UNIVERSITÀ DEGLI STUDI DI MILANO

FACOLTÀ DI SCIENZE E TECNOLOGIE

PhD SCHOOL in INDUSTRIAL CHEMISTRY

XXIX Cycle

Amphiphilic, biodegradable and biocompatible polymers for industrial applications

Coordinator: PROF. MADDALENA PIZZOTTI
Tutor: PROF. ELISABETTA RANUCCI

PhD student: **CAPUANO GIOVANNA**
R10587

INDEX

AIM OF THE PhD THESIS

The aim of this PhD work was to establish the synthetic procedures for new families of biocompatible and biodegradable and/or bioeliminable biomaterials that can be differently processed to obtain nanoparticles, core-shell nanofibres and hydrogel slabs or conduits, respectively. Depending on composition, size and morphology, these biomaterials may be intended for applications as drug delivery systems and/or tissue regeneration.

Specifically, the research project has been developed along two main lines:

- *Synthesis of poly(lactic-glycolic acid)-g-poly(1-vinylpyrrolidin-2-one) (PLGA-g-PVP) copolymers whose architecture consisted of a long PLGA backbone with oligomeric PVP pendants. These were obtained by the radical polymerisation of 1-vinylpyrrolidin-2-one in molten PLGA 50:50, acting as chain transfer agent. The procedure was a single pot - single step one. Copolymers were characterized by FTIR, ^{1}H- and ^{13}C-NMR and thermal analyses. They were saponified giving, besides PLGA degradation products, also un-degraded PVP. This was isolated and analysed by size exclusion chromatography, to evaluate the molecular weights of grafted PVP chains. MALDI-TOF analysis allowed identifying the chemical structure of PVP terminals and unambiguously establishing that PVP chains had been grafted onto PLGA backbone PLGA-g-PVP with different PVP content were formulated as drug nanocarriers by different procedures. Doxorubicin-loaded nanoparticles were prepared by the solvent diffusion method and fully characterised. In vitro drug release kinetics were studied and in vitro biological activity evaluated on several antitumoral cell lines.*

  PLGA-g-PVP were also used as coatings of lipid nanocapsules for the delivery of curcumin and artemisinin as antimalarials. Drug loaded-lipid micro-dispersions were first prepared by oil in water emulsion. The lipid drops were converted into nanometric ones by high pressure homogenization and finally surface coated by adding a DMSO/acetone PLGA-g-PVP solution. Growth inhibition assay were conducted on plasmodium falciparum (3D7) cultures. Haemoltic assays were conducted on healthy red blood cells.

  PLGA-g-PVP- and PLGA-based scaffolds consisting of nanofibrous mats were produced by electrospinning. Starting materials were electrospun and their morphology was evaluated by scanning electron microscopy and wettability by contact angle measurements. Coaxial electrospinning of two materials, in which PLGA formed the core and PLGA-g-PVP the shell of fibres, were also conducted and compared with those obtained by mixed solutions of staritng materials. Chemical composition was evaluated

by TGA, morphology by scanning electron microscopy and wettability by contact angle measurements. Nanofabric scaffold produced will be evaluated for drug release and tissue engineering applications.

- Synthesis of a new classes of poly(saccharide)-poly(aminoamine)s 3D-network intended as scaffolds for the regeneration of liver.

  In particular, hyaluronic acid-polyamidoamine and hyaluronic acid-gelatin-polyamidoamine hydrogels were synthesised by amidation reaction between the carboxylic acid group of hyaluronic acid and amine groups of gelatin and or an NH_2-functionalized PAA, promoted by 4-(4,6-dimethoxy-1,3,5-triazin-2-yl)-4-methylmorpholinium chloride (DMTMM) as coupling agent. Chemical-physical characterization were carried out on hydrogels. In order to promote hepatic cell proliferation serotonin was bonded to both hydrogels, adding it to the initial recipe, exploiting the above reaction between carboxylic acid group of hyaluronic acid and amine group of serotonin. Serotonin-loaded hydrogels were tested in vitro to evaluate biological efficacy.

In "Introduction" the broad definitions, classification and roles of biomaterials have been discussed. In the following chapters, chapter is launched with a brief and more narrow introduction on the chapter matter.

1.1 BIOMATERIALS: DEFINITION

"*A biomaterial is a nonviable material used in a medical device, intended to interact with biological systems.*"[i]

David Franklyn Williams, 1987

The increase in global average life expectancy, particularly in industrialised countries, a more active lifestyle and the onset of a large number of diseases, have generated a rising demand of medical devices, allowing to return the recovery of functionality of compromised body parts resulting in patient's survival. In order to build effective medical devices capable to perform these functions, the constituting materials must have the ability to interact with biological systems. These materials are named biomaterials. A number of definitions has been developed for this term.

At Consensus Conference of the European Society for Biomaterials (1987, Chester, England), D.F. Williams gave the most famous and used definition, reported at the begin of this paragraphs. These definition do not include materials for controlled drug and biological active molecules deliveries, as much as, all material-cell combinations.[ii,iii,iv] The currently accepted broader definition of biomaterial, always defined by D.F. William in 1991, is:[i]

"*A biomaterial is a man-made or man-modified viable or non-viable material intended to interface with biological systems to evaluate, treat, augment, or replace any tissue, organ, or function of the body.*"

INTRODUCTION TO BIOMATERIALS

1.1.1 Generations of biomaterials

As for the definition of biomaterials, also their purpose has changed over time, leading to three different generations. These three generations are not only a chronological sequence, but, mainly a conceptual evolution carrying change of requirements and properties of the materials involved. A first generation of biomaterials was developed starting from 1960-1970s, with the goal of "*achieve a suitable combination of physical properties to match those of the replaced tissue with a minimal toxic response in the host*".[v] They consisted in implanted prostheses that must be biological inert or have a minimal interaction with its surrounding tissue once putted in the body. By the mid-1980s, a second generation of biomaterials was reported with the peculiarity to be bioactive, meant as the ability to interact with the biological environment through the establishment of tissue-biomaterial surface bonding in order to enhance a specific biological response. During those years various compositions of bioactive glasses, ceramics, glass-ceramics and composites underwent clinical trials. The third generation biomaterials combined bioactivity with progressive and controlled chemical breakdown and resorption. This generation was created to aid both regeneration or restoration, and not simply replacement, of injured or lost tissues or body functions and delivery of biochemical factors and drugs. Thus, temporary structures that stimulate cellular invasion, attachment and proliferation fall in this area.[vi,vii,viii]

It is important to underline that new generation biomaterials do not necessarily override the use of those of a previous generation, but have only a different "modern" application. For example, bioinert materials are used to build temporary urinary catheter, bottles or body fluid containers and needles; bioactive materials for body implants and grafts; bioresorbable one are used in drug delivery and tissue engineering.

1.1.2 Biocompatibility

Bioinertness, bioactivity and bioresorbability are features describing how the host tissue interacts with an implanted or injected biomaterial, and how it impacts the biomaterial. Host response and how the host response impact biomaterials are two subjects of a single matter: biocompatibility.[iv,ix,x]

INTRODUCTION TO BIOMATERIALS

Biocompatibility is the most important property of a biomaterial and also the essential one to define a material as biomaterial. It is defined as *"the ability of a material to perform with an appropriate host response in a specific application".[xi]*
For a lay person this definition is very general and so self-evident that it is not of any real help in advancing knowledge of biocompatibility concept, but it is the only one always true and that takes in account all specific and different mechanisms involved in the interaction between biomaterials and tissues.

Table 1.1. Host response and host variables influence host response

Major characteristic of the generic response to biomaterials	Most material variables that could influence the host response
Protein adsorption and desorption characteristics Generalized cytotoxic effects Neutrophil activation Macrophage activation, foreign body giant cell production, granulation tissue formation Fibroblast behaviour and fibrosis Microvascular changes Tissue/organ specific cell responses Activation of clotting cascade Platelet adhesion, activation, aggregation Complement activation Antibody production, immune cell responses Acute hypersensitivity/anaphylaxis Delayed hypersensitivity Mutagenic responses, genotoxicity Reproductive toxicity Tumour formation	Bulk material composition, micro-(or nano)-structure, morphology Crystallinity and crystallography Elastic constants Water content, hydrophobic-hydrophilic balance Macro-,micro-, nano-porosity Surface chemical composition, chemical gradients, surface molecular mobility Surface topography Surface energy Surface electrical/electronic properties Corrosion parameters, ion release profile, metal ion toxicity (for metallic materials) Degradation profile, degradation product form and toxicity (for polymeric materials) Leachable, additives, catalysts, contaminants and their toxicity (for ceramic materials) Wear debris release profile

These specific mechanisms and the consequent host response depend on the general application and specific context. As an example, for long term bone implants, where the goal is bone integration of biomaterials, biocompatibility needs to take in account the rate of release of corrosion or degradation products and the tissue response to them, the rate of wear debris release and the tissue response to this debris. For systems injected in the bloodstream, host response may be acute, sub-acute and chronic inflammation, partially due to the mechanical injury of injection, but mainly to the presence of foreign substances

INTRODUCTION TO BIOMATERIALS

in blood that activate immunological response, leading high concentration of monocytes and macrophages in circulation. In the above cited examples, the main requirements of biomaterials is that they do not generate negative effects, that is, do not generate release of chemical substance, debris formation, inflammation phenomena and immune response, or that these phenomena are minimised. Major generic host response and major biomaterial variable influencing the host response are listed in Table 1.1 (A and B) and some test to evaluate biocompatibility depending on body tissue contact and contact duration, regulated by ISO 10993·1, are listed in Table 1.2.[xii,xiii]

Table 2. ISO 10993·1. Biocompatibility testing selection criteria.

Medical device categorization by			Biological effect [a]									
Nature of body contact												
Category	Contact	Contact duration [b]	Cytotoxicity	Sensitization	Irritation or intracutaneous reactivity	Acute Systemic Toxicity	Subchronic toxicity	Genotoxicity	Implantation	Haemocompatibility	Chronic toxicity	Carcinogenicity
Surface device	Skin	A	X	X	X							
		B	X	X	X							
		C	X	X	X							
	Mucosal Membrane	A	X	X	X							
		B	X	X	X	o	o		o			
		C	X	X	X	o	X	X	o		o	
	Breached or compromised surface	A	X	X	X	o						
		B	X	X	X	o			o			
		C	X	X	X	o	X	X	o		o	
External communicating device	Blood path, indirect	A	X	X	X	X				X		
		B	X	X	X	X	o			X		
		C	X	X	o	X	X	X	o	X	o	
	Tissue/ bone/dentin	A	X	X	X	o						
		B	X	X	X	X	X	X	X			
		C	X	X	X	X	X	X	X		o	o
	Circulating blood	A	X	X	X	X		o		X		
		B	X	X	X	X	X	X	X			
		C	X	X	X	X	X	X	X		o	o
Implant device	Tissue/bone	A	X	X	X	o						
		B	X	X	X	X	X	X	X			
		C	X	X	X	X	X	X	X		o	o
	Blood	A	X	X	X	X			X	X		
		B	X	X	X	X	X	X	X	X		
		C	X	X	X	X	X	X	X	X	o	o

a) The "X" indicates data endpoint that can be necessary for a biological safety evaluation, based on a risk analysis. The "o" indicates data endpoint that can be advisable for a biological safety evaluation. Where existing data are adequate, additional testing is not required. b) A= limited ($\leq$ 24h); B= prolonged (from > 24h to 30d); C= permanent (> 30d).

1.2 MATERIALS USED AS BIOMATERIALS

The majority of biomaterials are classifiable into three main classes: metals, ceramics and polymers. All others are composites and biologically-derived materials.
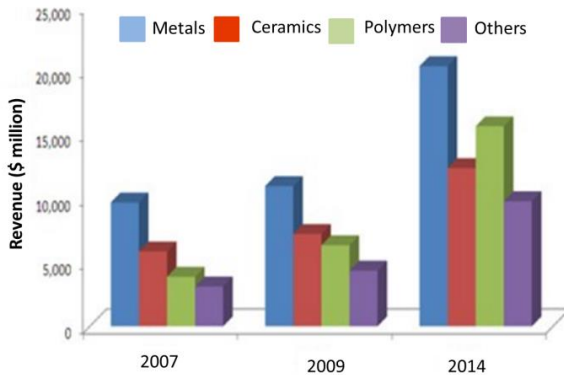
Figure 1.1. Biomaterial market by composition. Figure adapted from reference.[xiv]

The worldwide biomaterials market is poised to reach USD 130.57 Billion by 2020, growing at a CAGR (Compounded Average Growth Rate) of 16% during the forecast period between 2015 and 2020.[xv] As shown in Figure 1.1, the metallic segment accounted for the largest share of the market in 2014. The growth of this segment is driven by the benefits of metal biomaterials, such as strength and resistance to breakage, which makes them suitable for usage in various medical applications requiring strength and toughness. However, polymeric biomaterials form the fastest-growing segment in the coming years

INTRODUCTION TO BIOMATERIALS

owing to continuous research and advancements for highly biocompatible polymers and the increasing application areas of these biomaterials.

1.2.1 Polymeric biomaterials

Strong points of polymeric biomaterials compared to metal or ceramic materials are ease of manufacturability to produce various shapes (latex, film, sheet, fibres, etc.), reasonable cost and availability with desired mechanical and physical properties. These benefits have been evident since the dawn of polymer science. Virtually every new synthetic polymer found its way into biomedical experimental studies soon after its invention.[xvi,xvii] Nylon sutures were reported in the early 1940s, after only 5 years from the invention, by Wallace Hume Carothers.[xviii]

Polymers are macromolecules composed of a combination of many small units that repeat themselves along the long chain. The small starting molecules are called monomers, and unit, which repeats itself along the chain is called the repeating unit. Polymeric biomaterials can be produced by polymerization of one or more monomers, used to impart desirable chemical, physical, and biological properties to biomaterials. It is possible to produce polymers containing specific hydrophilic or hydrophobic entities, biodegradable repeating units, or multifunctional structures that can become points for three-dimensional 3D network. Moreover, many properties the chemical structure of the bulk polymer is unable to impart can be reached by chemical or physical modification of polymer surface.[xix,xx,xxi]

Considering the multitude of available polymers and of their applications, it may be useful to classify them into categories that highlight important aspects for their practical application.

In this section, polymers will be classified based on the presence or absence of degradation phenomena in a biological environment, that is, depending on their belonging to the second or third generation biomaterials (see section 1.1.2).

Non-degradable polymers have been extensively used in medicine as fillers, orthopaedic implants, ocular lens, heart valves, bone cements, vascular grafts, and tissue engineering scaffolds for long term devices.[xiii,xxii] Degradable

polymeric biomaterials are preferred candidates for developing therapeutic temporary devices such as prostheses, resorbable three-dimensional porous structures as scaffolds for tissue engineering and as drug delivery vehicles with controlled/sustained release.[xv,xxiii,xxiv,xxv]

1.2.2 Degradation and erosion of polymers in biological environment

According to the International Union of Pure and Applied Chemistry (IUPAC), polymer degradation is defined as "*changes in the values of in-use properties of the material because of macromolecule cleavage and molar mass decrease*". In contrast, erosion refers to "*degradation that occurs at the surface and progresses from it into the bulk*".[xxvi] Prefix *bio-* is added to both terms when degradation is due to cell-mediated or bacteria-mediated phenomena.[xxvii,xxviii,xxix]

In biological environment, hydrolysis is the most common chemical process by which polymers degrade, but degradation can also occur via oxidative, photodegradative, and enzymatic mechanisms.[iii] Hydrolytically degradable polymers are generally preferred because they are not affected by site-to-site and patient-to-patient variations, compared to enzymatically degradable ones.[xxx]

1.2.3 Hydrolically degradable polymers

Hydrolytic cleavage is dictated by the nature of the chemical bonds that make up the polymer backbone. In general, a carbon-carbon bond is chemically and biological inert. The C-C bond inertia can be decreased by oxidation of the carbon backbone. Therefore, an ester and urethane bond is easier to degrade than a ketone or a sulfone bond, which is easier to degrade than an ether bond. Other important factors are molecular weight, porosity and morphology (crystalline, amorphous forms). In particular, degradation phenomena slow down increasing the molecular weight and crystallinity of polymer and decreasing its porosity (a low ratio of exposed surface area to volume).[xlix,xxxi]

In extracellular fluids hydrolysis are promoted by the presence of ions, such as, H^+, Na^+, K^+, Mg^{2+}, Ca^{2+}, OH^-, Cl^-, HCO_3^-, PO_4^{3-}, and SO_4^{2-}. It has been shown that certain ions are effective hydrolysis catalysts, enhancing, for example, reaction rates of polyesters by several orders of magnitude.[xxxii] Ion catalysis can be enhanced increasing hydrophilicity percentage of the polymer.

Very hydrophobic polymers absorb negligible concentrations of ions. Whereas hydrogels, absorbing large amounts of water, act as ions sieves with consequent bulk hydrolysis via acid, base or salt catalysis.[iii]

1.2.4 Enzymatically degradable polymers

Enzymatically degradable polymers are materials possessing bonds that are hydrolytically sensitive, but require catalysis to degrade in physiological conditions. Most of the naturally occurring polymers undergo enzymatic degradation, like protein (*e.g.* silk, collagen, gelatin, fibrinogen), polyaminoacids (*e.g.* poly-γ-glutamic acid) and polysaccharides (cellulose, hyaluronic acid, dextran, alginate). Most of these polymers contain ether, amide or glycosidic bonds, which have hydrolytic degradation rates much lower than the polymers discussed before.[xxxiii] As an instance, polyurethanes biodegradation degree in the presence of cholesterol esterase enzyme is about 10 times higher than in the presence of buffer alone.[xxxiv] Hydrolytic reactions may be catalysed by enzymes known as hydrolases. These include proteases, esterases, glycosidases, and phosphatases, among others.

Enzymatically induced hydrolysis is a heterogeneous process, affected by the mode by which enzymes and polymeric chains interact. It typically involves four steps: (1) diffusion of the enzyme from the bulk solution to the polymeric surface, (2) adsorption of the enzyme on the surface with the following formation of the enzyme-polymer complex, (3) occurrence of the hydrolysis reaction, and (4) diffusion of the soluble degradation products from the solid surface to the solution.[xxxv] The slowest step controls the reaction rate.

In order to affect the enzymatic degradation rate, chemical modifications of polymers (crosslinking, removal, or introduction of chemical groups in the polymer chain) are usually done. Practically these modifications may compromise the ability of the enzyme to recognize the modified substrate. For instance, lysozyme (enzyme responsible for the degradation of peptidoglycan and also chitin materials) exhibited low activity toward chitosans with high degrees of deacetylation or crosslinked chitosan.[xxxvi,xxxvii,xxxviii]

The hydrolitically and enzimatically degradable polymers employed in this PhD work are briefly described below.

INTRODUCTION TO BIOMATERIALS

1.2.3.1 Poly(α-esters)

Due to the relative ease of their synthesis (via ring-opening or condensation polymerization)[xxxix,xl] and commercial availability, poly(α- esters)[xli,xlii] have been the most researched degradable polymers. They contain aliphatic bonds in their backbone. Only polymer having short aliphatic chains can be utilized as degradable polymers for biomedical applications.

Poly(glycolic acid)[xliii,xliv](PGA), poly(lactic acid)[xlv,xlvi,xlvii] (PLA), poly(lactic-co-glycolic acid)[xlviii,xlix,l] (PLGA) and poly (caprolactone)[li,lii,liii] (PCL) are the most common poly(α- esters) used (Figure 1.2).

PGA's rapid degradation and insolubility in many common solvents limited research for drug delivery devices. Typical application field that involving PGA is the short-term tissue engineering, in which it acts as filler material coupled with other degradable polymer networks.[liv] The additional methyl group in PLA causes polymer to be much more hydrophobic and stable against hydrolysis than PGA. PLA is extensively utilized in drug delivery and in tissue engineering applications ranging from scaffolds for bone, cartilage, tendon, neural, and vascular regeneration.[lv,lvi] PLGA is the most investigated degradable polymer for biomedical applications and has been used in sutures, drug delivery devices and tissue engineering scaffolds.[lvii,lviii,lix,lx] PCL has very low *in vivo* degradation rate and high drug permeability, it has found favour as a long-term implant delivery device.[lxi]
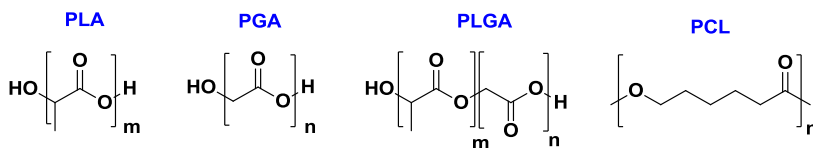
Figure 1.2. Structure of the most common poly(α-esters) used as biomaterials.

1.2.3.2 Polysaccharides

The term polysaccharides refers to a class of compounds consisting of monosaccharide units linked together by glycosidic linkages.[lxii,lxiii] They are

normally obtained by biosynthesis in plants (including algae) or in microorganisms. Therefore, they are produced by extraction and purification from renewable sources.[lxiv] A great share of polysaccharides constitutes a source of biomaterials for the most varied applications, especially in the domain of tissue engineering,[lxv,lxvi] drug delivery,[lxvii,lxviii] visco-supplementation[lxix]. The list of polysaccharides commonly used for biomedical applications include cellulose,[lxx] chitin/chitosan,[lxxi] starch,[lxxii] alginate,[lxxiii] hyaluronic acid,[lxxiv] pullulan[lxxv]and glycosaminoglycan[lxxvi] (Figure 1.3). Many natural polymers are found in the extracellular matrix components of organisms, including humans, and participate in inter and intracellular cell signalling, contributing to cell growth.[lxxvii] Thanks to these features, polysaccharides are often used to impart materials biological recognition ability, biocompatibility, and bioactivity. In spite of many benefits, they suffer from several drawbacks, including variation in material properties based on source, microbial contamination, uncontrolled water uptake, poor mechanical strength, and unpredictable degradation pattern.[lxxviii] Many polysaccharides have been chemically modified to achieve consistent physicochemical properties including mechanical stability, degradation, and bioactivity and processed into micropartides, hydrogels, and 3D porous structures for tissue regeneration applications.[lxxix,lxxx]
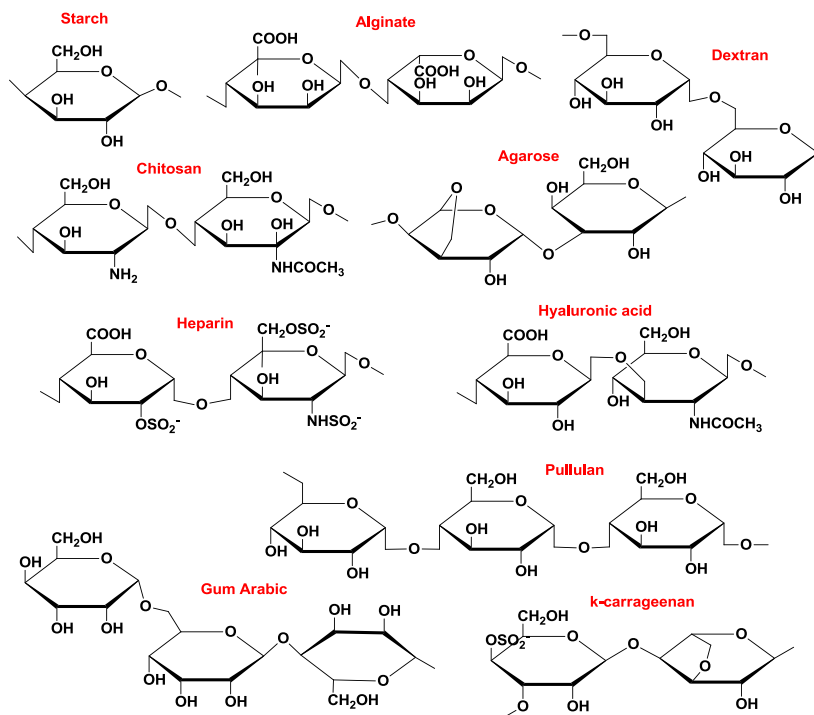
Figure 1.3. Structure of the most common polysaccharides used as biomaterials.

1.2.3.3 Polyamidoamines

PAAs are a family of biodegradable and biocompatible polymers with recognised potential in the pharmaceutical field.[lxxxi,lxxxii,lxxxiii,lxxxiv] PAAs are obtained by stepwise Michael type polyaddition reaction of primary or bis-secondary amines to bisacrylamids (Figure 1.4). The polymer obtained presents tert-amino and amido groups regularly arranged along the main chain. Polymerization reaction takes place in protonated solvents, such as water and alcohols, without catalysts. Amphoteric PAAs can be prepared using starting monomers, carboxyl groups not influencing the polyaddition reaction.[lxxxv,lxxxvi]
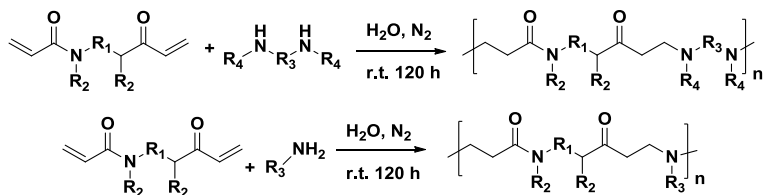
Figure 1.4. Reaction scheme of linear PAAs. Reaction was conducted in inert atmosphere to avoid radical polymerization of acrylamides.

It is possible to obtain cross-linked PAAs using polyfunctional monomers, such as bis-primary amine, by totally or partly replace the bis-functional amine monomer during the reaction (Figure 1.5). An alternative crosslinking method consists of triggering the radical polymerization of vinylic terminated PAA by UV irradiation, water soluble diazocompounds, or redox systems. In both cases crosslinked scaffolds were obtained, mostly used as inorganic pollutants adsorbents for water purification,[lxxxvii,lxxxviii,lxxxix] as optical dyes for metals detection,[xc] for the release of bioactive molecule[xci] and as scaffold for cell proliferation in tissue engineering application.[xcii,xciii,xciv] Conversely, linear PAAs were used as DNA,[xcv] protein[xcvi] carriers, in drug delivery for anticancer[xcvii] and antimalarial[xcviii] treatments, and also as macromolecular drug for antimetastatic[xcix] and antiviral applications[c]. Linear PAAs showed complex forming properties versus metallic ions dissolved in aqueous solutions.
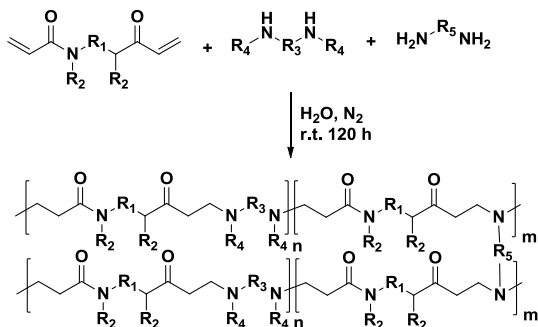
Figure 1.5. Reaction scheme of crosslinked PAAs. Reaction was conducted in inert atmosphere to avoid radical polymerization of acrylamides.

All PAAs are degradable in aqueous solution. The mechanism seems to be purely hydrolytic as no vinyl groups, such as those which would have derived from a β-elimination reaction, could be determined. Degradation rate in aqueous media is strongly influenced by pH and temperature. Degradation seems not to be affected by the presence of isolated lysosomal enzymes at pH 5.5.[ci,cii,ciii]

1.3 BIOMATERIALS: APPLICATIONS

The main applications of biomaterials can be classified into the categories, depending on the tissue or organ that they repair or, more generally, with which they come in contact. Each category has a different weight on global market (Figure 1.6). In particular, cardiovascular and orthopaedic application segments are the most revenue-bearing fields. The first dominates the global biomaterials market in terms of share due to the high prevalence rates of cardiovascular diseases, above all in rich countries like USA. The orthopaedic segment is the second largest market thank to health problems due to advancement of population average age.[xli,xlii]
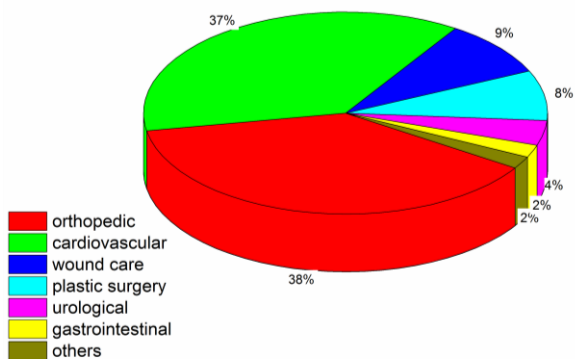
Figure 1.6. Biomaterials market by applications.

Typical applications in these fields are related to substitution, scaffolding or splinting of tissues that are not able to self-renew. In this way, a great number of implants and grafts have been produced.[civ,cv,cvi] Examples are heart valves, endovascular stents, vascular grafts, stent grafts, reconstructive implants,

fracture management products, arthroscopy products, electrical stimulation products for cardiovascular and orthopaedic application areas.[cvii,cviii,cix,cx]

Adhesive and sealant biomaterials are used to fill a space, replacing some part of lost natural tissue, as bone cements in orthopaedics, or to protect surfaces or prevent leakage, as pit and fissure sealants in dentistry.[cxi,cxii,cxiii]

Biomaterials are not only intended for internal body applications but also as device constituents for external body applications. They are used for drugs, organs and blood packaging, but also for many disposable medical devices, such as syringes, injection pipes, surgical gloves, lancets, cotton pads, and *in vitro* biological devices, such as pipette, micropipette, well-plates, test tubes.[cxiv]

A broad class of biomaterials is used to provide bioelectrodes and biosensors.[cxv,cxvi,cxvii] Bioelectrodes are sensors used to transmit information into or out of the body. Surface or transcutaneous electrodes used to monitor or measure electrical events that occur in the body, like in electrocardiography, electroencephalography, and electromyography. A biosensor is a sensor that uses biological molecules, tissues, organisms or principles to measure chemical or biochemical concentrations. Biosensors can work by changes in pH, ions, blood gases (O_2, CO_2 and etc.), drugs, hormones, proteins, viruses, bacteria.

1.3.1 Tissue engineering and regenerative medicine

When tissues and/or organs fail, their replacement is usually the only solution. Regrettably, the number of compatible donors and the consecutive number of organs is really limited. For these reason, artificial prostheses are essential to save and improve lives of millions of patients.

At first, implants were made of materials well known in the technological field, but not in origin thought for biomedical applications. Stainless steel, alloys and high-density polyethylene were used for bone implant, methacrylate polymers as bone cement in dental medicine, polyethylene tetraphthalate fibres for the production of grafts for blood vessel reconstructions. These materials had initial problem with integration of host tissues, by triggering a host immune response compromising the healthy tissue around the implant.[cxviii]

INTRODUCTION TO BIOMATERIALS

By modifying the chemical composition of either the bulk or the surface of implants, tissue-implant interactions are improved with a remarkable reduction of inflammations, immune responses, systemic toxicity and imminent infection.

On the other hand, due to the normal cellular and tissue activity, materials are subject to continue stress that over time produces damage in the implant, eventually leading to its failure. Fatigue fracture and wear combined with the formation of debris, have been identified as some of the major problems associated with implant failure in long term. These events force patients to frequent substitution of implanted prostheses, resulting in a great bother.

A solution for this problem may be developing procedures that do not replace the damaged tissue/organ but favour their regeneration.

The goal of regenerative medicine is the healing (or at least partially restoring) of damaged tissue, supporting the regeneration of diseased or injured organs. Regenerative medicine usually takes advantage of tissue engineering materials.[cxix,cxx,cxxi,cxxii]

Tissue engineering is defined as: *"the creation (or formation) of new tissue for the therapeutic reconstruction of the human body, by the deliberate and controlled stimulation of selected target cells through a systematic combination of molecular and mechanical signals"*.[i]

Tissue engineering takes advantage of 3D structures, named scaffolds, that provide a template for cells to attach, proliferate, maintain their differentiated function and organize in order to restore structure and function to damaged tissues. Essentially, scaffolds act as a synthetic analogue of the natural extracellular matrix. [cxxiii]
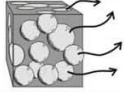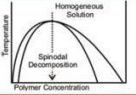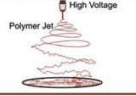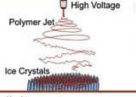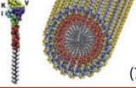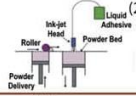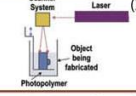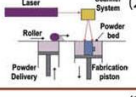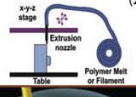
Two main strategies have been used in tissue engineering: transplantation of a *in vitro* grown tissue, and in situ tissue regeneration. The first consists of *in vitro* cultured cells on an artificial scaffold in presence of growth factors until forming a natural tissue followed by transplantation. The second is a combination of an artificial scaffold and growth factors used as a template to induce host cell regeneration of the tissue *in vivo*. In this case the host's body works as a bioreactor to construct new tissues.

In general, an ideal scaffold should have: i) three-dimensional highly porous structure with an interconnected pore network to facilitate cell/tissue growth and diffusion of nutrients, metabolic waste, and paracrine factors; ii) a biodegradable or bioresorbable network with degradation and resorption rates that match tissue growth both in vitro and in vivo; iii) a suitable surface chemistry for cell attachment, proliferation, and differentiation; iv) mechanical properties similar to those of tissues at the site of implantation; v) easy manufacturing, in order to be able to produce a variety of shapes and sizes.[cxxiv,cxxv]

1.3.1.1 Types of scaffolds

Large numbers of scaffolds from different biomaterials are available for clinical use with the aim of repair and regenerate lost or damaged tissue and organs. These scaffolds include porous scaffold, fibrous scaffold, hydrogel scaffold and solid free form one. The fabrication technique for scaffolds depends almost entirely on the bulk and surface properties of the biomaterial and the proposed function of the scaffold (Figure 1.7).

As before mentioned, the formation of a highly porous structure is the main goal of scaffold fabrication. Most usual methods used to made porous scaffolds, including particulate leaching,[cxxvi] freeze drying,[cxxvii] gas infusion,[cxxviii] and phase separation.[cxxix] Porous are developed by introducing particles or gas bubbles when the scaffold is in a fluid form and are later removed by solvent action (organic one, water) or under vacuum after scaffold solidification, leading an interconnected network of pores. The porosity and pore structure is dependent on the amount of porogen the size of porogen dissolved in the material, and the diffusion rate of it through the material.[cxxx] Phase separation is based on thermodynamic demixing of a homogeneous polymer-solvent solution into a polymer-rich phase and a polymer-poor phase, by exposure to an immiscible solvent or by cooling the solution below a binodal solubility curve. Solvents are removed by freeze-drying, leaving behind the polymer as a foam. These techniques are relatively simple but suffering of uncontrolled pore size and connectivity, poor mechanical strength, and residual solvent/porogens.[cxxxi]

	Scaffold Name	Porosity & Size	Schematic
Conventional Scaffold	Particulate leaching	Porosity < 90% Pore size 5-600µm	
	Thermal Induced Phase Separation (TIPS)	Porosity < 90% Pore size 5-600µm	
Nano-scale Scaffold	Electrospinning	Porosity < 90% Pore size <1-10µm	
	Electrospinning onto ice crystals	Porosity < 95% Pore Size 20-200µm	
	Self-assembling Nanofibers	Porosity < 95% Pore Size 200-800µm	(7)
Solid Freeform Fabrication (SFF) Scaffolds	3 Dimensional Printing (3DP)	Porosity < 45-60% Pore Size 45-1600µm	(2)
	Stereolithography	Porosity < 90% Pore size 20-1000µm	(2)
	Selective Laser sintering (SLS)	Porosity < 40% Pore size 30-2500µm	(2)
	Fused deposition modelling	Porosity < 80% Pore size 100-2000µm	(2)
	Direct Writing	Porosity < 90% Pore Size 5-100µm	(12)

Figure 1.7. Snapshot of techniques for preparing porous polymer scaffolds for tissue engineering. Figure from reference.[cxxxii]

Fibre-based scaffold are highly studied due to the possibility to have high surface area to volume ratio, leading to a microporous structure that favours cell

adhesion, proliferation, migration, and differentiation. All of these features are highly desired ones for tissue engineering applications.[cxxxiii] Three techniques are mostly used for them synthesis: electrospinning[cxxxiv], self-assembly,[cxxxv] and phase separation[cxxxvi]. Of these, electrospinning is the most widely studied technique, at contrary, nanofibres synthesized by self-assembly and phase separation have had relatively limited studies. By electrospinning of polymers, continuous micro- or nanoscale diameter fibres can be generated. In addition, it is possible to control orientation of fibres. However, it is difficult to control the distance between fibres and impossible to produce scaffold with volume and usually mechanical properties of collected scaffolds are poor.[cxxxvii]

Solid free form fabrication techniques are based on computerized modelling to produce highly complex three-dimensional physical objects.[cxxxviii] The result is a porous scaffold with enhanced control over its three-dimensional organization. Specifically, a two-dimensional image of a target specimen was acquired by a non-destructive imaging, then was later developed in a three-dimensional architecture with software and finally fabrication of the three-dimensional matrix with highly precise and automated layer-by-layer SFF processes.[cxxxix] Typical processes include laser-based, ink-jet type printing-based, and nozzle-based approaches. These methods offer precise control of the three-dimensional structure of the scaffolds; however, they are associated with higher costs and require more complex equipment compared to classical methods.

Hydrogels are hydrophilic polymer networks which may absorb up to thousands of times their dry weight in water. Hydrogels are formed when the network is covalently crosslinked.[cxl] In general, polymers with reactive moieties are polymerized into three-dimensional networks in the presence of cross-linkers. Photo-crosslinkable or thermo-crosslinkable hydrogels are the most frequently used.[cxli] Hydrogel properties can be tuned in order to satisfy a range of application needed by controlling the structure with defined cross-linking density, mechanical properties, mass transport, and degradation characteristics. In particular the degradation rates of hydrogel scaffolds must be matched to the rate of various cellular processes in order to optimize tissue regeneration.[cxlii,cxliii] Hydrogels are appealing scaffold because they are structurally similar to the extracellular matrix of many tissues, can often be processed under relatively mild conditions, and may be delivered in a minimally invasive manner.[cxliv]

Furthermore, hydrogels can be chemically modified to improve cell adhesion and proliferation on the gel matrices through inclusion of adhesion peptides. However, major problems with using hydrogels include structural instability and overall inferior mechanical properties for placement within dynamic environments.[cxlv]

1.3.2 Drug delivery systems

Delivery systems are mainly intended to achieve either a temporal or spatial controlled delivery of some pharmacological interesting molecules, such as drugs, proteins, DNA, RNA, growth factors and hormones. Delivery systems offer numerous advantages compared to conventional dosage forms, in particular when they have a "sustained" or "prolonged" molecule release.

1.3.2.1 Type of delivery systems

Different types of drug delivery systems have been developed with a wide range of sizes from tens of micrometres to tens or hundreds of nanometres. [cxlvi,cxlvii] Drug carriers can be divided in three categories by its composition: lipid carriers, polymeric carriers and inorganic ones as also depicted in Figure 1.8. Lipid and polymeric carriers are below examined.

Liposomes, micro/nano-emulsions, solid lipids nanoparticles are the most frequently used lipid carriers. Liposomes are spherical structures composed of a phospholipid bilayer surrounding an aqueous reservoir. Liposome vesicles are composed of unilamellar or multilamellar lipid bilayers which alternate aqueous. In general, hydrophobic compounds are well entrapped in liposomes compared to hydrophilic compounds.[cxlviii] Micro/nano-emulsions consist in oily drops dispersed in an aqueous surfactants solution, leading to a milky suspensions.[cxlix] Solid lipid nanoparticles (SLN) are similar to liposome, but they have only a single membrane and are based on solid lipids stabilized by surfactants. SLN have a mean particle size of 50-1000 nm. Different types of solid lipids such as glycerides, waxes, and fatty acids have been used in the fabrication of SLN.[cl]

Polymeric carriers count several types of micro or nanosized particles with different structures. Nanocristals (nanotized particles), drug-polymer

conjugates, solid micro or nanoparticles, micelles, layer by layer conjugates, dendrimers and polymersomes are the most famous.

Nano-crystals consist in large insoluble drug crystals are milled to form nano-sized particles with less than 2 μm. To prevent particle aggregation, surfactants such as surface active agents and polymers are normally required for stabilization.[cli] Polymer-drug conjugates are based on drug molecules linked on hydrophilic polymers. The drugs remain attached to the polymer and are not activated until the enzymes associated with the diseased tissue are present.[clii] Nanoparticles consist in polymeric aggregates in a solid state suspended in water solution, in presence or not of surfactants. Two kind of nanoparticles are usually described: nanosphere and nanocapsules. Nanospheres have a homogeneous structure in the whole particle, in which the drug is dissolved. Nanocapsules are nano-vesicular systems that exhibit a typical core-shell structure; the drug is confined to a reservoir or a cavity.[cliii] Micelle are organized self-assembled aggregates composed of amphiphilic macromolecules, in general amphiphilic di- or tri-block copolymers made of hydrophilic and hydrophobic blocks. Micelles are characterized by critical micellar concentration, (CMC), that is the minimum concentration of polymer in solution to reach micelle structure. Therefore, micelle formation and stability are concentration-dependent.[cliv] Dendrimers are monodispersed macromolecules with highly branched structures around an inner core. The terminal groups of dendrimers mostly control the dendrimer interactions with the molecular environment. The interior of a dendrimer can show hydrophilic characteristics while the exterior surface of a dendrimer is hydrophobic or vice versa.[clv] Polymersomes are made using amphiphilic block copolymers to form the vesicle membrane, with radii ranging from 50 nm to 5 μm or more. Most reported polymersomes contain an aqueous solution in their core and are useful for encapsulating and protecting sensitive hydrophilic drugs. They are the polymeric alternative to liposomes.[clvi]
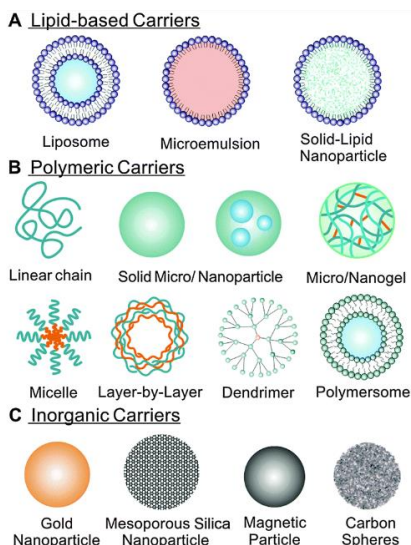
Figure 1.8. Nanosized carrier mainly used in drug delivery. Figure take from reference.[cxlvi]

A significant technological and medical breakthrough in the evolution of drug carriers is the shift in size from tens of micrometres to tens or hundreds of nanometres. Thanks to their sub-cellular and sub-micron size, nanocarriers can penetrate deep into tissues through fine capillaries, cross the fenestration present in the epithelial lining and are generally taken up efficiently by the cells.[clvii,clviii] For instance, nanoparticles 100 nm in size showed 2.5-fold higher uptake in Caco-2 cells compared to 1 μm particles and 6-fold higher compared to 10 μm particles.[clix]

1.3.2.2 Drug loading

A successful carrier should have a high drug-loading capacity in order to reduce the number of administrations. Drug can be loaded or be conjugated into the carrier. Drug conjugation allows high degree of incorporation. Physical incorporation of drugs may take place on nanoparticle preparation obtained by incubating them with a concentrated drug solution; c) by chemical conjugation

INTRODUCTION TO BIOMATERIALS

of drug into carriers. It is evident that a larger amount of drug is entrapped passing from method to incorporation one to conjugation one.[clx,clxi,clxii]

Drug loading depends on the solid-state drug solubility in polymeric matrix (solid dissolution or dispersion), which is related to polymer composition, molecular weight, drug polymer interaction (hydrophobic/hydrophilic interaction and ionic interaction)[clxiii,clxiv], and presence of end-functional groups.[clxv,clxvi,clxvii]

1.3.2.3 Time control

These systems are related to all devices able to maintain a desired tissue (blood) concentration within the molecule therapeutics index (TI) for long periods of time. Focusing upon drugs, TI is the ratio of two concentrations limits: the higher one, above which the drug produces undesirable (e.g., toxic) side-effects, and the lower one, below which it is not therapeutically effective. Drug delivery systems with prolonged release are able to release drugs for long periods of time without reaching a toxic level or dropping below the minimum effective level (Figure 1.9).[clxviii,clxix]
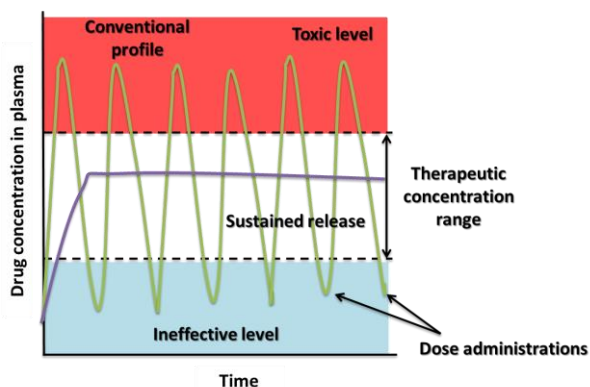
Figure 1.9. Kinetic profiles of standard dose forms (green line), sustained release systems (purple line).

Drug solubility and diffusion and biodegradation of the matrix materials govern the release process. [clxx] In the case of nanospheres, where the drug is uniformly

distributed, the release occurs by diffusion or erosion of matrix under biological conditions. If the diffusion of the drug is faster than erosion, the release mechanism is largely controlled by diffusion. The rapid initial release or 'burst' is mainly attributed to weakly bound or adsorbed drug to the large surface of nanoparticles.

1.3.2.4 Spatial control

Spatial controlled release is achieved thanks to two targeting mechanisms, i.e. passive and active. Passive targeting is dependent on the physicochemical properties of the drug-carrier system. Tailoring delivery system properties, it is possible to profit of physiological properties of target tissues, minimizing uptake into undesired tissues. Surface charge, hydrophobicity, size and shape of the carrier system are usually take in account.[clxxi] For instance, large macromolecule-drug conjugates and nanoparticles take advantage of the enhanced permeability and retention (EPR) effect, usually present in solid tumours. EPR is due to the presence in blood vessels of poorly aligned defective endothelial cells with wide fenestrations and the absence of effective lymphatic drainage that allow accumulation of drug carrier in the tumour tissue much more than in normal tissues.[clxxii,clxxiii]

Active targeting is achieved by conjugating a tissue- or cell-specific ligand to the carrier.[clxxiv,clxxv] The ideal active targeting is attained when the target receptor is not expressed in significant quantities anywhere else in the body or is over-expressed in diseased cells. Targeting ligands are either monoclonal antibodies (mAbs) and antibody fragments or non-antibody ligands (such as peptidic one).[clxxvi] Usually after internalization, nanocarriers escape the endo-lysosomes and enter the cytoplasm. Other organuli can be reached adding specific ligand, as, for example, by conjugating NLS (nuclear localization signal) for nuclear compartment cell. [clxxvii]

1.4 BIOMATERIALS: PROPERTIES

Properties (physical, mechanical and surface properties) of biomaterial are designed and modelled as a function of the application and of the host tissue. Examples of biomaterial properties affecting their performance in drug delivery and tissue engineering are reported in Figure 10.
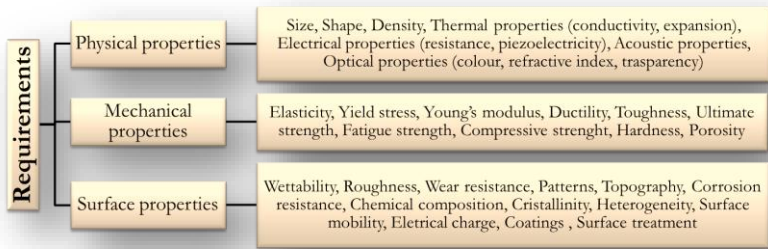
Figure 10. Physical, mechanical and surface requirements.

1.4.1 Size and shape

In the field of drug delivery, size and shape of carriers are fundamental for several *in vivo* functions. These include circulation times, extravasation, targeting, immunogenicity, internalization, intracellular trafficking, degradation, flow properties, clearance and uptake mechanisms (Figure 1.11, panel A).[clxxviii,clxxix,clxxx,clxxxi] A problem usually observed during intravenous injection of some kind of drug carriers is the phagocytosis by macrophages of the reticulo-endoplasmatic system (RES). Phagocytosis represents an immunological response of body that recognises as foreign these carriers and eliminate them from the bloodstream. To promote long persistence in the blood, phagocytosis must be avoided. Some carrier properties are modified to reach this target. Phagocytosis mechanism is influenced by particles size instead of particle shape influences phagocytosis outcomes and kinetic. Particles greater than 500 nm can be phagocytised by macrophages. Instead, smaller particles can be endocytosed by phagocytic or non-phagocytic cells.[clxxxii,clxxxiii] Encountering a fully pointed end of an elliptical particle, macrophage internalizes the particle in a few minutes, while if it hits the flat region of the same elliptical particle, phagocytosis does not occur for over 12 hrs. As shown in Figure 1.11-panel B, the local shape of the particle, characterized by an Ω angle, influences the start of phagocytosis (Figure 1.11-panel C).[clxxxiv] In particular, phagocytosis velocity decreased with increasing Ω.
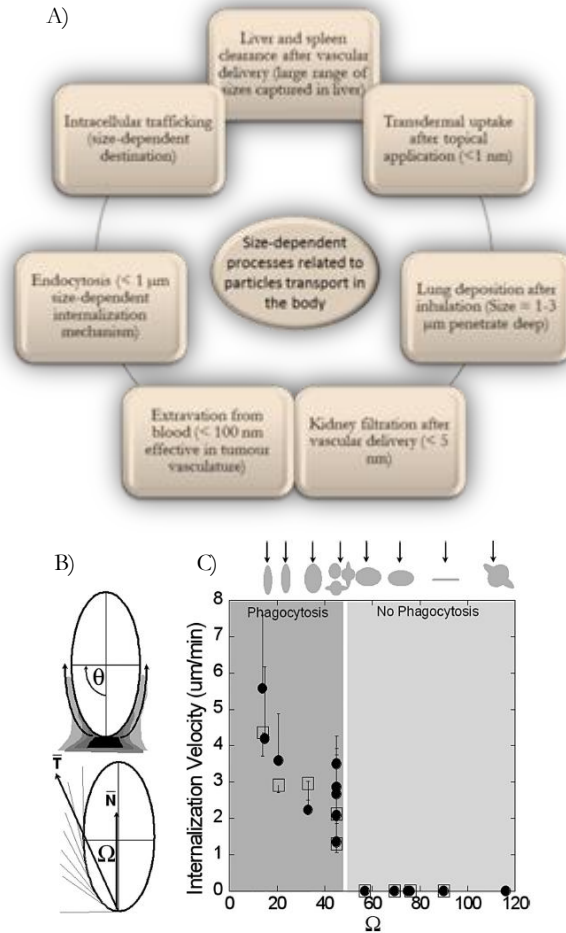
Figure 1.11. A) *In vivo* functions influenced by particle size. B) A schematic diagram illustrating how membrane progresses tangentially around an elliptical particle. T represents the average of tangential angles from $\theta = 0$ to $\theta = \pi/2$. Ω is the angle between T and membrane normal at the site of attachment, N. (C) Membrane velocity (distance traveled by the membrane divided by time to internalize, n $\geq$3; error bars represent SD) decreases with increasing Ω for a variety of shapes and sizes of particles. Figure adapted from reference.[clxxxiv]

1.4.2 Mechanical properties

In tissue engineering, mechanical properties represent important features.[clxxxv,] To help in selecting biomaterials, mechanical property maps, known as Ashby maps, are used to compare a large amount of physical properties from various material groups and compared with those of biological systems (Figure 1.12, A and B panels).[clxxxvi,clxxxvii] Human tissues have a wide range of modulus values, from soft materials (brain, about 0.5 kPa), to moderately stiff (skin and muscles, around 10 kPa) to stiff ones (precalcified bone, >30 kPa). Scaffolds for regenerative medicine should ideally have the same strength and Young's modulus of the tissue they will restore.[clxxxviii,clxxxix] This general law is valid for all the kinds of mechanical moduli. As shown in Figure 1.13, the scaffold elasticity drives lineage specification of mesenchymal stem cells (MSCs).[cxc]
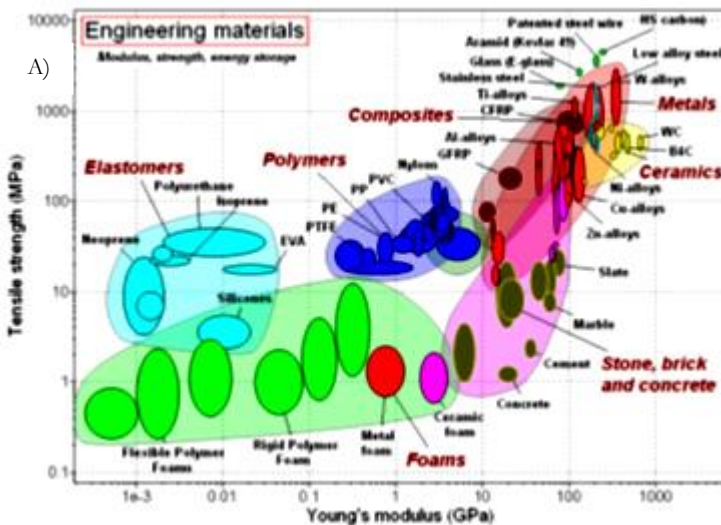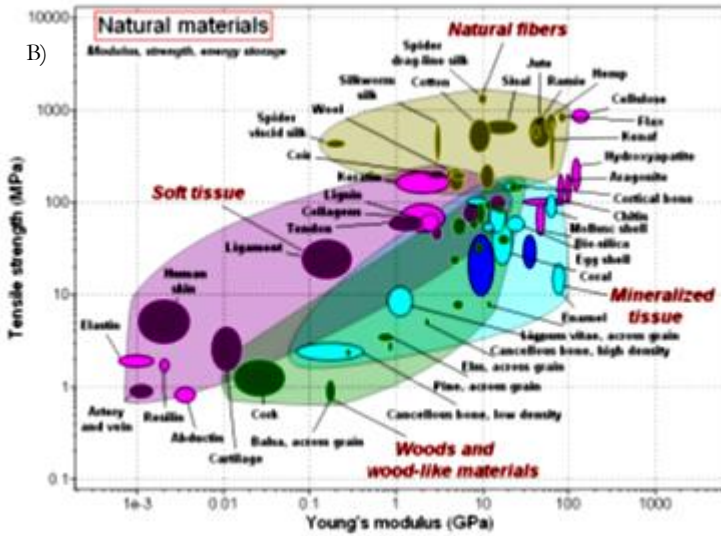
Figure 1.12. A) Young's modulus and tensile strength of engineering material; B) Young's modulus and tensile strength of natural material on exactly the same axes of panel A. Figure take from reference.[clxxxvi]

INTRODUCTION TO BIOMATERIALS
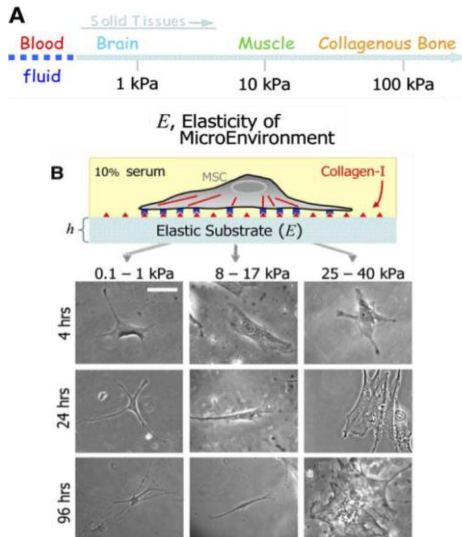
Figure 1.13. (A) Solid tissues exhibit a range of stiffness, as measured by the elastic modulus, E. B) Naive MSCs of a standard expression phenotype are initially small and round but develop increasingly branched, spindle, or polygonal shapes when grown on matrices respectively in the range typical of E_{brain}(0.1–1 kPa), E_{muscle}(8–17 kPa), or stiff crosslinked-collagen matrices (25–40 kPa). Scale bar is 20 mm. Figure adapted from reference.[cxc]

1.4.3 Surface properties

Surface is the biomaterial section in contact with neighbouring tissues and, subsequently, it greatly influences biological responses in all applications. [cxci,cxcii] Therefore, the evaluation of surface properties of biomaterials is of paramount important. Surfaces have free energy associated with the discontinuity and asymmetry of the interface that tends to actively minimize through continual processes of molecule adsorption, restructuring, and chemical reactions. When an object is inserted in a biological environment, the first molecule it comes in contact is water with. Wetting is the ability of water (or in general of a liquid) to maintain contact with a solid surface. The balance between adhesive and cohesive forces determines the degree of wetting (wettability). Adhesive forces compel a water drop to spread across the surface (hydrophilic surfaces). Cohesive forces compel the drop to ball up and avoid contact with the surface (hydrophobic surfaces). Wettability influences interaction with biological materials.[cxciii,cxciv,cxcv]

In tissue engineering, wettability influences the interaction between surface scaffold and cell adhesion protein (transmembrane glycoproteins) that are the first to attach the surface and promote cell adhesion. Adhesion proteins include selectins, integrins, syndecans, and cadherins. In Figure 1.14 Panel A, the influence of siloxane-coated polystyrene wettability on osteosarcoma cells (MG63) is reported. Increasing hydrophobicity of the surface (increasing contact angle) cell adhesion decreases.[cxcvi]
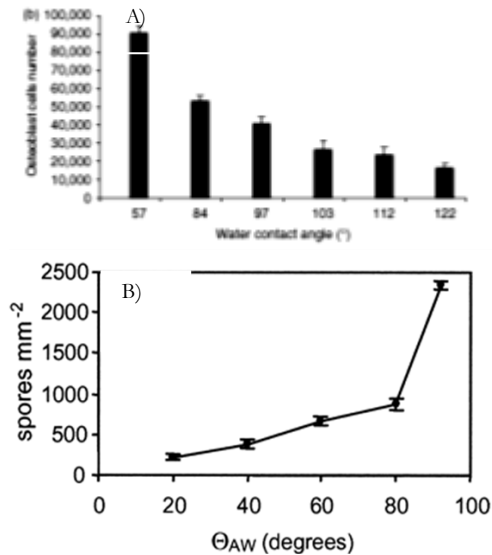
Figure 1.14. Influence of siloxane-coated rough surface PS water contact angle on MG63 cell adhesion. B) Attachment of Enteromorpha zoospores on patterned CH_3/OH SAMs of varying wettabilities ($\boldsymbol{\theta}$AW) Figures take from references.[cxcvi,cxcvii]

Wettability influences also bacteria adhesion (Figure 1.14, Panel B), but in this case increasing hydrophobicity of surfaces adhesion is favoured.[cxcvii] If bacteria spread on scaffold surface, an infection is developed with the consequent rejection of the scaffold from the host tissue. For this reason, bacteria adhesion and proliferation must be avoided (Figure 1.15).[cxcviii] Also other properties are tuned to obtain antifouling activity, such as roughness, topography, surface tension, surface charge etc. For example, bacterial membranes are generally negatively charged and so, in general, a negatively charged biomaterial surface could reduce adhesion, due to repulsion forces.[cxcix]
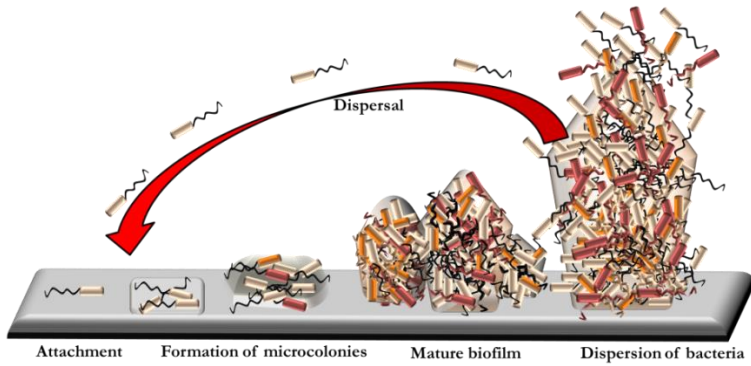
Figure 1.15. Main stages of bacteria biofilm formation.

Wettability influences the in vivo fate of micro- and nanopartides. Hydrophobic partides are normally recognized by the host immune system (RES). To minimize opsonization, hydrophobic partides are coated with hydrophilic polymers/surfactants or bonded to them, obtaining amphiphilic copolymers.

INTRODUCTION TO BIOMATERIALS

BIBLIOGRAPHY

[i] D.F. Williams, *Biomaterials*, **2009**, 30, 5897-5909

[ii] K.D. Jandt, *Advanced Engineering Materials*, **2007**, 9, 1035-1050

[iii] B.D. Ratner, A.S. Hoffman, F.J. Schoen, J.E. Lemons, *Biomaterials science: an introduction to materials in medicine*, 3rd ed., Oxford: Elsevier/AP, **2013**

[iv] V. Migonney, *Biomaterials*, Bioengineering and health science series, Wiley-ISTE, **2014**

[v] L. Hench, *Biomaterials Science*, **1980**, 208, 826–831

[vi] G. Heness, B. Ben-Nissan, *Materials forum*, **2004**, 27, 104-114

[vii] L.L. Hench, I. Thompson, *Journal of the royal society of interface*, **2010**, 7, S379-S391

[viii] M. Navarro, A. Michiardi, O. Castano, J.A. Planell, *Journal of The Royal Society Interface*, **2008**, 5, 1137-1158

[ix] B.D. Ratner, S.J. Bryant, *Annual Review of Biomedical Engineering,* **2004**, 6, 41-75

[x] R. Langer, D.A. Tirrell, *Nature*, **2004**, 428, 487-492

[xi] B.D. Ratner, *Journal of Cardiovascular Translational Research,* **2011**, 4, 523-527

[xii] Available from:
https://www.medtechintelligence.com/feature_article/biological-evaluation-of-medical-devices/

[xiii] A.J.T. Teo, A. Mishra, I. Park, Y.J. Kim, W.T. Park, Y.J. Yoon, *ACS Biomaterials Science and Engineering,* **2016**, 2, 454-472

[xiv] Available from: http://slideplayer.com/slide/7677086/

[xv] Avalaible from: http://www.marketsandmarkets.com/Market-Reports/biomaterials-393.html

[xvi] M. Vert. *Progress in Polymer Science*, **2007**, 32, 755-761

[xvii] D. Ozdila, H. M. Aydin, *Journal of Chemical Technology and Biotechnology,* **2014**, 89, 1793-1810

[xviii] N. Angelova, D. Hunkeler, *Trends in biotechnology*, **1999**, 17, 409-421

[xix] B.L Seal, T.C. Otero, A. Panitch, *Material Science and Engineering*, **2001**, 34, 147-230

[xx] L.G. Griffith, *Acta Materialia*, **2000**, 48, 263-277

[xxi] M.F. Maitz, *Biosurface and Biotribology*, 2015, 161-176

[xxii] V.P. Shastri, *Current Pharmaceutical Biotechnology*, **2003**, 4, 331-337

[xxiii] B.D. Ulery, L.S. Nair, C.T. Laurencin, *Journal of Polymer Science Part B: Polymer Physics,* **2011**, 49, 832-864

[xxiv] H. Tian, Z. Tang, X. Zhuang, X. Chen, X. Jing, *Progress in Polymer Science*, **2012**, 37, 237-280

[xxv] G.E. Luckachan, C.K.S. Pillai, *Journal of Polymers and the Environment,* **2011**, 19, 637-676

xxvi Terminology for biorelated polymers and applications, *Pure and Applied Chemistry,* **2012**, 84, 377-410

xxvii Available from:

http://www.treccani.it/enciclopedia/biomateriali_(Enciclopedia-della-Scienza-e-della-Tecnica)/

xxviii L.S. Nair, C.T. Laurencin, *Progress in Polymer Science*, **2007**, 32, 762–798

xxix A. Göpferich, *Biomaterials*, **1996**, 17, 103-114

xxx D.S. Katti, S. Lakshmi, R. Langer, C.T. Laurencin, *Advanced Drug Delivery Reviews*, **2002**, 54, 933-961

xxxi F. Alexis*, Polymer International,* **2005**, 54, 36-46

xxxii G.E. Zaikov, *Journal of Macromolecular Science, Part C: Polymer Reviews*, **1985**, 25, 551-597

xxxiii R.L. Reis, J. San Román, *Biodegradable Systems in Tissue Engineering and Regenerative Medicine*, CRC Press, Taylor& Francis group, **2004**

xxxiv J.P. Santerre, R.S. Labow, D.G. Duguay, D. Erfle, G.A. Adams, *Journal of Biomedical Materials Research Part A,* **1994**, 28, 1187-1199

xxxv M Rahmouni, F Chouinard, F Nekka, V Lenaerts, J.C. Leroux, *European Journal of Pharmaceutics and Biopharmaceutics*, **2001**, 51, 191-198

xxxvi R.J. Nordtveit, K.M. Varum, O. Smidsrod, *Carbohydrate Polymers,* **1996**, 29, 163-167

xxxvii K. Tomihata, Y. Ikada, *Biomaterials*, **1997**, 18, 567-575

xxxviii F.L. Mi, Y.C. Tan, H.C. Liang, R.N. Huang, H.W. Sung, *Journal of Biomaterials Science, Polymer Edition,* **2001**, 12, 835-850

xxxix O. Dechy-Cabaret, B. Martin-Vaca , D. Bourissou, *Chemical Reviews,* **2004**, 104, 6147-6176

xl M. Ajioka, H. Suizu, C. Higuchi, T. Kashima, *Polymer Degradation and Stability*, **1998**, 59, 137-143

xli M. Vert, *Biomacromolecules*, **2005**, 6, 538-546

xlii A.A. Ignatius, L.E. Claes, *Biomaterials*, **1996**, 17, 831-839

xliii J.B. Herrmann, R.J. Kelly, G.A. Higgins, *Archives of surgery,* **1970**, 100, 486-490

xliv K.B. Lee, D.J. Kim , Z.W. Lee , S.I. Woo, I.S. Choi, *Langmuir*, **2004**, 20, 2531-2535

xlv D. Garlotta, *Journal of Polymers and the Environment*, **2001**, 9, 63-84

xlvi Y. Cheng, S. Deng, P. Chen, R. Ruan, *Frontiers of Chemistry in China,* **2009**, 4, 259-264

xlvii A.J.R. Lasprilla, G.A.R. Martinez, B.H. Lunelli, A.L. Jardini, R. Maciel Filho, *Biotechnology Advances*, **2012**, 30, 321-328

xlviii H.K. Makadia, S.J. Siegel, *Polymers*, **2011**, 3, 1377-1397

xlix J.M. Lü, X. Wang, C. Marin-Muller, H. Wang, P.H. Lin, Q. Yao, C. Chen, *Expert Review of Molecular Diagnostics*, **2009**, 9, 325-341

l R.A. Jain, *Biomaterials*, **2000**, 21, 2475-2490

[li] D. Goldberg, *Journal of environmental polymer degradation*, **1995**, 3, 61-67

[lii] M. Labet, W. Thielemans, *Chemical Society Reviews,* **2009**, 38, 3484-3504

[liii] T.K. Dash, V.B. Konkimalla, *Journal of Controlled Release*, **2012**, 158, 15-33

[liv] X.H. Zong , Z.G. Wang , B.S. Hsiao, B. Chu, *Macromolecules*, **1999**, 32, 8107-8114

[lv] A.J. Lasprilla, G.A. Martinez, B.H. Lunelli, A.L. Jardini, R.M. Filho, *Biotechnology Advances,* **2012**, 30, 321-328

[lvi] K.M. Nampoothiri, N.R. Nair, R.P. John, *Bioresource Technology,* **2010**, 101, 8493-8501

[lvii] H.K. Makadia, S.J. Siegel, *Polymers,* **2011**, 3, 1377-1397

[lviii] P. Gentile, V. Chiono, I. Carmagnola, P.V. Hatton, *International Journal of Molecular Sciences,* **2014**, 15, 3640-3659

[lix] I. Bala, S. Hariharan, M.N.V. Ravi Kumar, *Journal Critical Review in Therapeutic Drug Carrier Systems*, **2004**, 21, 387-422

[lx] S. Li, *Journal of Biomedical Materials Research*, **1999**, 48, 342-353

[lxi] J.M. Williams, A. Adewunmi, R.M. Schek, C.L. Flanagan, P.H. Krebsbach, S.E. Feinberg, S.J. Hollister, S. Das, *Biomaterials*, **2005**, 26, 4817-4827

[lxii] M. Rinaudo, *Polymer International,* **2008***,* 57, 397-430

[lxiii] N.B. Shelke, R. James, C.T. Laurencin, S.G. Kumbar, *Polymers for Advanced Technologies,* **2014**, 25, 448-460

[lxiv] L. Liu, Y. Liu, J. Li, G. Du, J. Chen, *Microbial Cell Factories,* **2011**, 10, 99

[lxv] V. Sinha, R. Kumria, *International Journal of Pharmaceutics*, **2001**, 224, 19-38

[lxvi] J. Lee, J. Park, J. Robinson, *Journal of Pharmaceutical Sciences,* **2000**, 89, 850-866

[lxvii] A. Aravamudhan, D. Ramos, J. Nip, M. Harmon, R. James, M. Deng, C. Laurencin, X. Yu, S. Kumbar, *Journal of Biomedical Nanotechnology,* **2013**, 9, 719-731

[lxviii] Y. Cheng, D. Ramos, P. Lee, D. Liang, X. Yu, S.G. Kumbar, *Journal of Biomedical Nanotechnology,* **2014**, 10, 287-298

[lxix] H.R. Shao, Y. Jin, G.Y. Han, P. Jiang, X.Q. Zhu, F. Liu, Z.G. Song, M. Li, P.X. Ling, *Biorheology*, **2014**, 51, 305-314

[lxx] R.J. Moon, A. Martini, J. Nairn, J. Simonsen, J. Youngblood, *Chemical Society Reviews,* **2011**, 40, 3941-3994

[lxxi] M.N.V Ravi Kumar, *Reactive and Functional Polymers*, **2000**, 46, 1, 1-27

[lxxii] S.C. Zeeman, J. Kossmann, A.M. Smith, *Annual Review of Plant Biology*, **2010**, 61, 209-234

[lxxiii] K.Y. Lee, D.J. Mooney, *Progress in Polymer Science,* **2012**, 37, 106-126

[lxxiv] G.D. Prestwich, *Journal of Controlled Release*, **2011**, 155, 193-199

[lxxv] K.C. Cheng, A. Demirci, J.M. Catchmark, *Applied Microbiology and Biotechnology,* **2011**, 92, 29-44

[lxxvi] J. Salbach, T.D. Rachner, M. Rauner, U. Hempel, U. Anderegg, S.Franz, J.C. Simon, L.C. Hofbauer, *Journal of Molecular Medicine*, **2012**, 90, 6, 625-635

lxxvii L. Sherman, J. Sleeman, P. Herrlich, H. Ponta, *Current Opinion in Cell Biology,* **1994**, 6, 726-733

lxxviii C. Alvarez-Lorenzo, B. Blanco-Fernandez, A. Puga, A. Concheiro, *Advanced Drug Delivery Reviews,* **2013**, 65, 1148-1171

lxxix S. Verma, A.J. Domb, N. Kumar, *Nanomedicine*, **2010**, 6, 157-181

lxxx N.B. Shelke, R. Kadam, P. Tyagi, V.R. Rao, U.B. Kompella, *Drug Delivery and Translational Research,* **2011**, 1, 76-90

lxxxi C. Lin, Z. Zhong, M.C. Lok, X. Jiang, W.E. Hennink, J. Feijen, J.F.J. Engbersen, *Bioconjugate Chemistry,* **2007**, 18, 138-145

lxxxii N. Lavignac, M. Lazenby, J. Franchini, P. Ferruti, R. Duncan, *International Journal of Pharmaceutics,* **2005**, 300, 102-112

lxxxiii P.C. Griffith, A. Paul, Z. Khayat, K.W. Wan, S.M. King, I. Grillo, R. Schweins, P. Ferruti, J. Franchini, R. Duncan, *Biomacromolecules*, **2004**, 5, 1422-1427

lxxxiv S.C.W. Richardson, N.G. Pattrick, Y.K.S. Man, P. Ferruti, R. Duncan, *Biomacromolecules*, **2001**, 2, 1023-1028

lxxxv P. Ferruti, *Journal of Polymer Science Part A Polymer Chemistry*, **2013**, 51, 2319-2353

lxxxvi P. Ferruti, M.A. Marchisio, R. Barbucci, *Macromolecular Rapid Communications*, **2002**, 23, 332-355

lxxxvii P. Ferruti, C. Bertoglio Riolo, T. Soldi, M. Pesavento, *Journal of Applied Polymer Science*, **1982**, 27, 2239-2248

lxxxviii M. Pesavento, T. Soldi, P. Ferruti, R. Barbucci, M. Benvenuti, *Journal of Applied Polymer Science*, **1983**, 28, 3361-3368

lxxxix M. Pesavento, T. Soldi, P. Ferruti, R. Barbucci, M. Benvenuti, *Journal of Applied Polymer Science*, **1983**, 28, 3361-3368

xc L. Sartore, M. Penco, S. Della Sciucca, G. Borsarini, V. Ferrari, *Sensors and Actuators B: Chemical*, **2005**, 111, 160-165

xci M.K. Nguyen, D.S. Lee, *Macromolecular Research*, **2010**, 18, 284-288

xcii P. Ferruti, S. Bianchi, E. Ranucci, F. Chiellini, V. Caruso, *Macromolecular Bioscience*, **2005**, 5, 613-622

xciii P. Ferruti, S. Bianchi, E. Ranucci, F. Chiellini, A.M. Piras, *Biomacromolecules*, **2005**, 6, 2229-2235

xciv V. Magnaghi, V. Conte, P. Procacci, G. Pivato, P. Cortese, R. Cavalli, G. Pajardi, E. Ranucci, F. Fenili, A. Manfredi, P. Ferruti, *Journal of Biomedical Materials Research Part A*, **2011**, 98, 19-31

xcv R. Cavalli, A. Bisazza, R. Sessa, P. Luca, F. Fenili, A. Manfredi, E. Ranucci, P. Ferruti, *Biomacromolecules,* **2010**, 11, 2667-2674

xcvi G. Coué, J.F.J. Engbersen, *Journal of Controlled Release*, **2011**, 152, 90-98

xcvii E.H. Schacht, P. Ferruti, R. Duncan, European Community, Luxembourg, WO 9,505,200, **1995**

[xcviii] E. Ranucci, P. Ferruti, F. Fenili, A. Manfredi, N. Mauro, X. Fernandez-Busquets, P. Urban, EP12192633.1, **2012**

[xcix] P. Ferruti, F. Danusso, G. Franchi, N. Polentarutti, S. Garattini, *Journal of Medicinal Chemistry*, **1973**, 16, 496-499

[c] P. Ferruti, R. Cavalli, E. Ranucci, D. Lembo, A. Manfredi, *PCT – The International Patent System*, WO2011145056 A120111124, **2011**

[ci] P. Ferruti, E. Ranucci, F. Bignotti, L. Sartore, P. Bianciardi, M. A. Marchisio, *Journal of Biomaterials Science, Polymer Edition,* **1994**, 6, 833-844

[cii] P. Ferruti, E. Ranucci, L. Sartore, F. Bignotti, M.A. Marchisio, P. Bianciardi, F.M. Veronese, *Biomaterials*, **1994**, 15, 1235-1241

[ciii] E. Ranucci, G. Spagnoli, P. Ferruti, D. Sgouras, R. Duncan, *Journal of Biomaterials Science, Polymer Edition*, **1991**, 2, 303-315

[civ] L. Xue, H.P. Greisler, *Journal of Vascular Surgery*, **2003**, 37, 472-480

[cv] J.B. Brunsky, D.A. Puleo, A. Nanci, *The International Journal of oral and maxillofacial implants*, **2000**, 15, 15-46

[cvi] G. Balasundaram, T.J Webster, *Nanomedicine*, **2006,** 1, 169-176

[cvii] S. Ravi, E.L. Chaikof, *Summary Regenerative Medicine,* **2010**, 5, 107-120

[cviii] L. Xue, H.P. Greisler, *Journal of Vascular Surgery*, **2003**, 37, 472-480

[cix] L.M. Cross, A. Thakur, N.A. Jalili, M. Detamore, A.K. Gaharwar, *Acta Biomaterialia*, **2016**, 42, 2-17

[cx] K.L. Ong Brian M. Yun, J.B. White, *Orthopedic Research and Reviews*, **2015**, 7, 107-130

[cxi] O. Lupescu, M. Nagea, C. Patru, G. Popescu, N. Marcov, *Key Engineering Materials*, **2016**, 695, 99-105

[cxii] M. Kazemzadeh-Narbat, N. Annabi, A. Khademhosseini, *Materials Today*, **2015**, 18, 176-177

[cxiii] A. Frassetto, L. Breschi, G. Turco, G. Marchesi, R. Di Lenarda, F.R. Tay, D.H. Pashley, M. Cadenaro, *Dental Materials,* **2016**, 32, e41–e53

[cxiv] H.R. Rezaie, L. Bakhtiari, A. Öchsner, *Biomaterials and Their Applications*, Springer Briefs in Materials, **2015**

[cxv] A. Karimi, A. Othman, A.Uzunoglu, L. Stanciub, S. Andreescu, *Nanoscale*, **2015**, 7, 6909-6923

[cxvi] A.P.F. Turner, *Chemical Society Reviews*, **2013**, 42, 3184-3196

[cxvii] M. Holzinger, A. Le Goff, S. Cosnier, *Frontiers in Chemistry*, **2014**, 2, 1-10

[cxviii] T. Velnar, G. Bunc, R. Klobucar, L. Gradisnik, *Bosnian Journal of Basic Medical Sciences,* **2016**, 16, 82-90

[cxix] J. Jagur-Grodzinski, *Polymers for Advanced Technologies,* **2006**, 17, 395-418

[cxx] B.V. Slaughter, S.S. Khurshid, O.Z. Fisher, A. Khademhosseini, N.A. Peppas, *Advanced Materials*, **2009**, 21, 3307-3329

[cxxi] E. Engel, A. Michiardi, M. Navarro, D. Lacroix, J.A. Planell, *Trends in biotechnology*, **2008**, 26, 39-47

cxxii G.C. Gurtner, M.J. Callaghan, M.T. Longaker, *Progress and Potential for Regenerative Medicine*, **2007**, 58, 299-312

cxxiii M.E. Furth , A. Atala , M.E. Van Dyke, *Biomaterials*, **2007**, 28, 5068-5073

cxxiv J.E. Babensee, L.V. McIntire, A.G. Mikos, *Pharmaceutical Research*, **2000**,17, 497-504

cxxv V. Karageorgiou, D. Kaplan, *Biomaterials*, **2005**, 26, 5474-5491

cxxvi A.G. Mikos, A.J. Thorsen, L.A. Czerwonka, Y. Bao, R. Langer, D.N. Winslow, J.P. Vacanti, *Polymer,* **1994**, 35, 1069-1077

cxxvii K. Whang, C.H. Thomas, K.E. Healy, *Polymer*, **1995**, 36, 837-842

cxxviii D.J. Mooney, D.F. Baldwin, N.P. Suh, J.P. Vacanti, R. Langer, *Biomaterials*, **1996**, 17, 1417-1422

cxxix C. Schugens, V. Maquet, C. Grandfils, R. Jerome, P. Teyssie, *Polymer*, **1996**, 37, 1027-1038

cxxx S. Yang, K.F. Leong, Z. Du, C.K. Chua, *Tissue Engineering*, **2016**, 7, 679-689

cxxxi B. Dhandayuthapani, Y. Yoshida, T. Maekawa, D.S. Kumar, *International Journal of Polymer Science*, **2011**, Article ID 290602

cxxxii P.D. Dalton, T. Woodfield, D.W. Hutmacher, *Biomaterials*, **2009**, 30, 2420

cxxxiii Z. Ma, M. Kotaki, R. Inai, S. Ramakrishna, *Tissue Engineering*, **2005**, 11, 101-109

cxxxiv T.J. Sill, H.A. von Recum, *Biomaterials*, **2008**, 29, 1989-2006

cxxxv P. Berndt, G.B. Fields, M. Tirrell, *Journal of the American Chemical Society*, **1995**, 117, 9515-9522

cxxxvi R. Zhang, P.X. Ma, *Journal of Biomedical Materials Research*, **1999**, 45, 285-293

cxxxvii R.L. Dahlin, F.K. Kasper, A.G. Mikos, *Tissue Engineering Part B Reviews* **2011**, 17, 349-364

cxxxviii K.F. Leong, C.M. Cheah, C.K. Chua, *Biomaterials,* **2003**, 24, 2363-2378

cxxxix S.J. Hollister, *Nature Materials*, **2005**, 4, 518-524

cxl A.S. Hoffman, *Annals of the New York Academy of Sciences*, **2001**, 944, 62-73

cxli L.S. Ferreira, S. Gerecht, J. Fuller, H.F. Shieh, G. Vunjak-Novakovic, R. Langer, *Biomaterials*, **2007**, 28, 2706-2717

cxlii J.A. Hubbell, *Current Opinion in Biotechnology*, **1999**, 10, 123-129

cxliii K.Y. Lee, D.J. Mooney, *Chemical Reviews*, **2001**, 101, 1869-1879

cxliv J.L. Drury, D.J. Mooney, *Biomaterials*, **2003**, 24, 4337-4351

cxlv A.S. Hoffman, *Advanced Drug Delivery Reviews,* **2012**, 64, 18-23

cxlvi R. Mo, T. Jiang, J. Di, W. Taiac, Z. Gu, *Chemical Society Reviews*, **2014**, 43, 3595-3629

cxlvii S. Caban, E. Aytekin, A. Sahin, Y. Capan, *OA Drug Design and Delivery,* **2014**, 18, 2

cxlviii B.S. Pattni, V.V. Chupin, V.P. Torchilin, *Chemical Reviews*, **2015**, 115, 10938-10966

cxlix N. Anton, T.F. Vandamme, *Pharmaceutical Research*, **2011**, 28, 978-985

[cl] M.K. Sarangi, S. Padhi, *Journal of Critical Reviews*, **2016**, 3, 5-12

[cli] J.A.H. Junghanns, R.H. Müller, *International Journal of Nanomedicine*, **2008**, 3, 295-310

[clii] J. Singh, S. Desai, S. Yadav, B. Narasimhan, H. Kaur, *Current Pharmaceutical Design,* **2016**, 22, 2821-2843

[cliii] N. Kamaly, B. Yameen, J. Wu, O.C. Farokhzad, *Chemical Reviews*, **2016**, 116 2602-2663

[cliv] D.H. Shin, Y.T. Tam, G.S. Kwon, *Frontiers of Chemical Science and Engineering,* **2016**, 10, 348

[clv] K. Madaan, S. Kumar, N. Poonia, V. Lather, D. Pandita, *Journal of Pharmacy and Bioallied Sciences*, **2014**, 6, 139-150

[clvi] R.G. Tuguntaev, C.O. Ikechukwu, J. Xu, C. Li, P.C. Wang, X.J. Liang, *Current Pharmaceutical Design*, **2016**, 22, 2857-2865

[clvii] J. Panyam, V. Labhasetwar, *Advanced Drug Delivery Reviews,* **2003***, 55, 329-347

[clviii] S.V. Vinagradov, T.K. Bronich, A.V. Kabanov, *Advanced Drug Delivery Reviews,* **2002**, 54, 223-233

[clix] M.P. Desai, V. Labhasetwar, E. Walter, R.J. Levy, G.L. Amidon, *Pharmaceutical Research*, **1997**, 14, 1568-1573

[clx] M.J. Alenso, C. Losa, P. Calvo, J.L.Vila-Jato, *International Journal of Pharmaceutics,* **1991**, 68, 69–76

[clxi] M. Ueda, A. Iwara, J. Kreuter, *Journal of Microencapsulation*, **1998**, 15, 361-372

[clxii] H.S. Yoo, J.E. Oh, K.H. Lee, T.G. Park, *Pharmaceutical Research,* **1999**, 16, 1114-1118

[clxiii] Y. Chen, R.K. McCulloch, B.N. Gray, *Journal of Controlled Release*, **1994**, 31, 49-54

[clxiv] Y. Chen, V.J. Mohanraj, J.E. Parkin, *Letters in Peptide Science*, **2003**, 10, 621-627

[clxv] T. Govender, S. Stolnik, M.C. Garnett, L. Illum, S.S. Davis, *Journal of Controlled Release,* **1999**, 57, 171-185

[clxvi] T. Govender, T. Riley, T. Ehtezazi, M.C. Garnett, S. Stolnik, L. Illum, S.S. Davis, *International Journal of Pharmaceutics,* **2000**, 199, 95-110

[clxvii] J. Panyam, D. Williams, A. Dash, D. Leslie-Pelecky, V. Labhasetwar, *Journal of Pharmaceutical Sciences,* **2004**, 93, 1804-1814

[clxviii] A.L. Weiner, B.C. Gilger, *Veterinary Ophthalmology*, **2010**, 13, 395-406

[clxix] K.E. Uhrich, S.M. Cannizzaro, R.S. Langer, K.M. Shakesheff, *Chemical Reviews,* **1999**, 99, 3181-3198

[clxx] B. Magenheim, M.Y. Levy, S. Benita, *International Journal of Pharmaceutics*, **1993**, 94, 115-123

[clxxi] S. Cai, K. Vijayan, D. Cheng, E.M. Lima, D.E. Discher, *Pharmaceutical Research*, **2007**, 24, 2099-2109

[clxxii] Y. Matsumura, H. Maeda, H, *Cancer Research,* **1986**, 46, 6387-6392

INTRODUCTION TO BIOMATERIALS

[clxxiii] J. Fang, H. Nakamura, H. Maeda, *Advanced Drug Delivery Reviews*, **2011**, 63, 136-151

[clxxiv] A. Lamprecht, N. Ubrich, H. Yamamoto, U. Schafer, H Takeuchi, P. Maincent, Y. Kawashima, C.M. Lehr, *Journal of Pharmacology and Experimental Therapeutics,* **2001**, 299, 775-781

[clxxv] F. Scherer, M. Anton, U. Schillinger, J. Henke, C. Bergemann, A. Kruger, B. Gansbacher, C. Plank, *Gene Therapy*, **2002**, 9, 102-109

[clxxvi] F. Danhier, O. Feron, V. Préat, *Journal of Controlled Release,* **2010**, 148, 135-146

[clxxvii] R. Misra, S.K. Sahoo, *European Journal of Pharmaceutical Sciences*, **2010**, 39, 152-163

[clxxviii] S. Mitragotri, J. Lahann, *Nature Materials*, **2009**, 8, 15-23

[clxxix] D.S. Kohane, *Biotechnology and Bioengineering*, **2007**, 96, 203-209

[clxxx] M. Singh, A. Chakrapani, D. O'Hagan, *Expert Review of Vaccines,* **2007**, 6, 797-808

[clxxxi] M.N. Ravi Kumar*, Journal of Pharmacy and Pharmaceutical Sciences,* **2000**, 3, 234-258

[clxxxii] J. Rejman, V. Oberle, I.S. Zuhorn, D. Hoekstra, *Biochemical Journal*, **2004**, 377, 159-169

[clxxxiii] R.C. May, L.M. Machesky*, Journal of Cell Science,* **2001**, 114, 1061-1077

[clxxxiv] J.A. Champion, S. Mitragotri, *PNAS, Proceedings of the National Academy of Sciences*, **2006**, 103, 4930-4934

[clxxxv] F.J. O'Brien, *Materials Today*, **2011**, 14, 88-95

[clxxxvi] M.F. Ashby, *The CES EduPack Database of Natural and Man-Made Materials,* Cambridge University and Granta Design, Cambridge, UK, **2008**

[clxxxvii] T.P.J. Knowles, M.J. Buehler, *Nature Nanotechnology*, **2011**, 6, 469-479

[clxxxviii] K. Metavarayuth, P. Sitasuwan, X. Zhao, Y. Lin, Q. Wang, *Biomaterials Science and Engineering*, **2016**, 2, 142-151

[clxxxix] T. Yeung, P.C. Georges, L.A. Flanagan, B. Marg, M. Ortiz, M. Funaki, N. Zahir, W. Ming, V. Weaver, P.A. Janmey, *Cell Motility and the Cytoskeleton*, **2005**, 60, 24-34

[cxc] A.J. Engler, S. Sen, H.L. Sweeney, D.E. Discher, *Cell*, **2006,** 126, 677–689

[cxci] R. Vasita, I.K. Shanmugam, D.S. Katt, *Current Topics in Medicinal Chemistry,* **2008**, 8, 341-353

[cxcii] V. PeŠŠková, D. Kubies, H. Hulejová, L. Himmlová, *Journal of Materials Science: Materials in Medicine,* **2007**, 18, 465-473

[cxciii] P.B. van Wachem, T. Beugeling, J. Feijen, A. Bantjes, J.P. Detmers, W.G. van Aken, *Biomaterials*, **1985**, 6, 403-408

[cxciv] M.L. Carman, T.G. Estes, A.W. Feinberg, J.F. Schumacher, W. Wilkerson, L.H. Wilson, M.E. Callow, J.A. Callow, A.B. Brennan, *Biofouling: The Journal of Bioadhesion and Biofilm Research*, **2006**, 22, 11-21

[cxcv] K. Webb, V. Hlady, P.A. Tresco, *Journal of Biomedical Materials Research*, **1998**, 41, 422-430

[cxcvi] D.P. Dowling, I.S. Miller, M. Ardhaoui, W.M. Gallagher, *Journal of Biomaterials Applications*, **2011**, 26, 327-347

[cxcvii] J.A. Finlay, M.E. Callow, L.K. Ista, G.P. Lopez, J.A. Callow, *Integrative and Comparative Biology,* **2002**, 42, 1116-1122

[cxcviii] P.Y. Chung, Y.S. Toh, *Pathogens and Disease,* **2014**, 70, 231-239

[cxcix] A. Roosjen, W. Norde, H. C. van der Mei, H. J. Busscher, *Progress in Colloid and Polymer Science*, **2006**, 132, 138-144

"The purpose of this research is to establish the synthetic procedures to obtain a new family of amphiphilic biodegradable and bioeliminable biomaterials for the construction of drug nanocarriers, core-shell nanofibres for tissue regeneration. These new biomaterials are based on PLGA-g-PVP copolymers, where PLGA forms a linear backbone on which short arms of PVP are randomly distributed. PLGA-g-PVP copolymers were synthesised by the one-step one-pot radical polymerization of 1-vinylpyrrolidin-2-one (VP) in molten PLGA that acted as chain transfer agent. Modulating the initial VP/PLGA ratio different grafting degrees of PVP chains having different molecular weights were obtained. Saponification of PLGA-g-PVP gave, besides PLGA degradation products, also un-degraded PVP. This was isolated and analysed by size exclusion chromatography (SEC), to evaluate the molecular weights of grafted PVP. MALDI-TOF analysis allowed identifying the chemical structure of PVP terminals and unambiguously establishing that PVP chains were originally grafted onto PLGA backbone. PLGA-g-PVP spontaneously formed nanoparticles when dispersed in water, irrespective of PVP content.

2.1 POLY(LACTIC-CO-GLYCOLIC) ACID

In the last twenty years aliphatic polyester-based polymeric structures[i,ii,iii] have been receiving special attention because they are sensitive to hydrolytic degradation and their physical and mechanical properties can be tailor-made by tuning the chemical structure of the repeating unit. Among polyesters, the most extensively studied one in the biomedical field is the copolymer poly(lactic-co-glycolic) acid (PLGA). Different copolymers have been commercially developed and are usually identified in regard to the monomer ratio (for instance PLGA 75:25 identifies a copolymer containing 75% lactic acid and 25% glycolic acid).

SYNTHESIS AND CHARACTERIZATION OF PLGA-g-PVP COPOLYMERS

Two general reaction mechanisms are used to synthesize PLGA and all other poly (α-hydroxyesters): condensation polymerization and ring opening polymerization. The condensation of hydroxyl-acids monomers or mixtures of diacids and diols is usually conducted at high temperatures for long reaction times, usually leading limited molecular weight chains of few tens of thousands ($\overline{M}_n$ 30 kDa) and often subjected to side reactions, such as racemization.[iv]

High-molecular weight aliphatic polyesters can be prepared by ring opening polymerization (ROP) (in melt or in solution, emulsion or dispersion) of lactones of different ring-size, with or without (protected) functional groups. Reactions are carried out in presence of a catalyst or a initiator. Depending on the initiator, the polymerization proceeds according to three different major reaction mechanisms, i.e. cationic, anionic or coordination-insertion mechanisms.[v]

PLGA's properties depend on lactic/glycolic acids monomer ratio. For instance, PLGA 75:25 is amorphous, PLGA 80:20 semi-crystalline. The degree of crystallinity and melting point of PLGA copolymers are also related to their molecular weight. In addition, unlike poly(lactic) acid and poly(glycolic) acid homopolymers, PLGAs are soluble in wide range of solvents including chlorinated solvents, tetrahydofuran, acetone and ethyl acetate.[ii]

PLGAs degrade by hydrolysis of its ester linkages, through bulk erosion, in aqueous environments. Lactic acid rich PLGAs are more hydrophobic than glycolic acid reach ones and absorb lower amounts of water and degrade more slowly, also due to the superior steric hindrance effect. As a rule, higher glycolic acid contents lead to faster degradation rates with the exception of PLGA 50:50, which exhibits the fastest degradation, due to a less crystallinity present in the copolymer.[vi]

PLGA is approved by Food and Drug Administration and is mainly proposed as component of drug delivery systems,[vii,viii] as scaffold for tissue engineering[ix, x] and as structural material for hard tissue reparation.[xi] PLGA has been used for preparing nano- or microsized particles as carriers of hydrophobic drugs, but also DNA, RNA, vitamins, and proteins, in different parts of the body and for different applications.[xii]

SYNTHESIS AND CHARACTERIZATION OF PLGA-g-PVP COPOLYMERS

As already described in Chapter 1 Paragraph 1.4.3, hydrophobic nanoparticles. are cleared by phagocytes from the circulation, PLGA nanoparticles exhibit the same behaviour. They are usually be taken up by the liver, followed by the spleen and lungs.[xiii] Coating strategies with hydrophilic polymers and amphiphilic copolymers are extensively present in literature. In particular the synthesis of linear PEG-PLGA[xiv] di-block and PEG-PLGA-PEG[xv] tri-block copolymers have been widely used in drug delivery. In both kinds of copolymers PEG is oriented to the external aqueous phase, instead PLGA is in the internal part of a micelle. PEG layer acts as a barrier and do not allow the interactions with foreign molecules by steric and hydrated repulsion, resulting in an enhanced shelf stability.[xvi]. Faster release kinetics from formulations of di-block copolymers have been observed in comparison to PLGA alone. Various mechanisms of targeted delivery of drugs from di-block PEG-PLGA-nanoparticles have also been reported[xvii] [xviii] [xix]

Despite of abundance of studies that demonstrate the positive effects of PEG on biocompatibility of hydrophobic nanoparticles, PEG leads to some adverse reactions. Indeed PEG induced blood clotting and clumping of cells, leading to embolism.[xx] It is also reported to activate complement (C),[xxi] leading to hypersensitivity reactions and ultimately to anaphylactic shock.[xxii,xxiii,xxiv] Pegylated surfaces exhibited also the accelerated blood clearance (ABC) phenomenon.[xxv] Monomethyl-PEG liposome concentration in rats was drastically decreased after a second injection performed after 4h the first injected dose (from 52.6% to 0.6% after the second injection).[xxvi] ABC phenomenon also occurred when the second injection was administered after five days.[xxvii] These results indicated that a recurring injection of Pegylated liposomes can alter the circulation time, affecting bioavailability of the drug. Also passive targeting is decreased, in fact the second dose was shown to preferentially accumulate in Kupffer cells of the liver, due to the action of immunological system. In liver accumulation could cause severe liver damage, particularly in the case of highly toxic therapeutics.

A study on the ABC phenomenon induced by different hydrophilic coating on PLA nanoparticles showed that ABC phenomenon was not induced upon repeated injection of PVP-coated nanoparticles at various time intervals,

dosages, or frequencies, whereas it was elicited by PEG-coated nanoparticles (Figure 2.1).[xxviii]
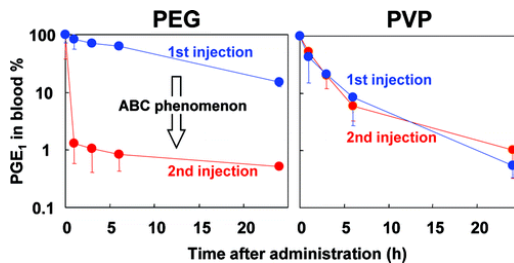
Figure 2.1. Induction of the ABC phenomenon upon injections of prostaglandin (PGE$_1$)-loaded PEG/PLA NPs and PVP/PLA-NPs. A) PEG/PLA NPs: blue line, first dose; red line second dose administered 7 d after the first injection. B) PVP/PLA NPs: blue line, first dose; red line second dose administered 7 d after the first injection

2.2 POLY(VINYLPYRROLIDONE)

Poly(vinylpyrrolidone) (PVP) have been used in this work to modulate the hydrophobicity of PLGA.

PVP was first reported in 1938 by Reppe.[xxix] PVP has excellent physiological compatibility, low chemical toxicity, and good solubility in water and most organic solvents.[xxx] PVP forms complexes with numerous low molecular weight compounds as well as with many polymers, acting as solubilizer.[xxxi,xxxii] It has adhesion properties of pharmaceutical materials,[xxxiii] and in general it is used as glue on glass, metal and plastics, paper, fabric surface and as pressure-sensitive adhesive.[xxxiv] It is not biodegradable and for this reason the parenteral administration of high molecular weight PVP is not practiced. Only PVP chains, able to be eliminated by renal clearance, can be used. In particular PVP having molecular weights below 30 000, has diameter below 7 nm, the same of capillaries of human kidney, and is able to pass through the kidney and to be excreted.[xxxv] In low molecular weight form is widely used in many industries such as pharmaceuticals, cosmetics, beverages, adhesives, detergents, paints, electronics, and biological engineering materials. [xxxvi,xxxvii,xxxviii,xxxix]

SYNTHESIS AND CHARACTERIZATION OF PLGA-g-PVP COPOLYMERS

PVP having molecular weights from 2500 to about 1 million is mainly obtained by radical polymerization of 1-vinyl-2-pirrolidone (VP) in aqueous solution. Obtained polymers have hydroxyl and carbonyl end groups. More stable end groups can be obtained by polymerization in solvents, which may act as chain transfer agents and which produce low molecular weight products.[xl] Different techniques allow synthesizing PVP in a controlled manner, tuning precisely number-average molar mass, dispersity, end-groups, and architecture. Organo-cobalt-mediated radical polymerization (OCMRP)[xli], organo-heteroatom-mediated radical polymerization (OHMRP)[xlii], reversible addition–fragmentation chain transfer polymerization using xanthates (RAFT/MADIX)[xliii], and atom transfer radical polymerization (ATRP)[xliv] allowed controlled radical polymerization of VP.

2.3 PVP-POLYESTERS COPOLYMERS AND BLENDS

PVP was bonded to other polyesters by different reaction mechanisms. Linear PVP block copolymers with polyesters such as poly-ε-caprolactone (PCL) or PLA have been extensively reported.[xlv,xlvi,xlvii,xlviii,xlix,l,li,lii,liii] Most of these copolymers were prepared by ROP of ε-caprolactone or lactides with end-hydroxylated PVP oligomers, which are obtained by conventional radical polymerization of N-VP in the presence of hydroxylated compounds, as for instance 2-isopropoxyethanol(Figure 2.2-A).[liv] Vice-versa, starting from end-functionalized PCL and PLA oligomers that were respectively employed as ATRP or RAFT macroinitiators for PVP polymerization (Figure 2.2-B). PLA-b-PVP copolymers were also synthesised by polymerization of N-VP in the presence of mercapto-terminated PLA (Figure 2.2-C).[lv] Surface-grafted PVP chains onto PLLA films were obtained by physical methods[lvi]or by radical copolymerization of NVP with ω-methacryloxy-PLLA.[lvii]

Nevertheless the ability to obtain well-tuned copolymers, reactions listed above have a number of flaws that limit their use, in particular in industrial field. The use of very complex and expensive macroinitiators, requiring very long synthetic procedures, at least of 3,4 steps, with a reduction of the final yield, and the use of heavy metal derivates, really difficult to isolate and expensive to dispose of, are some examples on this issue.

SYNTHESIS AND CHARACTERIZATION OF PLGA-g-PVP COPOLYMERS
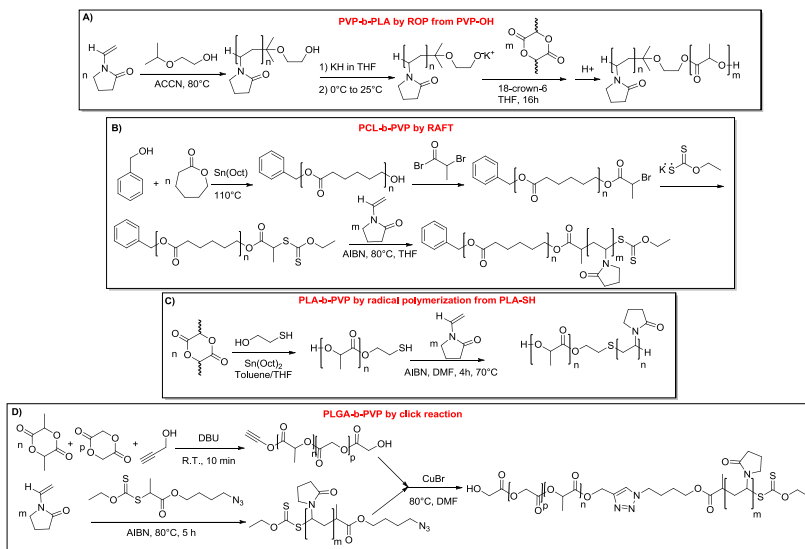
Figure 2.2. A) Synthesis of PVP-b-PLA by ring opening polymerization stating from hydroxylate- terminated PVP, obtained by radical polimerization of N-VP in the presence of 2-isopropoxyethanol, followed by KH treatment; B) Synthesis of PCL-b-PVP by RAFT polymerization starting from a PLA macroinitiator; C) Synthesis of PLA-b-PVP by radical polimerization of N-VP in presence of mercapto-terminated PLA; D)PLGA-b-PVP synthesis by click reaction between azide-terminated PVP and alkyne-terminated PLGA.

In literature one example of linear di-block PLGA-b-PVP copolymer was reported, obtained by click reaction between alkyne-terminated PLGA and azide-terminated PVP (Figure 2.2- D).[lviii] Synthetic procedure consisted in three steps, one of which use a metallic compound as catalyst, and each step needed purification of product from the initial monomers and by-products, using a great amount of solvents. As result a really expensive process is obtained with the unlikelihood of easy industrial scale-up.

Several examples of blends (PLGA/PVP) are also reported to form fibres and particles. PLGA/PVP fibres were prepared by coaxial electrospinning of PLGA and PVP.[lix] PLGA/PVP microparticles and nanoparticles were formed when

SYNTHESIS AND CHARACTERIZATION OF PLGA-g-PVP COPOLYMERS

PVP acts as surfactant of PLGA particles[lx] or by spray-dried.[lxi] These systems, providing the only physical interaction, have a narrow stability over time, due to separation of the two blocks in aqueous matrix.

Previous researches conducted by this group have discussed on ester-terminated PVP oligomers prepared by radical polymerization of N-VP in the presence of aliphatic esters, acting in the meantime as solvents and chain transfer agents.[lxii,lxiii,lxiv,lxv,lxvi,lxvii,lxviii,lxix]

The purpose of this thesis research is to use, not aliphatic ester molecules, but polymeric esters, as instance PLGA, as chain transfer agents. By using of initiator, radicals are generated in α to the ester function on the PLGA main backbone, and consequently, VP monomers are radically polymerized on. This provides a simple and direct one-step synthesis of PLGA-g-PVP comb like copolymers.[lxx] PVP side chain molecular weight can be modulated modulating the initial ratio of monomer and chain transfer agents. The great benefit of this procedure is the easy scale up of the synthesis, thank you the absence of solvents and of really expensive reagents and the quantitative yield of product, that make useless any further purification steps. The aim of this research is to report on this issue, with a focusing on properties and application in drug delivery and tissue engineering.

2.4 EXPERIMENTAL PART

2.4.1 Materials

1-Vinylpyrrolidin-2-one (VP) (99%, Sigma Aldrich) was purified by vacuum distillation (bp100 °C/15 tor) just before use. 2,2'-Azobis(2-methylpropionitrile) (AIBN) (98%, Sigma Aldrich) was recrystallized from methanol just before use. Ester-terminated poly(lactic-co-glycolic) acid (PLGA) 50:50 $\overline{M}_n$ = 45000-55000 was purchased from PolySciTech (Indiana, USA) and used as received. NMR analysis showed that the lactide/glycolide ratio was actually 52:48, meaning that the average molecular weight of the repeating units was 65:35. Poly(1-vinylpyrrolidin-2-one) (PVPK40, $\overline{M}_w$ = 40000), anhydrous N,N-dimethylformamide (DMF, 99.9%) (obtained in sealed glass bottles over molecular sieves), diethyl ether, chloroform, deuterium oxide (D$_2$O, 99.9 atom D%), hydrochloric acid (HCl, 37% w/w), sodium hydroxide (NaOH, 98.5%),

SYNTHESIS AND CHARACTERIZATION OF PLGA-g-PVP COPOLYMERS

dithranol MALDI-MS >98%, dichloromethane (99.9%) CHROMASOLV Plus and methanol (99.9 %) CHROMASOLV Plus were purchased from Sigma Aldrich and used as received.

2.4.2 Instruments and methods

^{1}H and ^{13}C NMR spectra and 2D Heteronuclear Single-Quantum Correlation (HSQC) experiments were run at 25 °C on a Brüker Avance 400 spectrometer operating at 400.132 and 100.623 MHz, respectively.

Size exclusion chromatography (SEC) traces of PVP samples were obtained using a Knauer Pump 1000 equipped with a Knauer Autosampler 3800, TKS gel G4000 PW and G3000 PW Toso Haas columns connected in series, light scattering/viscometer Viscotek 270 Dual Detector and refractive-index detector Waters 2410. The combination of these detectors gave a triple low-angle light scattering, right-angle light scattering and refractive index detector. The mobile phase was a 0.1 M Tris buffer pH = 8.1 ± 0.05 with 0.2 M sodium chloride. The sample concentration was 2% (w/v) and the flow rate 1 mL min^{-1}.

IR spectra were obtained with an FT-IR 4100 Jasco spectrometer on films cast from dichloromethane solutions onto KBr plates.

MALDI-TOF mass analyses were obtained with a MALDI TOF-TOF AUTOFLEX III Brüker Daltonics instrument on samples prepared as follows: a 10 mg mL^{-1} dithranol chloroform solution (20 mL) was mixed with a 7 mg mL^{-1} chloroform solution (20 mL) of the polymer sample. Aliquots of the final solution (20 µL) were cast onto stainless steel targets and dried.

Differential scanning calorimetric (DSC) analyses were carried out with a Mettler Toledo DSC823 (Mettler Toledo, Italy) equipped with the STAR Software and the FRS5 Mettler Toledo ceramic sensor. The instrument was calibrated with indium for melting point and heat of fusion. Tests were performed using standard aluminium pans with an empty pan as reference. Samples (5-10 mg) underwent a four-step thermal cycle: a) heating from 0 °C to 100 °C at 10 °C min^{-1}; b) 10 min isocratic step at 100 °C; c) cooling from 100 °C to 0 °C at 10 °C min^{-1}; d) heating from 0 °C to 250 °C at 10 °C min^{-1}. All tests were carried under 20 mL min^{-1} nitrogen flow.

SYNTHESIS AND CHARACTERIZATION OF PLGA-g-PVP COPOLYMERS

TGA analyses were performed with a Perkin Elmer TGA 4000 on 10 mg samples in the range $30 - 600\ °C$, with $30\ °C\ min^{-1}$ heating rate and under 50 mL min^{-1} nitrogen flow.

Dynamic light scattering (DLS) and ζ-potential analyses were carried out using a Malvern NanoZS instrument (Malvern Instruments, Worcestershire UK) with a laser fitted at 532 nm and fixed 173° scattering angle.

2.4.3 Synthetic procedures

2.4.3.1 Synthesis of PLGA-g-PVP$_{10:1}$

PLGA (2.012 g) and VP (0.203 g, 1.83 mol) were added to dichloromethane (30 mL) in a two-necked 100 mL flask equipped with a stir bar. The resultant solution was purged 5 min with nitrogen and AIBN (2.1 mg, 0.013 mmol) was added. Dichloromethane was then eliminated at room temperature and 0.2 tor. After three nitrogen-vacuum cycles, the reaction mixture was heated to 100 °C, maintained at this temperature under nitrogen for 2.5 h, cooled to room temperature and dissolved in dichloromethane (100 mL). The solution was poured drop-wise in diethyl ether (1 L) under vigorous stirring and the resultant slurry stirred for further 2 h. The precipitated product was finally retrieved by filtration, washed with fresh ether (200 mL) and dried under vacuum. Yield: 96.4%. This product was identified as the "main product" (MP), according to the fractionation scheme (Fig. 13) reported below in "Results and discussion". The mother liquors were evaporated to dryness *in vacuo* and the small residue, identified as "unidentified by-products and impurities" (UBPI), analyzed by FT-IR and NMR. It contained a little residual VP, lactic acid, glycolic acid and some residual tin catalyst present in the starting PLGA.

PLGA-g-PVP$_{10:2}$ and PLGA-g-PVP$_{10:3}$ were prepared by the same procedure. The amounts of PLGA, VP and AIBN used were 2.013 g, 0.408 g, 4.2 mg and 2.016 g, 0.6134 g, 6.1 mg, respectively. Yield: 93.0% for PLGA-g-PVP$_{10:2}$ and 95.2% for PLGA-g-PVP$_{10:3}$.

2.4.3.2 Saponification of PLGA-g-PVP MP samples (typical procedure)

SYNTHESIS AND CHARACTERIZATION OF PLGA-g-PVP COPOLYMERS

PLGA-g-PVP$_{10:1}$ (0.999 g) was suspended in a 1 M NaOH solution (22 mL) and stirred 30 days at room temperature. The polymer gradually dissolved. The resultant solution was neutralized with 1 M HCl solution and then ultrafiltered through a membrane with nominal molecular weight cut-off 500. The retained fraction was freeze-dried giving PVP as a yellowish solid. Yield: 0.093 g; $\overline{M}_n$ = 2700, $\overline{M}_w$ = 5600, PD = 2.07. PLGA-g-PVP$_{10:2}$ and PLGA-g-PVP$_{10:3}$ were similarly treated yielding 0.176 g and 0.234 g PVP of $\overline{M}_n$ = 12100, $\overline{M}_w$ = 31000, PD 2.56 and $\overline{M}_n$ = 28000, $\overline{M}_w$ = 49500, PD 1.77, respectively.

2.4.3.3 Fractionation of PLGA-g-PVP (MP samples)

PLGA-*g*-PVP (2 g) was dissolved in dichloromethane (20 mL) and added drop-wise to a stirred 1:1 methanol/water mixture (200 mL). The resultant white suspension was centrifuged at 7500 rpm for 20 min and the insoluble fraction (F2) retrieved, re-suspended in the same solvent mixture (10 mL), centrifuged and retrieved again, and finally dried to constant weight at 0.2 tor. The soluble fraction (F1) was filtered through a 0.2 µm HPLC filter, the solvent evaporated and the residue dried as above. Two equal aliquots of F2 fraction were extracted with methanol (50 mL) and ethyl acetate (50 mL), respectively. The obtained suspensions were vigorously stirred for 2 h and then centrifuged at 7500 rpm for 30 min. The insoluble fractions (F4 and F6, respectively) were retrieved, extracted with fresh solvent (25 mL) and dried to constant weight. The methanol and ethyl acetate phases (F3 and F5, respectively) were separately evaporated to dryness and the resultant solids retrieved.

2.4.3.4 Preparation and fractionation of PLGA/PVPK40 blends

Measured volumes of chloroform PLGA and PVP solutions containing 0.2 g polymer in 6 mL solvent were mixed and poured in 50 volumes diethyl ether. After drying to constant weight, the precipitate was extracted either with ethyl acetate or methanol, leaving an insoluble portion that, in turn, was completely soluble either in methanol or in ethyl acetate, respectively.

SYNTHESIS AND CHARACTERIZATION OF PLGA-g-PVP COPOLYMERS

2.4.3.5 Synthesis of low molecular weight PVP in DMF solution (PVP$_{DMF}$)

A 500 mL two-necked flask, equipped with a stir bar and a thermometer, was charged with VP (5.713 g, 0.052 mol) and DMF (136.78 g, 1.871 mol). The solution was purged with nitrogen for 5 min at 75 °C, then AIBN (57.1 mg) was added and the reaction mixture allowed reacting for 2 days. After cooling to room temperature, the mixture was added drop-wise to diethyl ether (1 L) under vigorous stirring and left under stirring for 2 h. The reaction product was recovered by filtration, extracted overnight with fresh ether (150 mL) and dried to constant weight at room temperature and 0.2 tor. Yield: 5.35 g. $\bar{M}_n$ = 4500, $\bar{M}_w$ = 7300, PD = 1.62.

2.4.3.6 Preparation of PLGA/PVP blends (PLGA/PVP$_{DMF}$ 10:1)

PLGA (1.016 g) and PVP$_{DMF}$ (0.103 g) were dissolved in dichloromethane (2 mL), precipitated in diethyl ether (30 mL), centrifuged 5 min at 7500 rpm, the supernatant discarded, the precipitate extracted with a fresh portion of diethyl ether, centrifuged again, retrieved and dried to constant weight under vacuum. PLGA/PVP$_{DMF}$ 10:2 and 10:3 w/w blends were prepared following the same procedure and the amounts of PLGA and PVP$_{DMF}$ were 1.020 g and 0.200 g, 1.103 g and 0.334 g, respectively.

2.4.3.7 Fractionation of PLGA/PVP$_{DMF}$ blends

PLGA/PVP$_{DMF}$ blends (0.12 g) were dissolved in dichloromethane (2 mL) and precipitated in a 1:1 methanol/water mixture (30 mL), obtaining white suspensions that were centrifuged 10 min at 7500 rpm. The insoluble portion was extracted with the same methanol/water mixture, centrifuged again, retrieved and dried to constant weight at 0.2 tor. The remaining solutions were filtered through a 0.2 μm HPLC filter, evaporated to dryness in vacuo and the residues brought to constant weight at 0.2 tor.

2.4.3.8 Synthesis of PVP in water

In a round bottom flask VP (3.000 g, 0.027 mol) was dissolved in water (10 mL). The solution was purged 3 min with nitrogen, then AIBN (20.0 mg, 0.122 mmol) was added. The solution was then immersed in an oil bath pre-heated to 100 °C

SYNTHESIS AND CHARACTERIZATION OF PLGA-g-PVP COPOLYMERS

and allowed to polymerize 2 h. The product was finally recovered by liophilization: $\bar{M}_n$ =128200, $\bar{M}_w$ =197000, PD 1.54.

2.4.3.9 Determination of the IR calibration curve relevant to the ester/amide C=O stretching

The FT-IR spectra of PLGA/PVP blends with compositions ranging from 9:1 to 0.5:1 w/w were obtained by casting onto KBr plates 300 μL aliquots of mixed PLGA/PVP dichloromethane solutions prepared by dissolving the relevant amounts of PLGA50:50 and PVPK40 in 4 mL solvent (Table 1). These spectra were analyzed in the absorption mode, and the areas of the C=O$_{PLGA}$ and C=O$_{PVP}$ bands, centered at 1760 cm^{-1} and 1660 cm^{-1} respectively, obtained using the valley-to-valley method to determine the peak baselines. (Figure 2-A). All band area measurements were performed in triplicate on spectra obtained from at least two distinct PLGA/PVP films. The calibration curve (Figure 2-B) was obtained by plotting the PLGA/PVP weight ratio against the corresponding C=O$_{PLGA}$/C=O$_{PVP}$ band area ratio.

2.4.3.10 PLGA-g-PVP-based aqueous nanodispersions

All fractions of PLGA-g-PVP copolymer were tested to form nanoparticles in water, without using of stabilizers or surfactants. In details, 3 mg of each fractions were dissolved in acetone (1% w/v) and diluted with 10 volumes of water. Later, acetone was removed by flashing for 30 min at room temperature. Obtained nanodispersions (NDS) were stored at room temperature (about 22°C) or 4°C.

The same procedure was followed with native PLGA, 10:1, 10:2 and 10:3 w/w native PLGA/PVP$_{DMF}$ blends, and 8:2 w/w PLGA/PLGA-g-PVP$_{10:1}$, PLGA-g-PVP$_{10:2}$ and PLGA-g-PVP$_{10:3}$ blends. Particle size, ζ-potential, stability on time (1h, 24h, 7d) and re-dispersion in water after lyophylization of the resultant NDS were assessed.

2.5 RESULTS AND DISCUSSIONS

2.5.1 Synthesis

End-functionalized PVP oligomers were previously prepared by radical polymerization of VP in presence of aliphatic esters acting as both solvents and chain transfer agents. In the present study, it was found that running the reaction at 100 °C and substituting PLGA for the esters provided a one-step procedure to PLGA-*g*-PVP copolymers. At that temperature, the reaction mixture was in the fluid state. The reaction scheme is reported in Figure 2.3. Three batches were performed with 10:1, 10:2 and 10:3 w/w PLGA/VP ratios and 1% w/w (based on VP) AIBN as initiator. As the AIBN decomposition rate at 100 °C is $kd=$ 1.5 x 10-3 s-1, with less than 10 min half-life, the reaction was considered completed within 2.5 hours. All reaction mixtures were homogeneous, highly viscous liquids that solidified on cooling. After cooling, they were dissolved in dichloromethane and re-precipitated with ether for eliminating residual VP. No dichloromethane-insoluble fractions were noticed, indicating absence of cross-linked byproducts.
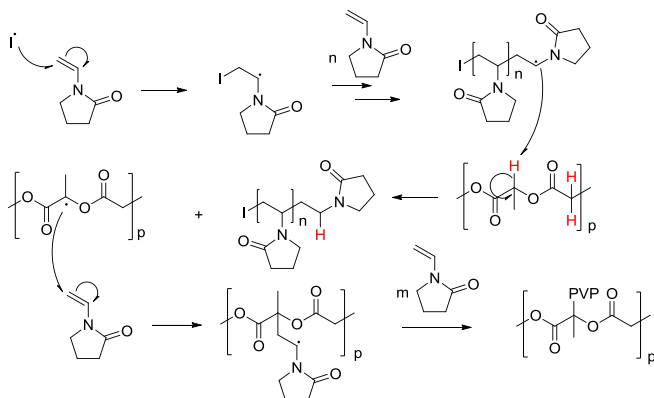
Figure 2.3. Synthesis of PLGA-g-PVP copolymers by radical polymerization of NVP in molten PLGA.

Evaporating to dryness the mother liquors and drying the residue at room temperature and 0.1 tor yielded small amounts of unidentified by-products and impurities (UBPI) that were no further processed.

SYNTHESIS AND CHARACTERIZATION OF PLGA-g-PVP COPOLYMERS

The precipitate main products, henceforth collectively named PLGA-*g*-PVP MP or individually PLGA-*g*-PVP$_{10:1}$, PLGA-*g*-PVP$_{10:2}$ and PLGA-*g*-PVP$_{10:3}$, were extracted several times with ether and dried to constant weight at room temperature and 0.1 tor. Their FT-IR spectra, reported in Figure 2.4, clearly showed both ester and amide C=O bands. The composition of all PLGA-*g*-PVP samples were determined after these band ratio using a calibration curve obtained from PLGA/PVP blends of known composition as reported in Table 2.1 and Figures 2.5 (A and B). The found values for PLGA-*g*-PVP$_{10:1}$, PLGA-*g*-PVP$_{10:2}$ and PLGA-*g*-PVP$_{10:3}$ expressed as PVP wt % were, respectively, 6.7, 18.8 and 23.5.

The ^{1}H and ^{13}C NMR spectra of the MP samples were consistent with the presence of both PLGA and PVP portions. The NMR spectra of PLGA-*g*-PVP$_{10:3}$ MP samples are shown in Figure 2.6.
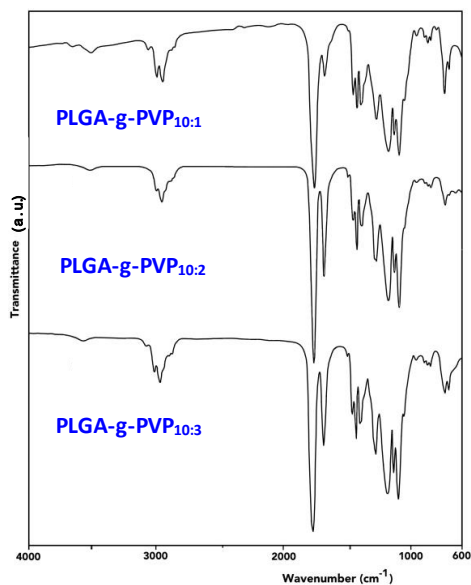
Figure 2.4. Infrared spectra of PLGA-g-PVP MP samples.

SYNTHESIS AND CHARACTERIZATION OF PLGA-g-PVP COPOLYMERS

Table 2.1. PLGA50:50/PVPK40 blends for IR calibration.

PLGA50:50 (mg)	PVPK40 (mg)	PLGA/PVP (w/w)	$C=O_{PLGA}/C=O_{PVP}$ band area ratio
22.0	44.0	0.50	0.54
36.6	41.1	0.89	1.07
46.6	20.0	2.33	2.38
82.0	22.0	3.73	3.74
100.0	19.8	5.05	5.10
140.0	21.0	6.67	6.87
154.4	18.0	8.33	8.65
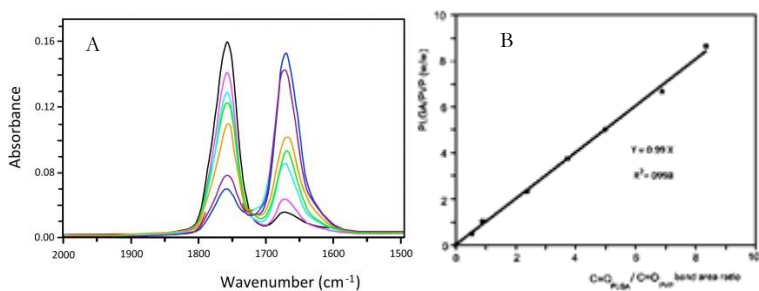
Figure 2.5. A) FT-IR spectra of PLGA/PVP blends with different w/w ratios in the 2000 - 1500 cm^{-1} range.(--) PLGA/PVP 0.50; (--) PLGA/PVP 0.89;(--) PLGA/PVP 2.33;(--) PLGA/PVP 3.73; (--) PLGA/PVP 5.05; (--) PLGA/PVP 6.67; (--) PLGA/PVP 8.33. **B)** FT-IR calibration curve.

SYNTHESIS AND CHARACTERIZATION OF PLGA-g-PVP COPOLYMERS
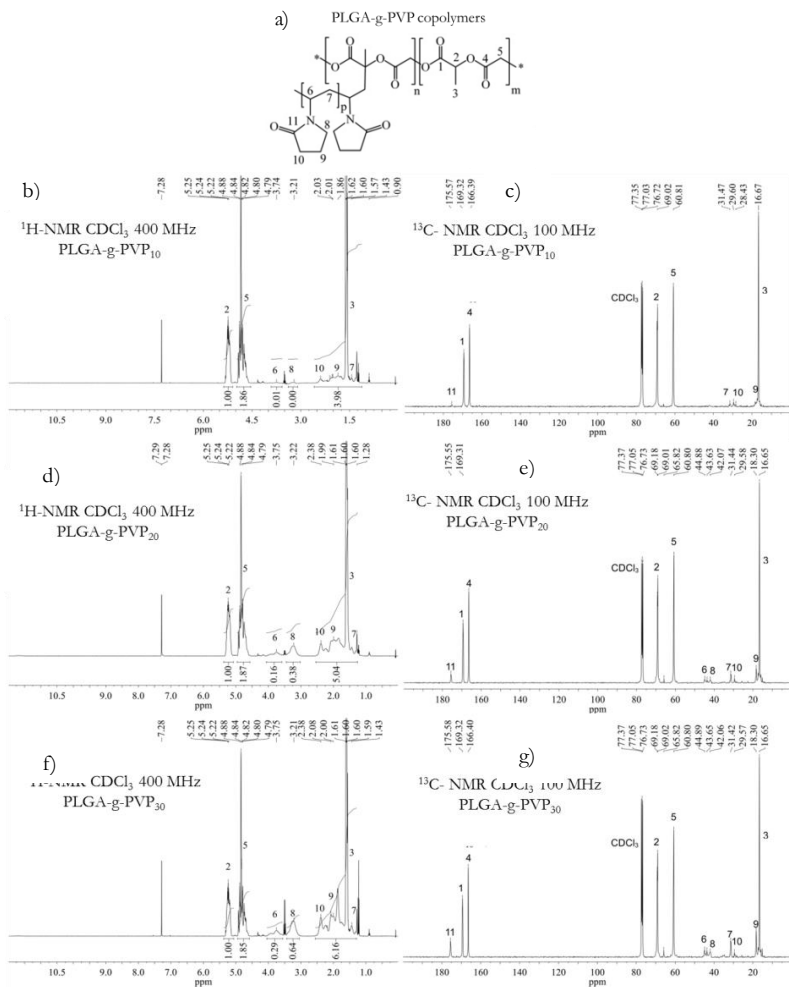
Figure 2.6. (a)PLGA-g-PVP copolymer's structure and assessments.(b) ^{1}H-NMR and (c) ^{13}C-NMR spectra of PLGA-g-PVP$_{10:1}$in CDCl$_3$. (d) ^{1}H-NMR and (e) ^{13}C-NMR spectra of PLGA-g-PVP$_{10:2}$in CDCl$_3$. (f) ^{1}H-NMR and (g) ^{13}C-NMR spectra of PLGA-g-PVP$_{10:3}$in CDCl$_3$.

SYNTHESIS AND CHARACTERIZATION OF PLGA-g-PVP COPOLYMERS

2.5.2 Thermal analysis

The DSC thermograms of PLGA-g-PVP$_{10:1}$, PLGA-g-PVP$_{10:2}$ and PLGA-g-PVP$_{10:3}$ MP samples were compared with those of virgin PLGA and PVPK40 (Figures 2.7a and 2.7b, respectively). The glass transition temperatures, Tg, of the PLGA and PVP portions of PLGA-g-PVP MP and of virgin PLGA and PVP are reported in Table 2.2. It may be noticed that the Tg of the PLGA portion was higher than that of virgin PLGA and steadily increased with the PVP content following the same trend of PLGA/PVP mixtures, as previously observed and attributed to partial phase miscibility of the two components.[lxxi]
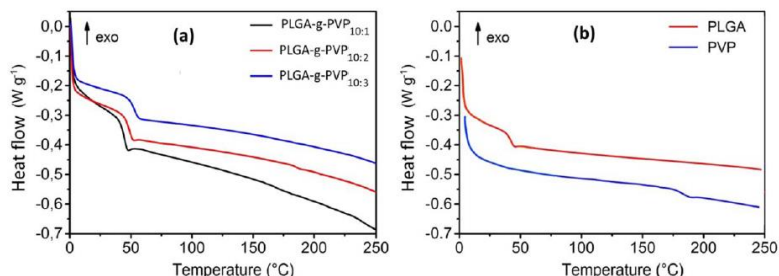
Figure 2.7. (a) DSC traces of PLGA-g-PVP MP samples and (b) of PLGA 50:50 and PVPK40. Second heating cycle, heating rate: 10 °C min^{-1}.

The Tg of the PVP portions were hardly detectable in the spectra of PLGA-g-PVP$_{10:1}$ and PLGA-g-PVP$_{10:3}$, whereas the spectrum of PLGA-g-PVP$_{10:2}$ showed a barely detectable inflection roughly corresponding to the Tg of pure PVPK40. The TGA thermograms of PLGA-g-PVP$_{10:1}$, PLGA-g- PVP$_{10:2}$ and PLGA-g-PVP$_{10:3}$ (MP samples) are reported in Figure 2.8. All thermograms showed two distinct zones, ascribed to the degradation of the PLGA and PVP portions, with a decomposition temperatures at 5% weight loss of 308 °C and 387 °C, respectively, in line with the values normally reported for the virgin polymers.[lxxii][lxxiii]

Passing from PLGA-g-PVP$_{10:1}$ to PLGA-g-PVP$_{10:2}$ and PLGA-g-PVP$_{10:3}$ the thermograms showed the expected increase of the PVP-related portions. The TGA estimates of the wt% PVP, namely 5.0, 13.2 and 21.9 were fairly consistent with the IR assessments.

SYNTHESIS AND CHARACTERIZATION OF PLGA-g-PVP COPOLYMERS
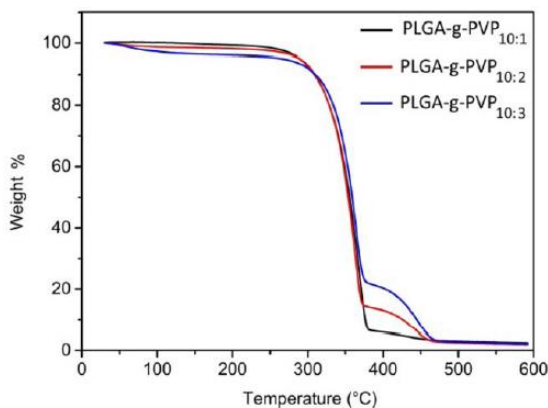
Figure 2.8. TGA thermograms of PLGA-g-PVP$_{10:1}$, PLGA-g-PVP$_{10:2}$ and PLGA-g-PVP$_{10:3}$ (MP samples).

Table 2.2. Glass transition temperatures, T$_g$, of the PLGA and PVP portions of PLGA-g-PVP$_{10:1}$, PLGA-g-PVP$_{10:2}$ and PLGA-g-PVP$_{10:3}$ (MP samples) as well as those of virgin PLGA and PVP

Sample	$T_{g\text{-PLGA}}$[a] (°C)		$T_{g\text{-PVP}}$[b] (°C)	
	onset	offset	onset	offset
PLGA-g-PVP$_{10:1}$	38.3	58.3	nd[c]	nd[c]
PLGA-g-PVP$_{10:2}$	45.0	58.3	~180.0	~190.0
PLGA-g-PVP$_{10:3}$	49.2	55.0	nd[c]	nd[c]
PLGA 50:50	33.0	50.0	-	-
PVPK40	-	-	162.4	185.6

[a] $T_{g\text{-PLGA}}$ = T$_g$ of the PLGA portion. [b] $T_{g\text{-PVP}}$ = Tg of the PVP portion. [c] nd = not detected.

2.5.3 Estimate of the average Chain Transfer Constant of PLGA repeating units

The PLGA main chains of PLGA-g-PVP MP samples were saponified with dilute aqueous sodium hydroxide at room temperature (~20 °C) and the side

SYNTHESIS AND CHARACTERIZATION OF PLGA-g-PVP COPOLYMERS

PVP chains isolated by acidifying the reaction mixture to pH ~ 3, ultrafiltering the resultant clear solution through a membrane with nominal molecular weight cut-off 500 and lyophilizing the retained portion. The molecular weights of the PVP side chains were then determined by SEC-LALS (Table 2.3).

The average chain transfer constant (C_T) of the PLGA units under the adopted conditions was estimated by means of Eq. 2.1, previously developed and successfully employed for determining the C_T values of low molecular weight aliphatic esters employed as both solvents and chain transfer agents in VP polymerizations aimed at obtaining end-functionalized PVP oligomers.[lxxiv]

$$C_T = \frac{\log\left(1 - \frac{[M]_o Y_t}{[T]_o \bar{\bar{X}}_{n,t}}\right)}{\log(1 - Y_t)} \qquad Eq.\,2.1$$

Where $\bar{\bar{X}}_{n,t}$ = cumulative number average polymerization degree at t time; $[M]_o$ and $[T]_o$ = initial monomer and chain transfer agent concentrations; Y_t = monomer conversion at t time. Eq. 2.1 was obtained from the well-known Lewis and Mayo equation (Eq. 2.2) by a mathematical elaboration of its simplified version reported in Eq. 2.3:

$$\frac{1}{\bar{X}_n} = \frac{1}{\bar{X}_{n,o}} + C_T \frac{[T]}{[M]} \qquad Eq.\,2.2$$

$$\bar{X}_n = \frac{1}{C_T} \frac{[M]}{[T]} \qquad Eq.\,2.3$$

where $\bar{X}_n$ is the instantaneous number average polymerization degree and $\bar{X}_{n,o}$ is the instantaneous number average polymerization degree in the absence of the chain transfer agent.

Eq. 2.3 is valid if $1/\bar{X}_{n,o}$ is negligible compared with $1/\bar{X}_n$, that is, if a sufficiently high $[T]_o/[M]_o$ ratio (which depends on C_T) renders chain termination much less frequent than chain transfer. Bulk VP polymerization was ruled out as a mean to estimate the $\bar{X}_{n,o}$ value of PVP under the same polymerization conditions, since at medium-high conversions the so-called "gel" effect was likely to occur and, in the meanwhile, it was difficult to stop the

SYNTHESIS AND CHARACTERIZATION OF PLGA-g-PVP COPOLYMERS

reaction at low conversions. A PVP sample prepared by polymerizing N-VP at 100 °C as 30% aqueous solution had $\bar{X}_n$ = 1200. This was considered as a reasonable approximation of $\bar{X}_{n,o}$. By comparing this value with the $\bar{X}_n$ values of the PVP side chains of the three PLGA-*g*- PVP MP samples (Table 3), it appeared that the validity condition of Eq. 2.1 was fulfilled for PLGA-*g*-PVP$_{10:1}$, whereas PLGA-*g*-PVP$_{10:2}$ was borderline and PLGA-*g*-PVP$_{10:3}$ was off limits. All considered, it was reasonably concluded that the average C_T of the PLGA units at 100 °C was approximately 1 x 10^{-3}, that is, fell in the 1 x 10^{-2} ÷ 5 x 10^{-4} range of the C_T values of low molecular weight esters previously determined at 70 - 80°C.[lxxv] The grafting degree, that is, the average number of PVP side chains per PLGA main chain of PLGA-*g*-PVP MP samples (calculated from the number average molecular weight of the PLGA main chain, the number average of the PVP pendants and the PLGA/PVP w/w ratio) were 1.5, 1.1 and 1.0. The grafting degree was proportional to the [T]/[M] ratio, therefore decreased by increasing the VP content in the feed. By contrast, the molecular weight of the PVP side chains was inversely proportional to the [T]/[M] ratio, hence the PVP/PLGA w/w ratio in the resultant PLGA-*g*-PVP increased.

Table 2.3. Molecular weights of the PVP side chains and average C_T of the PLGA repeating units

Sample	PLGA RU[a]/VP (mol/mol)	PVP $\bar{M}_n$	PVP $\bar{M}_w$	PVP $\bar{X}_n$[b]	Y_t[c]	C_T x 10^3	Grafting degree[d]
PLGA-*g*-PVP$_{10:1}$	17.0	2700	5600	24	0.88	1.02	1.5
PLGA-*g*-PVP$_{10:2}$	8.5	12100	31000	109	0.69	0.64	1.1
PLGA-*g*-PVP$_{10:3}$	5.7	28000	49500	252	0.79	0.36	1.0

[a]PLGA repeating units. [b] Number average polymerization degree. [c] Monomer conversion, see Table 2.4. [d] Average number of PVP side chains per PLGA main chain.

2.5.4 MALDI-TOF analysis of PVP side chains

The PVP samples obtained by saponification of the PLGA-*g*-PVP MP samples were analyzed by MALDI-TOF mass spectrometry. This allowed gaining unquestionable evidence of grafting occurrence by determining the nature of the PVP terminal groups. The spectra of the saponification products of all samples

SYNTHESIS AND CHARACTERIZATION OF PLGA-g-PVP COPOLYMERS

were much similar notwithstanding the different PVP content and the different average molecular weight of the PVP portions. This reflected the identity of all fractions in the same m/z range as well as the obvious flying limits of the polydisperse PVP under the adopted conditions. The whole spectrum of PLGA-g-PVP$_{10:1}$ saponification product in the 800-5000 m/z range is reported in Figure 2.9, together with its expanded 1420-1530 m/z spectral range. The corresponding spectral regions of the saponification products of PLGA-g-PVP$_{10:2}$ and PLGA-g-PVP$_{10:3}$ are shown in Figures 2.10 and 2.11.
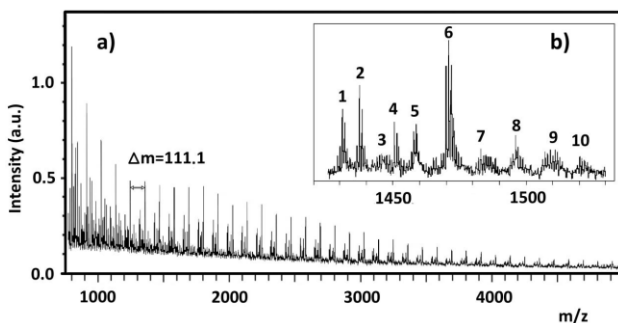
Figure 2.9.(a) MALDI-TOF spectrum of the saponification products of PLGA-g-PVP$_{10:1}$ MP. (b) Expanded 1420-1530 m/z spectral range.
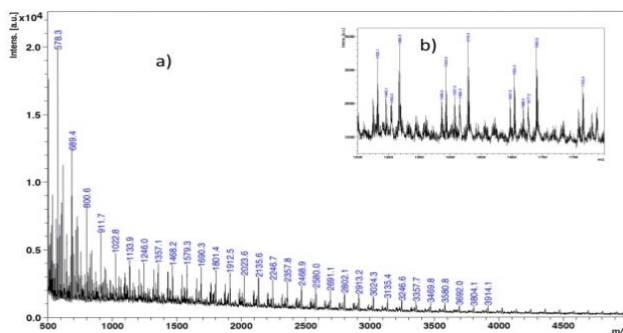
Figure 2.10. MALDI-TOF spectra of the saponification products of PLGA-g-PVP$_{10:2}$ in the ranges (a) 800 − 5000 m/z and (b)1400 − 1800 m/z.
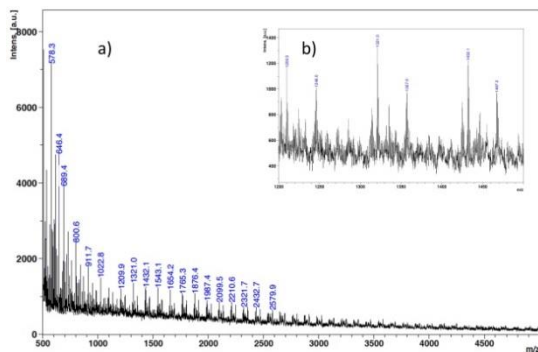
Figure 2.11. MALDI-TOF spectra of the saponification products of PLGA-g-PVP$_{10:3}$ in the ranges (a) $800 - 5000$ m/z and (b)$1400 - 1800$ m/z.
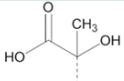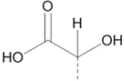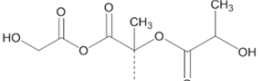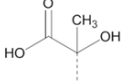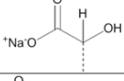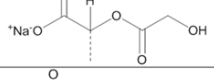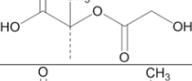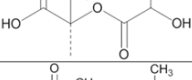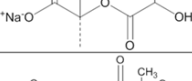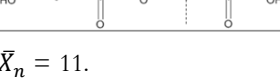
The whole spectra of all samples consisted of a succession of ten-peak motifs of four moderately intense peaks followed by a single peak of paramount intensity and five weakly intense peaks. The m/z difference of the corresponding peaks belonging to consecutive motifs was constantly 111.1, that is, the mass of the VP unit.

The m/z values of the recovered PVP, including terminals, was expressed by Eq. 4:

$$^{m}/_{z_{PVP}} = 111.1 \times X_{n,PVP} + m_{T_2} + m_{cation} \quad Eq.4$$

where 111.1 is the mass of the VP unit, m_{T_1} and m_{T_2} are the masses of the chain terminals, and m_{cation} is the mass of the cation(s), mainly H$^+$ or Na$^+$. It may be noticed that T_1 is hydrogen, as the abstraction of a different PLGA atom by the propagating PVP radical could hardly be imagined. The consequent peak assignments are reported in Table 2.4. They were consistent with the presence at one chain end of residues from lactic acid (L), and glycolic acid (G), all their dimers (LG), the lactic-lactic-glycolic trimer (LLG), and the lactic-lactic-glycolic-glycolic tetramer (LLGG). No PVP homopolymer and PLGA-PVP-PLGA traces in MALDI-TOF spectra were highlighted.

Table 2.4. Terminal groups of PLGA-g-PVP$_{10:1}$ saponification product, corresponding to $\bar{X}_n = 12$.

SYNTHESIS AND CHARACTERIZATION OF PLGA-g-PVP COPOLYMERS

Peak	T$_1$	Terminals T$_2$	Cation	m/z Experimental	m/z Expected
1	H		H+	1425.1	1424.8
2	H		Na+	1432.1	1431.7
3	H		H+	1443.3	1443.7
4	H		Na+	1447.0	1445.7
5	H		Na+	1455.1	1453.7
6	H		H+	1469.0	1468.8
7	H		H+	1482.0	1482.8
8	H		H+	1497.0	1496.8
9	H		Na+	1511.0	1511.7
10	H		Na+	1522.0	1522.7

a)   For $\bar{X}_n = 11$.

SYNTHESIS AND CHARACTERIZATION OF PLGA-g-PVP COPOLYMERS

2.5.5. Fractionation of PLGA-*g*-PVP copolymers

The PLGA-*g*-PVP MP samples were fractionated to assess their compositional dispersion. To this purpose, preliminary tests were performed on PLGA and both low - and high -molecular weight PVP (the former purposely prepared by polymerizing VP in DMF solution). It was found that ethyl acetate and methanol were selective extraction solvents from blends (the IR spectra of the recovered solids were superimposable to those of PLGA and PVP, respectively, Figure 2.12, while the 1:1 (v/v) water-methanol mixture was a selective precipitation medium from mixed dichloromethane solutions (Figure 2.13). In both cases, the original PLGA and PVP components were quantitatively recovered.
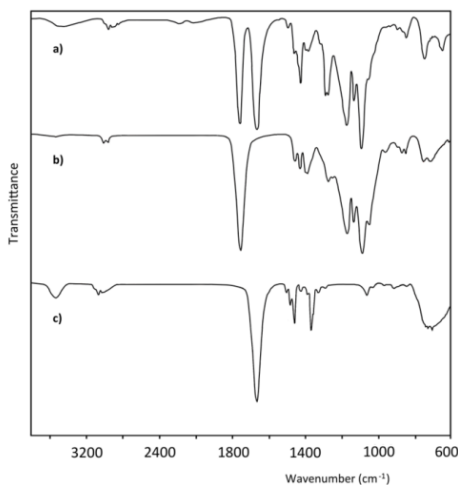
Figure 2.12. IR spectra of the fractions retrieved from the extraction fractionation of PLGA/PVP blends with ethyl acetate and methanol. a) PLGA/PVP blend; b) ethyl acetate soluble fraction; c) methanol soluble fraction.

SYNTHESIS AND CHARACTERIZATION OF PLGA-g-PVP COPOLYMERS
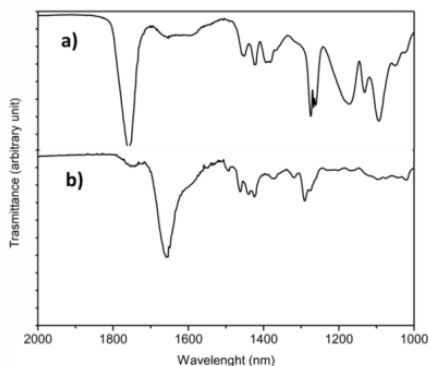
Figure 2.13. IR spectra of the products of PLGA/PVP$_{DMF}$ precipitation from DCM into a 1:1 methanol/water mixture. a) Methanol/water insoluble portion; b) methanol/water soluble portion.

The same treatments were adopted for fractionating the PLGA-g-PVP MP samples. The whole fractionation scheme adopted for each PLGA-g-PVP copolymer is reported in Figure 2.14, which encompasses the previously mentioned precipitation from dichloromethane with ether of the crude reaction mixture, leading to the main product (MP) and leaving unidentified impurities and byproducts (UBPI) in the mother liquors.
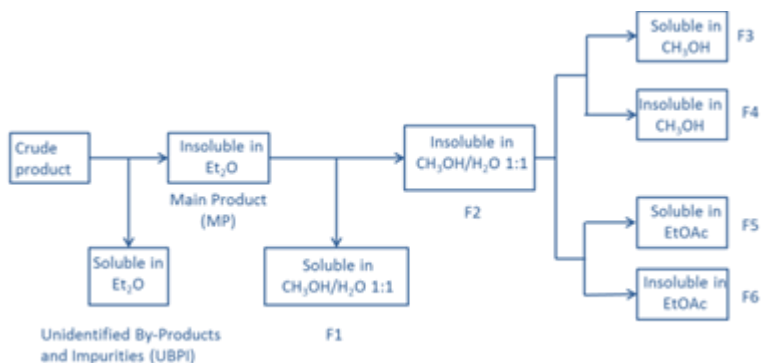
Figure 2.14. Fractionation scheme of PLGA-*g*-PVP copolymers.

SYNTHESIS AND CHARACTERIZATION OF PLGA-*g*-PVP COPOLYMERS

All PLGA-*g*-PVP MP samples were dissolved in dichloromethane and re-precipitated with 1:1 water-methanol. The mother liquors contained a small soluble fraction (F1). The insoluble fraction (F2) was further fractionated by selective extractions with ethyl acetate and methanol. On the whole, each PLGA-*g*-PVP copolymer was subdivided in two intermediate (MP and F2) and six terminal (UBPI, F1, F3, F4, F5, F6) fractions. Their compositions are evaluated by FTIR (Figure 2.15) reported in Table 2.5. The grafting degrees of the terminal fractions, defined as the number of PVP chains per PLGA chain, are reported in Table 6. The above results demonstrate that the fractionation process effectively separated PLGA-rich and PVP-rich fractions, but failed to isolate either PLGA or PVP. As reported in Table 2.3, the grafting degrees of PLGA-*g*-PVP$_{10:1}$, PLGA-*g*- PVP$_{10:2}$ and PLGA-*g*-PVP$_{10:3}$ were 1.5, 1.1 and 1.0, respectively.
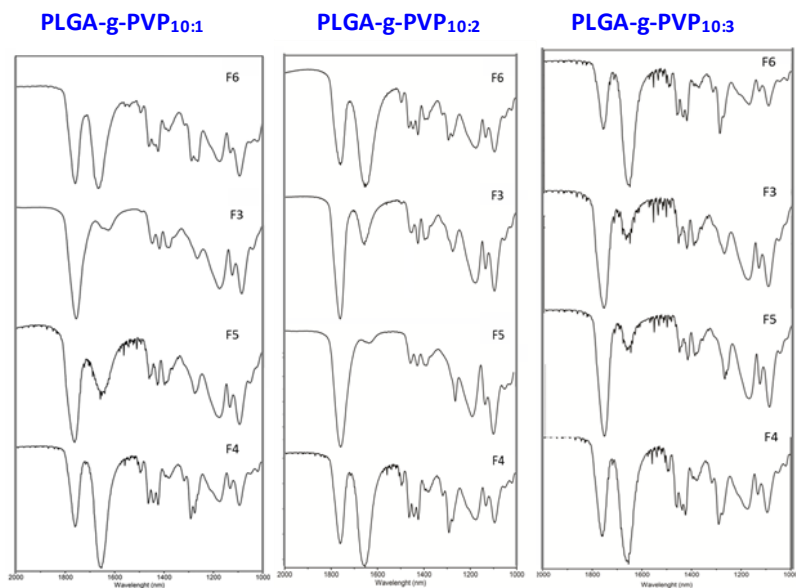
Figure 2.15. IR spectra of F3-F6 fractions of PLGA-g-PVP copolymers.

SYNTHESIS AND CHARACTERIZATION OF PLGA-g-PVP COPOLYMERS

Table 2.5. Weight and composition of PLGA-*g*-PVP fractions

PLGA-*g*-PVP$_{10:1}$			PLGA-*g*-PVP$_{10:2}$			PLGA-*g*-PVP$_{10:3}$		
Code	PLGA (%)	PVP (%)	Code	PLGA (%)	PVP (%)	Code	PLGA (%)	PVP (%)
UBPI (0.090 g)	64.1	35.9	UBPI (0.095 g)	66.0	34.0	UBPI (0.105 g)	70.6	29.4
MP (2.119 g)	93.3	6.7	MP (2.299 g)	81.2	18.8	MP (2.560 g)	67.8	32.2
F1 (0.046 g)	60.8	39.2	F1 (0.059 g)	42.2	57.8	F1 (0.093 g)	25.5	74.5
F2 (1.962 g)	nd[a]	nd[a]	F2 (2.186 g)	nd[a]	nd[a]	F2 (2.457 g)	nd[a]	nd[a]
F3 (0.079 g)	42.1	57.9	F3 (0.090 g)	41.2	58.8	F3 (0.195 g)	35.9	64.1
F84 (1.003 g)	94.9	5.1	F4 (1.004 g)	92.5	7.5	F4 (1.093 g)	94.4	5.6
F5 (0.867 g)	99.8	1.6	F5 (0.933 g)	95.5	4.5	F5 (0.815)	91.6	8.4
F6 (0.051 g)	42.0	58.0	F6 (0.070 g)	38.8	61.2	F6 (0.202 g)	37.5	62.5
Recovery (%)	97.3	87.7	Recovery (%)	97.9	68.5	Recovery (%)	100.3	78.5

[a] Not determined. [b] Regarded as the VP conversion. Probably, most wanting VP in respect of the feed was unreacted monomer remaining in the dichloromethane mother liquors of the main products (MP) precipitation and subsequently lost while retrieving the UBPI fraction by high vacuum solvent elimination.

As shown in Table 2.6, the PVP chains were not evenly distributed. All PLGA-*g*-PVP MP samples contained minority PVP-rich fractions (F1, F3,F6) with grafting degrees ranging from 13 to 28 (PLGA-*g*-PVP$_{10:1}$), 6.5 to 7.5 (PLGA-*g*-PVP$_{10:2}$) and 3 to 6 (PLGA-*g*-PVP$_{10:3}$), together with major PLGA-rich fractions (F2, F4, F5) with grafting degrees ranging from 0.3 to 1.1 (PLGA-*g*- PVP$_{10:1}$), 0.2-to 0.4 (PLGA-*g*-PVP$_{10:2}$) and 0.1 to 0.2 (PLGA-*g*-PVP$_{10:3}$). It is apparent that the fractions of the latter group contained significant amounts of virgin PLGA. A possible explanation of this uneven distribution is that PVP grafting on a PLGA chain facilitated further grafting on the same chain. The first step of the chain transfer reaction was hydrogen abstraction from a PLGA chain by a PVP

SYNTHESIS AND CHARACTERIZATION OF PLGA-g-PVP COPOLYMERS

macroradical, which preferentially approached an already PVP-grafted PLGA for which it had greater affinity than for virgin PLGA.

Table 2.6. Grafting degree of PLGA-*g*-PVP fractions

	Grafting degree [a]		
Code	PLGA-*g*-PVP$_{10:1}$	PLGA-*g*-PVP$_{10:2}$	PLGA-*g*-PVP$_{10:3}$
UBPI	11.6	2.4	0.8
F1	13.4	6.3	5.8
F2	nd[b]	nd[b]	nd[b]
F3	28.5	6.6	3.6
F4	1.1	0.4	0.1
F5	0.3	0.2	0.2
F6	28.6	7.4	3.3

a) Average number of PVP side chains per PLGA main chain.
b) Not determined.

2.5.6 PLGA-*g*-PVP-based aqueous nanodispersions

In preliminary experiments, all PLGA-*g*-PVP MP samples gave nanodispersions (NDS) by diluting their 1% acetone solutions with 10 volumes water and then getting rid of acetone by nitrogen flushing at room temperature. For comparison purposes, the same procedure was followed with native PLGA, 10:1, 10:2 and 10:3 w/w native PLGA/PVP$_{DMF}$ blends, and 8:2 w/w PLGA/PLGA-*g*-PVP$_{10:1}$, PLGA-*g*-PVP$_{10:2}$ and PLGA-*g*-PVP$_{10:3}$ blends. Particle size, ζ-potential, stability on time and re-dispersion in water after lyophylization of the resultant NDS were assessed.

The properties of native PLGA NDS were recorded as formed and after 1 and 2 days standing at room temperature. As formed, PLGA NDS had large dimensions (>250 nm) and highly negative surfaces (-40 mV). Their size rapidly increased and sediments were produced within after 1-2 days (data not shown). They were no further considered.

In all other cases, the NDS size and ζ- potential were recorded after standing 1 h, 24 h and 7 days at room temperature. The results are shown in Figure 2.16. The PLGA-*g*-PVP MP NDS were smaller (150 - 180 nm) than those of PLGA,

SYNTHESIS AND CHARACTERIZATION OF PLGA-g-PVP COPOLYMERS

their size did not strictly depend on PVP content, remained constant and formed no sediments throughout the observation time. Moreover, in the absence of added cryoprotectors they could be lyophilized and subsequently re-dispersed in water with a moderate increase of size to 300-400 nm and a significant reduction of their negative surface charge, possibly due to structural rearrangement (Figure 2.17). PLGA-PVP blends gave somewhat larger NDS (220-350 nm) that within 48 h produced sediments and if treated with water after lyophilization gave a solid cake (Figure 2.18).
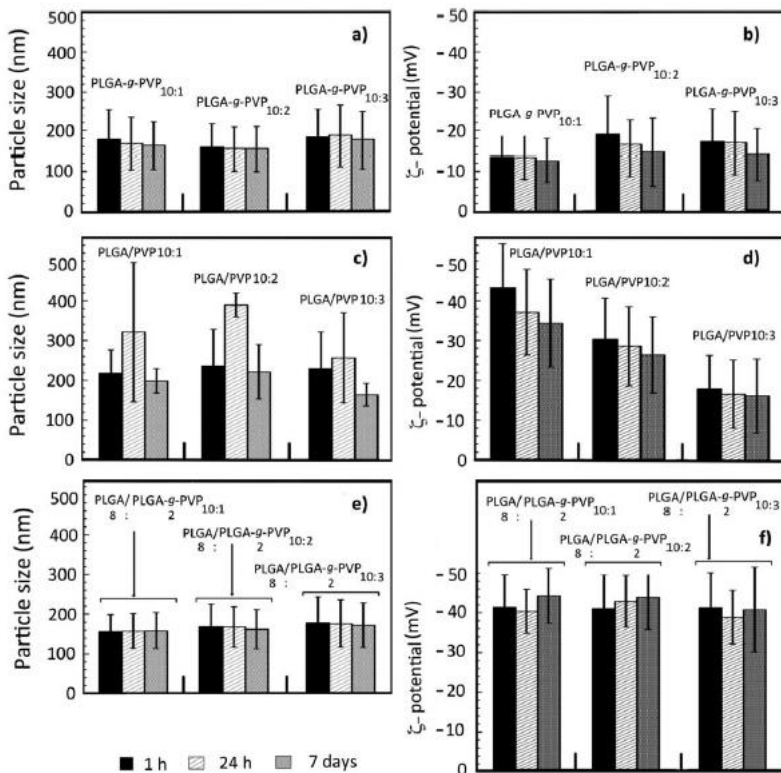
Figure 2.16. Particle size and ζ-potential of nanodispersions from (a,b) MP fractions; (c,d) PLGA/PVP; (e,f) PLGA/MP blends.

SYNTHESIS AND CHARACTERIZATION OF PLGA-g-PVP COPOLYMERS
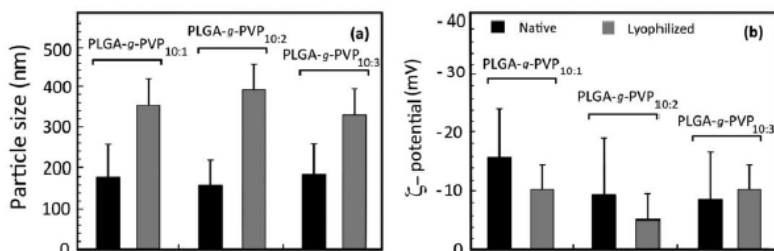
Figure 2.17. (a) Partide size and (b) ζ-potential of pristine and lyophilized MP nanodispersions.

Figure 2.18. PLGA/PVP 10:3 blend and PLGA-*g*-PVP$_{10:3}$ MP sample re-dispersed in water after lyophilization of the pristine nanodispersions.

Interestingly, NDS of 8:2 PLGA/PLGA-*g*-PVP$_{10:3}$ blends behaved exactly as those of PLGA-*g*-PVP, apart from the formation of little sediment by re-dispersing after lyophilization. These results suggest that in all NDS PVP protruded in the aqueous phase. However, it was only loosely bound to- and easily extracted from PLGA/PVP blends, but stably bound to- and hardly extractable from both PLGA-*g*-PVP and PLGA/PLGA-*g*-PVP blends.

The ζ-potentials of both PLGA-*g*-PVP and PLGA/PLGA-*g*-PVP blend NDS were the same as those of native PLGA, that is ~ - 40 mV. They did not depend from the PVP content and remained constant throughout the observation period. The ζ-potential of PLGA/PVP blend NDS was also negative, ranging from - 30 to - 40 mV, but depended on the PVP content and did not remain

SYNTHESIS AND CHARACTERIZATION OF PLGA-g-PVP COPOLYMERS

constant with time, but within the observation period halved to -15- -20 mV, possibly owing to the gradual PVP migration to the surface.

Size and ζ-potential of fractions F3-F6 NDS are shown in Figure 2.19 (a and b). Confirming the above observation, higher PVP contents did not lead to better performances under the experimental conditions adopted, notwithstanding most of the F4 and F5 fractions grafting degrees ranged in the range 0.1 - 0.4. Therefore, they contained significant amounts of virgin PLGA and were, in fact, PLGA/PLGA-g-PVP intimate blends similar to the purposely prepared ones reported above. Logically, they performed similarly.
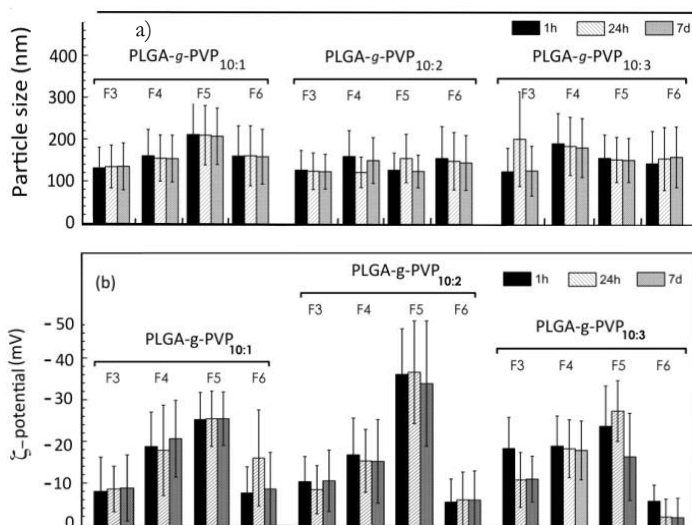
Figure 2.19. (a) Particle size and (b) ζ-potential of nanodispersions from F3-F6 fractions.

For all cases, particle size and ζ-potential were collected after standing at 1h, 24h and 7 days at 4°C (Figure 2.20). Generally, particle sizes are smaller and less sensitive to spending time than those of room temperature. Also in this condition, NDS obtained from MP are the smallest (less of 160 nm) and independent on PVP content, only ζ-potential changed, in particular moduli decrease increasing PVP portion. PLGA/PVP NDS presented sizes of about

SYNTHESIS AND CHARACTERIZATION OF PLGA-g-PVP COPOLYMERS

200 nm and as ζ-potentialmoduli of about -35 - -40 mV. These values did not vary during the observation time and respect to PVP content, on the contrary of room temperature standing NDS. Probably the lower temperature slows down agreement mechanisms in which PVP covers PLGA surface of NDS.F3-F6 NDS confirmed the trend and values observed at room temperature.
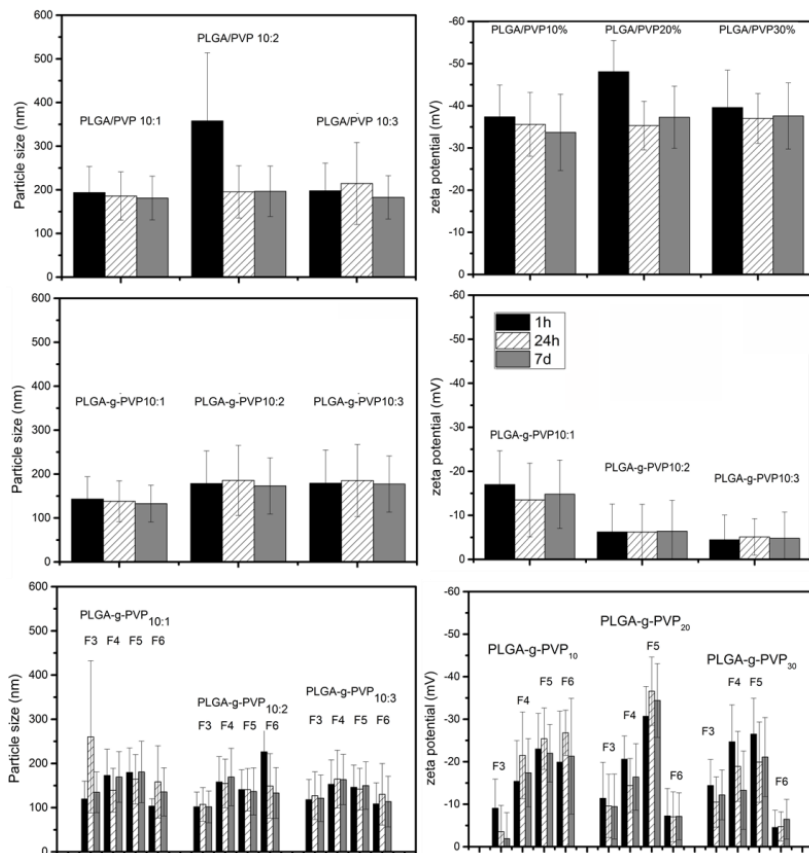
Figure 2.20. Particle size and ζ-potential of nanodispersions from (a,b) PLGA/PVP; (c,d) MP fractions; (e,f) from F3-F6 fractions at 4°C.

SYNTHESIS AND CHARACTERIZATION OF PLGA-g-PVP COPOLYMERS

2.6 CONCLUSIONS

The results reported in this paper demonstrate that the radical polymerization of VP dissolved in commercial medical grade PLGA at 100 8C provides a one-step straightforward preparation of hitherto undescribed PLGA-g-PVP copolymers by a chain-transfer mechanism. The saponification of the PLGA portion allowed determining the molecular weight of the PVP side chains as a function of the PLGA/VP ratio in the reaction feed. This allowed estimating the chain-transfer constant (C_T) of PLGA repeating units to be 1 x 10^{-3}, that is, within the range of those previously determined for non-polymeric aliphatic esters, notwithstanding the PLGA high molecular weight. The resultant copolymers consisted of a long PLGA main chain and PVP pendants whose molecular mass could be kept well below the renal elimination threshold by adjusting the PLGA/VP ratio in the feed. Thus, they are entirely bioeliminable if employed as injectable drug delivery systems.

The MALDI-TOF spectra of the PVP obtained by saponification of the PLGA-g-PVP main products were consistent with oligomeric PVP chains terminated at one end by hydrogen and at the opposite end by L-, G-, LG-, LLG, and LLGG residues. This unequivocally demonstrated the occurrence of PVP grafting onto PLGA. On average, PLGA-g-PVP$_{10:1}$, PLGA-g-PVP$_{10:2}$, and PLGA-g-PVP$_{10:3}$ carried, respectively, 1.5, 1.1, and 1.0 PVP side chains per PLGA main chain. The fractionation by the orthogonal solvent pair ethyl-acetate/ methanol, whereas able to quantitatively separate in a pure state the PLGA and PVP components of PLGA/PVP intimate blends, if used to fractionate crude PLGA-g-PVP failed to isolate either pure PLGA or pure PVP. However, it separated PLGA- and PVP-rich fractions with widely different compositions, demonstrating that the PVP grafting was unevenly distributed.

The mass balance of the fractions showed that one or more PVP chains grafted onto a PLGA chains probably facilitated further grafting on the same chain. Moreover, the PLGA-rich fractions probably contained some native PLGA. All main PLGA-g-PVP products and single fractions gave stable nanodispersions in water by the solvent evaporation technique, irrespective of the PVP content. Similar results were obtained with PLGA/PLGA-g-PVP intimate blends, but not with PLGA/PVP blends. Admittedly, these preliminary results need to be

SYNTHESIS AND CHARACTERIZATION OF PLGA-g-PVP COPOLYMERS

substantiated by further, specifically addressed research. However, they suggest that the new PLGA-g-PVP copolymers reported in this article, notwithstanding the uneven distribution of PVP grafting among the PLGA chains, have a potential as bioeliminable nanodispersed drug delivery systems.

SYNTHESIS AND CHARACTERIZATION OF PLGA-g-PVP COPOLYMERS

BIBLIOGRAPHY

[i] D. K. Schneiderman, M.A. Hillmyer, *Macromolecules*, **2016**, 49, 2419-2428

[ii] M. Vert, *Biomacromolecules*, **2005**, 6, 538-546

[iii] K.M. Zia, A. Noreen, M. Zuber, S. Tabasum, M. Mujahid, *International Journal of Biological Macromolecules*, **2016**, 82, 1028-1040

[iv] N.Wanga, X. S.Wub, L.-U.Hanniac, E.Donahued, A.Siddiquie, *Journal of Biomaterials Science: Polymer Edition*, **1997**, 8, 905-917

[v] S. Li, M. Vert, *Macromolecules*, **2003**, 36, 8008-8014

[vi] M.L. Houchin, E.M. Topp, *Journal of Applied Polymer Science*, **2009**, 114, 2848-2854

[vii] H. K. Makadia, S.J. Siegel, *Polymers,* **2011**, 3, 1377-1397

[viii] F. Danhier, E. Ansorena, J. M. Silva, R. Coco, A. Le Breton, V. Préat, *Journal of Controlled Release*, **2012**, 161, 505-522

[ix] B. Dhandayuthapani, Y. Yoshida, T. Maekawa, D.S. Kumar, *International Journal of Polymer Science,* **2011**, ID 290602

[x] Z. Pan, J. Ding, *Interface Focus*, **2012**, 2, 366-377

[xi] M.I. Sabir, X. Xu, L. Li, *Journal of Materials Science*, **2009**, 44, 5713-5724

[xii] A. Kumari, S.K. Yadav, S.C. Yadav, *Colloids and Surfaces B: Biointerfaces*, **2010**, 75, 1-18

[xiii] H.M. Redhead, S.S. Davis, L. Illum, *Journal of Controlled Release*, **2001**, 70, 353-363

[xiv] J. Cheng, B.A. Teply, I. Sherifi, J. Sung, G. Luther, F.X. Gu, E. Levy Nissenbaum, A.F. Radovic-Moreno, R. Langer, O.C. Farokhzad, *Biomaterials*, **2007**, 28, 869-876

[xv] K. Ramesh, R.K. Gundampati, S. Singh, K. Mitra, A. Shukla, M.V. Jagannadham, D. Chattopadhyay, N. Misra B. Ray, *RSC Advances*, **2016**, 6, 25864-25876

[xvi] M. Tobio, R. Gref, A. Sanchez, R. Langer, M.J. Alonso, *Pharmaceutical Research,* **1998**, 15, 270-275

[xvii] J. Cheng, B.A. Teply, I. Sherifi, J. Sung, G. Luther, F.X. Gu, E. Levy-Nissenbaum, A.F. Radovic-Moreno, R. Langer, O.C. Farokhzad, *Biomaterials*, **2007**, 28, 869-876

[xviii] S. Dhar, F.X. Gu, R. Langer, O.C. Farokhzad, S.J. Lippard, *Proceedings of the National Academy of Sciences*, **2008**, 105, 17356-17361

[xix] H.S. Yoo, T.G. Park, *Journal of Controlled Release*, **2004**, 96, 273-283

[xx] K. Knop, R. Hoogenboom, D. Fischer, U.S. Schubert, *Angewandte Chemie International Edition*, **2010**, 49, 6288-6308

[xxi] J. Szebeni, L. Baranyi, S. Savay, J. Milosevits, R. Bunger, P. Laverman, J.M. Metselaar, G. Storm, A. Chanan-Khan, L. Liebes, F.M. Muggia, R. Cohen, Y. Barenholz, C.R. Alving, *Journal of Liposome Research*, **2002**, 12, 165-172

SYNTHESIS AND CHARACTERIZATION OF PLGA-g-PVP COPOLYMERS

xxii A. Chanan-Khan, J. Szebeni, S. Savay, L. Liebes, N.M. Rafique, C.R. Alving, F.M. Muggia, *Annals of Oncology*, **2003**, 14, 1430-1437

xxiii J.M. Metselaar, *Dissertation*, Utrecht Institute for Pharmaceutical Sciences, Utrecht University, The Netherlands, **2006**

xxiv M.C.H. de Groot, B.J. van Zwieten-Boot, A.C. van Grootheest, *Journal of Nederlands Tijdschrift voor Geneeskunde*, **2004**, 148, 1887-1888

xxv T. Ishida, M. Ichihara, X.Y. Wang, H.Kiwada, *Journal of Controlled Release,* **2006**, 115, 243-250

xxvi E.T.M. Dams, P. Laverman, W.J.G. Oyen, G. Storm, G.L. Scherphof, J.W.M. van der Meer, F.H.M. Corstens, O.C. Boerman, *Journal of Pharmacology and Experimental Therapeutics*, **2000**, 292, 1071-1079

xxvii T. Ishida, M. Harada, X.Y.Wang, M. Ichihara, K. Irimura, H. Kiwada, *Journal of Controlled Release*, **2005**, 108, 305-317

xxviii T. Ishihara, T. Maeda, H. Sakamoto, N. Takasaki, M. Shigyo, T. Ishida, H. Kiwada, Y. Mizushima, T. Mizushima, *Biomacromolecules*, **2010**, 11, 2700-2706

xxix W. Reppe, "*Polyvinylpyrrolidon,*" VerlagChemie, Weinheim, **1954**

xxx X. Liu, Y. Xu, Z. Wu, H. Chen, Macromolecular Bioscience, **2013**, 13, 147-154

xxxi Y.E. Kirsh, T.A. Soos, T.M. Karaputadze, *European Polymer Journal,* **1979**, 15, 223-228

xxxii M.K. Chun, C.S. Cho, H.K. Choi, *Journal of Controlled Release*, **2002**, 81, 327–334

xxxiii J. Lee, *Macromolecular Bioscience*, **2005**, 5, 1085-1093

xxxiv Available from:
http://www.pvpworld.com/en/pvp_info.aspx?News_Id=67&CateId=88

xxxv F. Haaf, A. Sanner, F. Straub, *Polymer Journal*, **1985**, 17, 143-152

xxxvi V. Bühler, *Polyvinylpyrrolidone Excipients for Pharmaceuticals - Povidone, Crospovidone and Copovidone*, Springer Berlin Heidelberg; New York, **2005**

xxxvii B. V. Robinson, F.M. Sullivan, J.F. Borzelleca, S.L. Schwartz, *PVP: A Critical Review of the Kinetics and Toxicology of Polyvinylpyrrolidone (Povidone),* CRC Press Inc., **1990**

xxxviii V. Ferrari, D. Marioli, A. Taroni, E. Ranucci, P. Ferruti, *IEEE transactions on ultrasonics, ferroelectrics, and frequency control*, **1996**, 43, 601-608

xxxix E. Ranucci, P. Ferruti, P. Opelli, V. Ferrari, D. Marioli, A. Taroni, *Sensors and Materials*, **1994**, 5, 221-229

xl F.Haaf, A.Sanner, F. Straub, *Polymer Journal*, **1985**, 17,143-152

xli A.Debuigne, N. Willett, R. Jérôme, C.Detrembleur, *Macromolecules,* **2007**, 40, 7111-7118

xlii S. Yamago, B. Ray, K. Iida, J. Yoshida, T. Tada, K. Yoshizawa, Y. Kwak, A. Goto, T. Fukuda, *Journal of the American Chemical Society*, **2004**, 126, 13908-13909

SYNTHESIS AND CHARACTERIZATION OF PLGA-g-PVP COPOLYMERS

xliii A. Guinaudeau, O. Coutelier, A. Sandeau, S. Mazières, H.D. Nguyen Thi, V. Le Drogo, D.J. Wilson, M. Destarac, *Macromolecules,* **2014**, 47, 41-50

xliv X. Lu, S. Gong, L. Meng, C. Li, S. Yang, L. Zhang, *Polymer*, **2007**, 48, 2835−2842

xlv A. Benahmed, M. Ranger, J.C. Leroux, *Pharmaceutical Research*, **2001**, 18, 323-328

xlvi H.J. Jeon, Y.C. You, J.H. Youk, *Journal of Polymer Science Part A: Polymer Chemistry*, **2009**, 47, 3078-3085

xlvii Y. Hu, Z. Jiang, R. Chen, W. Wu, X. Jiang, *Biomacromolecules,* **2010**, 11, 481-488

xlviii Z. Zhu, Y. Li, X. Li, R. Li, Z. Jia, B. Liu, W. Guo, W. Wu, X. Jiang, *Journal of Controlled Release*, **2010**, 142, 438-446

xlix A.K. Mishra, V.K. Patel, N.K. Vishwakarma, C.S. Biswas, M. Raula, A. Misra, T.K. Mandal, B. Ray, *Macromolecules,* **2011**, 44, 2465-2473

l L.B. Luo, M. Ranger, D.G. Lessard, D. Le Garrec, S. Gori, J.C. Leroux, S. Rimmer, D. Smith, *Macromolecules,* **2004**, 37, 4008-4013

li I. Bartolozzi, R. Solaro, E. Schacht, E. Chiellini, *European Polymer Journal*, **2007**, 43, 4628-4638

lii Z. Zhu, C. Xie, Q. Liu, X. Zhen, X. Zheng, W. Wu, R. Li, Y. Ding, X. Jiang, B. Liu, *Biomaterials*, *2011*, 32, 9525-9535

liii S. Shi, J. Liu, Y. Xia, S. Jiao, X. Li, *Advanced Materials Research*, **2006**, 11-12, 461-464

liv F.M. Veronese, L. Sartore, P. Caliceti, O. Schiavon, E. Ranucci, P. Ferruti, *Journal of Bioactive and Compatible Polymers*, **1990**, 5, 167-178

lv T. Ishihara, T. Maeda, H. Sakamoto, N. Takasaki, M. Shigyo, T. Ishida, H. Kiwada, Y. Mizushima, T. Mizushima, *Biomacromolecules*, **2010**, 11, 2700-2706

lvi U. Edlund, M. Källrot, A.C. Albertsson, *Journal of the American Chemical Society*, **2005**, 127, 8865-8871

lvii J.L. Eguiburu, M.J. Fernandez-Berridi, J. San Román, *Polymer*, **1996**, 37, 3615-3622

lviii K. Ramesh, S. Singh, K. Mitra, D. Chattopadhyay, N. Misra, B. Ray, *Colloid and Polymer Science*, **2016**, 294, 399-407

lix T. Zhu, S. Chen, W. Li, J. Lou, J. Wang, *Journal of Applied Polymer Science*, **2015**, 132, 41982-41983

lx M. Murillo, J.M. Irache, M. Estevan, M.M. Goñi, J.M. Blasco, C. Gamazo, *International Journal of Pharmaceutics*, **2004**, 271, 125-135

lxi J. Meeus, D.J. Scurr, K. Amssoms, M.C. Davies, C.J. Roberts, G. Van den Mooter, *Molecular Pharmaceutics*, **2013**, 10, 3213-3224

lxii L. Sartore, E. Ranucci, P. Ferruti, P. Caliceti, O. Schiavon, F.M. Veronese, *Journal of Bioactive and Compatible Polymers*, **1994**, 9, 411-428

lxiii E. Ranucci, G. Spagnoli, L. Sartore, F. Bignotti, P. Ferruti, O. Schiavon, P. Caliceti, F. M. Veronese, *Macromolecular Chemistry and Physics*, **1995**, 196, 763-774

SYNTHESIS AND CHARACTERIZATION OF PLGA-g-PVP COPOLYMERS

lxiv P. Caliceti, O. Schiavon, M. Morpurgo, F.M. Veronese, L. Sartore, E. Ranucci, P. Ferruti, *Journal of Bioactive and Compatible Polymers*, **1995**, 10, 103-120

lxv E. Ranucci, M. Tarabic, M. Gilberti, A.C. Albertsson, *Macromolecular Chemistry and Physics,* **2000**, 201, 1219-1225

lxvi M. Tarabic, E. Ranucci, *Macromolecular Bioscience,* **2001**, 1, 126-135

lxvii C. Baldoli, C. Oldani, S. Maiorana, P. Ferruti, E. Ranucci, M. Bencini, A. Contini, *Journal of Polymer Science Part A: Polymer Chemistry*, **2008**, 46, 1683-1698

lxviii E. Ranucci, L. Macchi, R. Annunziata, P. Ferruti, F. Chiellini, *Macromolecular Bioscience*, **2004**, 4, 706-713

lxix E. Ranucci, P. Ferruti, R. Annunziata, I. Gerges, G. Spinelli, *Macromolecular Bioscience*, **2006**, 6, 216-227

lxx E. Ranucci, G. Capuano, A. Manfredi, P. Ferruti, *Journal of Polymer Science: Part A: Polymer Chemistry*, **2016**, 54, 1919-1928

lxxi J. Meeus, D. J. Scurr, K. Amssoms, M.C. Davies, C.J. Roberts, G. Van den Mooter, *Molecular Pharmaceutics*, **2013**, 10, 3213-3224

lxxii A. Mathew, T. Fukuda, Y. Nagaoka, T. Hasumura, H. Morimoto, Y. Yoshida, T.T. Maekawa, K. Venugopal, D.S. Kumar *PLoS Public Library of Science*, **2012**, 7, 3

lxxiii C. Peniché, D. Zaldivar, M. Pazos, S. Paz, A. Bulay, J. San Roman, *Journal of Applied Polymer Science*, **1993**, 50, 485-493

lxxiv E. Ranucci, F. Bignotti, End-Functionalized Oligomers by Chain-transfer Techniques - In The Polymeric Materials Encyclopedia; Salamone, J. C. Ed.; CRC Press: Boca Raton, **1996**

lxxv E. Ranucci, P. Ferruti, R. Annunziata, I. Gerges, G. Spinelli, *Macromolecular Bioscience*, **2006**, 6, 216-227

CHAPTER 3

FORMULATIONS OF PLGA-g-PVP COPOLYMERS

"The purpose of this piece of work is to establish the best formulation technologies to transform PLGA-g-PVP copolymers into nanosized carriers, namely nanoparticles and lipid nanocapsules, for the delivery of anticancer and antimalarial drugs"

3.1 NANOPARTICLES

Polymeric nanoparticles (NPs) are colloidal structures composed of natural, synthetic or semi-synthetic polymers with sizes generally around 5-1000 nm, more centred on 100-500 nm. Depending on the process used for NP preparation, nanospheres or nanocapsules can be obtained (Figure 3.1).[i] Nanospheres have a homogeneous structure in the whole particle, the drug is dissolved, entrapped, encapsulated or uniformly attached to polymer matrix.[ii] Nanocapsules are nano-vesicular systems that exhibit a typical core-shell structure where the drug is confined to a reservoir or within a cavity surrounded by a polymer membrane or coating. The reservoir can be a liquid oily core or in a solid form.[iii]
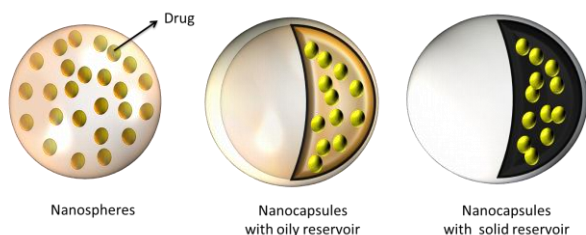
Figure 3.1. Nanosphere and nanocapsule structures.

3.2 NP PREPARATION METHODS

NPs are usually prepared by bottom-up procedure, mainly based on two methods: solvent evaporation and solvent displacement.[iv] All the other methods proposed in the literature are derived from them, with little difference.

Solvent evaporation method: the polymer and drug are dissolved in an organic solvent such as dichloromethane, chloroform and ethyl acetate, and then emulsified into an aqueous solution to make oil (O) in water (W) (O/W emulsion) by using a surfactant or an emulsifying agent. After the formation of a stable emulsion, the organic solvent is evaporated either by increasing the temperature under pressure or by continuous stirring. A similar procedure is adopted for (W/O)/W method, usually used for preparing water-soluble drug-loaded NPs. This approach consists in two consecutive emulsions: the former useful to solubilise the drug in the polymer solution, and the latter to form the NPs.[v]

Solvent displacement method/ nanoprecipitation: a water-soluble solvent with intermediate polarity, such as acetone, ethanol or methanol, is used to initially solubilise both polymer and drug. This phase is thus injected into a stirred aqueous solution in the presence or not of surfactants. Polymer deposition on water/organic solvent interface, caused by the fast diffusion of solvent, leads to the instantaneous formation of a colloidal suspension. The solvent displacement technique allows for preparing nanocapsules when a small volume of nontoxic oil is incorporated in the organic phase.

Emulsification/solvent diffusion method: this is a modified version of solvent evaporation method. The encapsulating polymer is dissolved in a partially water-soluble solvent, such as propylene carbonate and saturated with water. The polymer-water saturated solvent phase is emulsified in an aqueous solution, already containing a stabilizer, leading to solvent diffusion to the external phase and the formation of nanospheres or nanocapsules, according to the oil-to-polymer ratio. Finally, the solvent is eliminated by evaporation.

Salting out method: it is a modification of the solvent displacement method, in which the separation of a water miscible solvent from aqueous solution is via a salting out effect. Polymer and drug are initially dissolved in a solvent such as acetone, which is subsequently emulsified into an aqueous gel containing the

salting-out agent (electrolytes, such as magnesium chloride, calcium chloride, and magnesium acetate, or non-electrolytes such as sucrose) and a colloidal stabilizer such as polyvinylpyrrolidone or hydroxyethylcellulose. This oil/water emulsion is diluted with a sufficient volume of water or aqueous solution to enhance the diffusion of acetone into the aqueous phase, thus inducing the formation of nanospheres.

Dialysis: polymer is dissolved in a water miscible solvent and placed inside a dialysis tube with proper molecular weight cut off. The displacement of the solvent inside the membrane is followed by the progressive aggregation of polymer, due to a loss of solubility and the formation of homogeneous suspensions of nanoparticles. The solvent used in the preparation of the polymer solution affects the morphology and particle size distribution of the nanoparticles obtained.

Supercritical fluid technology: polymer is dissolved in a supercritical fluid to form a solution, followed by the rapid expansion of the solution across an orifice or a capillary nozzle into ambient air or in an aqueous solution. The high degree of super saturation, accompanied by the rapid pressure reduction in the expansion, results in homogenous nucleation and, thereby, the formation of well-dispersed particles.

Even top-down methods have been developed taking advantage of instruments such as desktop or high-pressure homogenizers or ball-milling equipment able to reduce the particle size from micrometres to nanometres.[vi]

3.3 ANTITUMOUR DRUGS

Cancers are a large family of diseases that involve abnormal cell growth with the potential to invade and/or spread to other parts of the body. All tumour cells show the five hallmarks: a) cell growth and division in absence of the proper signals or in presence of contrary ones; b) avoidance of programmed cell death; c) limitless number of cell divisions; d) promoting blood vessel construction; and e) tissue invasion and metastasis formation.[vii]

Cancers figure among the leading causes of morbidity and mortality worldwide, with approximately 14.0 million new cases and 8.2 million cancer related deaths in 2012.[viii]

FORMULATION OF PLGA-g-PVP COPOLYMERS

Research aims at developing ever more potent treatments, able to get definitive ablation of the disease.

3.3.1 Doxorubicin

Doxorubicin hydrochloride (Adriamycin®)[ix,] is one of the most potent antineoplastic agents approved by the Food and Drug Administration, effective against a wide range of cancers, including breast cancer[x,xi], myeloma[xii], lung cancer[xiii], glioma[xiv], leukaemia[xv], and lymphoma[xvi].

Its cytotoxic role is explicated in nuclear compartment of cells, by binding DNA associated enzymes[xvii] and intercalating the base pairs of the DNA's double helix with consequently inhibition of both DNA replication and RNA transcription. [xviii,xix]

Doxorubicin in form of hydrochloride salt (Dox) achieves a high degree of solubility in water; conversely, doxorubicin in the free base form (Dox$_B$) is hydrophobic. Dox has a high biodistribution, it is quickly accumulated into many tissues (like liver, kidney, bone marrow), leading to a rapid extinction in the blood stream.[xx,xxi] It is not selective against tumour cells, therefore it results toxic for the healthy cells, in particular is considered cardiotoxic.[xxii]

Modification of biodistribution and reducing of toxicity toward healthy cells can be achieved by entrapping the drug in carriers.

Dox-loaded PLGA carriers are intensively studied in the literature. These systems include PLGA microparticles,[xxiii,xxiv,xxv,xxvi,xxvii] PLGA NPs,[xxviii,xxix,xxx,xxxi,xxxii,xxxiii,xxxiv] PLGA-PEG micelles,[xxxv,xxxvi,xxxvii,xxxviii] covalently bounded PLGA-Dox NPs,[xxxix] PLGA-Dextran micelles,[xl] [P(NIPAAm-co-DMAAm)-PLGA micelle,[xli] hyaluronic acid NPs coated with PLGA-PEI,[xlii,xliii] magnetic NPs coated with PLGA,[xliv,xlv,xlvi] PLGA-Vitamin E TPGS NPs,[xlvii] PLGA-laponite-F68 nanocomposite (PNC) vesicles,[xlviii] magnetic NPs coated with PLGA-PEG,[xlix] PEG-PLGA-porphirin NPs[l].

3.3.3 Aim of research

In this research work PLGA-g-PVP NPs are prepared by solvent displacement method to be used in antitumor treatment.

Despite great benefits obtained by using above carriers in Dox delivery, they suffer of some drawbacks in term of efficacy and stability over time, as already

mentioned. Microparticles cannot reach tumour and need to be *in situ* implanted. Micelles are prone to dilution phenomenon that occurred when intravenous injected, leading to premature drug release.[li] Hydrophobic NPs coated by hydrophilic had poor affinity, sometimes leading to separation of the two blocks over time. NPs based on amphiphilic copolymers, like those obtained from PLGA-g-PVP copolymers, should not be prone to these pitfalls. Modulating PVP content in the initial PLGA-g-PVP copolymer, it was possible to vary the hydrophobicity degree of NPs matrix and, thus, affinity of nanocarrier with drugs with different lipophilicity. Drugs used to study NPs properties were Dox and its basic analogue doxorubicin base (Dox_B).

Chemical-physical characterizations of NPs were conducted by evaluation of sizes, morphologies, ζ-potentials, pH and osmolarities. Over time stability and drug release kinetics were studied. To highlight efficacy against tumour cells Dox-loaded NPs and Dox_B-loaded-NPs, 2D and 3D *in vitro* studies were carried out.

3.4 ANTIMALARIAL DRUGS

Malaria is the most prevalent parasitic disease in the world. By 2015, it was estimated that the worldwide number of malaria cases is 214 million and the number of deaths to 438 000.[lii] It is caused by the apicomplex protozoan of the *Plasmodium* genus and transmitted to humans by the bites of the female mosquito vector of the *Anopheles* genus.[liii,liv] *P. falciparum* is the most dangerous of the four malarial parasites that can infect humans and is most prevalent on the African continent. *P. falciparum* resists to rigorous climate and has developed resistance to several drugs.[lv]

Nanosized carriers have been receiving special attention with the aim of minimizing the side effects of drug therapy, poor bioavailability and drug resistance. Particularly lipid-based carriers (e.g., liposomes,[lvi,lvii,lviii,lix] solid lipid nanoparticles[lx,lxi,lxii] and nano or microemulsions[lxiii,lxiv,lxv]) and polymeric nanocarriers [lxvi,lxvii,lxviii,lxix] have been already studied. All these nanocarriers are currently used to fight the disease with good results.

3.4.1 Artemisinin as antimalarial drug

Artemisinin (Art) is a sesquiterpene lactone peroxide, extracted from the wormwood *Artemesia annua Longa*. Usually used as anti-malarial drug, anticancer activity of Art was discovered by Woerdenbag et al in 1990.[lxx] Art and its derivatives (dihydroartemisinin, arthemeter, and artesunate) are the most used antimalarial drugs together with quinine derivatives (chloroquine, primaquine and mefloquine). Artemisinin has a very fast action and parasite clearance times are shorter when compared with other malarial drugs. Cytotoxicity of Art is explicated by the endoperoxide moiety present in its structure that reacts with Fe^{2+} ions present in haem (Figure 3.2).[lxxi]
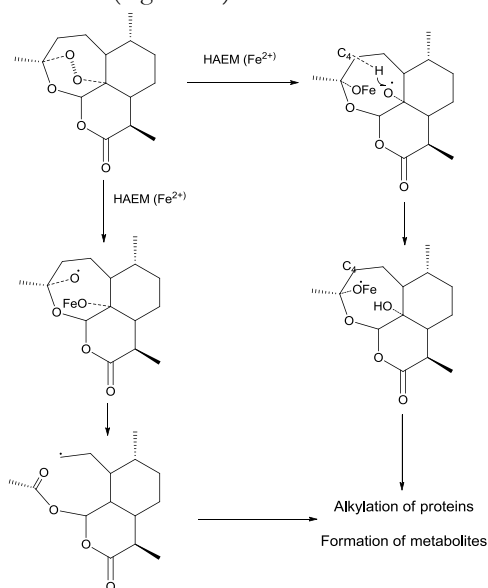
Figure 3.2. Mechanism of interaction of Art with Fe^{2+} present in haem, leading to radicals.

The malaria parasite is rich in haem-iron, derived from the proteolysis of host cell haemoglobin. This could explain why artemisinin is selectively toxic to parasites.[lxxii] In parasite cultures treated with Art, adducts of haem and Art have been isolated.[lxxiii] Free radicals formed by the reaction alkylate protein and damage the microorganelles and membranes of the parasites.[lxxiv] Drawbacks of

FORMULATION OF PLGA-g-PVP COPOLYMERS

Art are low water and oil solubility, poor bioavailability, and a short half‑life in vivo (~2.5h).[lxxv,lxxvi] For these reasons, it is usually loaded in several drug delivery systems, such as nanoparticles[lxxvii] and liposomes[lxxviii,lxxix]. Liposomal formulation of Art for antimalarial treatments is reported.[lxxx,lxxxi] Cyclodextrins[lxxxii,lxxxiii,lxxxiv] and albumin-Art conjugated[lxxxv] are other typical nanocarriers. Only one formulation study of Art-loaded PLGA NPs was described in the literature.[lxxxvi] Art derivatives loaded in PLGA carriers are reported, *e.g.* artesunate-loaded and chitosan-coated PLGA NPs,[lxxxvii] dihydroartemisinin-loaded and PLGA-coated phospholipidic NPs[lxxxviii].

3.4.2 Curcumin

Curcumin (Cur) is a polyphenolic compound derived from turmeric, *Curcuma Longa* rhizomes, possesses diverse pharmacologic effects including anti-inflammatory,[lxxxix] antioxidant[xc] and anticancer activities[xci,xcii] In addition, curcumin possesses activities against bacteria,[xciii] fungi,[xciv,xcv] and protozoa[xcvi]. Cytotoxic effects of Cur on protozoan parasites have been demonstrated in cultures against *Leishmania*,[xcvii] *Trypanosoma*,[xcviii] *and Giardia*[xcix]. Cur antimalarial effects was demonstrated against *Plasmodium falciparum*[c,ci] and *Plasmodium Berghei*[cii] (the latter in combination with Art). Parasitical effect is due to the generation of reactive oxygen species and histone acetylation.[ciii] An excellent property of Cur is its safety even at very high doses when administrated to various animal models[civ] and humans[cv,cvi]. In spite of its efficacy and safety, Cur has not yet been approved as a therapeutic agent, due to its low solubility and low bioavailability.[cvii] To overcome these problems several carriers have been developed, among which nanotized Cur,[cviii] liposomal carrier,[cix] chitosan NPs,[cx] nanoemulsion,[cxi] lipid based systems,[cxii] sodium dodecyl sulphate (SDS) micelles,[cxiii] PMMA-PHEMA nanospheres[cxiv], PLGA-coated magnetic microspheres[cxv] and PLGA NPs[cxvi,cxvii,cxviii].

3.4.3 Aim of research

Even if a current decrease of mortality and morbidity due to malaria is reached, improvements are always requested, especially in formulations of monodose, not expensive treatments with prolonged permanence in bloodstream and

sustained release of drugs. This route is possible only developing carrier with real high drug entrapping degree and modified surface.

Lipid nanocapsules consisting of an oily core and PLGA-g-PVP surface were used as delivery systems of Cur and Art. The oily core chose to dissolve great amounts of drug was prepared by oil in water emulsion leading to microdrops in aqueous solution. Nanometric sizes were reached by using of high-pressure homogenizer. PLGA-g-PVP copolymers with two different PVP contents were deposited on, employing solvent displacement method. Modified surfaces were useful to modulate interactions between nanocapsules and cellular membranes of infected red blood cells in order to favour endocytosis inside. Chemical and physical characterizations of Art-loaded nanocapsules and Cur-loaded nanocapsules were carried out. Growth inhibition assay were conducted on *plasmodium falciparum* (3D7) culture.

3.5 ANTITUMORAL PROJECTS EXPERIMENTAL PART

3.5.1 METHODS

3.5.1.1 Materials

PLGA-PVP$_{10:1}$ and PLGA-PVP$_{10:2}$ were prepared according to the procedure reported in Chapter 2, Paragraphs 2.3.4.1. Poly(lactic-co-glycolic) acid (PLGA) 50:50 ($\bar{M}_n$= 45000-55000) was purchased from PolySciTech (Indiana, USA) and used as received. Doxorubicin hydrochloride salt (Dox) was purchased from Pharmacia & Upjohn; doxorubicin base (Dox$_B$) was prepared as following described and used without further purification. Pluronics F68 (Plu), Tween 20, Tween 80, poly(vinyl alcohol) (PVA), mucin from porcine stomach, bovine serum albumin (BSA) and other chemicals and solvents were supplied by Sigma- Aldrich (Italy) at reagent grade and used without further purification. For *in vitro* tests:

4T1 (mouse breast cancer), MDA-MB231 and CRL-2335 (human breast cancer) cells were obtained from the American Type Culture Collection (ATCC; Manassas, VA, USA). Human HCC1806 Breast Carcinoma cell line was purchased from LGC Standards, Sesto San Giovanni, Italy. Dulbecco's Modified Eagle Medium (DMEM), penicillin-streptomycin and foetal calf

serum were purchased by Invitrogen, Burlington, ON, Canada. MTT (3-(4,5-Dimethylthiazol-2-yl)-2,5diphenyltetrazolium bromide, thiazolyl blue tetrazolium bromide, RPMI medium and ultra-low attachment (ULA) 96-wells flat-bottom plates were supplied by Sigma- Aldrich St Louis, MA, USA. Colorimetric WST-1 test was obtained from Dojindo Europe, Germany.

3.5.1.2 Preparation of doxorubicin base

A saturated solution of Na_2CO_3 (1.4 g/mL) was added in deionized water Dox solution drop by drop. The precipitate was recovered by filtration and washed several times with cold deionised water. After drying, Dox_B was stored at room temperature in the dark.

3.5.1.3 Preparation of PLGA-PVP$_{10:1}$, PLGA-PVP$_{10:2}$ blank NPs and Dox- or Dox$_B$-loaded NPs

Doxorubicin-loaded and blank nanoparticles were prepared using a solvent displacement method. Briefly, different amount of Dox or Dox_B (1, 2 or 3 mg) were dissolved in benzyl alcohol (15 mg/mL) and added to a solution of 21 mg of PLGA-PVP$_{10:1}$ (or PLGA-PVP$_{10:2}$) in 800 µL 85:15 v/v acetone DMSO solution. This solution was drop-wise added to 7 mL of a 0.1 % (w/v) Pluronics F68 aqueous solution heated at 40°C under vigorous magnetic stirring. Following acetone was removed by 30 min of magnetic stirring and the suspension was kept under stirring overnight. Then the suspension was dialyzed against water using a dialysis tube with MW cut-off of 3500 for 1 h to remove any not encapsulated drug, benzyl alcohol and DMSO and lastly lyophilized.

Blank nanoparticles were similarly prepared. A 70:30 v/v acetone/DMSO polymeric solution (21 mg in 400 µL) was dripped in a 0.1 % (w/v) Pluronics F68 aqueous solution under vigorous magnetic stirring at 40°C. The latter was stirred for 30 min to remove acetone and kept under stirring overnight to form nanoparticles and eventually lyophilized.

FORMULATION OF PLGA-g-PVP COPOLYMERS

3.5.1.4 Physical-chemical characterization of NPs

Particle size and polydispersion index (PDI) were determined by photon correlation spectroscopy (PCS), employing a 90 PLUS Particle Size Analyzer at a fixed angle of 90° and a temperature of 25 °C. The laser light (He/Ne) wavelength was 678 nm. Two drops of sample were diluted directly into the cuvette sample holder with previously filtered water. All determinations were carried out in triplicate and the results were expressed as the average diameter (expressed in nm) and PDI as measure of the distribution width.

Differential scanning calorimetric (DSC) analyses were performed by a Mettler Toledo DSC823 (Mettler Toledo, Italy), equipped with the STAR Software and the FRS5 Mettler Toledo ceramic sensor. The instrument was calibrated with indium for melting point and heat of fusion. Tests were performed using standard aluminium pans with an empty pan as reference. Samples (5-10 mg) underwent a single heating step from 0 °C to 100 °C at 10 °C min^{-1} under 50 mL min^{-1} nitrogen flow.

Zeta potential measurements were determined using 90 PLUS Particle Size Analyzer. Nanoparticle solution was diluted with few drops of a 1 mM KCl solution. A minimum of five runs was obtained per sample.

Transmission electron microscopy (TEM) analysis was performed using a Philips CM10 instrument. Nanoparticle solution was stained with a 2% solution of osmium tetraoxide.

Optical microscopy analysis was carried out using a Motic AE 31inverted microscope equipped with Motic MHG – 100B using Ex D350/50x, DM 400DCLP and BA D460/50m. Magnification LWD 600x.

Osmolarity was measured using Semi-micro osmometer K-7400 with measuring head for glass vessels. 300 mOsmol solution of sodium chloride used for reference standard.

The pH was determined at 25°C by a calibrated pH meter 420 A (Orion).

3.5.1.5 Assay of doxorubicin loaded into NPs

The doxorubicin loading within NPs was determined by HPLC. HPLC system consists of a Shimadzu LC-9A pump C equipped with a Cromopack fluorescence detector and a Kinetex® 5 μm EVO C 18 100 Å column (250 ×4.6 mm²). Methanol-acetonitrile-phosphate buffer solution (10:25:65 v/v/v)

was used as eluent, in which buffer was a 0.01 M pH=1.4 phosphate aqueous solution. The flow rate was 1.0 mL min^{-1}. The column effluent was monitored at excitation and emission wavelengths of 480 and 560 nm, respectively.

A known amount of freeze-dried nanoparticles was completely dissolved in DMSO solution and after diluted in HPLC eluent. Drug concentration was calculated from the area using a calibration curve previously established.

For the calibration curve Dox was dissolved directly in HPLC eluent, Dox$_B$ was firstly dissolved in DMSO and after diluted with HPLC eluent. The experiment was performed in triplicate for both types of drugs.

Drug loading (DL) was calculated on the percentage amount of drug present per mg of nanoparticles, as follows:

$$D.L.\% = \frac{(\text{Concentration of drug (mg/mL)} \times \text{Solution volume (mL)})}{\text{Nanoparticles mass (mg)}} \times 100\%$$

(Equation 1)

Encapsulation efficiency (EE) was calculated based on the percentage ratio of the amount of doxorubicin incorporated into nanoparticles with respect to the initial amount used, as follows:

$$E.E.\% = \frac{\text{Encapsulated drug mass (mg)}}{\text{Initial drug mass (mg)}} \times 100\% \qquad \text{(Equation 2)}$$

3.5.1.6 *In vitro* release of doxorubicin from nanoparticles

In vitro drug release studies were performed at two different pHs by using a physiological solution (0.9% NaCl, pH = 5.55) and phosphate buffer solution (0.1 M, pH = 7.40). 1 mL of Dox-loaded and Dox$_B$-loaded nanoparticle suspensions (donor solutions) were kept in contact with 1 mL of physiological solution or buffer solution (receiver solutions) by a dialysis membrane with MW cut-off 12-14K. At specific time, the receiver solution was collected for analysis and replaced with fresh one. The amount of released doxorubicin was evaluated by HPLC as previously described.

3.5.1.7 Determination of bovine serum albumin (BSA) adsorption on NP surface

Interactions of BSA with selected NPs were monitored using a UV visible spectrophotometer. Lyophilized blank NPs were suspended in water (1.6 mg/mL) and diluted with a 10 mg/mL phosphate buffer BSA solution (0.1 M, pH = 7.4) in 20:80 volume ratio. Solution was stirred for 90 min, centrifuged (7500 rpm, 10 min) and then the supernatant was collected. The amount of BSA adsorbed on nanoparticles surface was evaluated using Uv-visible analysis at 278 nm taking into account the difference between BSA concentration present in the supernatant and a blank BSA solution at the same dilution. Each sample was assayed in triplicate.

3.5.1.8 Cell and culture conditions

4T1 (murine breast cancer), MDA-MB231 (human breast adenocarcinoma) and CRL-2335 (basal-like human breast carcinoma) cell lines were grown in culture dishes as a monolayer in DMEM supplemented with 10% penicillin-streptomycin and 10% foetal calf serum in a humidified atmosphere with 5% CO_2.

3.5.1.9 Cell proliferation test

MTT analysis was performed in 96-well plates incubated at 37 °C, 5% CO_2, for 72 h. Briefly, 1000 cells/well were seeded in 100 μL of complete medium and treated with different concentrations of Dox-loaded NPs (0.002-0.2 mM) and compared to those treated with blank NPs and free drug solutions at the same dilution. Subsequently, cells were supplemented with 11 μl of 5mg/ml thiazolyl blue tetrazolium bromide for 2 h. Later, the medium was removed and cells were lysed with 100 μl of DMSO. Absorbance was recorded at 570 nm by a 96-well-plate reader (PerkinElmer, Waltham, MA, USA).

3.5.1.10 Data analysis

Data concerning inhibition percentage as function of drug concentration are reported as average ± experimental error. A statistical analysis was performed with GraphPad Prism 3.0 software (San Diego, CA, USA) using the one-way

ANOVA and Dunnett test. IC_{50} (half maximal inhibitory concentration) has been investigated using the two tailed unpaired T test with Welch correction. The significance cut-off was p-value below 0.05.

3.5.1.11 Spheroids cultures

The human HCC1806 Breast Carcinoma cell line was grown in RPMI medium supplemented with 10% foetal bovine serum (FBS), 1% L-glutamine and 1% penicillin-streptomycin.

For spheroids formulation, at ~80% confluence, monolayer cells were dissociated with trypsin-EDTA (Ethylenediaminetetraacetic acid) into single-cell suspensions. The cells were then seeded on ultra-low attachment (ULA) 96-wells flat-bottom plates, at different initial concentrations, starting from 2500 to 50000 cells per well. Optimal seeding density was established such that HCC1806 spheroids fell within a size range of 200 to 500 μm in diameter on day 5. The initial concentration of 7500 cells/well was then considered appropriate for experimental studies.

After treatments with the different drug formulations, morphology was analysed under light microscope and cell viability by colorimetric WST-1 test.

3.5.2 RESULTS AND DISCUSSIONS: DOXORUBICIN LOADED NPs

3.5.2.1 Blank nanoparticle preparation

PLGA-PVP blank nanoparticles (PLGA-PVP Blk NPs) were successfully prepared using an solvent displacement method by dissolving copolymer (26 mg/mL) in organic solvent mixture (85:15 %v/v acetone:DMSO) and precipitating it as nanoparticles in an aqueous phase, having 0.1% w/v Pluronics F68 as a stabilizer, at 40°C (Figure 3.3). PLGA blank nanoparticles were similarly prepared.

This procedure was the result of a study performed for correlating the relationship between formulation parameters (namely, solvent composition, surfactant type and concentration, copolymer concentration, pH of aqueous

solution and temperature) and NP diameters. The collected data corresponding to PLGA-PVP$_{10:1}$ and PLGA-PVP$_{10:2}$ NPs are summarized in Tables 1 and 2. As results, NP size was highly influenced by solvent composition with a reduction of about 30 and 200 nm for PLGA-PVP$_{10:1}$ and PLGA-PVP$_{10:2}$, respectively, passing from pure acetone (DMC in Tables 3.1 and 3.2) to 85:15%v/v acetone:DMSO solution. This reduction can be ascribed to the higher solubilisation of PVP portion copolymer in DMSO. Poly(vinylalcohol) (PVA), glycerol, glucose and Pluronics F68 (Plu) were chosen as preferred surfactants; among them, Plu gave the smallest NPs with both copolymers in comparison with those prepared with the other surfactants in the same experimental condition. In addition, Plu concentration in water has proven to slightly affect the size distribution of PLGA-PVP$_{10:2}$ NPs, but highly influence those of PLGA-PVP$_{10:1}$ NPs. In particular, PLGA-PVP$_{10:1}$ precipitated in total absence of surfactant and formed particles of about 1 μm in presence of 0.5%w/v Plu solution, instead of 166 nm using 0.1%w/v one. PLGA-PVP$_{10:2}$ was able to form NPs even in absence of surfactants with formation of a thin film close adherent to vial walls and 134 nm particles in presence of the more concentrated Plu solution, minimum (131 nm) was also in this case fulfilled in 0.1%w/v solution. Finally, temperature of aqueous Plu solution influenced the rate of displacement and evaporation of solvents, resulting in a decreased NP diameter at 40°C instead of those obtained at room temperature, but 60°C heated solution favoured precipitation for both copolymeric compositions. High-pressure homogenizer was not able to a further reduction of NPs, conversely 426 and 335 nm were the final diameters of PLGA-PVP$_{10:1}$ and PLGA-PVP$_{10:2}$ NPs, respectively, after 30 min of treatment.

FORMULATION OF PLGA-g-PVP COPOLYMERS
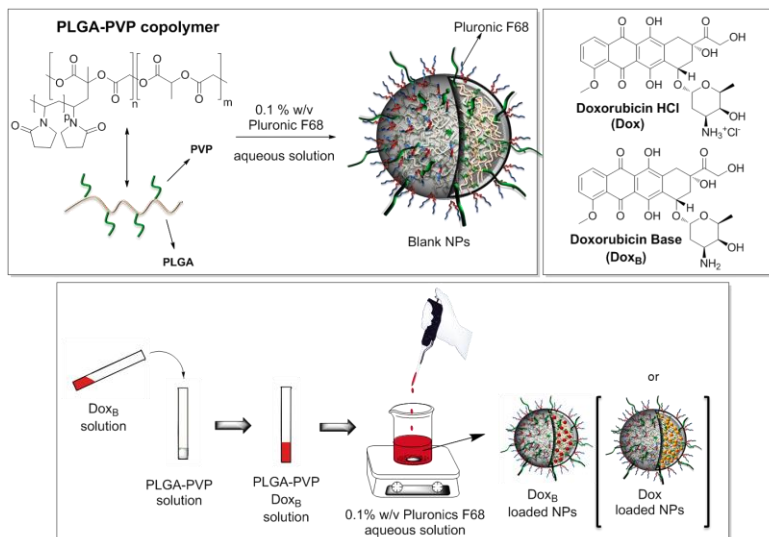
Figure 3.3. Preparation of PLGA-PVP Blk NPs and Dox$_B$ loaded and Dox loaded NPs by solvent displacement method. Chemical structure of Dox and Dox$_B$.

Table 3.1. Formulation parameters affecting PLGA-PVP$_{10:1}$ NPs size distribution.

PLGA-PVP$_{10:1}$ (mg)	Solvent /(µL)	Surfactant (%w/v)/ Vol (mL)	Size (nm)	PDI
10	DMC/ 200	Plu 0.1 / 5	222.2 ± 1.4	0.043 ± 0.013
10	DMC/ 200	Glycerol 2.4 / 5	280.6 ± 6.9	0.061 ± 0.029
10[a]	DMC/ 400	Plu 0.1 / 7	107.8 ± 0.9	0.153 ± 0.017
10[b]	DMC/ 400	Plu 0.1 / 7	109.3 ± 1.8	0.148 ± 0.021
21	DMC/ 800	Plu 0.1 / 7	210.4 ± 2.1	0.125 ± 0.016
21	DMC/ 800	PVA 0.3 / 7	216.0 ± 3.3	0.064 ± 0.013
21	DMSO:DMC 1:2/800	Plu 0.1 / 7	184.1 ± 5.9	0.061 ± 0.028
21[c]	DMSO:DMC 1:2/800	Plu 0.1 / 7	426.4 ± 15.7	0.194 ± 0.031
21[d]	DMSO:DMC 1:10/800	Plu 0.1 / 7	181.4 ± 6.1	0,105 ± 0,024
21[d]	DMSO:DMC 15:85/800	Plu 0.1 / 7	166.7 ± 0.8	0.115 ± 0.028

FORMULATION OF PLGA-g-PVP COPOLYMERS

21d	DMSO:DMC 15:85/800	Plu 0.5 / 7	897.3 ± 28.7	0.086 ± 0.046
21d	DMSO:DMC 15:85/800	only water/ 7	precipitate	--
21d	DMSO:DMC 15:85/800	NaCl 0.9 / 7	precipitate	--
21d	DMSO:DMC 15:85/800	Glucose 5 / 7	260.4 ± 9,7	0.142 ± 0.043
21e	DMSO:DMC 15:85/800	Plu 0.1 / 7	304.9 ± 7.5	0.231± 0.051

a) Dialysis against water milliQ; b) dialysis against 0.01M PBS buffer solution at pH=7.4; c) after 30 minutes of high pressure homogenization; d) temperature= 40°C; e) temperature= 60°C.

Table 3.2. Formulation parameters affecting PLGA-PVP$_{10:2}$ NPs size distribution.

PLGA-PVP$_{10:2}$ (mg)	Solvent /(μL)	Surfactant (%w/v)/Vol(mL)	Size (nm)	PDI
10	DMC/200	Plu 0.1 / 5	363.9 ± 4.2	0.141 ± 0.013
10	DMC/200	Glycerol 2.4 / 5	348.4 ± 10.7	0.238 ± 0.032
10a	DMC/400	Plu 0.1 / 7	216.0 ± 15.2	0.286 ± 0.011
10b	DMC/ 400	Plu 0.1 / 7	239.5 ± 2.5	0.274 ±0.001
21	DMC/ 400	Plu 0.1 / 7	318.1 ± 4.7	0.105 ± 0.039
21	DMC/ 400	PVA 0.3 / 7	329.2 ± 6.9	0.152 ± 0.022
21	DMSO:DMC 1:1/400	Plu 0.1 / 7	168.0 ± 2.6	0.115 ± 0.028
21c	DMSO:DMC 1:1/400	Plu 0.1 / 7	335.6 ± 3.2	0.098 ± 0.047
21d	DMSO:DMC 2:8/400	Plu 0.1 / 7	160.4 ± 1.7	0.093 ± 0.039
21d	DMSO:DMC 3:7/400	Plu 0.1 / 7	161.7 ± 0.6	0.064 ± 0.008
21d	DMSO:DMC 3:7/400	Plu 0.5 / 7	164.0 ± 2.0	0.066 ± 0.022
21d	DMSO:DMC 3:7/400	only water/ 7	166.2 ± 1.0	0.046 ± 0.023
21d	DMSO:DMC 3:7/400	NaCl 0.9 / 7	187.9 ± 5.2	0.034 ± 0.029
21d	DMSO:DMC 3:7/400	Glucose 5 / 7	204.4 ± 6.8	0.068 ± 0.019
21e	DMSO:DMC 3:7/400	Plu 0.1 / 7	153.4 ± 2.9	0.157 ± 0.042

a) Dialysis against water MilliQ; b) dialysis against 0.01M PBS buffer solution at pH=7.4; c) after 30 minutes of high pressure homogenization; d) temperature= 40°C; e) temperature= 60°C.

3.5.2.2 Drug loaded nanoparticle preparation and drug assay

Next step was the preparation of PLGA-PVP NPs loaded with doxorubicin hydrochloride salt (Dox) and doxorubicin free base (Dox_B). Several water miscible solvents (namely, acetone, methanol, ethanol, N-methylpyrrolidone, and benzyl alcohol) were tested to solubilise drugs. In detail, both forms of doxorubicin have proven to be practically insoluble in acetone. Methanol and ethanol were not compatible with copolymers causing their partial precipitation. When drugs are solubilised in N-methylpyrrolidone and subsequently added to copolymer, a clear solution was obtained. Unfortunately, this solution became a microemulsion when dripped in water. At the end, benzyl alcohol has proven as the best drug solvent; indeed, 15 mg/mL Dox and Dox_B solutions in benzyl alcohol were prepared and separately added to copolymeric acetone/DMSO ones giving a transparent orange and red solutions, respectively. These recipes were slowly added to a 0.1% Plu aqueous solution in order to formulate drug-loaded NPs.

In order to assess the drug loading percentage (D.L.%) and encapsulation efficiency percentage (E.E. %), three drug loadings (1, 2 or 3 mg) were tested for each copolymer composition and drug. To this aim, samples were dialyzed, lyophilised and analysed by HPLC.

As reported in Table 3.3, D.L. % of Dox was found to be between 0.73 and 3.32% w/w depending on copolymer type, resulting in a E.E. % ranged between 21.16 and 55.89% w/w. PLGA-PVP$_{10:2}$ always showed at least one percentage point more than PLGA-PVP$_{10:1}$ regardless of initial Dox amount. This finding can be attributed to the enhanced hydrophilicity of the PLGA-PVP$_{10:2}$ copolymer, resulting to a higher affinity with hydrophilic Dox. On the other hand, in the case of Dox_B, D.L. % varied from 0.11 to 3.20 % w/w and E.E.% from 19.11 to 36.24 % w/w. Save for 1mg case, in all other ones, PLGA-PVP$_{10:1}$ showed a better affinity with Dox_B than PLGA-PVP$_{10:2}$.

For comparison, Dox- and Dox_B- loaded PLGA NPs and blank PLGA NPs were similarly prepared as control. 3 mg of initial amounts of drugs were used.

FORMULATION OF PLGA-g-PVP COPOLYMERS

Really low D.L. % and E.E.% were obtained for Dox-loaded PLGA NPs, instead of Dox_B loaded PLGA NPs that showed the greater D.L.% value (3.69%) among others.

Table 3.3. Drug loading percentage and encapsulation efficacy varying doxorubicin amount initially added in solution.

Sample	Doxorubicin initial amount (mg)	D.L. % (w/w)	E.E %(w/w)
Dox-PLGA-PVP$_{10:1}$ NPs	1	0.73	21.2
	2	1.67	22.6
	3	2.55	21.3
Dox-PLGA-PVP$_{10:2}$ NPs	1	1.93	55.9
	2	2.76	38.7
	3	3.32	30.9
Dox$_B$-PLGA-PVP$_{10:1}$ NPs	1	1.14	33.0
	2	1.30	21.5
	3	2.27	24.2
Dox$_B$-PLGA-PVP$_{10:2}$ NPs	1	0.65	19.1
	2	1.36	21.2
	3	3.20	36.2
Dox-PLGA NPs	3	0.06	4.13
Dox$_B$-PLGA NPs	3	3.69	24.0

Physical state of the drug in PLGA-PVP NPs were investigated by DSC. Thermograms of Dox, Dox_B, copolymers alone, Plu, black NPs, and drug-loaded NPs were depicted in Figure 3.4 (Panel A-C). In blank NP thermograms an endothermic peak is present at 40-55°C corresponding to Plu melting point that partially covered PLGA glass transition temperature ranged at 45-53°C in copolymer thermograms. In all, PVP glass transition temperature was not visible. Dox exhibited a single endothermic melting peak at 236°C with onset at 180°C. Dox_B showed an exothermic peak at 220°C with onset at 170°C, due to its degradation.

FORMULATION OF PLGA-g-PVP COPOLYMERS
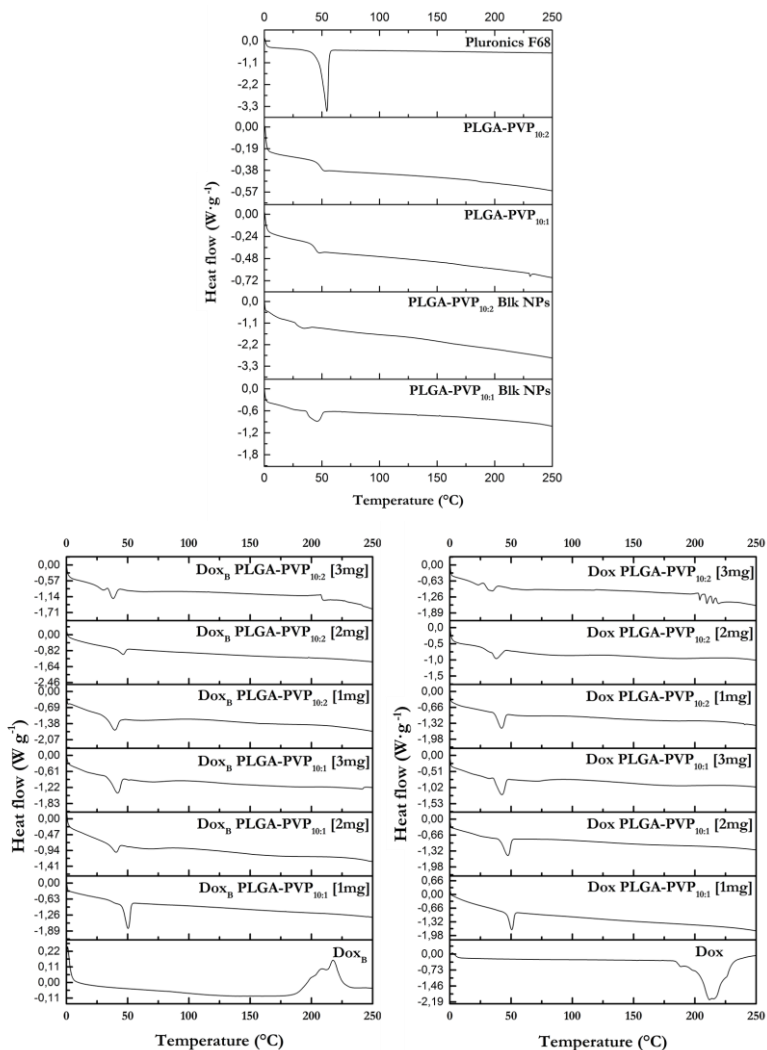
Figure 3.4. DSC thermograms of A) copolymers alone, pluronics, black PLGA-PVP NPs B) Dox_B free and Dox_B-loaded PLGA-PVP NPs and C) Dox free and Dox-loaded NPs.

In DSC thermograms of Dox-loaded and Dox_B-loaded PLGA-PVP NPs, Dox melting peak disappeared, as well as the degradation one of Dox_B, regardless to them initial loading. In addition, Plu melting point was always present. This indicated the absence of drug free in the delivery system and, thus, it was totally incorporated inside nanoparticles. Therefore, 3 mg of Dox and Dox_B were subsequently used as the standard concentration to prepare drug-loaded NPs.

3.5.2.3 Characterization of PLGA-PVP NPs

The physicochemical properties of NPs, in terms of their average diameter, polydispersity index, ζ potential, morphology, pH and osmolarity were evaluated and listed in Table 3.4 and Figure 3.5 and 3.6. The effect drug incorporation on such properties was also studied by comparing the results obtained with those for blank NPs, whose size and polydispersity index are also reported in order to facilitate result interpretation.

With respect to particle size analysis, all prepared PLGA-PVP systems were nanometric (average diameter <500 nm) and exhibited a narrow size distribution (polydispersity index <0.2). Freshly prepared blank NP suspensions showed unimodal size distribution having the average values in the range of 160 - 170 nm (Figure 3.6). PLGA Blk NPs similarly prepared had greater dimensions than PLGA-PVP ones and showed an aggregate at 5 µm. Thus, a downtrend in the particle size was observed as PVP content in copolymer increased. Lyophilized PLGA-PVP blank NP formulations showed larger particle size in the range of 300-450 nm compared to freshly prepared particles; lyophilisation process might induced particle aggregation. NP size after freeze-dry indicates that either a cryoprotectant or sonication is needed for maintaining the original size of the particle suspension. Sonicating for 10 min of a suspension of lyophilized NPs in MilliQ water was successfully able to break the aggregate and reduce the size of the particles to almost its original size before lyophilisation. PLGA Blk NPs were not able to be resuspendable.

FORMULATION OF PLGA-g-PVP COPOLYMERS

Table 3.4. Physiochemical characterisation of PLGA-PVP NP and PLGA NP suspensions.

NPs	Size $\pm\sigma$ (nm)	PDI$\pm\sigma$	Zeta potential $\pm\sigma$ (mV)	pH	Osmolarity (mOsmol)
PLGA-PVP$_{10:1}$ Blk	166.7 ± 0.8	0.115 ± 0.028	-28.71 ± 2.28	4.26	320
After lyophilisation	450.3 ± 10.2	0.136 ± 0.026	N.E.	N.E.	N.E.
After sonication	175.9 ± 5.6	0.125 ± 0.012	N.E.	N.E.	N.E.
PLGA-PVP$_{10:1}$ Dox	406.2 ± 2.09	0.053 ± 0.037	-12.33 ± 2.77	4.76	302
PLGA-PVP$_{10:1}$ Dox$_B$	223.1 ± 15.5	0.162 ± 0.006	-20.12 ± 2.76	4.96	327
PLGA-PVP$_{10:2}$ Blk	161.7 ± 0.6	0.064 ± 0.008	-17.03 ± 2.50	4.10	318
After lyophilisation	312.7 ± 6.4	0.067 ± 0.023	N.E.	N.E.	N.E.
After sonication	172.0 ± 2.3	0.103 ± 0.056	N.E.	N.E.	N.E.
PLGA-PVP$_{10:2}$ Dox	180.9 ± 2.8	0.065 ± 0.031	-9.88 ± 4.20	4.64	254
PLGA-PVP$_{10:2}$ Dox$_B$	196.4 ± 9.4	0.121 ± 0.027	-12.56 ± 2.30	4.69	347
PLGA Blk	240.1 ± 2.0	0.146 ± 0.026	-39.09 ± 5.40	5.09	201
PLGA Dox	860.9 ±162.4	0.005 ± 0.003	-37.26 ± 2.61	5.82	365
PLGA Dox$_B$	183.3 ± 8.4	0.197 ±0.018	-40.74 ± 4.10	5.40	446

Blk = Blank; N.E. Not evaluated
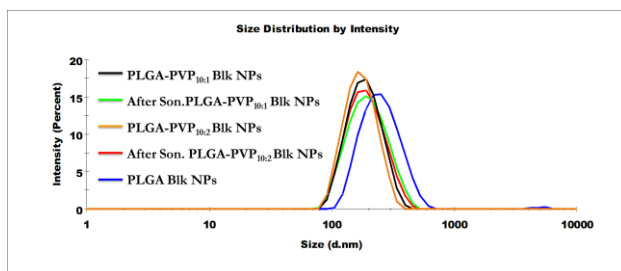
Figure 3.5. Size distribution by DLS of NPs before and after lyophilisation.

The drug addition to the formulations caused an increase of polymer particle size; despite this, such increase is considered acceptable for parenteral use. Its extent was affected by copolymer composition and drug form. With both drugs, PLGA-PVP$_{10:1}$ copolymer formed nanoparticles in solution always greater than those obtained using PLGA-PVP$_{10:2}$. This finding may be explained taking into account that a higher copolymer amount and relative higher PVP density are required by the system in order to completely cover all nanoparticles. PLGA-PVP copolymers formed NPs having different size in relation to the PVP content and drug form: indeed, PLGA-PVP$_{10:1}$ generated smaller NPs with the Dox$_B$, while the PLGA-PVP$_{10:2}$ with the Dox, accordingly to the drug hydrophilicity. The significant increment occurred in the case of Dox-loaded PLGA-PVP$_{10:1}$ NPs (three times respect to the reference, blank NPs), is likely due to a substantial change in their form, not observed elsewhere. In order to confirm this hypothesis, DLS data were supplemented with TEM observations (Figure 3.7). Dox-loaded PLGA-PVP$_{10:1}$ NPs showed rod-like morphologies with diagonals of 510 and 70 nm, respectively. Conversely, the other NPs exhibited approximately spherical morphologies with diameters consistent to those assessed by DLS.
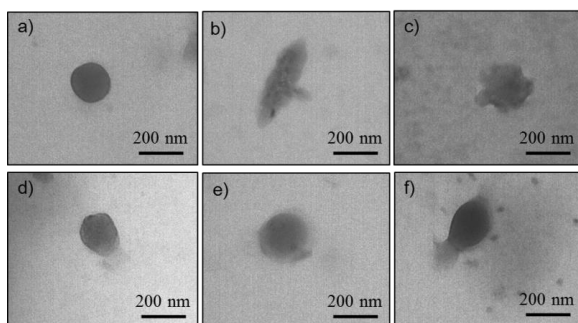
Figure 3.6. TEM images of a) Blk-PLGA- PVP$_{10:1}$ NPs; b) Dox-loaded PLGA- PVP$_{10:1}$ NPs; c) Dox$_B$-loaded PLGA- PVP$_{10:1}$ NPs; d) Blk-PLGA-PVP$_{10:2}$ NPs; e) Dox-loaded PLGA- PVP$_{10:2}$ NPs; f) Dox$_B$-loaded PLGA-PVP$_{10:2}$ NPs.

For a suspension system, zeta potential is an important index that reflects the intensity of repulsive forces among particles and the dispersion stability. Higher zeta potential modulus corresponds to higher repulsive forces.

Zeta potential of nanoparticles was negative due to the presence of terminal carboxylic groups in copolymers. Blank PLGA-PVP NPs zeta potential values ranged between −29 and −17 mV (PLGA-PVP$_{10:1}$ and PLGA-PVP$_{10:2}$, respectively) and were less negative than PLGA ones, namely, -39.9 mV. Probably, the lower negative value was due to the higher PVP density of copolymers, absent in PLGA NPs. The possibility that Plu chains on NP surface can also played a role in masking the surface charge of PLGA was also evaluated. No significant differences in the zeta potential values of PLGA NPs found in this work and typical ones reported in the literature (-40 mV) were observed. This showed that the residual Plu on the NP surface did not affect the real contribution of PVP density to surface charge reduction, hence surface properties of particles were only due to copolymer composition. The presence of Dox and Dox$_B$ in NPs always reduced the negative zeta potential value; probably, there was an additional masking effect of the superficial carboxylic groups by the drug in proximity of surface. This effect was intensified in the case of Dox due to the positive charge of quaternary ammonium group.

In order to determine whether nanoparticle suspensions may be incubated in cell cultures, pH and osmolarity were measured. The pH values of all suspensions were acidic, probably due to PVP protonation in water, ranging from 4.1 to 5.8. The osmolarity of PLGA-PVP suspensions were close to the isotonicity value (300 mOsmol), instead of PLGA suspensions that resulted ipertonic and, thus, requiring dilution. In conclusion, PLGA-PVP NP suspensions could be injected and kept in contact with cell cultures without further modifications. By this way, these systems were proven suitable for *in-vitro* tests.

3.5.2.4 *In vitro* drug release

It is well documented that the extracellular pH of tumours is slightly more acidic than the blood and normal tissue.[cxix] In addition, hypothesizing that nanoparticles are taken up by cells via an endocytosis process, pH drops to 5.5-6.0 in endosomes and approaches pH 4.5-5.0 in lysosomes.[cxx]

Therefore, *in vitro* release studies were performed in PBS (0.01 M, pH 7.4) and in physiological solutions (NaCl 0.9 %, pH 5.5) in order to evaluate the release kinetic of Dox or Dox$_B$ loaded NPs at the two different pHs. The cumulative release of drugs is shown in Figure 3.7. In Figure 3.8, release over 6 hours of

both drugs from Dox- and Dox$_B$-loaded PLGA NPs is reported. For all kinds of nanoparticles, the drug release followed a two-phase kinetics. In the first phase, the amount of drug released rapidly increases (burst effect). The second phase corresponds to a pseudo steady-state for which the release rate is constant and very slow.
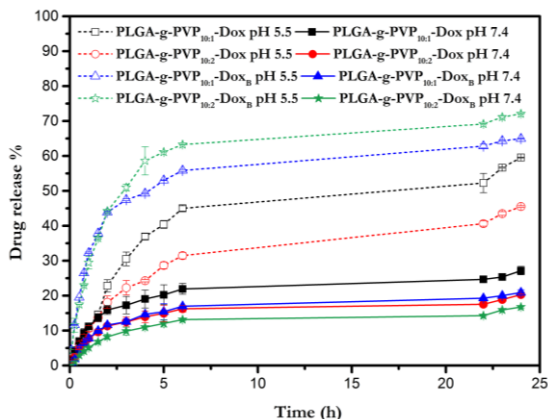
Figure 3.7. In vitro release profile of drug loaded in PLGA-PVP nanoparticles at different pHs.
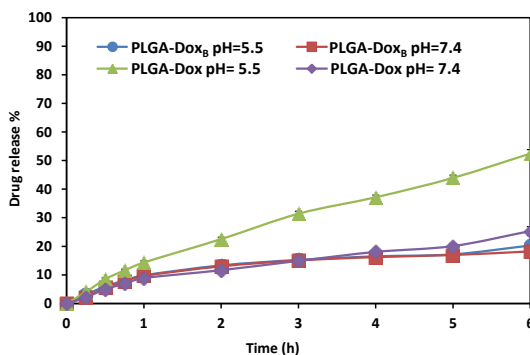
Figure 3.8. In vitro release profile of drug loaded in PLGA nanoparticles at different pHs.

At pH 7.4 both drugs were released in a lesser extent from different PLGA-PVP and PLGA NPs compared to those studied at pH 5.5. Specifically, within 6 h only about 10 - 20% of the doxorubicin was released; after 24 h the release rose to 25% as maximum, in the case of PLGA-PVP NPs. Lower amounts of drug released were detected, increasing PVP grating densities onto PLGA. PVP chains are easily oriented towards the NP surface, leading to effective surface coverage in the case of PLGA-PVP NPs, thus reducing the premature diffusion of drug towards the buffer aqueous phase. This might indicate the ability of the PLGA-PVP NP formulation to efficiently entrap and control Dox and Dox_B release over a prolonged period of circulation time, enough to reach tumour cells.

At pH 5.5, release percentage ranged between 30 and 65 % after 6 h for PLGA-PVP NPs, instead of 15-55 % in the case of PLGA NPs. The high extent of drug release was obtained in the case of Dox_B-loaded PLGA-PVP$_{10:2}$ NPs, in opposition to Dox_B-loaded PLGA NPs that released only the 15% of total amount of encapsulated drug. Other drug-loaded NPs had intermediate trend.

In literature, several mathematical models were developed in order to investigate the mechanism of drug release from nanoparticles/microparticles.[cxxi] The drug release depends on: i) adsorption or diffusion through the NP matrix, ii) particle erosion, iii) a combined erosion and diffusion process and iv) polymer degradation (chemical or enzymatic hydrolysis). The application of the correct mathematical model allowed for having informations about the release rate and mechanisms of drug release.[cxxii,cxxiii]

To study the mechanism of doxorubicin release from PLGA-PVP NPs, five mathematical models were taken in consideration: zero-order $(F=kt)$[cxxiv], first-order $(\ln(1-F)= -kt)$[cxxv], Higuchi´s model $(F=kt^{1/2})$[cxxvi], Hixon-Crowell´s model $(1-(1-F)^{1/3}= kt)$[cxxvii] and Korsmeyer-Peppas model, or "the power law", $(F=kt^n)$[cxxviii]. The squared correlation coefficients (R^2) and slope (rate constant, k) obtained after linear regression by mathematical models considering drug release fraction (F) and time (t), as respectively y and x variables, are listed in Table 3.5.

FORMULATION OF PLGA-g-PVP COPOLYMERS

In zero-order model, drug release would be directly proportional at time and totally independent of drug concentration; this means that release proceeds until the drug is totally consumed. Zero order release is typical of several types of delivery systems loaded with drugs with low solubility in water.[cviiii] In a first-order process, the rate of diffusion is directly proportional to concentration of the drug. First-order model describes the release profile from the delivery systems containing hydrophilic drugs dispersed in porous matrices.[cxxix] Hixon-Crowell model can be applied to the delivery systems whose drug release rate is proportional to the surface area of the system such as the erosion-dependent release systems. This model is used to describe the release profile keeping in mind the surface of the drug particles is diminished during the drug dissolution.

Using these three models to fit release curve of doxorubicin from PLGA-PVP NPs, the obtained squared correlation coefficients, that indicates how much the regression equation truly represent the set of data, is low. In particular, R^2 obtained with the zero-order model was ranged between 0.6 and 0.7. First-order kinetics gave a R^2 of 0.6-0.8. Hixson-Crowell's cube root model provided a R^2 of 0.6-0.8. Hence, these models cannot be used for describing the release from PLGA-PVP systems. A possible explanation was that Dox_B solubility in water is higher than the released amounts from NPs, thus it not represents the only threshold to diffusion of drug. In addition, PLGA-PVP NPs had not a porous matrix and this matrix were not prone to erosion, at least in the time interval of analysis.

Table 3.5. Squared correlation coefficient (R^2) and coefficients obtained after linear regression of the release data utilizing mathematical models for all drug-loaded PLGA-PVP NPs.

FORMULATION OF PLGA-g-PVP COPOLYMERS

Sample	Mathematical model (Part A)								
	$F=kt$			$\ln(1-F)=-kt$			$F=kt^{1/2}$		
	k		R^2	k		R^2	k		R^2
	Value	St.Error		Value	St.Error		Value	St.Error	
PLGA-g-PVP$_{10:1}$- Dox pH 5.5	0.028	0.004	0.776	0.040	0.005	0.841	0.130	0.007	0.957
PLGA-g-PVP$_{10:2}$-Dox pH 5.5	0.021	0.003	0.799	0.027	0.003	0.849	0.099	0.004	0.974
PLGA-g-PVP$_{10:1}$- DoxB pH 5.5	0.033	0.007	0.618	0.051	0.009	0.706	0.166	0.016	0.887
PLGA-g-PVP$_{10:2}$-DoxB pH 5.5	0.037	0.007	0.639	0.062	0.010	0.735	0.182	0.016	0.898
PLGA-g-PVP$_{10:1}$- Dox pH 7.4	0.013	0.002	0.659	0.015	0.003	0.685	0.065	0.005	0.911
PLGA-g-PVP$_{10:2}$-Dox pH 7.4	0.010	0.002	0.670	0.011	0.002	0.688	0.047	0.004	0.917
PLGA-g-PVP$_{10:1}$- DoxB pH 7.4	0.010	0.002	0.686	0.011	0.002	0.705	0.050	0.004	0.925
PLGA-g-PVP$_{10:2}$-DoxB pH 7.4	0.008	0.001	0.711	0.009	0.001	0.725	0.038	0.003	0.935

Sample	Mathematical model (Part B)								
	$1-(1-F)^{1/3}=kt$				$F=kt^n$				
	R^2	k		R^2	k		n		R^2
		Value	St.Error		Value	St.Error	Value	St.Error	
PLGA-g-PVP$_{10:1}$- Dox pH 5.5	0.957	0.012	0.001	0.820	0.168	0.906	0.402	0.046	0.906
PLGA-g-PVP$_{10:2}$-Dox pH 5.5	0.974	0.008	0.001	0.833	0.128	0.955	0.400	0.030	0.955
PLGA-g-PVP$_{10:1}$- DoxB pH 5.5	0.887	0.015	0.003	0.676	0.309	0.874	0.254	0.031	0.874
PLGA-g-PVP$_{10:2}$-DoxB pH 5.5	0.898	0.017	0.003	0.701	0.319	0.859	0.280	0.037	0.859
PLGA-g-PVP$_{10:1}$- Dox pH 7.4	0.911	0.005	0.001	0.676	0.113	0.903	0.281	0.030	0.903
PLGA-g-PVP$_{10:2}$-Dox pH 7.4	0.917	0.003	0.001	0.682	0.080	0.895	0.294	0.033	0.895
PLGA-g-PVP$_{10:1}$- DoxB pH 7.4	0.925	0.004	0.001	0.699	0.081	0.900	0.308	0.034	0.900
PLGA-g-PVP$_{10:2}$-DoxB pH 7.4	0.935	0.003	0.000	0.720	0.058	0.895	0.335	0.039	0.895

St.Error =Standard error

Higuchi´s model provided the highest values of R^2 (0.8 to 0.97). Higuchi's model has been based on the Fick's Law, where the release occurs by the diffusion of drugs within the delivery system. In this case, the cumulative released amount of the drug is proportional at square root of time. Under some experimental conditions, the release mechanism can deviate from Fickian diffusion, following an anomalous transport (no-Fickian release). In these

cases, Korsmeier-Peppas model based on a more generic equation can be used. This mathematical model relates the exponential drug release *versus* the elapsed time. The model used the release exponent (n) in order to characterize different release mechanism. If the n value is 0.5 or less, as in PLGA-PVP NPs cases, the release mechanism follow Fickian diffusion (Higuchi model), and higher values $0.5 < n < 1$ for mass transfer follow a non-Fickian model denominates anomalous transport.[cxlii]

Thus results obtained with the Korsmeyer-Peppas model corroborated the data obtained with the Higuchi model. The result suggests that the release of doxorubicin from PLGA-PVP NPs is controlled only by diffusion.

3.5.2.5 Plasma protein adsorption

Phagocytosis is mainly initiated by the attachment of the foreign nanoparticles to the surface receptors of the phagocytic cells.[cxxx] This phenomenon, leading to nanoparticle elimination, is facilitated by the adsorption of plasma proteins to the particle surface.[cxxxi] Therefore, possibility of plasma protein adsorption onto the NP surface was investigated and also the influence of different copolymeric matrix on it. Bovine serum albumin (BSA) is the most abundant protein in serum and for this reason was chosen for plasma protein adsorption study.

To estimate the potential interaction of BSA with nanoparticles, blank NPs were incubated with BSA (10 mg/mL in PBS) under physiological conditions for 1 hour, subsequently centrifuged at 7500 rpm for 10 min and supernatant recovered. UV-visible spectroscopy at 500 nm was used to determine percent adsorbed BSA on PLGA-PVP blank NPs. PLGA blank NPs was also included for comparison. Collected data are reported in Table 3.6. As expected, the level of protein adsorption gradually reduced along with the density of PVP chain in the copolymers. PLGA-PVP$_{10:2}$ blank NPs did not practically interact with BSA molecules. While PLGA showed a clear BSA adsorption tendency with average value of about 80%.

Table 6: Percentage of bovine serum albumin (BSA) adsorbed on PLGA-PVP blank NPs and PLGA blank NPs after incubation with BSA physiological solution.

FORMULATION OF PLGA-g-PVP COPOLYMERS

| Sample	Percentage of BSA adsorbed
PLGA Blk NPs	81.6 ± 2.5
PLGA-PVP$_{10:1}$ Blk NPs	25.0 ± 2.4
PLGA-PVP$_{10:2}$ Blk NPs	3.87 ± 1.6

3.5.2.6 Proliferation cell inhibition *in vitro*.

To test the response of cells to both Dox and Dox$_B$ loaded NPs, cell viability was assessed by MTT assay, after an exposure of 72 h, and compared with blank NPs and free drugs. Figure 3.9, 3.10 and 3.11 show the inhibition of MDA-MB-231 cells induced by drug loaded PLGA-PVP and PLGA formulations. In general, Dox was more ablative against tumour cell respect of Dox$_B$. This trend was confirmed in drug loaded NPs. Analyses revealed for all that inhibition trend was dose dependent. Inhibition of 30-35% was reached in cases of Dox$_B$-loaded PLGA and PLGA-PVP NPs, in contrast with the only 7% of free drug, at 0.2 M concentration. A maximum of activity was reached by Dox$_B$-loaded PLGA NPs.

A significant difference in inhibition between Dox-loaded PLGA-PVP$_{10:2}$ NPs and drug in free form was evident at all concentrations used. In particular in the case of 0.02 μM, Dox-loaded PLGA-PVP$_{10:2}$ NPs showed a high inhibition of vitality, more than 75%, instead of Dox free showed a moderate inhibition of vitality, less than 45%. At same concentration, Dox-loaded PLGA-PVP$_{10:2}$ NPs was significantly more ablative also respect to Dox-loaded PLGA-PVP$_{10:1}$ NPs and Dox-loaded PLGA NPs that showed an inhibition trend and values similar to those explicated by Dox in free form. The blank NPs did not show any toxicity even at highest doses, and the MTT values were similar to those obtained in untreated cells (data not shown).

To confirm efficacy of Dox-loaded PLGA-PVP NPs against tumour cells, human breast cancer cell line, namely 4T1 and CRL-2335 cell lines, were incubated with NPs and viability by MTT test evaluated (Figure 3.12 and 3.13). As previously reported, blank NPs did not explicated toxicity against cells at any concentrations. The inhibition effect was concentration dependent with some differences between the two cell lines and substances. Dox free form presented a percent inhibition of 70 and 65 % respectively against 4T1 and CRL-2335 cells at 0.2 μM. Similarly, Dox-loaded PLGA-PVP$_{10:1}$ NPs showed an inhibition percentage respectively of 50 and 70 %, while PLGA-PVP$_{10:2}$ ones had an inhibition values of 85 and 80 %. At a dose 10 time lower,

inhibition by Dox free form turned down to 30 and 10 % and by Dox- loaded PLGA-PVP$_{10:1}$ NPs to 15 and 20 %, instead of Dox-loaded PLGA-PVP$_{10:2}$ NPs that kept at high level inhibition, 65 and 70 %.
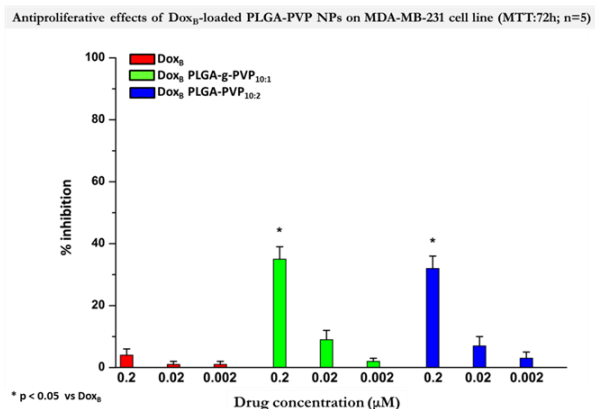
Figure 3.9. Inhibition percentage of Dox$_B$ free and loaded in PLGA-PVP NPs on MDA-MB-231 cell line.
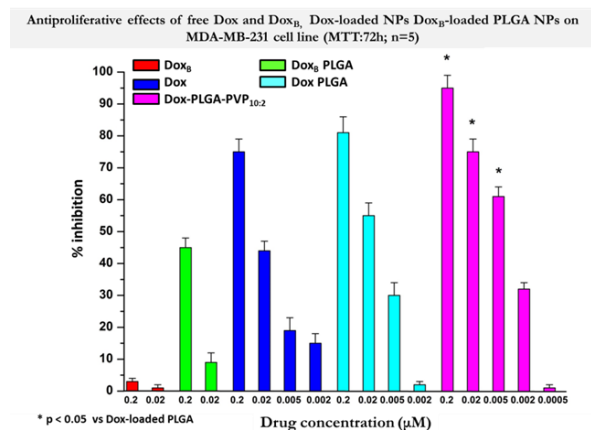
Figure 3.10. Inhibition percentage of Dox and Dox$_B$ free and loaded in PLGA NPs on MDA-MB-231 cell line.

FORMULATION OF PLGA-g-PVP COPOLYMERS
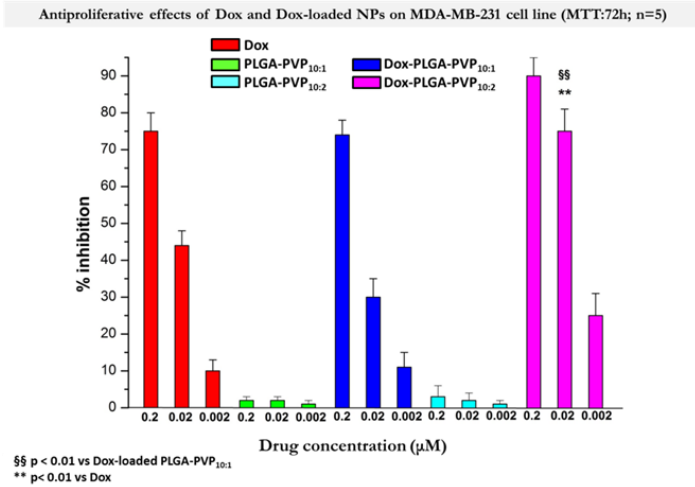
Figure 3.11. Inhibition percentage of Dox free and loaded in PLGA-PVP NPs on MDA-MB-231 cell line.
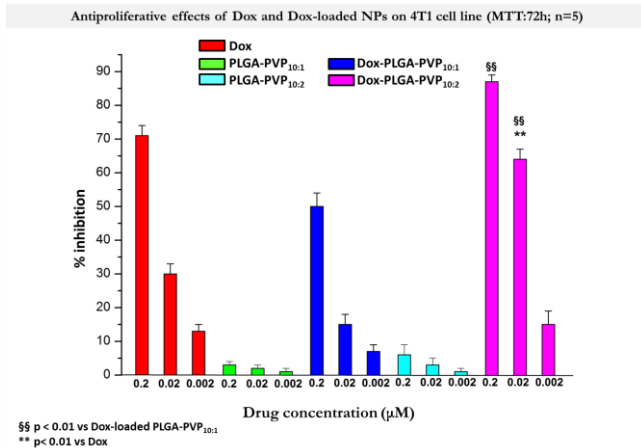
Figure 3.12. Inhibition percentage of Dox free and loaded in PLGA-PVP NPs on 4T1 cell line.

FORMULATION OF PLGA-g-PVP COPOLYMERS

Figure 3.13. Inhibition percentage of Dox free and loaded in PLGA-PVP NPs on CRL-2335 cell line.

3.5.2.7 Viability of PLGA-PVP$_{10:2}$ NPs on spheroid cultures

3D cell culture spheroids, present a powerful alternative to standard 2D cell culture for in vitro studies.[cxxxii] The 3D spheroid model is particularly useful to mimic solid-tumours from a physiologically relevant architectural perspective. For this reason, spheroid cultures of human breast cancer (HCC1906) cells were used to test viability of PLGA-PVP$_{10:2}$ NPs, that gave in 2D in vitro tests the best performance when loaded with Dox. HCC1906 was treated with blank PLGA-PVP$_{10:2}$ NPs, at different dilution, at day 5 from the seeding in ULA plates. After 72h of treatment, morphology was checked (Figure 3.14). No significant changes were observed even in the spheroid cultures treated with the highest quantity of blank PLGA-PVP$_{10:2}$ NPs.
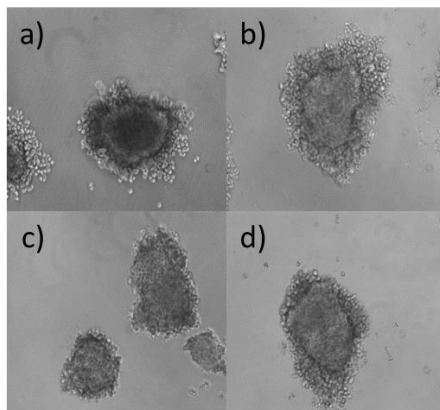
Figure 3.14. Spheroid cultures of HCC1906 cells treated with blank PLGA-PVP$_{10:2}$ NPs, at different dilution a) Control; b) dilution 1:100; c) dilution 1:1000; d) dilution 1:10000.

3.5.3 CONCLUSION: DOXORUBICIN

In conclusion, results obtained in the present study showed that PLGA-PVP copolymers could be used to prepare stable nanoparticles loaded with doxorubicin in base and salt forms, using a solvent displacement technique. Blank NPs had small dimension, 160 - 170 nm and spheroidal shape as evidenced by DLS and TEM respectively. Drug encapsulation led to an increase of size and in the case PLGA-PVP$_{10:1}$ a change in morphology, which showed a rod-like particles. Increasing initial amount of drug, in all prepared formulation an increase of drug loading was evidenced reaching values higher than 3 %. All particles presented a negative charged surface, probably due to carboxylic acid end-group of PLGA. Increasing PVP amount in copolymers, zeta potential values increase, leading to less negative surface; similar trend was evidenced also in the case of drug-loaded NPs. In particular Dox-loaded NPs had always lower negative surface than Dox$_B$-loaded ones. pH and osmolarity measurements confirmed the presence cell compatible solutions. BSA adsorption on PLGA-PVP NP surface was meaningfully reduced respect of PLGA NP one, indicating that were stealth nanoparticles. Data clearly indicated a lower inclination of PLGA-PVP NPs for opsonization phenomenon, ensuring a prolonged in circulation half-life compared to PLGA

FORMULATION OF PLGA-g-PVP COPOLYMERS

NPs one. Release studies of both drugs at pH 7.4 showed a doxorubicin retention by PLGA-PVP NPs during 24 h. An initial burst release and then sustained release phase were conversely typical trend at pH 5.5. At both pHs and for all studied systems, Higuchi kinetic model well-fitted release data indicating that diffusion was the principle mechanism involved. The cytotoxicity against MDA-MB 231 cell line of Dox_B-loaded NPs was slightly lower than that of Dox ones and for this reason they were not further investigated. MTT assays on MDA-MB 231 together with 4T1 and CRL-2335 cell lines evidenced that Dox-loaded PLGA-PVP$_{10:2}$ NPs highly affected cancer cell proliferation, allowed an inhibition activity of about 65-95 % at 0.02M. At the same concentration, Dox free inhibited proliferation of only 25% of treated cells. Thus, it can be concluded that Dox-loaded PLGA-PVP$_{10:2}$ NPs were capable of providing an efficient anticancer activity. In addition, in all considered cases blank PLGA-PVP NPs were safe and this result was confirmed by incubation with 3D spheroid cultures.

3.6 ANTIMALARIAL PROJECTS EXPERIMENTAL PART

3.6.1 METHODS

3.6.1.1 Materials and Instruments

PLGA-PVP$_{10:1}$ and PLGA-PVP$_{20:1}$ were prepared according to the procedure reported in Chapter 2, Paragraphs 2.3.4.1. Epikuron® 200 (soya phosphatidylcholine 95%) was purchased by Degussa GmbH, Hamburg, Germany. Mygliol® 812 (medium-chain triglycerides containing 57% caprylic acid (C8), 41.4% capric acid (C10) and 0.6% lauric acid (C12))was purchased from Cremer Oleo division (Hamburg, Germany). Pluronics F68, Tween 80, isopropyl myristate, dioctyl sulfosuccinate sodium salt (DOSS) and other chemicals and solvents were supplied by Sigma- Aldrich (Italy) at reagent grade and used without further purifications. Artemisinin (Art) was purchased from Tocris Bioscience (United Kingdom) and Curcumin (Cur) from Sigma-Aldrich (Spain). Ultra-Turrax SG215 homogenizer was from IKA Staufen, Germany. High pressure homogenizer was Emulsiflex C5 by Avestin, Canada. For biological tests, 96 well plates and Gibco™ RPMI 1640 Complete Medium were bought from Thermo Fisher Scientific, 0.2 M L-glutamine solution, phosphate buffered saline (PBS) powder and Triton™ X-100 from Sigma-Aldrich (Spain), SYTO® 11 Green Fluorescent Nucleic Acid Stain from Life Technologies by Thermo Fisher Scientific.

Particle size and polydispersion index (PDI) were determined by photon correlation spectroscopy (PCS), employing a 90 PLUS Particle Size Analyzer at a fixed angle of 90° and a temperature of 25 °C. The laser light (He/Ne) wavelength was 678 nm. Two drops of sample were diluted directly into the cuvette sample holder with previously filtered water. All determinations were carried out in triplicate and the results were expressed as the average diameter (expressed in nm) and PDI as measure of the distribution width.
Zeta potential measurements were determined using 90 PLUS Particle Size Analyzer. Nanoparticle solution was diluted with few drops of a 1 mM KCl solution. A minimum of five runs was obtained per sample.

Transmission electron microscopy (TEM) analysis was performed using a Philips CM10 instrument. Nanoparticle solution was stained with a 2% solution of osmium tetraoxide.

Optical microscopy analysis was carried out using a Motic AE 31inverted microscope equipped with Motic MHG - 100B using Ex D350/50x, DM 400DCLP and BA D460/50m. Magnification LWD 600x.

Osmolarity was measured using Semi-micro osmometer K-7400 with measuring head for glass vessels. 300 mOsmol solution of sodium chloride used for reference standard.

3.6.1.2 Formulation of drug loaded and blank nanocapsules

7.0 mg of artemisinin or curcumin and 70.0 mg of Epikuron 200 were dissolved in 220.0 mg di Tween 80 in presence of 300 μL of decanol and 300 μL isopropyl miristate under stirring at room temperature. Ultrafiltered water (10 mL) was added under vigorous stirring allowing to a milky mixture. This emulsion was dispersed for 5 minutes by Ultra-Turrax at 30000 rpm and for 1 hour by a high pressure homogenizer. 3.5 mL of each emulsion were putted in a 10 mL flask at 40°C and under vigorous magnetic stirring 400 μL of 15 mg/mL (15:75 v/v) DMSO/Acetone PLGA-PVP$_{10:1}$ or PLGA-PVP$_{10:2}$ solution was drop-wise added into. After 3 hours, drug loaded nanocapsules were collected and stored in fridge.

Blank nanocapsules were prepared by the same method in absence of drug.

3.6.1.3 Artemisinin assay

The quantitative determination of artemisinin was performed by reverse-phase high performance liquid chromatography using a Binary LC 250 pump (Perkin Elmer). Stationary phase was a Ultrasphere ODS (C18) 5-μm HPLC Columns (250×4.6 mm, Beckman). Mobile phase was acetonitrile/0.1% v/v acetic acid at a ratio 70:30 v/v; the flow rate was fixed at 1.0 ml/min and the detector UV (LC 95 UV/Visible detector, Perkin Elmer) at λ=254 ηm.

Experimental conditions for standard preparation was rearranged from a procedure previously described in literature.[cxxxiii] Briefly, 1 mg/mL of artemisinin solution in acetone was prepared was placed in a 10 mL measuring flask. Three dilutions of the stock solution were prepared adding in a 10 mL

measuring flask as follows: a) 0.2 mL of artemisinin solution and 0.8 ml of acetone; b) 0.5 ml of artemisinin solution and 0.5 ml of acetone; c) 1 ml of artemisinin solution alone without acetone. This was followed by the addition of 4 ml of 0.2 % NaOH solution to the three flasks respectively, and then, allowed to react at 50 °C for 30 min. After that, 0.08 mol/L acetic acid solution was used to reach the final volume.

In Art-loaded PLGA-PVP NCaps, Art content was evaluated preparing samples as follows: nanocapsules were dissolved 200 μL in 1.8 mL of acetone into a 5 mL measuring flask. 1 ml of 0.2 % NaOH solution was added to the flask and allowed to react at 50 °C for 30 min after which 0.08 mol/L acetic acid solution was added to fill up to the mark. All solutions were applied to HPLC-UV in order to evaluate Art encapsulation efficiency % (E.E. %) using Equation 3:

$$E.E.\% = \left(\frac{[Art]_{Exp}\ (mM)}{[Art]_{Theor}\ (mM)} \right) \times 100\% \qquad \text{Equation 3}$$

where $[Art]_{Exp}$ was Art concentration found experimentally by and $[Art]_{Theor}$ was theoretical concentration of Art present in NCaps if all the amount of drug was totally encapsulated, both concentrations were expressed in mM.

3.6.1.4 Curcumin assay

Cur loading of NCaps was evaluated using a Beckman Coulter DU® UV/Vis spectrophotometer. A standard solution 0.1 mg/mL of Cur in acetone was prepared dissolving 1 mg was accurately weighed and transferred in a 100ml volumetric flask. 5, 2.5, 1.25, 0.75, 0.375 mL of Cur standard solution were transferred in 10 mL measuring flasks and diluted to mark with acetone. 200 μL Cur-loaded PLGA-PVP NCaps was dissolved in acetone in a 10mL measuring flask. All solutions were analysed at wavelength of 425 ηm in triplicate. Entrapment efficacy was evaluated by equation 4:

$$E.E.\% = \left(\frac{[Cur]_{Exp}\ (mM)}{[Cur]_{Theor}\ (mM)} \right) \times 100\% \qquad \text{Equation 4}$$

where $[Cur]_{Exp}$ was Cur concentration found experimentally by and $[Cur]_{Theor}$ was theoretical concentration of Cur present in NCaps if all the amount of drug was totally encapsulated, both concentrations were expressed in mM.

3.6.1.5 Stability studies

Blank, Art-loaded and Cur-loaded NCaps were stored at room temperature (about 27°C) for thirty days. Stability was evaluated by comparing the initial particle size, PdI (polydispersity index) with those obtained from samples withdrawn after 1, 7, 14, 21, and 28 days of storage.

3.6.1.6 Growth Inhibition Assay

In order to perform a growth inhibition assay, Plasmodium falciparum (3D7) culture was synchronize by 5% sorbitol lysis before the experiment. Seventy-five μL of P. falciparum were plated in 96-well plate at 1.5% parasitemia and 3% haematocrit. Samples (2x) were added to the culture dissolved in 75 μL of RPMI complete medium as the culture. After 48h parasitemia was analysed by fluorescent-assisted cell sorting (FACS).

3.6.1.7 Haemolysis Assay

Human blood collected in citrate-phosphate-dextrose (CPD) buffer was washed and diluted in PBS to make a solution with 3% haematocrit. 100 μL of RBCs were placed into 96-well plate and 100 μL of each PLGA-g-PVP in different concentrations (2x) were added. Same amount of PLGA-g-PVP than in the GIA's was here tested. As controls, 1% Triton X-100, for the positive one, and PBS for the negative one were used. After incubating with the samples for 3h and 24h at 37°C, plates were centrifuge at 1500 rpm during 5 min and supernatants were measured at 541ηm.

3.6.2 RESULTS AND DISCUSSIONS: ARTEMISIMIN AND CURCUMIN LOADED NANOCAPSULES.

3.6.2.1 Polymeric lipid nanocapsules preparation

Polymeric nanocapsules (NCaps) are submicronic carriers consisted of an oily core surrounded by a polymeric shell with lipophilic and/or hydrophilic

surfactants assembled at the interface.[cxxxiv] The main advantages of polymeric NCaps are the possibility of loading high amount of water insoluble drug molecules into the oil core, their physicochemical stability, and protection against enzymatic degradation due to the presence of the polymeric wall.[cxxxv,cxxxvi] For these reasons NCaps were chosen as delivery system of artemisinin and curcumin, hydrophobic drugs, for antimalarial activity. PLGA-PVP copolymers were used as polymeric shell of NCaps, thank to their stealth properties, long term stability and drug retention as demonstrated in a previous work.

PLGA-PVP copolymers due to ester groups along PLGA chain and, in particular way, to the carboxylic acid as one terminal, present a negative zeta potential when used to form nanoparticles. This negative surface charge was here used to form stable shell on oily core of a nanocapsules, by ionic interactions. Oily core was thus prepared in order to have a positive surface charge. Epikuron 200 consisted in purified phosphatidylcholine was used as hydrophobic surfactant of mygliol 812, a triglyceride of the fractionated plant fatty acids with alkyl chains of C8 and C10, in presence of hydrophilic surfactants such as dioctylsulfosuccinate (DOSS), Pluronics F68 or Tween 80. Solids were firstly solubilised in mygliol and after the whole solution diluted with water under stirring. Microemulsion was obtained homogenizing for 5 min at 30000 rpm by Ultra-Turrax, and nanosized droplets after 1 hour treatment by high pressure homogenizer. Particle sizes and zeta potentials of obtained emulsions were evaluated and listed in Table 7. The smallest oily droplets (93 nm) with the most positive surface charge (+24 mV) was reached by using Tween 80 as surfactant. A further trials were attempted changing the oil and using ones with a longer alkyl chain, i.e. isopropyl-myristate (i-pr-myr, C14+C3), and oleic acid (C18). I-pr-myr in presence of Tween 80 and Epikuron 200 gave drop size of 94 nm and comparable zeta potential value of those obtained using mygliol 812. Probably size reduction was due to a more affinity between isopropyl groups and apolar chains in the hydrophilic head of both surfactants. Instead of oleic acid had similar behaviour of mygliol 812. Therefore, isopropyl-myristate was successively used to form nanocapsules. Amount of Tween 80 in recipe was adjusted. Both lower and higher amounts of surfactant caused droplet aggregation, but decreasing Tween 80 zeta potential increased. Despite last findings, 200 mg of Tween 80 was chosen.

Table 7. Zeta potentials and size of lipid core of nanoparticles varying emulsifier and lipid.

Sample	ζ Potential ± σ (mV)	Size ± σ (nm)	PDI ± σ
Epik[a), DOSS[b), Mygliol[c)	+20.04 ± 3.93	133.1 ± 16.1	0.30 ± 0.04
Epik, Plu[d), Mygliol	+18.12 ± 1.00	160.9 ± 12.2	0.301 ± 0.003
Epik, Tween 80, Mygliol	+20.18 ± 1.50	128.5 ± 1.4	0.280 ± 0.005
Epik, Tween 80, oleic acid	+21.89 ± 3.65	113.8 ± 2.7	0.304 ± 0.022
Epik, (200 mg) Tween 80, i-pr-myr[e)	+23.57 ± 1.19	94.7 ± 4.0	0.210 ± 0.02
Epik, (100 mg) Tween 80, i-pr-myr[e	+24.75 ± 1.85	118.2 ± 2.2	0.340 ± 0.008
Epik, (400 mg)Tween 80, i-pr-myr[e)	+16.89 ± 2.42	115.2 ± 1.2	0.299 ± 0.015

[a) Epikuron 200; [b) DOSS= dioctylsulfosuccinate; [c)Mygliol 810; [d) Pluronic F68; [e) isopropyl-myristate.

Influence of different alcohols on droplet size was evaluated. Butanol was knew to influence arrangements in lipid monolayer[cxxxvii] and it was hypothesised that could contribute also in rearrangement in oily droplet. Butanol like ethanol and other short chain alcohols (up to C6), by hydrogen bonds to carbonyl groups in the lipid headgroups, leads reducing interlipid van der Waals attraction, and increasing membrane elasticity.[cxxxviii,cxxxix] When used with mixture of satured and unsatured lipids, it reduced the tail mismatch between the two lipids.[clv]

In droplets, it was hypothesised that butanol and other alcohols act similarly, reducing tail mismatch between surfactant and i-pr-myristate, leading to size reduction. Results are depicted in Table 8.

In this study methanol, ethanol and propanol was not used, because they are incompatible with PLGA-PVP copolymers, leading to their precipitation. Thus, the first alcohol tested was butanol by using different volume to dissolve oil and surfactants. In all three tests a reducing of size was obtained, but the smallest dimension (39.9 nm) was reached using 300 µL of butanol. Using the same volume, hexanol, heptanol, decanol and benzyl alcohol were evaluated as

lipid compatibilizer. Benzyl alcohol did not affect droplet size, confirming that a long alkyl chain in alcohol structure was fundamental. 1-decanol gave the best result, reaching droplet size of 28.9 nm, instead of 94.7 nm of original recipe.

Table 8. Size dependence by kind and amount of alcohol used to dissolve oil and surfactants.

Alcohol	Volume (μL)	Particles size ±σ (nm)	PDI ±σ
No alcohol	--	94.7 ± 4.0	0.210 ± 0.02
1-Butanol	500	57.9 ± 3.0	0.295 ± 0.015
1-Butanol	300	39.9 ± 3.0	0.308 ± 0.017
1-Butanol	200	66.8 ± 2.4	0.258 ± 0.013
1-Hexanol	300	43.2 ± 3.3	0.211 ± 0.024
1-Heptanol	300	53.8 ± 2.2	0.237 ± 0.014
1-Decanol	300	28.9 ± 0.5	0.231 ± 0.012
Benzyl alcohol	300	84.7 ± 3.9	0.344 ± 0.005

3.6.2.2 Drug encapsulation

Once optimized formulation parameters for obtaining empty oily nanodroplets having small dimensions, anti-malarial drugs encapsulation was studied.

Three different concentrations of artemisinin and curcumin were prepared, 0.4, 0.7 and 1.0 mg/mL of each drug, and resulting droplet size and morphology were evaluated by DLS and optical microscopy. Results are listed in Table 9 and depicted in Figure 15.

In all cases a slight increase in size was observed. Focusing on Art encapsulation, it was possible to appreciate a droplet size decreasing, when drug concentration in recipe was increased. Nevertheless, in 1.0 mg/mL Art-loaded droplet, several crystals of not encapsulated Art were visible at optical

FORMULATION OF PLGA-g-PVP COPOLYMERS

microscope and thus 0.7 mg/mL solution was chosen for nanocapsule formation. On the other hand, Cur behaved differently with a minimum in size at 0.7 mg/mL. No crystals were detected when analysed by optical microscope (Figure 15).
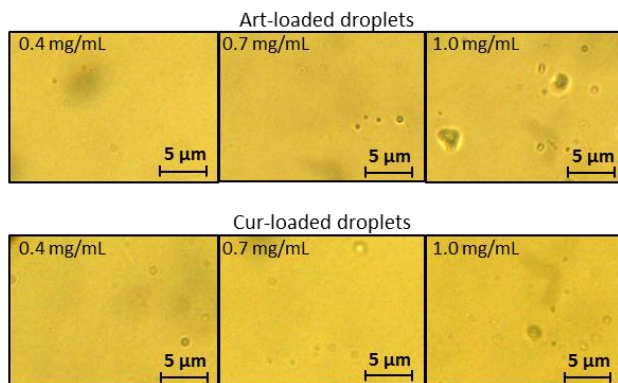
Figure 15. Optical microscopy pictures of Art-loaded droplets and Cur-loaded droplets with three different drug loading.

Table 9. Droplet sizes by DLS after encapsulation of different amounts of drugs.

Concentration (mg/mL)	Artemisinin		Curcumin	
	Particles size ±σ (nm)	PDI ±σ	Particles size ±σ (nm)	PDI ±σ
0.4	59.6 ± 0.3	0.19 ± 0.01	54.8 ± 0.7	0.21 ± 0.01
0.7	33.2 ± 0.5	0.19 ± 0.01	34.1 ± 0.2	0.13 ± 0.03
1.0	31.7 ± 0.5	0.22± 0.01	42.5 ± 0.5	0.20 ± 0.001

Final concentration of Art and Cur were evaluated by HPLC-UV and UV-Visible spectroscopy respectively, using calibration curve previously prepared (Figure 16 and 17). Drug concentration and encapsulation efficiency were listed in Table 10. Artemisinin was closely total encapsulated with an E.E.% of 99 %, instead of Cur that presented an E.E.% of 74%, confirming that in both case drugs and i-pr-myristate have a good compatibility.

FORMULATION OF PLGA-g-PVP COPOLYMERS
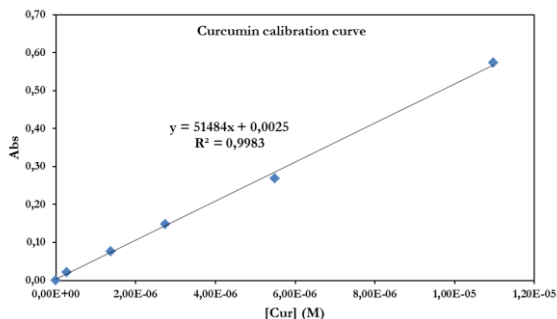
Figure 16. Calibration curve of curcumin by UV-Visible spectroscopy.
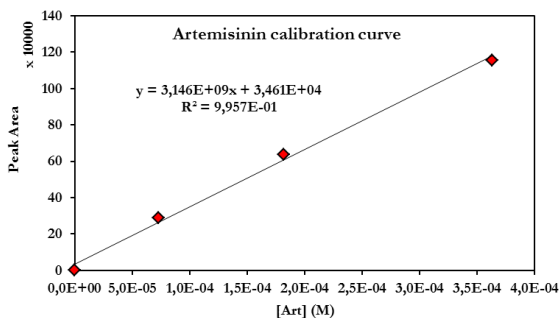
Figure 17. Calibration curve of artemisinin by HPLC-UV-Vis.

Table 10. Concentration of encapsulated drug in oily droplets and encapsulation efficacy percentage (E.E.%).

Anti-malarial drug	Concentration (mM)	E.E.%
Curcumin	1.42	74
Artemisinin	2.46	99

3.6.2.3 Drug-loaded PLGA-PVP NCaps characterization

Droplets were coated with PLGA-PVP copolymers by depositing of a layer of on oily droplet, dropping 400 µL a 30:70 DMSO/acetone copolymeric solution (15 mg/mL) under vigorous stirring. Schematic portrait of whole NCaps preparation was depicted in Figure 18 together with inserts of optical and TEM

image of oily droplets and final formulation of Art-loaded PLGA-PVP$_{10:2}$ NCaps.

PLGA-PVP$_{10:1}$ and PLGA-PVP$_{10:2}$ were used as copolymers, in order to study the dependence of drug-loaded NCap properties with PVP content in copolymers. As greatly described in Chapter 2, PVP weight content % in copolymers was 6.7 and 18.8, respectively for PLGA-PVP$_{10:1}$ and PLGA-PVP$_{10:2}$.

A thick copolymeric shell was obtained for all nanocapsules as demonstrated by the increase in particle size by DLS analysis and the variation of surface charge in negative sign from positive one, characteristic of nude oily droplets (Table 11 and 12), as showed by zeta potential analysis. In details, for PLGA-PVP$_{10:1}$ NCaps, diameters ranged between 57 to 75 nm with an increase in size of about 30 nm respect of the only oily droplets. For PLGA-PVP$_{10:2}$ NCaps, diameters ranged between 55 to 95 nm, and usually greater those obtained from PLGA-PVP$_{10:1}$ NCaps. In regard of kind of drug, passing from Cur- to Art-loaded NCaps a diameter increase was detected.
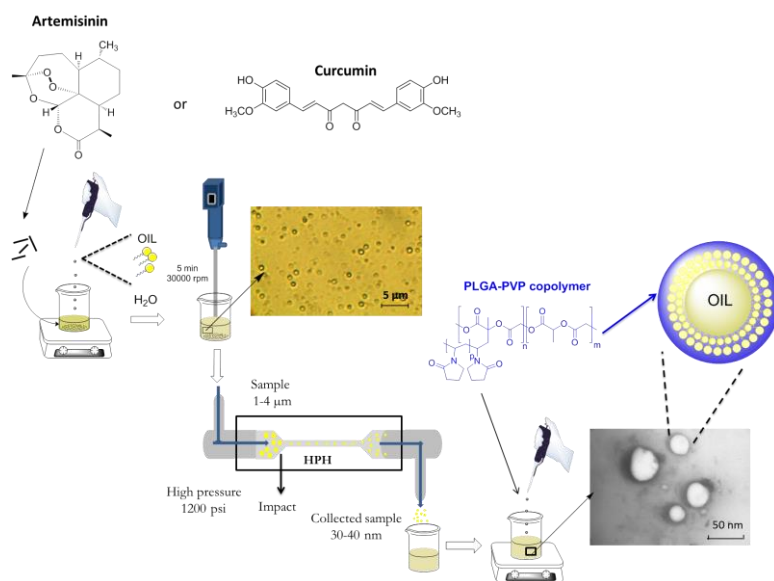
Figure 18. Schematic portrayal of drug-loaded PLGA-PVP nanocapsules, with insert of image of oily droplets (a) by optical microscope and Art-loaded PLGA-PVP$_{10:1}$ NCaps after at high pressure homogenization (HPH) treatment (b) by TEM.

Zeta potentials were more dependent from the kind of copolymer used to coated oily droplets and in particular PLGA-PVP$_{10:2}$ NCaps always showed less negative surface charges than PLGA-PVP$_{10:1}$ NCaps. No significant dissimilarities were observed changing kind of drug used. In Table 12 osmolarity values of PLGA-PVP NCaps were also listed.

It is essential to maintain isotonicity for the intravenous application of formulations. Osmolarity values varied from 130 to 240 mOsmol, indicated that all formulation were ipotonic. Thus, non-ionic substances such as glycerol or carbohydrate were recommended for use to reach isotonicity, before biological tests *in vitro* will be performed.

Table 11. Particle sizes by DLS of empty, Cur-loaded and Art-loaded nanocapsules with the two different copolymeric shells.

NCaps	PLGA-PVP$_{10:1}$		PLGA-PVP$_{10:2}$	
	Particles size $\pm\sigma$ (nm)	PDI $\pm\sigma$	Particles size $\pm\sigma$ (nm)	PDI $\pm\sigma$
Empty	57.1 ± 0.8	0.27 ± 0.01	69.5 ± 1.0	0.30 ± 0.01
Cur-loaded	67.6 ± 0.6	0.17 ± 0.03	54.7 ± 0.1	0.20 ± 0.01
Art-loaded	74.7 ± 0.7	0.20 ± 0.02	94.6 ± 0.7	0.26 ± 0.01

Table 12. Zeta potentials and osmolarity of empty, Cur-loaded and Art-loaded nanocapsules with the two different copolymeric shells.

NCaps	PLGA-PVP$_{10:1}$		PLGA-PVP$_{10:2}$	
	Zeta potential $\pm\sigma$ (mV)	Osmolarity (mOsmol)	Zeta potential $\pm\sigma$ (mV)	Osmolarity (mOsmol)
Empty	-11.54 ± 4.05	145	-7.56 ± 1.82	130
Cur-loaded	-12.37 ± 4.66	241	-10.78 ± 4.93	204
Art-loaded	-14.07 ± 2.94	200	-13.03 ± 2.39	160

3.6.2.4 Stability studies

Stability studies of empty and drug-loaded PLGA-PVP NCaps were performed in order to assess the influence of ingredients on the stability of the colloidal suspensions. For this purpose, mean diameter and PDI of PLGA-PVP NCaps dispersions were determined after different storage times (1, 7, 14, 21, 28 days) at room temperature (~27°C). Stability data are shown as average values and errors in Figure 19. After thirty days, PLGA-PVP NCaps dispersions were apparently homogeneous, without any visible precipitates, phase separation or flocculation. Furthermore, PLGA-PVP NCaps did not exhibit significant alterations in particle size, save at the end of experiment, slightly increase in size could be observed. PDI values were ranged between 0.10 and 0.30, indicating that a narrow distribution of particle size was present.
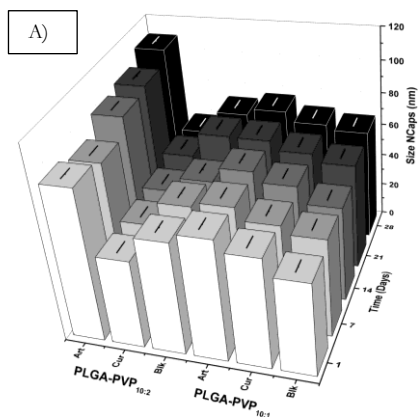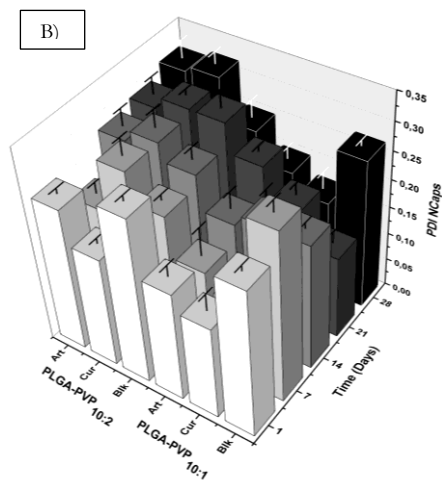
Figure 19. Stability study of blank and drug-loaded PLGA-PVP NCaps after 1, 7, 14, 21, 28 days, regarding of A) dimensional diameter (size in nm) and B) polydispersity (PDI) with their error bars.

3.6.2.5 *In vitro* biological studies

In an attempt to verify if PLGA-PVP NCaps could increase Art and Cur cytotoxicity, *in vitro* cytotoxicity studies were performed with FACS assay and *Plasmodium Falciparum* infected red blood cells (p-RBC) (3D7 culture lines). Nine different concentrations of free Cur (0.780-200 µM) and free Art (0.195-50 nM) were added to the cell culture, which was incubated for 48 h. From growth inhibition curve depicted in Figure 20, it was possible to infer the IC_{50} values for both free drugs, that were 7.93 µM and 29.7 nM, for Cur and Art respectively.

FORMULATION OF PLGA-g-PVP COPOLYMERS
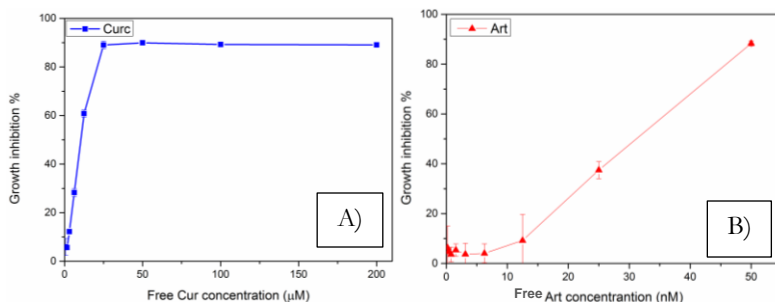
Figure 20. Growth inhibition % of pRGB in function of log of drug concentration: A) free curcumin; B) free artemisinin.

Similar experiments were conducted on Cur-loaded PLGA-PVP NCaps and emply ones. Tested drug amounts and the corresponding NCap concentrations were reported in Table 13. From preliminary results, after 48h of co-incubation, examination of p-RBC untreated group showed 100 % parasitemia, whereas a reduction of parasitemia was explicated after that pRBCs were treated with Cur-loaded PLGA-PVP NCaps (Figure 21). Also empty PLGA-PVP NCaps caused reduction of parasitemia, but in a lower extent respect of drug-loaded NCaps. IC_{50} of Cur loaded PLGA-$PVP_{10:1}$ NCaps was found to be 0.5 μM, instead of Cur-loaded PLGA-$PVP_{10:2}$ NCaps was 0.4 μM. Both IC_{50} values are significantly lower than IC_{50} of free curcumin (~8.0 microM).

By microscopic examinations, some p-RBCs were lysed when kept in contact with the formulation at highest concentration (1.56 μM). Nevertheless, more diluted formulations resulted not-toxic against p-RBCs, even if parasitemia was maintained.

Table 13. Cur concentrations tested during growth inhibition assay of Cur-loaded PLGA-PVP NCaps and corresponding NCap concentrations herein present.

Cur loaded in PLGA-$PVP_{10:1}$ (μM)	NCaps conc (μg/mL)	Cur loaded in PLGA-$PVP_{10:2}$ (μM)	NCaps conc (μg/mL)
1.56	8.47	1.17	6.34

FORMULATION OF PLGA-g-PVP COPOLYMERS

0.78	4.24	0.58	3.17
0.39	2.12	0.29	1.58
0.20	1.06	0.15	0.79
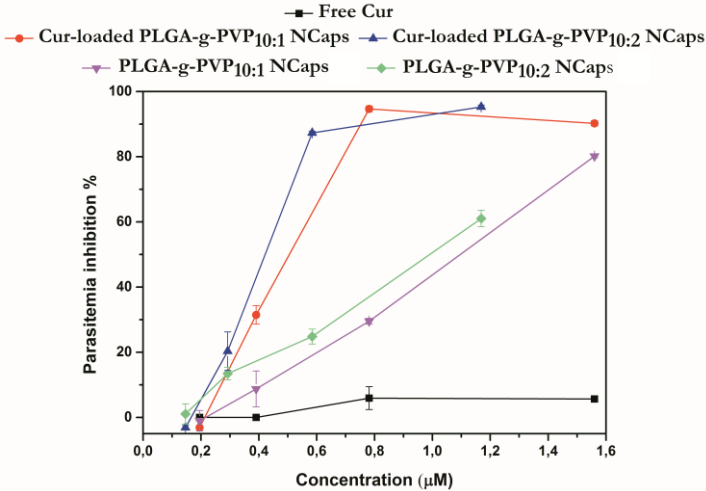
Figure 21. Growth inhibition curve of the free curcumin (black line), Cur-loaded PLGA-PVP$_{10:1}$ NCaps (red line) Cur-loaded PLGA-PVP$_{10:2}$ NCaps (blue line) and empty PLGA-PVP$_{10:1}$ NCaps (purple line) and empty PLGA-PVP$_{10:2}$ NCaps (green line).

Figure 22 reported the effect of Art-loaded formulations on pRBCs after 48h of incubation. At tested concentrations listed in Table 14, only PLGA-PVP$_{10:2}$ NCaps resulted efficient in p-RBC ablation, but the IC$_{50}$ value (38.8 nM) was greater than free Art (29.7 nM), indicating that Art was not easily released, but almost all retained inside the core of the particles. Empty NCaps did not inhibit p-RBC growth. No lysis of p-RBCs was evidenced during the experiment.

Table 14. Art concentrations tested during growth inhibition assay of Art-loaded PLGA-PVP NCaps and corresponding NCap concentrations herein present.

FORMULATION OF PLGA-g-PVP COPOLYMERS

Art loaded in PLGA-PVP NCaps (nM)	NCap conc (ng/mL)
50.0	165
25.0	82.3
12.5	41.1
6.25	20.6
3.13	10.3
1.56	5.14
0.78	2.57
0.39	1.29
0.20	0.64
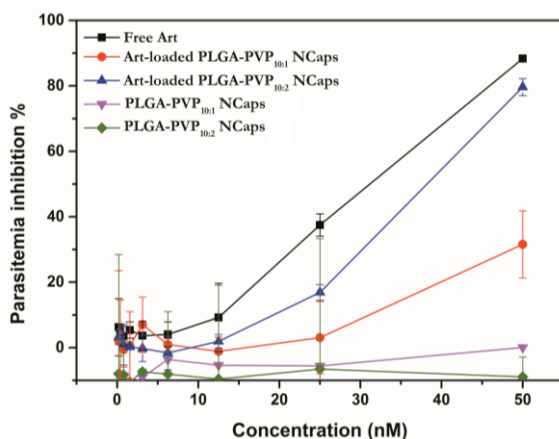
Figure 22. Growth inhibition curve of the free artemisinin, Art-loaded PLGA-PVP NCaps and empty PLGA-PVP NCaps.

To clarify if the lysis of pRBCs could contribute to inhibition of parasitemia, a haemolysis assay was performed with healthy red blood cells (RBCs) and blank PLGA-PVP NCaps. Seven dilution of empty PLGA-PVP NCaps were tested, covering all dilution range used in growth inhibition assays of drug-loaded NCaps (Table 15). After 3 h, no haemolysis properties was noted. After 24 h, only D1 caused slightly haemolysis, but further dilutions resulting totally safe. D1 dilution corresponded to double of first concentration used in growth inhibition assay. Thus, tested solutions resulted safe for healthy RBC cultures. Further experiments are planned to confirm all data.

Table 15. Dilutions of empty PLGA-PVP NCaps tested in haemolysis assay with healthy red blood cells.

Dilution code	NCap concentration (μg/mL)
D1	17.0
D2	8.47
D3	4.24
D4	2.12
D5	1.06
D6	0.164
D7	$6.43 \cdot 10^{-4}$
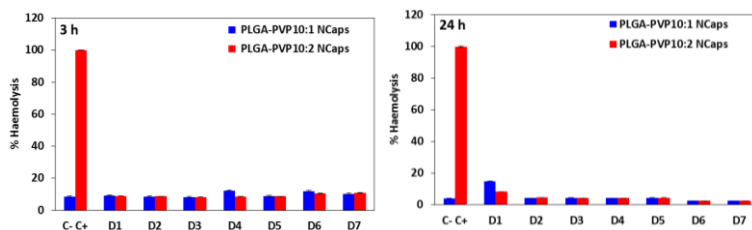
Figure 23. Haemolysis of RBCs at different concentration of empty PLGA-PVP NCaps after 3 and 24 h of incubation.

3.6.3 CONCLUSIONS: ARTEMISIMIN AND CURCUMIN LOADED NANOCAPSULES

In conclusion, results obtained in the present study showed that PLGA-PVP copolymers could be used as shell to prepare stable oily nanocapsules loaded with artemisinin and curcumin. Empty PLGA-PVP NCaps had small dimensions, about 50-60 nm as measured by DLS. Drug-loaded NCaps presented increased diameters, leading to 70-90 nm. High encapsulation efficacy was reached for all formulations, in particular in the case of artemisinin-loaded NCaps. Characterization of nanocapsules was conducted evaluating zeta potentials. All particles presented a negative charged surface, after PLGA-PVP deposition as shell. Increasing PVP amount in copolymers, zeta potential values increase, leading to less negative surface. No significantly difference between the two different drugs was evidenced. Stability studies of empty and drug-loaded PLGA-PVP NCaps were performed. After thirty days,

FORMULATION OF PLGA-g-PVP COPOLYMERS

PLGA-PVP NCaps dispersions were apparently homogeneous, without any visible precipitates, phase separation or flocculation. Furthermore, PLGA-PVP NCaps did not exhibit significant alterations in particle size.

Growth inhibition assay were evaluated after 48 h of incubation with *Plasmodium Falciparum* infected red blood cells of empty PLGA-PVP NCaps, drug-loaded PLGA-PVP NCaps and free drugs. Cur-loaded PLGA-PVP NCaps presented an IC_{50} ten times lower than one of free curcumin. In the case of Art-loaded NCaps, only PLGA-PVP$_{10:2}$ one resulted efficient in p-RBC ablation, but the IC_{50} value was greater than free Art, indicating that Art was not easily released, but almost all retained inside the core of the particles. Haemolysis assay of empty NCaps evidenced only a slight activity at higher concentrations than ones tested in growth inhibition assay.

This preliminary results indicated that both Cur-loaded PLGA-PVP NCaps were effective as antimalarial treatment. Art-loaded PLGA-PVP NCaps have to be perfect in order to promote drug release. Target could be reached by reducing PLGA-PVP shell or reducing stabiliser amounts at the start of preparation. Further experiments will be conducted.

Acknowledgements

FORMULATION OF PLGA-g-PVP COPOLYMERS

BIBLIOGRAPHY

[i] P. Couvreur, *Advanced Drug Delivery Reviews*, **2013**, 65, 21-23

[ii] A. Singh, G. Garg, P.K. *Sharma, International Journal of Pharmaceutical Sciences Review and Research*, **2010**, 5, 84-88

[iii] C.E. Mora-Huertas, H. Fessi, A. Elaissari, *International Journal of Pharmaceutics*, **2010**, 385, 113-142

[iv] K.S. Soppimath, T.M. Aminabhavi, A.R. Kulkarni, W.E. Rudzinski, *Journal of Controlled Release*, **2001**, 70, 1-20

[v] M.F. Zambaux, F. Bonneaux, R. Gref, P. Maincent, E. Dellacherie, M.J. Alonso, P. Labrude, C. Vigneron, *Journal of Controlled Release*, **1998**, 50, 31-40

[vi] B. Mishra, B.B. Patel, S. Tiwari, *Nanomedicine: Nanotechnology, Biology and Medicine,* **2010**, 6, 9-24

[vii] Available from: http://www.cancer.gov/about-cancer/understanding/what-is-cancer

[viii] Avalaible from: http://www.who.int/mediacentre/factsheets/fs297/en/

[ix] O. Tacar, P. Sriamornsak, C.R. Dass,. *Journal of Pharmacy and Pharmacology,* **2013**, 65, 157-170

[x] J.A. O'Shaughnessy, *Clinical Breast Cancer,* **2003**, 4, 318-28

[xi] G. Song, H. Gao, Z. Yuan, *Medical Oncology,* **2013**, 30, 1-8

[xii] R.Z. Orlowski, A. Nagler, P. Sonneveld, J. Bladé, R. Hajek, A. Spencer, *Journal of Clinical Oncology,* **2007**, 25, 3892-3901

[xiii] M.W. Nasser, J. Datta, G. Nuovo, H. Kutay, T. Motiwala, S. Majumder, *The Journal of Biological Chemistry,* **2008**, 283, 33394-3405

[xiv] P. Hau, K. Fabel, U. Baumgart, P. Rümmele, O. Grauer, A. Bock, *Cancer*, **2004**, 100, 1199-1207

[xv] R.Z. Orlowski, P.M. Voorhees, R.A. Garcia, M.D. Hall, F.J. Kudrik, T. Allred, *Blood*, **2005**, 105, 3058-3065

[xvi] D.E. Lopes de Menezes, L.M. Pilarski, T.M. Allen, *Cancer Research,* **1998**, 58, 3320-3330

[xvii] W.E. Ross, D.L. Glaubiger, K.W. Kohn, *Biochimica et Biophysica Acta*, **1978**, 519, 23-30

[xviii] D. Agudelo, P. Bourassa, G. Bérubé, H.A. Tajmir-Riahi, *Journal of Photochemistry and Photobiology B: Biology,* **2016**, 158, 274-279

[xix] D.A. Gewirtz, *Biochemical Pharmacology,* **1999**, 57, 727-741

[xx] K.J. Patel, O. Tre´dan, I.F. Tannock, *Cancer Chemotherapy and Pharmacology,* **2013**, 72, 127-138

xxi R. Danesi, S. Fogli, A. Gennari, P. Conte, M. Del Tacca, *Clinical Pharmacokinetics*, **2002**, 41, 431-444

xxii A. De Angelis, K. Urbanek, D. Cappetta, E. Piegari, L.P. Ciuffreda, A. Rivellino, R. Russo, G. Esposito, F. Rossi, L. Berrino, *Cardio-Oncology*, **2016**, 2, 1-8

xxiii M. Cetin, I. Vural, A. Atila, Y. Kadioglu, *Turkish Journal of Chemistry*, **2010**, 34, 509-516

xxiv S.H. Lee, H.H. Baek, J.H. Kim, S.W. Choi, *Macromolecular Research*, **2009**, 17, 1010-1014

xxv J.S. Park, J.C. Yang, S.H. Yuk, H.S. Shin, J.M. Rhee, M.S. Kim, H.B. Lee, G. Khang, *Polymer-Korea*, **2007**, 31, 189-193

xxvi R.Y. Lin, L.S. Ng, C.H. Wang, *Biomaterials*, **2005**, 26, 4476-4485

xxvii S.R. Mallery, P. Pei, J.C. Kang, G.M. Ness, R. Ortiz, J.E. Touhalisky, S.P. Schwendeman, *Anticancer Research*, **2000**, 20, 2817-2825

xxviii R. Misra, M. Das, B.S. Sahoo, S.K. Sahoo, *International Journal of Pharmaceutics,* **2014**, 475, 372-384

xxix L. Xu, H. Li, Y.B. Wang, F. Dong, H.B. Wang, S.T. Zhang, *Oncology Letters*, **2014**, 7, 387-392

xxx R. Misra, S.K. Sahoo, *Molecular Pharmaceutics*, **2013**, 10, 4746-4746

xxxi I. Amjadi, M. Rabiee, M.S. Hosseini, *Iranian Journal of Pharmaceutical Research*, **2013**, 12, 623-634

xxxii G. Romero, Y. Qiu, R.A. Murray, S.E. Moya, *Macromolecular Bioscience,* **2013**, 13, 234-241

xxxiii I. Amjadi, M. Rabiee, M.S. Hosseini, M. Mozafari, *Applied Biochemistry and Biotechnology*, **2012**, 168, 1434-1447

xxxiv F. Tewes, E. Munnier, B. Antoon, L.N. Okassa, S. Cohen-Jonathan, H. Marchais, L. Douziech-Eyrolles, M. Souce, P. Dubois, I. Chourpa, *European Journal of Pharmaceutics and Biopharmaceutics*, **2007**, 66, 488-492

xxxv G.L. Ma, C. Zhang, L.H. Zhang, H.F. Sun, C.X. Song, C. Wang, D.L. Kong, *Journal of Materials Science: Materials in Medicine*, **2016**, 27, Article ID: 17

xxxvi D. Li, J.X. Ding, Z.H. Tang, H. Sun, X.L. Zhuang, J.Z. Xu, X.S. Chen, *International Journal of Nanomedicine*, **2012**, 7, 2687-2697

xxxvii H. Wang, Y. Zhao, Y. Wu, Y.L. Hu, K.H. Nan, G.J. Nie, H. Chen, *Biomaterials*, **2011**, 32, 8281-8290

xxxviii H.Z. Zhao, L.Y.L. Yung, *International Journal of Pharmaceutics,* **2008**, 349, 256-268

xxxix M.T. Vu, Y.I. Jeong, C. Choi, J.P. Nam, D.H. Son, J.K. Park, W.S. Kim, M.Y. Kim, M.K. Jang, J.W. Nah, *Macromolecular Research,* **2010**, 18, 1115-1120

xl Y.I. Jeong, K.C. Choi, C.E. Song, *Archives of Pharmacal Research*, **2006**, 29, 712-719

xli S.Q. Liu, Y.W. Tong, Y.Y. Yang, *Biomaterials*, **2005**, 26, 5064-5074

xlii S.P. Wang, J. Zhang, Y.T. Wang, M.W. Chen, *Nanomedicine: Nanotechnology, Biology and Medicine*, **2016**, 12, 411-420

xliii H. Wang, P. Agarvval, S.T. Zhao, R.X. Xu, J.H. Yu, X.B. Lu, X.M. He, *Biomaterials*, **2015**, 72, 74-89

xliv I.N. Peca, A. Bicho, R. Gardner, M.M. Cardoso, *Journal of Nanoparticle Research*, **2015**, 17 Article Number: 427

xlv G. Tansik, A. Yakar, U. Gunduz, *Journal of Nanoparticle Research,* **2013**, 16, 2171

xlvi F. Li, J. Sun, H.S. Zhu, X.J. Wen, C. Lin, D.L. Shi, *Colloids and Surfaces B: Biointerfaces*, **2011**, 88, 58-62

xlvii J.X. Zhang, W. Tao, Y.H. Chen, D.F. Chang, T. Wang, X.D. Zhang, L. Mei, X.W. Zeng, L.Q. Huang, *Journal of Materials Science: Materials in Medicine*, **2015**, 26, Article Number: 165

xlviii B.P. Nair, C.P. Sharma, *Langmuir*, **2012**, 28, 4559-4564

xlix A. Akbarzadeh, H. Mikaeili, N. Zarghami, R. Mohammad, A. Barkhordari, S. Davaran, *International Journal of Nanomedicine*, **2012**, 7, 511-526

l S.S. Su, Y.P. Ding, Y.Y. Li, Y. Wu, G.J. Nie, *Biomaterials*, **2016**, 80, 169-178

li S. Draffehn, J. Eichhorst, B. Wiesner, M.U. Kumke, *Langmuir*, **2016**, 32, 6928-6939

lii *World malaria report*, World Health Organization, **2015**

liii N.P. Aditya, P.G. Vathsala, V. Vieira, R.S.R. Murthy, E.B. Souto, *Advances in Colloid and Interface Science*, **2013**, 201-202, 1-17

liv N.S. Santos-Magalhães, V.C. Furtado Mosqueira, *Advanced Drug Delivery Reviews*, **2010**, 62, 560-575

lv I. Petersen, R. Eastman, M. Lanzer, *FEBS Letters*, **2011**, 585, 1551-1562

lvi A.K. Agrawal, C.M. Gupta, *Advanced Drug Delivery Reviews*, **2000**, 41, 135-146

lvii A. Trouet, P. Pirson, R. Steiger, *Bull. World Health Organization*, **1981**, 59, 49-458

lviii J.E. Smith, P. Pirson, R.E. Sinden, *Annals of Tropical Medicine and Parasitology*, **1983**, 77, 379-386

lix L. Qiu, N. Jing, Y. Jin, *International Journal of Pharmaceutics*, **2008**, 361 56-63

lx Y. Gupta, A. Jain, S.K. Jain, *Journal of Pharmacy and Pharmacology*, **2007**, 59, 935-940

lxi M. Joshi, S. Pathak, S. Sharma, V. Patravale, *International Journal of Pharmaceutics,* **2008**, 364, 119-126

lxii S.A. Wissing, O. Kayser, R.H. Muller, *Advanced Drug Delivery Reviews,* **2004**, 56, 1257-1272

lxiii A.M. Dierling, Z. Cui, *International Journal of Pharmaceutics,* **2005**, 303, 143-152

lxiv K.K. Singh, S.K. Vingkar, *International Journal of Pharmaceutics,* **2008**, 347, 136-143

lxv M. Joshi, S. Pathak, S. Sharma, V. Patravale, *International Journal of Pharmaceutics,* **2008**, 362, 172-178

lxvi C. Vauthier, P. Couvreur, *Journal of Biomedical Nanotechnology*, **2007**, 3, 223-234

lxvii T. Xu, N. Zhang, H.L. Nichols, D. Shi, X. Wen, *Materials Science and Engineering: C*, **2007**, 27, 579-594

lxviii V.D. Labhasetwar, A.K. Dorle, *Journal of Controlled Release*, **1990**, 12, 113-119

lxix F. Föger, W. Noonpakdee, B. Loretz, S. Joojuntr, W. Salvenmoser, M. Thaler, A. Bernkop-Schnürch, *International Journal of Pharmaceutics,* **2006**, 319, 139-146

lxx H.J. Woerdenbag, T.A. Moskal, N. Pras, T.M. Malingré, F.S. el-Feraly, H.H. Kampinga, A.W. Konings, *Journal of Natural Products*, **1993**, 56, 849-856

lxxi S.R. Meshnick, *International Journal for Parasitology*, **2002**, 32, 1655-1660

lxxii P.J. Rosenthal, S.R. Meshnick, *Molecular and Biochemical Parasitology*, **1996**, 83, 131-139

lxxiii N.R. Meshnick, A. Thomas, A. Ranz, C.M. Xu, H.Z. Pan, *Molecular and Biochemical Parasitology*, **1991**, 49, 181-190

lxxiv S.R. Meshnick, *Med Trop Mars*, **1998**, 58, 13-17

lxxv Q. Li, P.J. Weina, W.K. Milhous, *Current Drug Therapy*, **2007**, 2, 210-223

lxxvi M. Ashton, D.S. Nguyen, V.H. Nguyen, T. Gordi, N.H. Trinh, X.H. Dinh, *Clinical Pharmacology and Therapeutics*, **1998**, 63, 482‑493

lxxvii Y. Chen, X. Lin, H. Park, R. Greever, *Nanomedicine: Nanotechnology, Biology and Medicine,* **2009**, 5, 316-322

lxxviii D. Neda, N. Dariush, C. Mohsen, E. Shamabadi Hassan, M. Seyed Mohammadreza, F.Ali, A. Akbarzadeh, *International Journal of Life science and Pharma Reviews*, **2013**, 2, 349-355

lxxix I. Leto, M. Coronnello, C. Righeschi, M.C. Bergonzi, E. Mini, A.R. Bilia, *ChemMedChem*, **2016**. doi: 10.1002/cmdc.201500586.

lxxx B. Isacchi, M.C. Bergonzi, M. Grazioso, C. Righeschi, A. Pietretti, C. Severini, A.R. Bilia, *European Journal of Pharmaceutics and Biopharmaceutics*, **2012**, 80, 528–534

lxxxi V. Rajendran, S. Rohra, M. Raza, G.M. Hasan, S. Dutt, P.C. Ghosh *Antimicrobial Agents and Chemotherapy*, **2016**, 60, 1304-1318

lxxxii M. Kakran, N.G. Sahoo, L. Li, Z. Judeh, *Chemical and Pharmaceutical Bulletin*, **2011**, 59, 646-652

lxxxiii J.W. Wong, K.H. Yuen, *Drug Development and Industrial Pharmacy*, **2003**, 29, 1035-1044

lxxxiv J.B.G. Yaméogo, A. Gèze, L. Choisnard, J.L. Putaux, A. Gansané, S.B. Sirima, R. Semdé, D. Wouessidjewe, *European Journal of Pharmaceutics and Biopharmaceutics*, **2012**, 80, 508-517

lxxxv N. Ibrahim, H. Ibrahim, A.M. Sabater, D. Mazier, A. Valentin, F. Nepveu, *International Journal of Pharmaceutics,* **2015**, 495, 671-679

lxxxvi M.Y. Want, M. Islamuddin, G. Chouhan, A.K. Dasgupta, A.P. Chattopadhyay, F. Afrin, *Journal of Colloid and Interface Science,* **2014**, 432, 258-269

lxxxvii H.N. Ho, T.H. Tran, T.B. Tran, C.S. Yong, C.N. Nguyen, *Journal of Nanomaterials*, **2015**, 2015, Article ID 674175

lxxxviii L. Wang, Y. Wang, X. Wang, L. Sun, Z. Zhou, J.Lu, Y. Zheng, *Journal of Microencapsulation*, **2016**, 33, 43-52

lxxxix R.C. Srimal, B.N Dhawan, *Journal of Pharmacy and Pharmacology*, **1973**, 25, 447-452

xc O. Sharma, *Biochemical Pharmacology*, **1976**, 25, 1811-1812

xci A.J. Ruby, G. Kuttan, K.D. Babu, K.N. Rajasekharan, R. Kuttan, *Cancer Letters*, **1995**, 94, 79-83

xcii C.C. Araujo, L.L. Leon, *Memórias do Instituto Oswaldo Cruz*, **2001**, 96 723-728

xciii Y. Wang, Z. Lu, H. Wu, F. Lv, *International Journal of Food Microbiology*, **2009**, 136, 71-74

xciv S. Han, Y. Yang, *Dyes and Pigments*, **2005**, 64, 157-161

xcv R. De, P. Kundu, S. Swarnakar, T. Ramamurthy, A. Chowdhury, G. B. Nair, A.K. Mukhopadhyay, *Antimicrobial Agents and Chemotherapy*, **2009**, 53, 1592-1597

xcvi H.B. Rasmussen, S.B. Christensen, L.P. Kvist, A. Karazmi, *Planta Medica,* **2000**, 66, 396-398

xcvii T. Koide, M. Nose, Y. Ogihara, Y. Yabu, N. Ohta, *Biological and Pharmaceutical Bulletin*, **2002**, 25,131-133

xcviii M. Nose, T. Koide, Y. Ogihara, Y. Yabu, N. Ohta *Biological and Pharmaceutical Bulletin*, **1998**, 21, 643-645

xcix L. Pérez-Arriaga, M. L. Mendoza-Magana, R. Cortes-Zarate, A. Corona-Rivera, L. Bobadilla-Morales, R. Troyo-Sanroman, M.A. Ramirez-Herrera, *Acta Tropica*, **2006**, 98, 152-161

c R.C. Reddy, P.G. Vatsala, V.G. Keshamouni, G. Padmanaban, P.N. Rangarajan, *Biochemical and Biophysical Research Communications,* **2005**, 326, 472-474

ci L. Cui, J. Miao, L. Cui, *Antimicrobial Agents and Chemotherapy*, **2007**, 51, 488-494

cii D.N. Nandakumar, V.A. Nagaraj, P.G. Vathsala, P. Rangarajan, G. Padmanaban, *Antimicrobial Agents and Chemotherapy*, **2006**, 50, 1859-1860

ciii L. Cui, J. Miao, L. Cui, *Antimicrobial Agents and Chemotherapy*, **2007**, 51, 488-494

civ T.N. Shankar, N.V. Shantha, H.P. Ramesh, I.A. Murthy, V.S. Murthy, *Indian Journal of Experimental Biology*, **1980**, 18, 73–75

cv C.D. Lao, M.T. Ruffin, D. Normolle, D.D. Heath, S.I. Murray, J.M. Bailey, M.E. Boggs, J. Crowell, C.L. Rock, D.E. Brenner, *BMC Complementary and Alternative Medicine*, **2006**, 6, 10

cvi A.L. Cheng, C.H. Hsu, J.K. Lin, M.M. Hsu, Y.F. Ho, T.S. Shen, J.Y. Ko, J.T. Lin, B.R. Lin, W. Ming-Shiang, H.S. Yu, S.H. Jee, G.S. Chen, T.M. Chen, C.A. Chen, M.K. Lai, Y.S. Pu, M.H. Pan, Y.J. Wang, C.C. Tsai, C.Y. Hsieh, *Anticancer Research*, **2001**, 21, 2895-2900

cvii P. Anand, A.B. Kunnumakkara, R.A. Newman, B.B. Aggarwal, *Molecular Pharmaceutics*, **2007**, 4, 807-818

cviii A. Ghosh, T. Banerjee, S. Bhandary, A. Surolia, *International Journal of Nanomedicine*, **2014**, 9, 5373-5387

cix D.N. Nandakumar, V.A. Nagaraj, P.G. Vathsala, P. Rangarajan, G. Padmanaban, *Antimicrobial Agents and Chemotherapy*, **2006**, 50, 1859-1860

cx F. Akhtar, M.M. Rizvi, S.K. Kar, *Biotechnology Advances*, **2012**, 30, 310-320

cxi A.P. Nayak, W. Tiyaboonchai, S. Patankar, B. Madhusudhan, E.B. Souto, *Colloids and Surfaces B: Biointerfaces*, **2010**, 81, 263-73

cxii P.B. Memvanga, R. Coco, V. Préat, *Journal of Controlled Release*, **2013**, 172, 904-913

cxiii S. Lapenna, A.R. Bilia, G.A. Morris, M. Nilsson, *Journal of Pharmaceutical Sciences*, **2009**, 98, 3666-3675

cxiv R.A. Sobh, W.S. Mohamed, A.B. Moustafa, H.E. Nasr, *Polymer-Plastics Technology and Engineering*, **2015**, 54, 1457-1467

cxv L. Hu, M. Huang, J. Wang, Y. Zhong, Y. Luo, *Journal of Applied Polymer Science*, **2016**, 133, Article Number: 43317

cxvi F. Li, *Osteoarthritis and Cartilage*, **2016**, 24, S166-S166

cxvii T. Harigae, K. Nakagawa, T. Miyazawa, N. Inoue, F. Kimura, I. Ikeda, T. Miyazawa, *International Journal of Nanomedicine*, **2016**, 11, 3009-3022

cxviii P. Anand, H.B. Nair, B. Sung, A.B. Kunnumakkara, V.R. Yadav, R.R. Tekmal, B.B. Aggarwal, *Biochemical Pharmacology*, **2016**, 102, 143-143

cxix K. Engin, D.B. Leeper, J.R. Cater, A.J. Thistlethwaite, L. Tupchong, J.D. McFarlane, *International Journal of Hyperthermia*, **1995**, 11, 211-216

cxx I. Mellman, R. Fuchs, A. Helenius, *Annual Review of Biochemistry*, **1986**, 55, 773-700

cxxi M.Barzegar-Jalali, K. Adibkia, H.Valizadeh, M.R. Siahi Shadbad, A. Nokhodchi, Y. Omidi, G. Mohammadi, S. H. Nezhadi, M. Hasan, *Journal of Pharmacy and Pharmaceutical Sciences*, **2008**, 11, 167-177

cxxii J. Siepmann, F. Siepmann, *International Journal of Pharmaceutics,* **2008**, 364, 328-343

cxxiii V. Azevedo de Mello, E. Ricci-Júnior, *Quimica Nova*, **2011**, 34, 933-939

cxxiv C.G. Varelas, D.G. Dixon, C. Steiner, *Journal of Controlled Release***, 1995**, 34, 185-192

cxxv N.V. Mulye, S.J. Turco, *Drug Development and Industrial Pharmacy*, **1995**, 21, 943-953

cxxvi T. Higuchi, *Journal of Pharmaceutical Sciences*, **1963**, 52, 1145-1149

cxxvii P. Costa, J.M.S. Lobo, *European Journal of Pharmaceutical Sciences*, **2001**, 13, 123-133

cxxviii S.T. Mathew, S.G. Devi, K.V. Sandhya, *Journal of PharmaSciTech*, **2007**, 8, E1

cxxix S. Dash, P.N. Murthy, L. Nath, P. Chowdhury, *Acta Poloniae Pharmaceutica Drug Research*, **2010**, 67, 217-223

cxxx M.K. Pratten, J.B. Lloyd, *Biochimica et Biophysica Acta*, **1986**, 881, 307-313

cxxxi T. Blunk, D.F. Hochstrasser, J.C. Sanchez, B.W. Müller, R.H. Müller, *Electrophoresis*, **1993**, 14, 1382-1387

cxxxii D.W. Grainger, *Advanced Drug Delivery Reviews*, **2014**, 69-70, vii-xi

cxxxiii A.O. Abolaji, U.M. Eteng, P.E. Ebong, A. Brisibe, A. Shakil, E. Shaista, C.M. Iqbal, *Pharmacognosy Journal*, **2010**, 2, 142-147

cxxxiv C.E. Mora-Huertas, H. Fessi, A. Elaissari, *International Journal of Pharmaceutics,* **2010**, 385, 113-142

cxxxv M.A. Pereira, V.C.F. Mosqueira, J.M.C. Vilelac, M.S. Andradec, G.A. Ramaldesd, V.N. Cardoso, *European Journal of Pharmaceutical Sciences*, **2008**, 33, 42-51

cxxxvi R.I. El-Gogary, N. Rubio, J. Tzu-WenWang, W.T. Al-Jamal, M. Bourgognon, H. Kafa, M. Naeem, R. Klippstein, V. Abbate, F. Leroux, S. Bals, G. Van Tendeloo, A.O. Kamel, G.A.S. Awad, N.D. Mortada, K.T. Al-Jamal, *ACS Nano*, 2014, 8, 1384-1401

cxxxvii Y. Kurniawan, C. Scholz, G.D. Bothun, *Langmuir*, **2013**, 29, 10817-10823

cxxxviii G.D. Bothun, L. Boltz, Y. Kurniawan, C. Scholz, *Colloids and Surfaces B: Biointerfaces*, **2016**, 139, 62-67

cxxxix H.V. Ly, M.L. Longo, *Biophysical Journal*, **2004**, 87, 1013-1033

NANOFIBRE FORMATION OF PLGA-g-PVP COPOLYMER BY
ELECTROSPINNING

CHAPTER 4

**NANOFIBRE FORMATION OF PLGA-g-PVP /PLGA BY
ELECTROSPINNING**

*"The purpose of this piece of work is to produce nanofibre based scaffolds of PLGA, having
a modulable wettability, by incorporating PLGA-PVP copolymer in the fibre structure.
Single and coaxial electrospinning techniques were employed for this aim."*

4.1 ELECTROSPINNING TECHNIQUE

Electrospinning technique was derived by modification the electrospraying
phenomenon. Indeed, both processes are based on the same physical and
electrical mechanisms, but differ in the geometry of final products, small
droplets by electrospraying, whereas continuous fibres by electrospinning are
formed.[i] The electrospray phenomenon was firstly described by Lord Rayleigh
in 1882,[ii] discovering that a highly-charged droplet was unstable when passed
through a voltage gradient with the consequence break down into smaller
droplets. Following experiment electrosprays of dilute polymer solutions were
performed by Dole.[iii] In 1934, Formhals granted a series of U.S. patents on
electrospun fine fibres from a cellulose acetate.[iv] In 1966, Simons found that
more viscous solutions favoured the formation of longer fibres.[v] Baumgarten
designed an apparatus with an infusion pump to electrospun acrylic fibres, and
discovered that the diameter of fibres could be controlled by the polymer feed
rate from the infusion pump.[vi] Finally, Larrondo and Manley electrospun
polypropylene and produced polyethylene nanofibres in 1981.[vii,viii,ix]

NANOFIBRE FORMATION OF PLGA-g-PVP COPOLYMER BY
ELECTROSPINNING

4.2 ELECTROSPINNING APPARATUS

The electrospinning apparatus consists of only three major components: a high voltage power supply, a polymer solution reservoir (usually a syringe, with a small diameter needle, named spinneret) with or without a flow control pump, and a metal collecting screen (Figure 4.1).
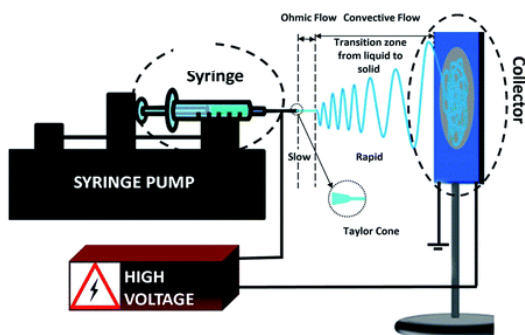
Figure 4.1. Schematic portrayal of a electrospinning apparatus. Figure adapted from reference. [x]

A syringe pump is typically used to force the polymeric solution through a small-diameter capillary, but also gravitational forces, or pressurized gas can be used for this aim. As consequence of this pressure, a hemispherical droplet of polymer solution is formed at the tip of the needle. Successively, an electrode from the high voltage source is immersed in the solution (or can be directly attached to the capillary if a metal needle is used) and when the voltage source is turned on, the electrode charges the polymeric solution. [x] With increasing voltage, the polymer droplet elongates to form a conical shape, known as the Taylor cone, causing a raising of surface charge on droplet over time. [xi,xii] Once the surface charge overcomes the surface tension of the polymer droplet, a polymer jet is initiated. If the molecular cohesion of the liquid is low, jet breakup occurs and polymer is electrosprayed and not electrospinned. [xiii] During travel to reach the collecting screen, the solvent in the polymer jet evaporates, increasing the surface charge that induces instability in the polymer

NANOFIBRE FORMATION OF PLGA-g-PVP COPOLYMER BY ELECTROSPINNING

jet when it passes through the electric field. To compensate this instability, the polymer jet divides geometrically, first into two jets, and then into many more as the process repeats itself. Eventually, fibre jet arrived by a helical motion (Figure 4.2) and deposited layer-by-layer on the metal collecting screen, forming a non-woven nanofibrous mat.[xiv,xv]

Figure 2. Particular of Taylor cone and helicoidally motion of fibre jet. Figure take from reference.[xvi]

Depending on the application a number of collector configurations can be used, including a stationary plate, rotating mandrel, solvent (e.g. water), etc. Typically the use of a stationary collector will result in the formation of a randomly oriented fibre mat. A rotating collector can be used to generate mats with aligned fibres, with the rotation speed playing an important role in determining the degree of anisotropy.[xvii] This technique allows for the production of polymer fibres with diameters varying from 3 nm to greater than 5 μm.[xviii]

4.3 PARAMETERS OF ELECTROSPINNING PROCESS

Electrospinning is a relatively simple and versatile method for forming non-woven fibrous mats, but a number of processing parameters must be tuned to adjust the properties of the generated fibres. Both extrinsic parameters, such as humidity and temperature, and intrinsic parameters, namely applied voltage,

NANOFIBRE FORMATION OF PLGA-g-PVP COPOLYMER BY ELECTROSPINNING

conductivity and viscosity of the polymer solution, need to be optimized to produce uniform nanofibres.[xix] Generally, the intrinsic parameters are more critical in determining the nanofibre structure.
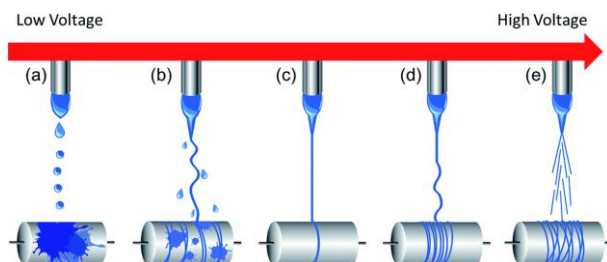
Polymer Solution Viscosity. Polymer solution viscosity is the most critical factor in controlling the structural morphology of the nanofibrous structure. It is directly proportional to the concentration of the polymer solution and to molecular weight of polymer. The polymer concentration determines the spinnability of a solution, namely whether a fibre forms or not.[xvi] For the formation of uniform and dimensionally narrow fibres, polymer viscosity should be in a specific range, depending on the type of polymer and solvent used. If the solution is too dilute, then, the polymer fibre will break up into droplets before reaching the collector, due to the effects of surface tension.[xx] With increasing polymer concentration and thus viscosity, spherical beads become elongated into spindle-shaped ones, and number of beads in the structure is reduced.[xxi] In some cases, increasing the concentration of a polymer solution can also affect its surface tension.[xxii] For solutions that are too concentrated (and therefore too viscous), the droplet dries out at the tip before jets could be initiated, preventing electrospinning.[xxiii] An example of how polymer concentration and viscosity influence morphology and diameter of fibres is showed in Figure 4.3.
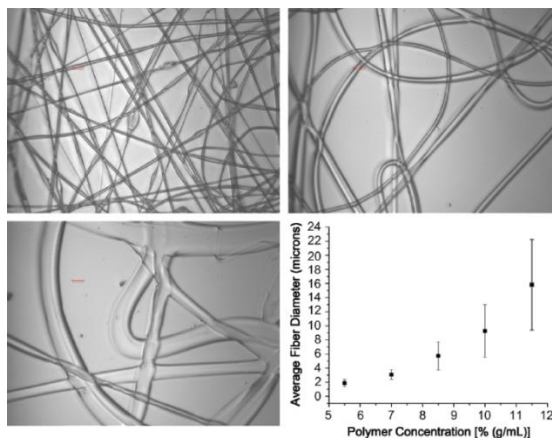
NANOFIBRE FORMATION OF PLGA-g-PVP COPOLYMER BY
ELECTROSPINNING

Figure 4.3. SEM Image. Effect of polymer concentration on fibre diameter. Fibres were electrospun from solutions containing varying concentrations of poly(ethylene- co -vinyl alcohol) in 70:30 (v/v) 2-propanol: DI water. Top left to bottom left: 5.5% (g/mL), 8.5% (g/mL) and 11.5% (g/mL) solutions. Bottom right plot of average fibre diameter against polymer concentration. Figure adapted from reference. [xxiii]

Applied Charge Density. Charge density is defined as the amount of charge per unit surface area of the polymer droplet. It is the sum of different contribute, namely the applied voltage, the distance between needle and collector of apparatus, and the conductivity of the polymer solution. The distance between capillary tip and collector can also influence fibre size by 1-2 orders of magnitude. Additionally, this distance can dictate whether the end result is electrospinning or electrospraying.[xxiv] Applied voltage (i.e. strength of electric field) alters shape of surface at which Taylor cone and fibre jet are formed.[xxv] In particular, at relatively low applied voltages, a polymeric pendant drop is formed at the tip of the capillary, having Taylor cone at the tip of the pendant drop. This configuration can lead to bead defects in the fibres or at lower values even failure in jet formation with the subsequently formation of only beads (Figure 4.4, a-b).[xxvi] Increasing the electric field strength decreases bead density, leading the formation of uniform fibres (Figure 4.4, c e d). High voltage conditions also creates a rougher fibre structure and the jet eventually moves around the edge of the tip, with no visible Taylor cone; at these conditions, the presence of many beads can be observed.[xxvii]

Figure 4.4. Schematic illustration of a jet spinning model of electrospinning from low to high voltages (from a to e). Figure take from reference.[xxviii]

NANOFIBRE FORMATION OF PLGA-g-PVP COPOLYMER BY ELECTROSPINNING

Polymer Solution Conductivity. The conductivity of a polymer solution is mainly determined by the polymer type, solvent used, and the availability of ionisable salts. A more conductive polymer solution carries more electric charge during the electrospinning process, with the as-spun fibres generating a stronger repulsive force, which facilitates the formation of bead-free, uniform fibres (Figure 4.5).[xxix,xxx] In case of non-conductive polymer choice of solvent plays an important role. Usually solvents with high dipole moment or dielectric constant are preferable, such as dimethylformamide, methanol, ethanol and so on.[xxxi,xxxii,xxxiii] Also, the productivity (number of fibres produced per unit time) of spinning polystyrene fibres is found to correlate with the dipole moment and dielectric constant. [xxxiv]
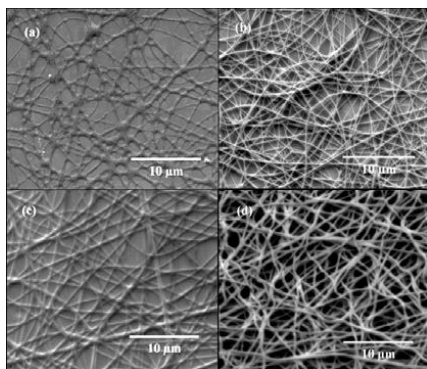
Figure 4.5. Representative SEM images (~10,000x) of 393 kDa poly SBMA electrospun nanofibres from solutions with varying concentrations of NaCl: (a) 1 M, (b) 0.5 M, (c) 0.25 M, (d) 0.17 M NaCl. Figure take from reference. [xxxv]

Flow rate. Flow rate was poorly investigated in literature, but the few present studies report that flow rate influences the homogeneity of nanofibres. In particular, too high flow rates result in rich bead defected mats since fibre jet have not a chance to dry prior to reaching the collector.[xxxvi,xxxvii] As well as, if the flow of solution through the capillary is insufficient to replace the solution ejected as the fibre jet, the cone shape at the tip of the capillary cannot be maintained.[xxxviii,xxxix]

NANOFIBRE FORMATION OF PLGA-g-PVP COPOLYMER BY ELECTROSPINNING

Solvent volatility. Choice of solvent is also critical as to whether fibres are capable of forming, as well as influencing fibre porosity. In order for sufficient solvent evaporation to occur between the capillary tip and the collector a volatile solvent must be used. As the fibre jet travels through the atmosphere toward the collector a phase separation occurs before the solid polymer fibres are deposited, a process that is greatly influenced by the volatility of the solvent.[xl,xli] Highly volatile solvents give fibres with a high density of pores, resulting in an increase of surface area. Less volatile solvent leads to a complete loss of microtexture with the formation of smooth fibres. Example of this behaviour is shown in Figure 4.6, where different ratio of DMF (less volatile solvent; b.p.= 154°C) and THF (more volatile solvent; b.p. = 66°C) solutions were used to electrospun poly(styrene).[xlii]
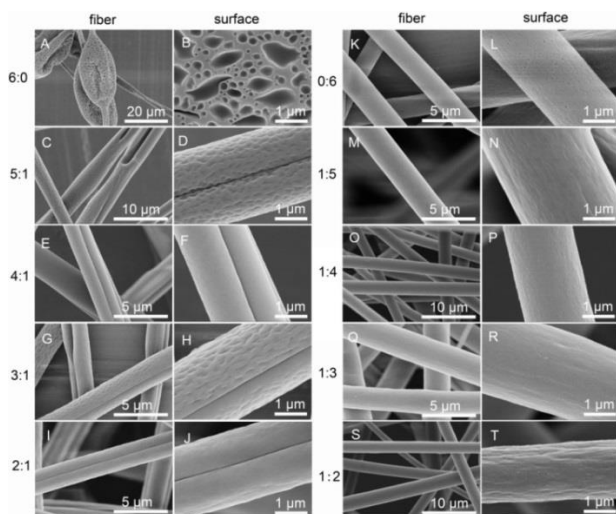

Figure 4.6. SEM pictures of fibres and their surfaces fabricated by electrospinning 20% (w/v) PS solutions with various THF/DMF ratios. (A, B) 6:0, (C, D) 5:1, (E, F) 4:1, (G, H) 3:1, (I, J) 2:1, (K, L) 0:6, (M, N) 1:5, (O, P) 1:4, (Q, R) 1:3, and (S, T) 1:2, v/v. RH 60%, collecting distance 15 cm, feeding rate 1.5 ml/h, and applied voltage 12 kV. Figure take from reference. [xlii]

NANOFIBRE FORMATION OF PLGA-g-PVP COPOLYMER BY
ELECTROSPINNING

Ambient parameters. Temperature and humidity are classified as ambient
parameters of the electrospinning process, and they have some influence of
the appearance of fibrous mats. In particular, temperature influences viscosity
of polymeric solution, leading to a decrease of this parameter when
temperature increases.[xliii] As a results, a decreased fibre diameter is usually
observed. Humidity influences porous morphology of fibrous surfaces.
Increasing the humidity leads to the appearance of small circular pores on the
surface of the fibres, with further increase pores have the tendency to
coalescing phenomenon.[xliv] Figure 4.7 illustrates the effects of both parameters
on poly(caprolactone) fibres by keeping all other parameters constant.
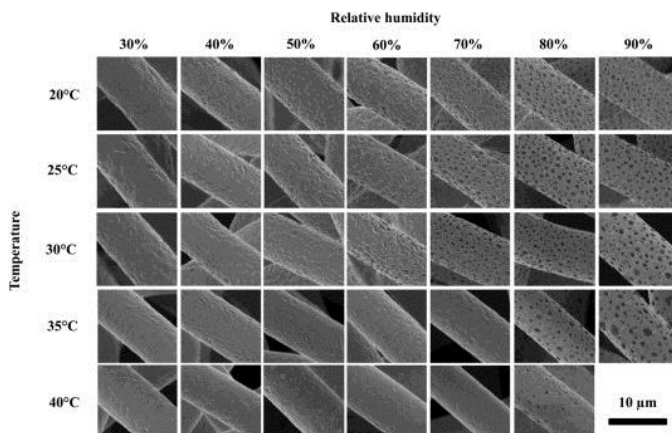
Figure 4.7. SEM micrographs of PCL fibres spun from a 15 % w/w solution
in CHCl$_3$ at the different temperatures and relative humidities. Figure take
from reference. [xlv]

4.4 MODIFICATION OF BASIC ELECTROSPINNING PROCESS: COAXIAL ELECTROSPINNING

Modification of the spinneret and/or the type of solution can allow for the
creation of fibres with unique structures and properties. One such
modification that has gained much attention and holds great promise in a
variety of applications is preparation nanofibres using "co-axial
electrospinning" are also called "two-fluid electrospinning".[xlvi,xlvii,xlviii]

NANOFIBRE FORMATION OF PLGA-g-PVP COPOLYMER BY
ELECTROSPINNING

As deducible by the name, in this process, two dissimilar materials are
delivered independently through a co-axial capillary and drawn to generate
nanofibres in core-sheath configuration. This opens up the possibility of
creating composite fibres which can have a wide range of uses: for instance, a)
to isolate and/or protect an unstable component and minimizing its chances
of decomposition under a highly reactive environment; b) to release with time
a substance to a particular receptor; c) to reinforce a material improving its
mechanical properties; d) to serve as scaffold for engineering tissues in which a
less biocompatible polymer is surrounded by a more biocompatible
material.[xlix,l,li]

The general set up adopted is quite similar to that used for electrospinning
described before (Figure 4.8). A modification is made in the spinneret by
inserting a smaller (inner) capillary that fits concentrically inside the bigger
(outer) capillary to make co-axial configuration. Since the process of co-axial
electrospinning is similar to that of the conventional electrospinning, all
variables that govern the quality of the process and the morphology of the
fibres in the latter also affects the behaviour in the former.[lii]
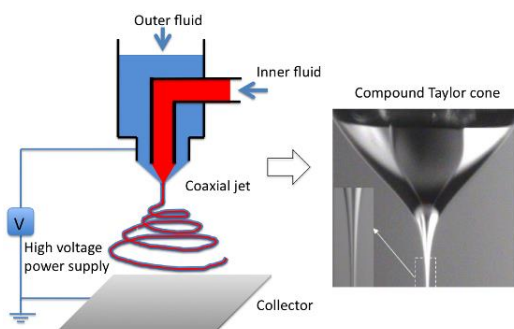
Figure 4.8. Schematic portrayal of Coaxial electrospinning apparatus, with a
magnification of Taylor cone.

NANOFIBRE FORMATION OF PLGA-g-PVP COPOLYMER BY
ELECTROSPINNING

4.5 AIM OF RESEARCH

In this work, PLGA-based scaffolds were produced by electrospinning for
biomedical applications. PLGA is a hydrophobic copolymer, as extensively
described in chapter 2. To improve biocompatibility and cell attachment on
PLGA-based scaffold, its hydrophobic must be reduced. Wettability of the
PLGA-basesd scaffolds was thus modulated by the use of a new synthetic
copolymer consisting of a main chain of PLGA with grafts lateral chains
constituted by highly hydrophilic units of poly(vinylpyrrolidone), named
(PLGA-g-PVP). Different strategies were followed for the production of
highly wettable fibres. In particular, fibres of blend solutions of both
copolymers and coaxial fibres, in which PLGA formed the core and PLGA-g-
PVP formed the shell of coaxial fibres, were produced and analysed.

4.6 EXPERIMENTAL PART

4.6.1 Materials

PLGA-g-PVP$_{10:1}$ (named PLGA-g-PVP in this work) was synthesised
following procedure reported in Chapter 2, Paragraph 2.2.3. Poly (lactide-
glycolide) 50:50 (PLGA) was purchased from Evonik Industries AG (Essen).
Polyvinylpyrrolidone (PVP) $\bar{M}_n$ 360000 g/mol was obtained by Sigma-Aldrich
(Italy). Solvents were purchased from Sigma-Aldrich and used without any
further purification steps.

4.6.2 Film formation by spin coating

A Laurell WS-650MZ-23NPP/LITE spin coater was used for 60 s at 1000
rpm with initial acceleration of 300 rpm/sec to spin-coat the polymeric
solutions on 24 x 24 mm glass. Spin-coating was used to make a uniform
distribution of 0.5 mL of 5 % w/v copolymeric solution (PLGA or PLGA-g-
PVP) in chloroform.

NANOFIBRE FORMATION OF PLGA-g-PVP COPOLYMER BY
ELECTROSPINNING

4.6.3 Scaffold preparation by single electrospinning

The electrospinning apparatus was composed of a high voltage power supply (Spellman, SL 50 P 10/CE/230), a syringe pump (KD Scientific 200 series), a glass syringe, a stainless-steel blunt-ended needle (inner diameter 0.51 mm) connected with the power supply electrode and a grounded aluminium plate-type collector. The polymer solution was dispensed through a teflon tube to the needle that was vertically placed on the collecting plate. Distance between needle and collector was in all cases of 20 cm.

Electrospinning parameters for all compositions are listed in Table 4.1.

PLGA solution was prepared at room temperature by dissolving the copolymer in DCM:DMF = 70:30 v/v at a concentration of 22 % and 26 % w/v, named respectively $PLGA_{22}$ and $PLGA_{26}$.

PLGA-g-PVP scaffolds were fabricated from a solution of PLGA-g-PVP in DCM:DMF = 70:30 v/v, at a concentration of 30 and 37% w/v. The two solutions were identified as $PLGA-g-PVP_{30}$ and $PLGA-g-PVP_{37}$, respectively.

PLGA/PLGA-g-PVP blend scaffolds were fabricated by using solution at two different concentration of PLGA-g-PVP, 13% w/w and 37% w/w, named $Blend_{13}$ and $Blend_{37}$ respectively. Blend solutions were prepared at room temperature dissolving both copolymers in DCM:DMF = 70:30 v/v, obtaining a total polymeric concentration of 25% w/v.

Obtained electrospun mats were kept under vacuum over P_2O_5 at room temperature overnight in order to remove residual solvents.

4.6.4 Scaffold preparation by coaxial electrospinning

The home-made electrospinning apparatus is composed of a high voltage power supply (Spellman SL 50 P 10/CE/230), two syringe pumps (KD Scientific 200 series), a glass syringe, a stainless steel coaxial needle connected to the power supply electrode and a grounded aluminium collector (10 cm ×10 cm). The coaxial needle used in the present work is constituted by an inner

needle (internal diameter = 0.55 mm) positioned concentrically to the outer
needle (internal diameter = 1.5 mm).

Core solution is constituted by 26 % w/v PLGA in 70:30 DCM:DMF
solution. Sheath solution is formed by PLGA-g-PVP in 70:30 DCM:DMF
solution. Three different copolymer concentrations, 13 %, 25% and 37% w/v,
was used, giving three different mats, named $Coax_{13}$, $Coax_{25}$ and $Coax_{37}$.
Electrospinning parameters for all coaxial fibres were listed in the following
Table 1. Electrospun fibres were kept under vacuum over P_2O_5 at room
temperature overnight in order to remove residual solvents.

4.6.5 Characterization of polymeric films and electrospun fibres

Scanning Electron Microscope (SEM) were performed SEM Philips 515
operating at 15 kV. Samples were fixed on aluminium stubs by double-sided
carbon adhesive tape and sputter-coated with gold prior to examination. The
distribution of electrospun fibre diameters was determined through the
measurement of fibres by means of an acquisition and image analysis software
(EDAX Genesis) and the results were given as the average diameter ±
standard deviation.

Thermogravimetric analysis (TGA) measurements were performed with a TA
Instruments TGA2950 Thermograms were recorded on 10-15 mg of samples
from RT to 700°C by heating rate of 10 °C/min, using gas nitrogen to purge
furnace (75 mL/min) and balance (55 mL/min).

Differential scanning calorimetry (DSC) was carried out using a TA
Instruments Q100 DSC equipped with the LNCS (Liquid Nitrogen Cooling
System) accessory. DSC scans were performed in helium atmosphere from -
50° to 210°C. A rate of 20°C/min was used during heating scans whereas the
cooling scans were performed at a rate of 10°C/min.

Static water contact angle measurements were performed at room temperature
under ambient conditions by using an optical contact angle and surface tension
meter KSV's CAM 100 (KSV, Espoo, Finland). Milli-Q water was used for
measurements. The water drop profile images were collected in a time range of

NANOFIBRE FORMATION OF PLGA-g-PVP COPOLYMER BY ELECTROSPINNING

0–30 s, every 1 s. Optical contact angle and pendant drop surface tension software was used for image processing. Results were averaged on at 10-12 measurements obtained at different areas of the sample.

Table 4.1. Electrospinning parameter used to prepare polymeric fibres at different composition.

Samples	Syringe diameter (mm)	Applied voltage (kV)	Flow rate core sol. (mL/h)	Flow rate sheath sol. (mL/h)	Temperature (°C)	Humidity %
PLGA$_{22}$	11.8	15.2	1.2	--	25	60
PLGA$_{26}$	11.5	15.1	0.9	--	22	58
PLGA-g-PVP$_{30}$ / PLGA-g-PVP$_{37}$	12.2	18	0.9	--	21	82
Blend$_{13}$	12.2	17.0	0.9	--	26	76
Blend$_{37}$	12.2	16	0.9	--	21	65
Coax$_{13}$	12.2	17.0	1.0	0.10	27	63
Coax$_{25}$	12.2	18.5	0.97	0.23	27	62
Coax$_{37}$	12.2	17.0	0.85	0.35	26	64

4.7 RESULTS AND DISCUSSIONS

4.7.1 Thermal characterization of native polymers.

Starting materials, namely the PLGA copolymer, the PVP homopolymer and PLGA-g-PVP copolymer, were characterized in their thermal properties by means of thermogravimetry (TGA) and differential scanning calorimetry (DSC).

The thermogravimetric analysis measuring the sample weight loss in function of temperature, due to substances volatilization or deriving from the thermal degradation. This technique allows to have information relating to the composition of samples. Figure 4.9 shows thermogravimetric curves of three starting polymers. In Table 4.2 degradation temperature and the corresponding weight losses of each sample are collected.

NANOFIBRE FORMATION OF PLGA-g-PVP COPOLYMER BY ELECTROSPINNING
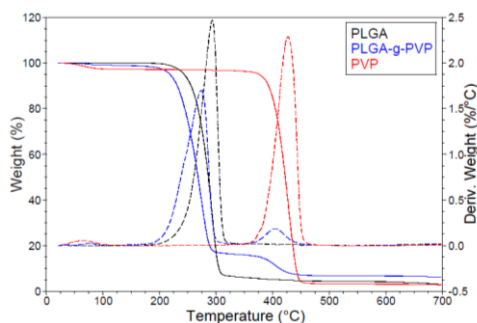
Figure 4.9. Overlapping of PVP (red curve), PLGA (black curve), PLGA-g-PVP (blue curve) TGA. For each sample is reported of the weight loss percentage as a function of temperature (continuous line) and the corresponding derivative (dashed line).

Table 4.2. Percentage of weight loss (Δm) and temperatures of the maximum degradation rate of starting polymers.

Sample	Δm (%) RT - 150°C	Δm (%) 150°C - 340°C	Δm (%) 340°C - 500°C	PLGA $T_{degradation}$ (°C)	PVP $T_{degradation}$ (°C)
PLGA	0.051	96	0	293	-
PVP	2.8	0	94	-	427
PLGA-g-PVP$_{10:1}$	1.1	83	9.3	274	404

PLGA degraded essentially through a single degradation step, which corresponds to a weight loss of about 96%, with a maximum degradation rate at 293 °C. Both PVP and PLGA-g-PVP, both have a small loss of weight at low temperatures (T <150 °C) respectively of 2.9% and 1.1% due to the evaporation of adsorbed water from samples. In fact, the presence of vinylpyrrolidone units makes these very hygroscopic polymers and, despite the samples are maintained under anhydrous conditions prior to analysis, in a few minutes in contact with atmospheric humidity absorb significant amounts of water. Following the loss of water, PVP degraded via a single step with a maximum degradation rate at 427 °C, accomplishing by a weight loss of 94%.

NANOFIBRE FORMATION OF PLGA-g-PVP COPOLYMER BY ELECTROSPINNING

PLGA-g-PVP instead presented two weight losses, at 274 °C equal to 83% and a 404 °C of about 9%. By comparing the TGA curves of the PLGA-g-PVP with those of the PVP and the PLGA is noted that the two weight losses shown by the PLGA-g-PVP are respectively attributable to thermal degradation of PLGA backbone (T = 274 °C) and PVP side chains (T = 404 °C). From PVP weight loss % is possible to define PVP content in copolymers, i.e. approximately 10%.

The differential scanning calorimetry (DSC) was used to detect the chemical-physical transformations taking place in the polymers and involving enthalpy or heat capacity changes. The DSC measurements were showed in Figure 4.10 and DSC data listed in Table 4.3.
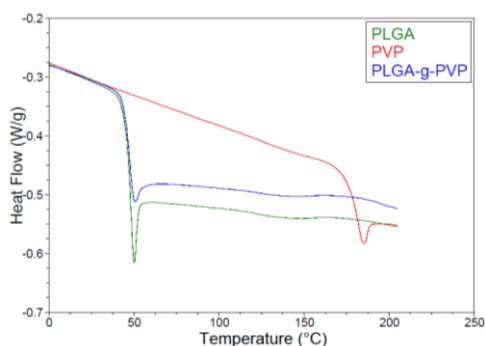
Figure 4.10. Overlapping of PVP, PLGA and PLGA-g-PVP DSC. Second scan from -50°C to 210°C with a temperature ramp of 20°C/min.

Table 4.3. Glass transition temperatures and variation of the heat capacity of the starting polymers.

Sample	PLGA Tg (°C)	PVP Tg (°C)	PLGA ΔC_p (J/(g·°C))	PVP ΔC_p (J/(g·°C))
PLGA	46	-	0.60	-
PVP	-	178	-	0.33
PLGA-g-PVP$_{10:1}$	46	ND[a]	0.52	ND[a]

[a]ND = not detected

NANOFIBRE FORMATION OF PLGA-g-PVP COPOLYMER BY
ELECTROSPINNING

Thermogram corresponding to PLGA analysis showed a glass transition
temperature (Tg) at 46 °C associated to a variation of heat capacity (ΔC_p) equal
to 0.60 J/g·°C. While, the PVP has Tg at 178 °C with a ΔC_p equal to 0.33 J/g·
°C. PVP and PLGA homopolymers are reported to be poorly miscible.[liii] In
DSC thermograms, the presence of two separated not miscible phases are
represented in two glass transitions in correspondence of those of the
individual component. Each glass transition is associated to ΔC_p proportional
to weight amount of each component. Thus, for PLGA-g-PVP copolymer,
two different glass transitions were expected, with two ΔC_p values
proportional to PLGA and PVP amounts present herein. However, PLGA-g-
PVP showed only a single transition at 46 °C with a ΔC_p equal to 0.52 J/g·°C,
corresponding to PLGA Tg. The associated ΔC_p was lower than that of not-
grafted PLGA (0.52 J/g·°C vs 0.60 J/g·°C). Taking advantage of
proportionality law that correlate ΔC_p to material weight and applying the
Equation 1, it is possible to calculate the PLGA weight amount in the
copolymer PLGA-PVP (x), amounting to 87%:

$$\Delta C_p^{PLGA} : 100 = \Delta C_p^{PLGA-PVP} : x \qquad \text{Equation 4.1}$$

TGA analysis described above provided PLGA weight content of 90%. Within
experimental error associated with the two techniques (± 5%), the two
characterizations provide comparable results. The absence of a glass transition
in correspondence of the PVP Tg can be attributed to the low PVP content.

### 4.7.2 Electrospinning and characterization of PLGA fibres

Non-woven fabric was spun starting from a $PLGA_{26}$ solution in 70:30 v/v
DCM:DMF. Preliminary observations by optical microscopy evidenced fibres
of micrometric dimensions. Several experimental observations[liv,lv,lvi] have
reported the influence of solution concentration on fibre morphology. In
particular, at low concentrations, the polymer was spun in form of micro and
nanobeads, increasing concentration very rich of beads thin fibres are
obtained, further increasing allow to electrospun fibres of larger diameter
devoid of defects. This behaviour is closely related to the number of physical
linkages between chains in solution.[lvii] In consideration of the above, to

NANOFIBRE FORMATION OF PLGA-g-PVP COPOLYMER BY ELECTROSPINNING

decrease fibre sizes under submicron diameters, polymer concentration was decreased to 22% w/v using the same solvent mixture, obtaining PLGA$_{22}$. This solution was electrospun and analysed by scanning electron microscope and SEM images at both polymer concentration are reported in Figure 4.11.

SEM images of Figure 4.11a and Figure 4.11b of PLGA$_{26}$ fibres showed no beads but diameters between 0.9 and 1.9 μm. While, scaffold obtained instead from the solution at a lower concentration, PLGA$_{22}$, presented fibres with an average size between 0.1 and 0.5 μm. However, having a less stable concentrated jet, fibrous structure possessed high number of beads and irregular diameter distribution. Probably, the spinning of a PLGA solution at an intermediate concentration would have allowed to obtain sub-micrometre fibres devoid of beads with homogeneous diameter distribution. But this optimization was not carried out, because unnecessary for the purposes of the work.
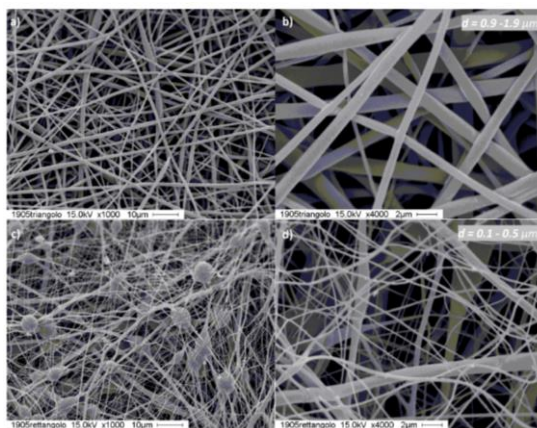
Figure 4.11. SEM images. a) 1000x PLGA$_{26}$, b) 4000x PLGA$_{26}$, C) 1000x PLGA$_{22}$, d) 4000x PLGA$_{22}$.

Nonwoven fabric were further characterized by measuring contact angle of a drop of water deposited on the sample surface, providing informations on the wettability of the material (for more in deep information on wettability see chapter 1 paragraph 1.4.3).

NANOFIBRE FORMATION OF PLGA-g-PVP COPOLYMER BY
ELECTROSPINNING

Table 4.4 compares the average contact angles obtained for the two nonwoven
fabrics PLGA and for a film of the same copolymer.

**Table 4.4.** Contact angle of a water drop deposited on PLGA-based materials.

Sample	Average water contact angle $\pm\sigma$ (°)
PLGA$_{26}$ **(diameter: 0.9-1.9 µm)**	99 $\pm$ 4
PLGA$_{22}$ **(diameter: 0.1-0.5 µm)**	132 $\pm$ 6
Film	69 $\pm$ 1

Contact angle measurements provided different values, despite the same
chemical composition of materials. In particular, wettability was greater in the
case of the film and smaller in the case of nonwoven fabrics, probably due to
the different surface roughness. A smooth surface, as in the case of the PLGA
film, had a contact angle lesser than a porous material, as the case of
electrospinned fibres. Furthermore, for the same reason, the two scaffolds had
two different contact angle. The presence of beads and thin fibres, in the case
PLGA$_{22}$, made its surface less uniform and more wrinkled, giving greater angle
of contact, compared to a more homogeneous surface of PLGA$_{26}$. Similar
results have been reported in the literature in the case of non-woven-fabrics of
other polymeric materials.[lviii,lix]

4.7.3 Electrospinning and characterization of PLGA-g-PVP fibres

Preliminary electrospinning tests of PLGA-g-PVP were conducted using a
solution of 30% w/v in 70:30 DCM:DMF. Results indicated that very thin and
full of beads fibres were obtained (Figure 4.12a). Instead, in the case of PLGA-
g-PVP$_{37}$, homogenous fibres with few imperfections were electrospinned
(Figure 4.12b, Figure 4.12c). PLGA-g-PVP$_{37}$ fibres had an average diameter
between 0.2 and 1 µm.

NANOFIBRE FORMATION OF PLGA-g-PVP COPOLYMER BY ELECTROSPINNING
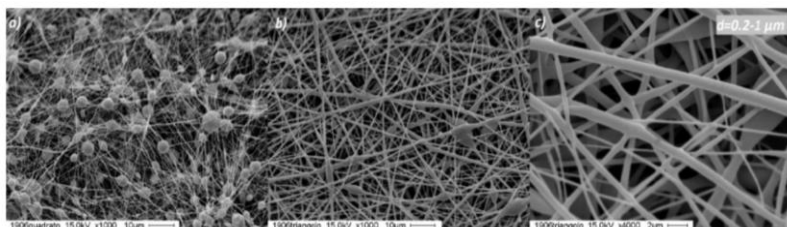
Figure 4.12. SEM images. a) 1000x PLGA-g-PVP$_{30}$, b) 1000x PLGA-g-PVP$_{37}$, c) 4000x PLGA-g-PVP$_{37}$.

Wettability of scaffolds were evaluated by contact angle measurements. Trend over time is reported in Figure 4.13. Graph is representative of a single drop on the non-woven PLGA-g-PVP fabric and a single drop on a film of the same composition.
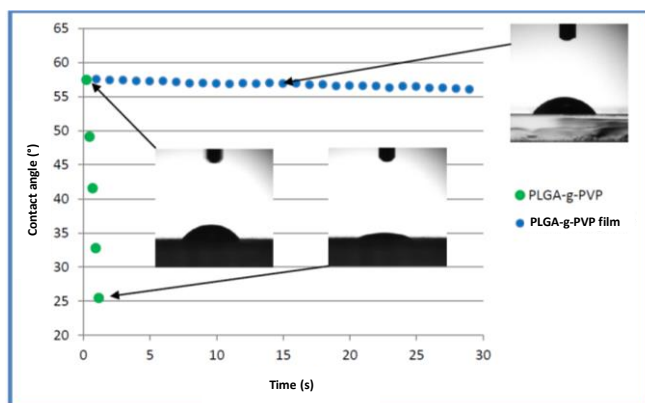
Figure 4.13. Contact angle results as a function of time for a PLGA-g-PVP$_{37}$ non-woven fabric and for a PLGA-g-PVP films (representative 2 drops).

The trend of angle of contact of fibrous scaffold was not constant over time and decreased rapidly within 2 seconds, after which the droplet was completely absorbed by the porous structure of the sample. Furthermore, the initial contact angle (approximately 58°) was significantly lower than the contact

163

angle values of PLGA fibres, a consequence of PVP grafts on the main backbone of PLGA that increased copolymer hydrophilicity.

The PLGA-g-PVP$_{37}$ films instead presented an contact angle practically constant over time with a mean value of $57° \pm 6°$. The addition of PVP chains on PLGA significantly increases the wettability. Indeed, comparing its contact angle value with those obtained from PLGA, a greater wettability was highlighted for PLGA-g-PVP compared to PLGA, also in the case of films. It is noted that the PVP is a water-soluble polymer and had not been therefore conducted contact measurements on this polymer.

### 4.7.3 Electrospinning and characterization of PLGA/PLGA-g-PVP fibres

Above described contact angle measurements have shown that the non-woven fabric of PLGA was strongly hydrophobic and a drop of water did not penetrate inside the porous structure. The scaffold of PLGA was therefore not wettable by water. In contrast, the PLGA-g-PVP was wet in a few seconds due to the addition of PVP chains grafted on PLGA chains. To modulate the wettability of the scaffolds, minimizing the use of non-commercial PLGA-g-PVP, fibres of PLGA containing small amounts of PLGA-g-PVP were produced.

PLGA-g-PVP was introduced into the fibres by adopting two strategies: 1) Electrospinning of mixtures. Copolymers were solubilised in the same solvent system and the obtained solution was electrospun leading to scaffolds with different content of PLGA-g-PVP depending on the concentration in the starting solution; 2) Coaxial electrospinning: were prepared two separate solutions of PLGA and PLGA-g-PVP and electrospunned simultaneously by two needles arranged in a coaxial configuration. The PLGA-g-PVP solution was kept in the outside needle while that of PLGA in the inner needle. The PLGA-g-PVP content in the fibres depended both from concentration and flow rate of the two solutions.

NANOFIBRE FORMATION OF PLGA-g-PVP COPOLYMER BY
ELECTROSPINNING

4.7.3.1 Electrospinning of blends

SEM images in Figure 4.14 show in both cases, fibres with only a few beads. Blend$_{13}$ fibre diameter was between 0.4 and 0.9 µm, while those of Blend$_{37}$ were thicker fibres with a diameter between 0.6 and 1.5 µm.
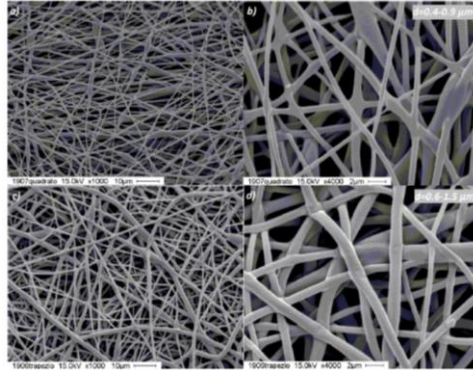
Figure 4.14. SEM images. a) 1000x of Blend$_{13}$ b) of 4000x Blend$_{13}$ c) of 1000x Blend$_{37}$ d) of 4000x Blend$_{37}$.
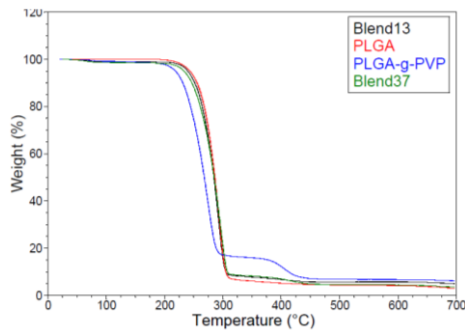
Figure 4.15. TGA overlapping of non-woven fabrics of Blend13, Blend37 and the starting polymer (PLGA, PLGA-g-PVP). temperature ramp of 10 °C/min.

NANOFIBRE FORMATION OF PLGA-g-PVP COPOLYMER BY ELECTROSPINNING

To assess the composition of produced nonwoven fabrics, thermogravimetric analysis was carried out. In Figure 4.15, TGA thermograms of the blend along with that of the two components for comparison were depicted. Both blend fabrics had a small weight loss at a low temperature due to adsorbed water and two degradation step, one at a lower temperature (T ~ 290 °C) and one at a higher temperature (T ~ 400 °C). As described in paragraph 4.5.3, the second weight loss is attributable to the PVP degradation. PVP weight loss was of 2.3% for the $Blend_{13}$ and of 4.0% for the $Blend_{37}$, index that a greater PVP content was present $Blend_{37}$.

The overall wettability of the non-woven fabric was evaluated by contact angle measurements for both samples. In both cases, contact angle values were constant over time. Results are collected in Table 4.5, data relating to PLGA scaffold were also reported for comparison. It was noted that the contact angles of PLGA/PLGA-g-PVP blend were independent of the PLGA-g-PVP content. In addition, sample wettability did not increase; contact angle values were similar to that of $PLGA_{22}$ and $PLGA_{26}$ fabrics.

Table 4.5. Comparison of the mean contact angle of blends based on PLGA / PLGA-g-PVP and non-PLGA-woven fabrics.

Sample	Average contact angle (°)
$Blend_{13}$ (fibre diameter: 0.4-0.9 μm)	122 ± 6
$Blend_{37}$ (fibre diameter: 0.6-1.5 μm)	122 ± 3
$PLGA_{26}$ (fibre diameter: 0.9-1.9 μm)	99 ± 4
$PLGA_{22}$ (fibre diameter: 0.1-0.5 μm)	132 ± 6

Results evidenced that fibre surface of $Blend_{13}$ and $Blend_{37}$ is not enough rich of PVP units to significantly decrease the hydrophobicity of the fabric when compared to those of only PLGA. The strategy of mixing the copolymers was not so effective, at least up to concentrations of PLGA-g-PVP equal to 37%. Evidently, the total amount of PVP in $Blend_{37}$ (4.0%) was homogenously

distributed along the section of the fibre and was not enough to influence surface property.

4.7.3.2 Coaxial electrospinning of copolymers

In order to increase the wettability of the fibres of PLGA, without using too high concentrations of PLGA-g-PVP, the latter was introduced into the fibres by adopting a different strategy to that described in the previous paragraph. The electrospinning was therefore conducted using two coaxial needles, the outer one containing the PLGA-g-PVP solution and the internal one containing the PLGA solution. In this configuration, it is expected that the surface of so produced fibres is richer PLGA-g-PVP compared to fibres obtained by electrospinning of mixtures, at equal copolymer content in the fibre.

The global composition of fibres was modulated by varying the flow rate of the two starting solutions. Three scaffolds with three PLGA-g-PVP percentage in the fibre (13%, 25% and 37% w/w) were electrospun and named $Coax_{13}$, $Coax_{25}$, $Coax_{37}$ respectively. Figure 4.16 showed SEM images of fabrics obtained by coaxial electrospinning. All samples have sub-micrometre fibres. Morphology was not perfectly smooth, but some beads very elongated were present, particularly in low-PLGA-g-PVP content samples (i.e. $Coax_{13}$ and $Coax_{25}$).

Composition of the nonwoven fabrics produced was evaluated by thermogravimetric analysis. Figure 4.17 shows the thermograms of the samples by coaxial electrospinning together with that of the two pure components for comparison.

The TGA curves of Coax samples show similar trends of PLGA-g-PVP sample. A first weight loss at low temperature (T <150 °C) due to the loss of adsorbed water, a second weight loss after 200 °C, given by the degradation of PLGA chains, and the last weight loss around 400 °C, attributable to the degradation of grafted PVP chains. The last weight loss can provide informations on the composition of samples in terms of PVP weight amount.

NANOFIBRE FORMATION OF PLGA-g-PVP COPOLYMER BY ELECTROSPINNING

Table 4.6 shows these values of weight loss for samples Coax and for comparison the values for the samples Blend.
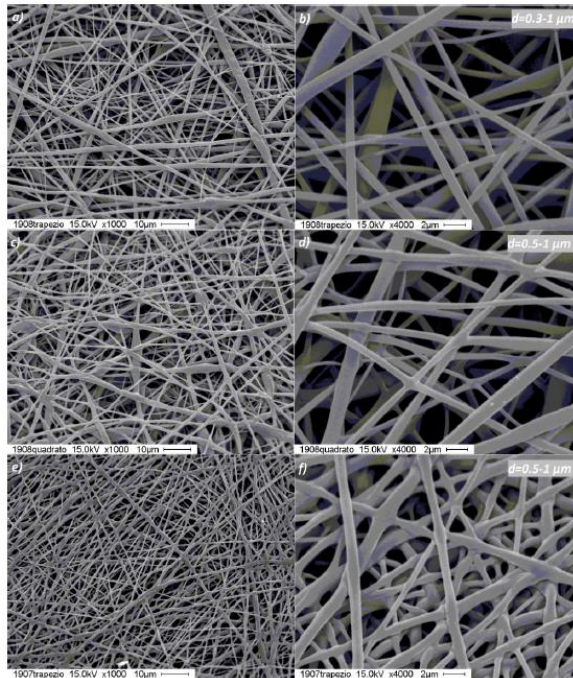
Figure 4.16. SEM images) of 1000x Coax13, b) of 4000x Coax13, c) of 1000x Coax25, d) of 4000x Coax25, e) of 1000x Coax37, f) of 4000x Coax37.

NANOFIBRE FORMATION OF PLGA-g-PVP COPOLYMER BY
ELECTROSPINNING
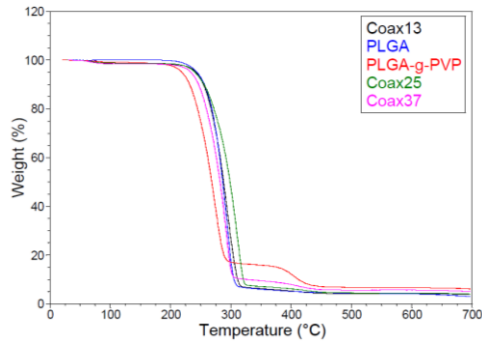
Figure 4.17. TGA overlapping tissue-non-tissue of $Coax_{13}$, $Coax_{25}$ and $Coax_{37}$ and of the starting polymers PLGA and PLGA-g-PVP. Temperature ramp of 10 °C/min.

Table 4.6. PVP weight loss% of Coax and Blend samples from TGA analysis.

Sample	Δm (%) 350°C - 500°C
$Coax_{13}$	2.1
$Coax_{25}$	2.7
$Coax_{37}$	3.9
$Blend_{13}$	2.1
$Blend_{37}$	3.7

$Coax_{13}$, $Coax_{25}$, $Coax_{37}$ presented increasing weight amount of PVP in fibres, as expected by increasing flow rate of external solution. Comparing the values obtained from $Coax_{13}$ and $Coax_{37}$ and the respective $Blend_{13}$ $Blend_{37}$, PVP content was comparable.

Contact angle values of Coax samples and for comparison also those Blend were reported in Table 4.7. In this case fibre diameters were not shown because all samples had sub-micrometre dimension and similar morphology. $Coax_{13}$ and $Coax_{25}$ samples were still hydrophobic, while $Coax_{37}$ was wettable. In contrast, the blend with the same composition, i.e. $Blend_{37}$, was hydrophobic. Therefore, coaxial needle favoured PLGA-g-PVP location on fibre surface and a quantity of 37% by weight appears to be sufficient to wet the scaffold. It is noted that the drop of water is absorbed by the $Coax_{37}$

NANOFIBRE FORMATION OF PLGA-g-PVP COPOLYMER BY
ELECTROSPINNING

sample in about 25 seconds, time significantly greater than that of the pure
PLGA-g-PVP non-woven fabric, about 2 sec.

Table 4.7. Comparison of the mean contact angle of samples Blend and Coax
samples.

Sample	Average contact angle (°)
Coax₁₃	126 ± 7
Coax₂₅	121 ± 6
Coax₃₇	Decreasing trend over time Drop was adsorbed after 25 s
Blend₁₃	122 ± 6
Blend₃₇	122 ± 3

4.8 CONCLUSIONS

In this work, PLGA-based scaffolds were produced by electrospinning for
biomedical applications. In order to modulate the wettability of the scaffolds
PLGA, which is a hydrophobic copolymer, has been used in combination to a
synthetic copolymer consisting of a main chain of PLGA with grafts lateral
chains constituted by highly hydrophilic units of poly(vinylpyrrolidone), named
(PLGA-g-PVP).

Measurements of contact angle conducted on only PLGA film and only
PLGA-g-PVP has confirmed the increased wettability of the latter with respect
to the only PLGA. Comparing the wettability of the corresponding non-
woven-fabrics for the difference in wettability is even more obvious: the
scaffold is PLGA is highly hydrophobic, while the scaffold is PLGA-g-PVP
absorbs water drops in a few seconds. Then, comparing contact angle values
obtained from the same materials but with different surface roughness, it was
found that a film with a smooth surface by the use of a spin coater, had
smaller contact angles and was therefore more wettable with respect to the
fibrous scaffolds, that it is a porous material with a highly corrugated surface at
micrometre level.

To modulate the wettability of the scaffolds, minimizing the amount of
synthetic PLGA-g-PVP, PLGA fibres containing small amounts of PLGA-g-

NANOFIBRE FORMATION OF PLGA-g-PVP COPOLYMER BY ELECTROSPINNING

PVP were electrospinned adopting two different strategies: (1) by electrospinning of mixtures of PLGA and PLGA-g-PVP to obtain fibres with different content of copolymers depending on their concentration in the starting solution; (2) by coaxial electrospinning, in which PLGA-g-PVP solution fed the external needle and PLGA solution fed the internal one. PLGA-g-PVP content in the fibres depends by solution concentrations and flow rates.

The composition of the scaffolds products was verified by TGA measures and the wettability by contact angle measurements.

From contact angle measurements on scaffolds produced by electrospinning of blends, it was concluded that the addition of PLGA-g-PVP to PLGA solution with w/w percentage of 37%, did not vary significantly the wettability of the material. Most likely, having PLGA-g-PVP a low amount of PVP (10% w/w , as valuated by TGA analysis), it was assumed that the few PVP chains were homogeneously distributed along the fibre section, and thus, did not lead to a significant increase of material hydrophilicity.

Therefore, PLGA-g-PVP was tried to locate on fibre surface in order to better exploit the hydrophilicity of this copolymer to modify scaffold wettability, by using coaxial electrospinning. Analysing three products containing increasing percentages of PLGA-g-PVP, only the sample having 37% w/w appeared to be well wettable: indeed, a water drop was absorbed by the porous structure in approximately 25 seconds. In addition, this scaffold was more wettable than that of one produced by electrospinning of the mixture having similar composition. Therefore, it can be concluded that coaxial electrospinning was useful to prepare wettable PLGA-based non-woven fabric. It was also demonstrated that wettability of nonwoven fabrics was influenced both by the morphology of the same fabric, both on the chemical composition of the fibres.

NANOFIBRE FORMATION OF PLGA-g-PVP COPOLYMER BY ELECTROSPINNING

BIBLIOGRAPHY

[i] W.J. Li, R.M. Shanti, R.S. Tuan, *Electrospinning Technology in Nanofibrous Scaffolds in Tissue Engineering from Nanotechnologies for the Life*, Sciences, by John Wiley and Sons, Inc. **1999-2012**

[ii] J.W.G. Rayleigh, *London, Edinburgh and Dublin Philosophical Magazine and Journal of Science*, **1882**, 14, 184-186

[iii] M. Dole, L.L. Mack, R.L. Hines, *Journal of Chemical Physics*, **1968**, 49, 2240-2249

[iv] Patent 1,975,504. **1934**

[v] Patent 3,280,229. **1966**

[vi] P.K. Baumgarten, *Journal of Colloid Interface Science*, **1971**, 36, 71-79

[vii] L. Larrondo, R.S.J. Manley, *Journal of Polymer Science Part B: Polymer Physics*, **1981**, 19, 909-920

[viii] L. Larrondo, R.S.J. Manley, *Journal of Polymer Science Part B: Polymer Physics*, **1981**, 19, 921-932

[ix] L. Larrondo, R.S.J. Manley, *Journal of Polymer Science Part B: Polymer Physics*, **1981**, 19, 933-940

[x] D.H. Reneker, I. Chun, *Nanotechnology*, **1996**, 7, 216-223

[xi] G.I. Taylor, *Proceedings of the Royal Society of London*, **1969**, 453-475

[xii] G.I. Taylor, *Proceedings of the Royal Society of London*, **1964**, 383-397

[xiii] A. Frenot, I.S. Chronakis, *Current Opinion in Colloid and Interface Science*, **2003**, 8, 64-75

[xiv] S. Kidoaki, I.K. Kwon, T. Matsuda, *Biomaterials*, **2005**, 26, 37-46

[xv] J.J. Stankus, J. Guan, K. Fujimoto, W.R. Wagner, *Biomaterials*, **2006**, 27, 735-744

[xvi] Patent US 8758668 B2, **2014**

[xvii] T.J. Sill, H.A. von Recum, *Biomaterials*, **2008**, 29, 1989-2006

[xviii] T. Subbiah, G.S. Bhat, R.W. Tock, S. Pararneswaran, S.S. Ramkumar, *Journal of Applied Polymer Science*, **2005**, 96, 557-569

[xix] J. Doshi, D.H. Reneker, *Journal of Electrostatics*, **1995**, 35, 151-160

[xx] H.S. Kim, K. Kim, H.J. Jin, I.J. Chin, *Macromolecular Symposia*, **2005**, 224,145-154

[xxi] Z. Jun, H.Q. Hou, A. Schaper, J.H. Wendorff, A. Greiner, *E-Polymers*, **2003**, 3, 102-110

[xxii] J.M. Deitzel, J. Kleinmeyer, D. Harris, N.C.B. Tan, *Polymer*, **2001**, 42, 261-272

[xxiii] X.H. Zong, K. Kim, D.F. Fang, S.F. Ran, B.S. Hsiao, B. Chu, *Polymer*, **2002**, 43, 4403-4412

[xxiv] R. Jaeger, M.M. Bergshoef, C.M.I. Batlle, H. Schonherr, G.J. Vancso, *Macromolecular Symposia,* **1998**, 127, 141-150

xxv J.M. Deitzel, J. Kleinmeyer, D. Harris, N.C.B. Tan, *Polymer*, **2001**, 42, 261-272

xxvi M.M. Demir, I. Yilgor, E. Yilgor, B. Erman, *Polymer*, **2002**, 43, 3303–3309

xxvii C. Meechaisue, R. Dubin, P. Supaphol, V.P. Hoven, J. Kohn, *Journal of Biomaterials Science, Polymer Edition,* **2006**, 17, 1039-1056

xxviii Y.S. Huang, C.C. Kuo, C.C. Huang, S.C. Jang, W.C. Tsen, F.S. Chuang, B.Y. Chen, J.J. Chen, J.D. Chow, Y.C. Shu, *RSC Advances*, **2015**, 5, 88857-88865

xxix P. Baumgarten, *Journal of Colloid and Interface Science*, **1971**, 36, 71-79

xxx C.X. Zhang, X.Y. Yuan, L.L. Wu, Y. Han, J. Sheng, *European Polymer Journal*, **2005**, 41, 423-432

xxxi C. Pattamaprom, W. Hongrojjanawiwat, P. Koombhongse, P. Supaphol, T. Jarusuwannapoo, R. Rangkupan, *Macromolecular Materials and Engineering*, **2006**, 291, 840-847

xxxii J. Liu, S. Kumar, *Polymer*, **2005**, 46, 3211-3214

xxxiii T. Jarusuwannapoom, W. Hongroijanawiwat, S. Jitjaicham, L. Wannatong, M. Nithitanakul, C. Pattamaprom, P. Koombhongse, R. Rangkupan, P. Supaphol, P. *European Polymer Journal*, **2005**, 41, 409-421

xxxiv L. Wannatong, A. Sirivat, P. Supaphol, *Polymer International*, **2004**, 53, 1851-1859

xxxv E. Emerick, S. Grant, M. Bernards, *Chemical Engineering and Process Techniques*, **2013**, 1, N°1003

xxxvi W.W. Zuo, M.F. Zhu, W. Yang, H. Yu, Y.M. Chen, Y. Zhang, *Polymer Engineering and Science*, **2005**, 45, 704-709

xxxvii X.Y. Yuan, Y.Y. Zhang, C.H. Dong, J. Sheng, *Polymer International*, **2004**, 53, 1704-1710

xxxviii X.H. Zong, K. Kim, D.F. Fang, S.F. Ran, B.S. Hsiao, B. Chu, *Polymer*, **2002**, 43, 4403-4412

xxxix S. Megelski, J.S. Stephens, D.B. Chase, J.F. Rabolt, *Macromolecules*, **2002**, 35, 8456-8466

xl J.H. Chai, Q.S. Wu, J. Beilstein, *Nanotechnology*, **2013**, 4, 189-197

xli C.J. Luo, M. Edirisinghe, *Macromolecules*, **2014**, 47, 7930-7938

xlii W. Liu, C. Huang, X. Jin, *Nanoscale Research Letters*, **2014**, 9, 350, 10 pages

xliii C. Mit-Uppatham, M. Nithitanakul, P. Supaphol, *Macromolecular Chemistry and Physics*, **2004**, 205, 2327-2338

xliv C.L. Casper, J.S. Stephens, N.G. Tassi, D.B. Chase, J.F. Rabolt, *Macromolecules,* **2004**, 37, 573-578

NANOFIBRE FORMATION OF PLGA-g-PVP COPOLYMER BY ELECTROSPINNING

[xlv] Haoyi Li and Weimin Yang *Electrospinning Technology in Non-Woven Fabric Manufacturing, Non-woven Fabrics*, Han-Yong Jeon (Ed.), InTech, **2016**

[xlvi] M.F. Elahi, W. Lu, G. Guoping, F. Khan, *Journal of Bioengineering & Biomedical Science*, **2013**, 3, 121, 14 pages

[xlvii] H. Qu, S. Wei, Z. Guo, *Journal of Materials Chemistry A*, **2013**, 1, 11513-11528

[xlviii] A.L. Medina-Castillo, J.F. Fernández-Sánchez, A. Fernández-Gutiérrez, *Advanced Functional Materials*, **2011**, 21, 3488-3495

[xlix] Y.Z. Zhang, J. Venugopal, Z.M. Huang, C.T. Lim, S. Ramakrishna, *Biomacromolecules*, **2005**, 6, 2583-2589

[l] Y. Zhang, Z.M. Huang, X. Xu, C.T. Lim, S. Ramakrishna, *Chemistry of Materials*, **2004**, 16, 3406-3409

[li] I.G. Loscertales, A. Barrero, I. Guerrero, R. Cortijo, M. Marquez, *Science*, **2002**, 295, 1695-1698

[lii] C.P. Barnes, S.A. Sell, E.D. Boland, D.G. Simpson, G.L. Bowlin, *Advanced Drug Delivery Reviews*, **2007**, 59, 1413-1433

[liii] J. Meeus, X. Chen, D.J. Scurr, V. Ciarnelli, K. Amssoms, C.J. Roberts, M.C. Davies, G. Van Den Mooter, *Journal of Pharmaceutical Sciences*, **2012**, 101, 3473-3485

[liv] J.S. Choi, S.W. Lee, L. Jeong, S. Bae, B.C. Min, J.H. Youk, W.H. Park, *International Journal of Biological Macromolecules,* **2004**, 34, 249-256

[lv] E. Kenawy, J.M. Layman, J.R. Watkins, G.L. Bowl, *Biomaterials,* **2003**, 24, 907-913

[lvi] K.H. Lee, H.Y. Kim, H.J. Bang, Y.H. Jung, S.G. Lee, *Polymer,* **2003**, 44, 4029-4034

[lvii] S.L. Shenoy, W.D. Bates, H.L. Frisch, G.E. Wnek, *Polymer*, 2005, 46, 10, 3372-3384

[lviii] S. Huan, G. Liu, G. Han, W. Cheng, Z. Fu, Q. Wu, Q. Wang, *Materials*, 2015, 8, 2718-2734

[lix] C. Tsai, Y. Gu, K.G. Kornev, *Colloids and surfaces A: Physicochemical and engineering aspects* , **2014**, 459, 22-30

"Aim of this piece of work was the synthesis of a new classes of poly(saccharide-co-amidoamine) and poly(saccharide-protein-amidoamine) 3-D-networks intended as scaffolds for tissue regeneration. In particular, hyaluronan-polyamidoamine and hyaluronan-gelatin-polyamidoamine hydrogels were synthesised by amidation reaction between the carboxylate groups of hyaluronan and the amine groups of gelatin and of an NH$_2$-functionalized PAA, promoted by 4-(4,6-dimethoxy-1,3,5-triazin-2-yl)-4-methylmorpholinium chloride (DMTMM) as coupling agent. In order to promote hepatic cell proliferation serotonin was covalently linked to hydrogels, by adding it to the reaction mixture, exploiting the same coupling reaction."

5.1 HYDROGELS

Hydrogels are made up of cross-linked polymer networks and may be classified as: (i) chemical hydrogels and (ii) physical hydrogels. In (i), the polymer network is obtained by chemical cross-linking, whereas in physical hydrogels (ii), chains are held together by ionic, hydrogen bonding and or dipolar interactions. Linear homopolymers, linear copolymers, and block or graft copolymers having cross-linkable functional groups are usually used to form chemical cross-linked hydrogel, on the other hand, polyion-, polyion–polyion or H–bonded complexes as physical cross-linked matrix.[i] In both cases, cross-link density is crucial in determining the properties and applications of the gels, as it is responsible for the swelling behaviour and therefore for the combined solid-like and liquid-like characteristics.

Main property of hydrogels is the ability to absorb huge amounts of water, up to several thousand percentages, without dissolving.[ii] Equilibrium state is reached when osmotic driving forces, which encourage water to come into the hydrogel matrix, and cohesive ones exerted by hydrogel macromolecules are balanced. Cohesive forces depend primarily on hydrogel crosslinking density.[iii,iv] In general, the higher the cross-linking extent, the lower the gel swelling. Equally, the more hydrophilic the polymer matrix, the higher the amount of water absorbed by the hydrogel.[v] In the swollen state, hydrogels are

soft and rubbery, resembling to a great extent living tissues. For this reason, hydrogels have become attractive to the new field of 'tissue engineering' as matrices used for cell/tissue regenerating.[vi,vii,viii,ix,x,xi]

In order to be used as biomaterials, hydrogels must be biocompatible. Inflammatory response to a hydrogel can affect the immune response toward the transplanted cells and vice versa.[xii,xiii] In particular if they are components of or have macromolecular properties similar to the natural extracellular matrix (ECM).[xiv,xv,xvi]

5.2 HYALURONIC ACID

Hyaluronic acid[xvii,xviii,xix] is a naturally occurring, biocompatible, and biodegradable polysaccharide composed of repeating disaccharide units of D-glucuronic acid and N-acetyl-d-glucosamine linked by alternating β(1→4) and β(1→3) linkages. Carboxyl groups in the glucuronic acid residues are negatively charged at physiological pH and ionic strength, giving as result a polyanions sodium hyaluronate, referred as hyaluronan (HA). [xx] It is the simplest glycosaminoglycan (GAG) and an important component of ECM, it is ubiquitously present in many biological fluids and tissues, such as eyes, joints, and cartilage.[xxi,xxii] It is naturally synthesized by a class of integral membrane proteins called hyaluronan synthases,[xxiii] and degraded by a family of enzymes called hyaluronidases.[xxiv] Degradation products, i.e. oligomeric HA ($\bar{M}_n$<100 000), are usually found as inflammatory, immuno-stimulatory and angiogenic.[xxv] These chains are then fractionated in monosaccharide units by β-d-glucuronidase, and β-N-acetylhexosaminidase.[xxiv]

Its function in the body is, among others, to bind water and lubricate movable parts of the body, such as joints and muscles. HA is highly hygroscopic and this property is believed to be important for modulating tissue hydration and osmotic balance.[xxvi] In addition to its function as a passive structural molecule, HA also acts as a signalling molecule by interacting with cell surface receptors and regulating cell proliferation, migration, and differentiation.[xxvii,xxviii] Thanks to these favourable properties, HA has been intensively used as component of scaffolds for tissue engineering.[xxix,xxx,xxxi]

A pitfall of HA-based materials is the fast HA *in vivo* degradation. HA half-life after injection into skin and joints is lower than 24 h.[xxxii,xxxiii] This time is not enough to allow restoring of tissues and lost functionalities. Modifications of HA chemical structure are needed, in order to camouflage HA chains to enzymes.[xxxiv]

HYDROGELS FOR TISSUE ENGINEERING BASED ON HYALURONIC ACID, GELATIN AND AGMA1

HA can be chemically modified by two different ways: cross-linking or conjugation. HA conjugation and HA cross-linking can be in principle based on the same chemical reactions and only differ in that, in the first case, a compound is grafted onto one HA chain by a single bond only, whereas in the second case, different HA chains are linked together by two bonds or more, as depicted in Figure 5.1. Some methods are performed in water while others, need to be performed in organic solvents, such as dimethylformamide (DMF) or dimethylsulfoxide (DMSO).[xxxv,] In the latter case, native HA sodium salt first needs to be converted into its acidic form. Since HA is soluble in water, the easiest method is to perform the reaction in water. However, treatments in alkaline or acidic aqueous conditions induce hydrolysis of HA chains.[xxxvi,xxxvii]
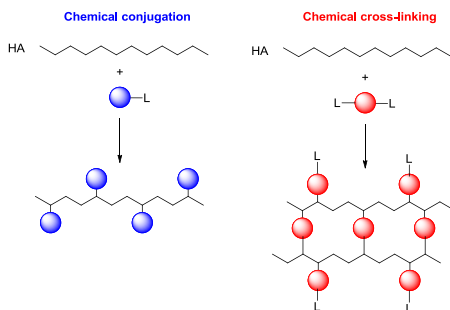
Figure 5.1. Schematic representation of chemical conjugation and cross-linking.

Typical partners in cross-link/conjugation products are polysaccharides (alginate[xxxviii], chitosan[xxxix], agarose[xl], etc), proteins or oligopeptide (fibronectin[xli], fibrin,[xlii] gelatin[xliii], collagen[xliv], etc) and also synthetic polymers, such as PLA,[xlv] PLGA[xlvi], PGA[xlvii] PHEMA[xlviii] and so on.[xlix] In addition to reduce degradation rate, improvement in cell adhesion onto HA-based scaffolds is reached when carboxylic acid groups are involved in reactions. It is due to a reduction of repulsive force between cell membranes (negative charged by presence of lipids) and carboxylic acid of HA.[l]

5.3 GELATIN

Gelatin is a soluble protein obtained by partial hydrolysis of collagen, the main fibrous protein constituent in bones, cartilages and skins; therefore, the source, age of the animal, and type of collagen, are all intrinsic factors influencing properties of the produced gelatin.[li] The acid-extracted gelatin is designated

HYDROGELS FOR TISSUE ENGINEERING BASED ON HYALURONIC
ACID, GELATIN AND AGMA1

"Type A" , whereas the product of the alkaline method is referred to as "Type B". Traditionally, hydrogen chloride and lime or sodium hydroxide are used for the types A and B methods, respectively.[lii]

Compared to its precursor, gelatin is economical and low-antigenic, and it has been presumed to retain some of the information signals, such as the RGD sequence of collagen,[liii] also if its biological activity of gelatin should be zero, due to the absence of the essential amino acid, i.e. tryptophan.[liv] The tripeptide arginyl-glycyl-aspartic acid (RGD) is an oligopeptide capable of reproducing the receptorial sites of proteins, such as fibronectin, vitronectin, and others playing a fundamental role in cell adhesion.[lv]

Gelatin is reported to contain 18 amino acids linked together in a partially ordered fashion. The various amino acids obtainable from some gelatins by complete hydrolysis, in grams per 100 grams of dry gelatin, are listed in Table 5.1.[lvi,lvii,lviii] No significant differences in the value of N-terminal residues as well as in the amino acid composition have been mentioned relating to the origin of gelatin. Type A gelatin has been reported to have an isoionic point of 7 to 9, and the isoionic point for lime (alkali) processed gelatin falls in the range of 4.8 to 5.1.[lix] Isoionic points are important values, determining the reactivity of gelatin, especially in pH-dependent coupling reaction.

Table 5.1. Amino acid composition of different type and source of gelatin.

Amino Acid	Type A	(Pork skin)	Type B	(Calf skin)	Type B	(Bone)
Alanine	8.6	10.7	9.3	11.0	10.1	14.2
Arginine	8.3	9.1	8.55	8.8	5.0	9.0
Aspartic acid	6.2	6.7	6.6	6.9	4.6	6.7
Cystine	0.1		Trace		Trace	
Glutamic acid	11.3	11.7	11.1	11.4	8.5	11.6
Glcine	26.4	30.5	26.9	27.5	24.5	28.8
Histidine	0.9	1.0	0.74	0.8	0.4	0.7
Hydroxlysine	1.0		0.91	1.2	0.7	0.9
Hydroxyproline	13.5		14.0	14.5	11.9	13.4
Isoleucine	1.4		1.7	1.8	1.3	1.5
Leucine	3.1	3.3	3.1	3.4	2.8	3.5
Lysine	4.1	5.2	4.5	4.6	2.1	4.4
Methionine	0.8	0.9	0.8	0.9	0.0	0.6
Phenylalanine	2.1	2.6	2.2	2.5	1.3	2.5
Proline	16.2	18.0	14.8	16.4	13.5	15.5
Serine	2.9	4.1	3.2	4.2	3.4	3.8
Threonine	2.2		2.2		2.0	2.4
Tyrosine	0.4	0.9	0.2	1.0	0.0	0.2
Valine	2.5	2.8	2.6	3.4	2.4	3.0

HYDROGELS FOR TISSUE ENGINEERING BASED ON HYALURONIC ACID, GELATIN AND AGMA1

Since gelatin has a sol-gel transition temperature around 30 °C, it should be chemically cross-linked in order to avoid dissolution at body temperature. Thanks to the fact that gelatin is composed of a large variety of side chains, a wide variety of chemical modification methods, introducing cross-linkable groups, have been proposed.[lx, lxi] The choice of potential reagents is limited to water-stable ones because gelatin only dissolves in water and in a number of alcohols.[lxii] In most cases, bifunctional reagents including glutaraldehyde,[lxiii] diisocyanates,[lxiv,lxv] carbodiimides,[lxvi] genipin,[lxvii] polyepoxy-compounds,[lxviii] and acyl azides[lxix] have been applied. When gelatin is combined with sugars (e.g., agarose), 1,1-carbonyldiimidazole can be applied as cross-linker.[lxx]

5.4 AGMA 1

The linear amphoteric poly(amidoamine) nicknamed AGMA1 is prepared by the Michael-type polyaddition of monoprotonated 4-aminobutylguanidine (agmatine) and 2,2-bis(acrylamido)acetic acid (BAC).[lxxi] Agmatine belongs to the family of biogenic amines and is involved in many physiological functions. Agmatine derives from the arginine decarboxylase-mediated decarboxylation of L-arginine, a semi-essential amino acid with interesting properties mostly attributed to its guanidine group. Agmatine and arginine play an important role in cell growth and proliferation, as well as in the synthesis of proteins and nucleic acids.[lxxii]

Table 5.2. Comparison of Some Structural Features of AGMA1 Repeating Unit and RGD Sequence

Structural features	AGMA 1 unit	RGD sequence
no. of guanidine groups	1	1
no. of carboxyl groups	1	1
no. of amidic groups	2	2
distance between guanidine and carboxyl groups	sequence of 10 atoms including 2 amidic groups	sequence of 11 atoms including 2 amidic groups

AGMA1 repeating unit carries both guanidine- and carboxyl groups and, therefore, shows a strong structural resemblance to the RGD sequence (Table 5.2). It was reported that AGMA1 is nontoxic and non-haemolytic *in vitro* within all pH ranges tested (4-7.5).[lxxi] Haemolysis is usually a function of the overall charge, reaching low value at physiological and neutral pHs. High toxicity was usually associated with the polycationic character of other studied PAAs.[lxxiii] As revealed from speciation curves (Figure 5.2), AGMA1's isoelectric point is at pH 10, corresponding to the intersection of the curves

relative to LH$^+$ and L$^-$. Charge distribution profiles show that this polymer is prevailingly cationic at all physiological pH values, the net average charge per unit varying from about 0.5 at pH 7.4, to about 1.0 at pH 5. Probably, the RGD-like repeating units exert a stabilizing action on cell membranes, overshadowing the membranolytic effect of the excess positive charges.

Grafted on a material's surface, RGD is capable of promoting a strong cell adhesion even at very low surface densities.[lxxiv] Similarly, AGMA1 hydrogels have exhibited good cell proliferation ability. In particular, AGMA1 hydrogel layers exhibited towards epithelial cells (Madin-Darby Canine Kidney epithelial cell line) a level of cell adhesion comparable to that of commercial plastic substrates for tissue culturing even in the presence of only 0.1% of fetal bovine serum.[lxxv] AGMA1 hydrogels were successfully used as scaffold for tissue engineering.[lxxvi] In particular, hydrogels with tubular shape proved to facilitate nerve regeneration, achieving good surgical outcomes with no signs of inflammation or neuroma.[lxxvii] In addition, AGMA1–montmorillonite composites with tunable stiffness were used as scaffolds for bone tissue-engineering applications.[lxxviii]
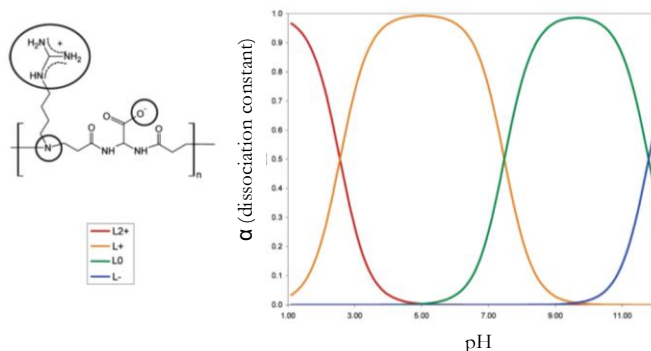
Figure 5.2. AGMA1 ionic speciation as a function of pH. Figure adapted from reference.[lxxiii]

5.5 Chemical design of hydrogels

Aim of this work was the production of chemical cross-linked hydrogels with potential as scaffolds for the regeneration of liver tissue. Sodium hyaluronate and gelatin (HA-Gel) were selected as scaffolding material to mimic the crucial components of ECM, in order to enhance cell proliferation, migration, and differentiation of liver tissue.

HYDROGELS FOR TISSUE ENGINEERING BASED ON HYALURONIC ACID, GELATIN AND AGMA1

HA-Gel scaffolds for tissue engineering were already described in literature.[lxxix] Leaving apart studies in which HA-Gel physical blends were used,[lxxx,lxxxi,lxxxii] all other works reported 3-4 step long synthetic schemes, consisting firstly in functionalization step of one terminus or pendant groups of both reagents followed by coupling reaction.[lxxxiii,lxxxiv,lxxxv,lxxxvi,lxxxvii,lxxxviii]

In one instance, the use of 1-ethyl-3-(3-dimethylaminopropyl) carbodiimide (EDC) as cross-linker agent in order to obtain hydrogels with a one-step process is reported.[lxxxix] In this work, HA-Gel scaffolds were fabricated by freeze-drying of blend solution and then immersed for 24h in EDC solution. In the resulting hydrogels, EDC efficacy was observed as gelatin cross-linker, but not for HA one. HA was only physical dispersed in the hydrogel structure, and gradually released when immersed in an aqueous solution. Furthermore, proliferation of L929 fibroblasts on the surfaces of these scaffolds after cell culturing showed a lower activity compared with control plate.

In this work, introducing AGMA1 in HA-Gel hydrogels was expected bring many benefits: on one side it will allow forming macroscopically homogeneous hydrogels with HA and gelatin, thanks to its easy coupling with both polymers. In addition, the RGD-mimic cationic AGMA1 units and their counteracting HA polyanionic nature, responsible for repulsive interactions with cell membranes, may improve cell adhesion and proliferation. As a further modification, serotonin (Ser) was introduced in the hydrogel structure to improve liver cell adhesion and proliferation. Serotonin is a biogenic monoamine neurotransmitter with variable effects on many different target organs.[xc] It is derived from the L-tryptophan, which is hydroxylated to 5-hydroxy-L-tryptophan (5-HTP) by tryptophane hydroxylase (Tph). Recent scientific studies highlighted the involvement of serotonin in the induction of hepatocyte DNA synthesis after a hepatectomy in the rat and human.[xci,xcii] Serotonin can be potentially associated with either beneficial or detrimental effects on liver regeneration and these actions are mediated through many different receptor subtypes located either centrally or peripherally.[xciii]

In this work, hydrogels were synthesised by a one-pot coupling reaction between the carboxylate groups of HA and the amine groups of Gel, AGMA1 and Ser, using 4-(4,6-dimethoxy-1,3,5-triazin-2-yl)-4- methylmorpholinium chloride (DMTMM) as coupling agent. DMTMM is a water-soluble cross-linker used for the amide bond formation of amines in presence of carboxylic group, without taking part in linkages.[xciv] According to literature reports, DMTMM efficacy is superior to that of EDC/NHS (1-ethyl-3-(3-dimethylaminopropyl) carbodiimide / N-Hydroxysuccinimide),[xcv] PyBOP ((Benzotriazol-1-yloxy)tripyrrolidinophosphonium hexafluorophosphate)[xcvi] for ligation of amines to carboxylate anions. Furthermore, it does not require accurate pH control or pH shift during the reaction to be effective.[xcvii]

HYDROGELS FOR TISSUE ENGINEERING BASED ON HYALURONIC ACID, GELATIN AND AGMA1

5.6 EXPERIMETAL SECTION

5.6.1 Materials

Sodium hyaluronate (HA) with a $\bar{M}n$ 260 000 (evaluated by Size Exclusion Cromatography, SEC) was obtained from Bioiberica, Gelatin powder from bovine skin (type B with bloom ~225 g) was purchased from Sigma Aldrich (Spain). 2,2-Bis(acrylamido)acetic acid (BAC) were synthesized as previously described and purity determined by Nuclear Magnetic Resonance (NMR) and titration.[xcviii] 4-Aminobutylguanidine sulphate (agmatine), lithium hydroxide monohydrate, 4-(4,6-dimethoxy-1,3,5-triazin-2-yl)-4-methylmorpholinium chloride (DMTMM), N-Boc-ethylenediamine, 37% hydrochloridic acid, serotonin, sodium nitrate, sodium phosphate monobasic were purchased from Sigma-Aldrich. Phosphate buffer solution (PBS) was prepared using Sigma Aldrich dry powder. All these reagents were used without further purification.

5.6.2 Methods

^{1}H-, ^{13}C-, HSQC-, and COSY- NMR spectra were recorded using a Bruker NMR spectrometer operating at 400 and 133.3 MHz. Spectra were recorded on samples dissolved in deuterium oxide (D$_2$O).

SEC analyses were obtained using a Shimadzu system comprising a DGU-20A3 solvent degasser, an LC-20AD pump, a CTO-20A column oven, an SIL-20A HT autosampler, an RID- 10A refractive index and an SPD-20A Shimadzu UV-VIS detector (flow rate: 1 mL min^{-1}, temperature: 40°C). The instrument was equipped with three columns (300 mm x 7.5 mm, 8 mm): PL-aquagel-OH 30 ^{TM}, PL-aquagel-OH 40^{TM} and PLaquagel- OH 50^{TM}, protected with a guard column (50 mm x 7.5 mm, 8 mm) (Polymer Laboratories). Calibration was performed with polysaccharide standards (Pullulan Polysaccharide, PL2090-0100 VARIAN) ranging from 180 to 708 000. The eluent was a pH 7 0.2 M NaNO$_3$ and 0.01 M NaHPO$_4$ buffer solution prepared using milli-Q water. Samples concentration 2 mg/mL.

Fourier Transformed Infrared (FTIR) spectra in Attenuated Total Reflection mode (ATR-FTIR) were obtained using a Perkin Elmer Spectrum One instrument. Spectra of reagents and dried hydrogels were recorded in the 4000 to 650 cm^{-1} range after 4 scans and with a resolution of 4 cm^{-1}.

Thermogravimetric analysis (TGA) was performed on 10 mg dry hydrogels with a TGA Q500 (TA Instruments) working from 25 to 600°C at 10°C/min

heating rate and under 50 mL/min nitrogen flow. Tests were repeated two times and data obtained as media of these measurements.

Differential scanning calorimetric (DSC) analyses were carried out with a Mettler Toledo DSC823 (Mettler Toledo, Italy) equipped with the STAR Software and the FRS5 Mettler Toledo ceramic sensor. The instrument was calibrated with indium for melting point and heat of fusion. The dry samples (5-10 mg) were placed in aluminium pans and heated from 0 to 200°C at a constant rate of 10°C min^{-1}. Empty pan was taken as reference. Tg was taken as the midpoint of the heat capacity transition.

Atomic force microscopy (AFM) experiments were performed in tapping mode using a Multimode AFM (Veeco Instruments, Santa Barbara, CA) equipped with a Nanoscope IVa control system (software version 6.14r1). Silicon tapping probes (RTESP, Veeco) were used with a resonance frequency of 300 kHz and a scan rate of 0.5 Hz. 3 µm² AFM images were taken for each sample. Topography was examined by topographical AFM, whereas composition was explored using phase imaging AFM.

5.6.3 Synthesis of AGMA$_{10}$ and AGMA$_{20}$

In a 200 mL flask, BAC (purity: 97%, 10.0 g, 0.049 mol) and lithium hydroxide monohydrate (2.04 g, 0.049 mol) were dissolved under stirring in distilled water (17 mL) and degassed with nitrogen. After complete dissolution, 4-Aminobutylguanidine sulphate (10.056 g, 0.044 mol) and lithium hydroxide monohydrate (1.88 g, 0.044 mol) were added. The clear reaction mixture was allowed to react for 5 days at room temperature in the dark. Mono-N-BOC-ethylenediamine (1.88 g, 0.012 mol) was then added under stirring and mixture allowed reacting for 1 day in the dark. After this time, the solution was acidified to pH 5 with few drops of a 3 M HCl aqueous solution and maintained under stirring for 15 min. The final product was purified by ultrafiltration with a membrane with nominal molecular weight cut-off 1000 and recovered by freeze-drying. Yield = 12.7 g (63.4%).

AGMA$_{20}$ was synthesized as described for AGMA$_{10}$ using the following reagent amounts: BAC (10.0 g, 0.049 mol), LiOH·H$_2$O (2.04 g, 0.049 mol), 4-Aminobutylguanidine sulphate (9.11 g, 0.039mol), LiOH·H$_2$O (1.66 g, 0.039), N-BOC-ethylenediamine (3.24 g, 0.020 mol). Yield = 2.97 g (15.5%). The NMR spectra were as reported for AGMA$_{10}$.

HYDROGELS FOR TISSUE ENGINEERING BASED ON HYALURONIC ACID, GELATIN AND AGMA1

^{1}H-NMR 400.132 MHz (D$_2$O, δ, ppm): 1.52-1.70 (m, NCH$_2$**CH$_2$**CH$_2$CH$_2$NH), 1.70-1.92 (br, NCH$_2$CH$_2$**CH$_2$**CH$_2$NH), 2.32-2.52 (br, NHCH$_2$**CH$_2$**NH$_2$), 2.69-2.88 (br, **CH$_2$**CONH), 2.88-2.95 (br, NH**CH$_2$**CH$_2$NH$_2$), 3.13-3.29 (m, NC**CH$_2$**CH$_2$CO), 3.40-3.62 (br, NC**CH$_2$**CH$_2$CH$_2$C**H$_2$**NH), 5.52 (s, C**H**-COO$^-$).

^{13}C NMR 100 MHz (D$_2$O, δ, ppm) 20.5 (NHCH$_2$CH$_2$**C**H$_2$), 25.1 (NHCH$_2$**C**H$_2$), 29.1 (NHCOCH$_2$**C**H$_2$), 35.8 (NHCH$_2$**C**H$_2$NH$_2$) 40.5 (CH$_2$N**C**H$_2$), 44.4 (NH**C**H$_2$CH$_2$NH$_2$) 49.3 (NHCO**C**H$_2$), 52.2 (NH**C**H$_2$), 56.0 (COOH**C**H), 155.1 (NH$_2$**C**NNH), 171.3 (NH**C**O), 173.5 (CH**C**OOH).

5.6.4 Synthesis of HA-Gel-AGMA, HA-AGMA and HA-Gel hydrogels

HA (0.500 g) and Gel (1.00 g) were dissolved in bidistilled water (10 mL) at 50ºC under vigorous stirring for 15 min. After complete dissolution, AGMA$_{10}$ (0.100 g) was added to the solution, followed by DMTMM (0.150 g). The resultant clear solution was poured in the wells (1 cm diameter, 0.2 cm thickness) of 12-well plate using a 10 mL syringe. The reacting mixtures were allowed reacting for totally 48 h at 37.5ºC in a humid atmosphere, even though the observed setting time was 5 min. The hydrogels were retrieved and freeze-dried.All hydrogels were prepared by following the general procedure described for the HA-Gel-AGMA$_{10}$ hydrogel and using the amounts of reagents reported in Table 5.3.

Table 5.3. Experimental parameters for hydrogel synthesis.

Sample	HA (g)	Gel (g)	Agma$_{10}$ (g)	Agma$_{20}$ (g)	DMTMM (g)	Vol H$_2$O (mL)
HA-Gel	0.500	1.00	-	-	0.150	10
HA-Gel-Agma20%	0.500	1.00	-	0.100	0.150	10
HA-Agma$_{10}$	0.500	-	0.100	-	0.150	10
HA-Agma$_{20}$	0.500	-	-	0.100	0.150	10

5.6.5 Synthesis of Serotonin containing hydrogels

HA (0.300 g), Gel (0.600 g) were dissolved in bidistilled water (6 mL) at 50ºC under vigorous stirring for 15 minutes. AGMA$_{10}$ (0.060 g) and Serotonin (0.015 g , % w/w regards to HA) were added into the solution followed by

DMTMM (0.090 g). Reagents were mixed, transferred in a 12 well-plate and allowed to proceed for 48h at 37.5ºC in a humid atmosphere. The hydrogels were retrieved and freeze-dried. Xerogels were sterilised by UV irradiation.

5.6.6 Water uptake measurement

Water uptake measurements were performed in 0.01 M pH 7.4 PBS at 37.5°C. Dry discs with 1 cm base diameter and 0.2 cm thickness were soaked in 25 mL buffer solution and maintained statically until maximum swelling for 24 h. After this time, discs were retrieved, wiped with filter paper to remove excess water and then weighed. The percentage water uptake was calculated as:

Water uptake % $= \frac{(W_s - W_o)}{W_o} \times 100$ 　　　　　　　　　Equation 5.1

where W_o is the initial hydrogel weight and W_s the wet hydrogel weight after 24h. Tests were performed in triplicate. Final values were expressed as the means $\pm$ standard error.

5.6.7 Flory-Rehner calculations

The hydrogel swelling ratio based on mass (Q_M) was calculated by dividing the hydrogel mass after swelling (W_s) by the xerogel mass (W_o). Flory-Rehner calculations were used to determine the crosslink density and mesh size of hydrogels.

The average molecular weight between crosslinks, $\bar{M}_c$, was calculated using a simplification of the Flory-Rehner equation:[xcix,c]

$$Q_V{}^{5/3} \cong \frac{\bar{\upsilon} \, \bar{M}_c}{V_1} \left(\frac{1}{2} - \chi \right)$$ 　　　　　　　　Equation 5.2

where Q_v is the volumetric swelling ratio, $\bar{\upsilon}$ is the specific volume of the dry polymer, $\bar{M}_c$ is the average molecular weight between crosslinks, V_1 is the molar volume of the solvent (18 mol/cm³ for water), and χ is the Flory polymer-solvent interaction parameter. Q_v was determined from the degree of mass swelling, Q_M:[ci]

$$Q_V = 1 + \frac{\rho_p}{\rho_s} (Q_M - 1)$$ 　　　　　　　　　　Equation 5.3

where ρ_p is the density of the dry polymer (1.229 g/cm³) and ρ_s is the density of the solvent (1 g/cm³ for water). The value of χ for HA was estimated to be

0.473, based on several assumptions. First, it was assumed that χ for HA is comparable to that for dextran, a well-studied polysaccharide, because HA and dextran have similar chemical structures. Finally, differences between soluble, unmodified polysaccharides and cross-linked polymers were assumed to be negligible.

The effective cross-link density, ν_c, was calculated as follows:[cii]

$$\nu_c = \frac{\rho_p}{\overline{M}_c} \qquad\qquad \text{Equation 5.4}$$

The swollen hydrogel mesh size, ξ, was determined with the following equation:[ciii,civ]

$$\xi = Q_V{}^{1/3}\sqrt{\overline{r_o}^2} \qquad\qquad \text{Equation 5.5}$$

where $\sqrt{\overline{r_o}^2}$ is the root-mean square distance between crosslinks and depends on the molecular weight between cross-links. For HA, the following root-mean-square end-to-end distance value was previously reported:[cv]

$$\left(\frac{\bar{r}_o^2}{2n}\right)^{1/2} \cong 2.4\ nm \qquad\qquad \text{Equation 5.6}$$

where n is the number of disaccharide repeat units for HA with a given molecular weight. [cvi]

5.6.8 Degradation studies

Hydrogel degradation was studied by monitoring the residual mass of hydrogels discs with 1 cm base diameter and 0.2 cm thickness soaked in 0.01 M pH 7.4 PBS at 37.5°C at different time points (1, 2, 7, 14, 21, 28 days). Residual mass measurements were obtained after freeze-drying, as:

$$Residual\ mass\ \% = \frac{(W_o - W_t)}{W_o} \times 100 \qquad\qquad \text{Equation 5.7}$$

where W_t represents the weight of dried hydrogel at time t and W_o is the initial weight of hydrogel. Tests were performed in triplicate. Final values were expressed as the means ± standard error.

HYDROGELS FOR TISSUE ENGINEERING BASED ON HYALURONIC
ACID, GELATIN AND AGMA1

5.6.9 Stress strain tests

Rheological measurements were carried out using a stress-controlled oscillatory rheometer ARG2 TA Instruments using parallel plate geometry. The test geometry was a 20 mm diameter standard steel parallel-plate. A dynamic mechanical analysis (stress–strain tests) was carried out to determine the viscoelastic properties of the HG, to obtain their storage (G') (elastic behaviour) and loss (G") (viscous behaviour) moduli. Hydrogel were prepared putting the reaction mixture in teflon moulds (diameter 20 mm, 0.2 mm thick). The reaction were conducted in a humid atmosphere at 37°C. The test methods employed were stress sweep, temperature ramp and frequency sweep. The stress sweep was set up by holding the temperature (37°C) and frequency (1 Hz) constant while increasing the oscillation torque from 0.1 to 10000 μN m. At this fixed oscillation torque (30 μN m) in the linear viscoelastic region and temperature (37°C), the oscillatory frequency was increased from 0.01 to 100 Hz. In the temperature ramp test, the evolution of G' and G" in the range of 25−100°C was measured at a heating rate of 5°C/min, with the same oscillation torque previously decided and frequency of 1Hz. Tests were performed in triplicate.

5.6.10 Biocompatibility test

Cell viability (CV) of hydrogels and starting reagents was assessed by a 3-(4,5-dimethylthiazol-2-yl)-2,5 diphenyltetrazolium bromide (MTT) assay. To evaluate the possibility of cytotoxic product formation, the samples were immerged (or solubilized) in 5 mL of FBS-free supplemented DMEM (Dulbecco's Modified Eagle's Medium with 4500mg L^{-1} glucose) and placed on a shaker at 37°C. The conditioned medium was collected and filtered at days 1, 2, 3, 7, 10, 15, 21 and stored at -20°C until required. BALB/3T3 Fibroblasts were seeded at a density of 8×104 cells·mL^{-1} in complete medium into a sterile 96-well plate and incubated to confluence. After 24 hours, the medium was replaced with the eluted extracts (100 μL /well) for each composite, the control sample and the Triton X-100 (positive control), and incubated at 37°C in humidified air with 5% CO_2 for 24 hours. An MTT solution (0.5 mg·mL^{-1}) was prepared in warm FBS-free supplemented DMEM and plates were incubated at 37°C for 4 hours. Excess medium and MTT were removed and dimethyl sulfoxide (100 μL) was added to all wells in order to dissolve MTT taken up by the cells. Finally, the absorbance was measured with a BioTek Synergy HT detector using a test wavelength of 570 nm. CV (%) was calculated with the following equation:

HYDROGELS FOR TISSUE ENGINEERING BASED ON HYALURONIC
ACID, GELATIN AND AGMA1

$$CV(\%) = 100 \times [(OD_S - OD_B)/(OD_C - OD_B)] \qquad \text{Equation 5.8}$$

OD_S, OD_B, and OD_C are defined as the optical density for sample (S), blank (B) (culture medium without cells), and control (C), respectively.

5.7 RESULTS AND DISCUSSIONS

### 5.7.1 Synthesis and characterization of soluble NH_2-end-capped AGMA1 oligomers

As previously pointed out, hydrogels were synthesised by a one-pot reaction between the carboxylate groups of HA and the amine groups present in Gel and AGMA1 and Ser, using DMTMM as coupling agent. AGMA1 precursors were NH_2-end-capped oligomers, in turn obtained from amide-end-capped oligomers prepared using non-stoichiometric acrylamide/amide ratios in the recipe (Figure 5.3). Different excess of BAC (namely 10% and 20%) were used. LiOH was used to neutralize the primary amine group of agmatine the carboxylic acid of BAC. The acrylamide-end-capped AGMA1 was finally converted to the NH_2-end-capped one by reaction with mono-N-BOC-ethylenediamine (added in excess), followed by strongly acidic treatment in order to remove the protecting group. The final AGMA1 products were nicknamed $AGMA_{10}$ and $AGMA_{20}$, respectively.
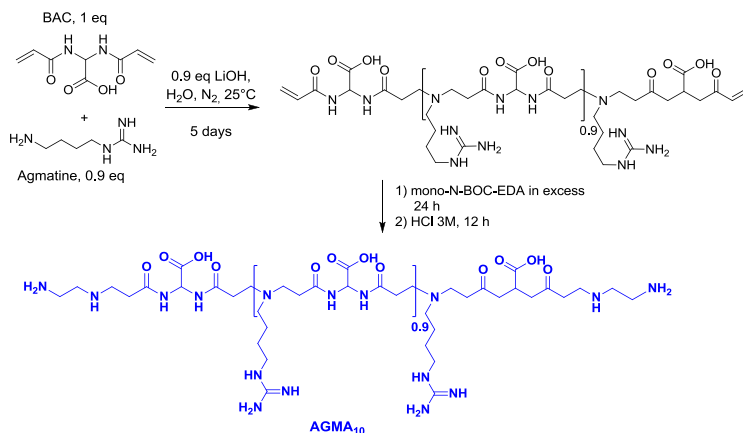
Figure 5.3. Synthesis of $AGMA_{10}$ product. $AGMA_{20}$ was prepared similarly by using a 1:0.8 BAC:agmatine ratio.

HYDROGELS FOR TISSUE ENGINEERING BASED ON HYALURONIC ACID, GELATIN AND AGMA1

^{1}H-NMR and ^{13}C-NMR confirmed AGMA$_{10}$ and AGMA$_{20}$ structures and are depicted in Figure 5.4 together with assignments. The percentages of amine end-terminated groups observed by NMR were 8 and 19% for respectively AGMA$_{10}$ and AGMA$_{20}$, in agreement with the theoretical data. By ^{1}H-NMR spectrum of products was possible calculate also number average molecular weight of AGMA$_{10}$ and AGMA$_{20}$, that was 2680 and 1370 respectevely.
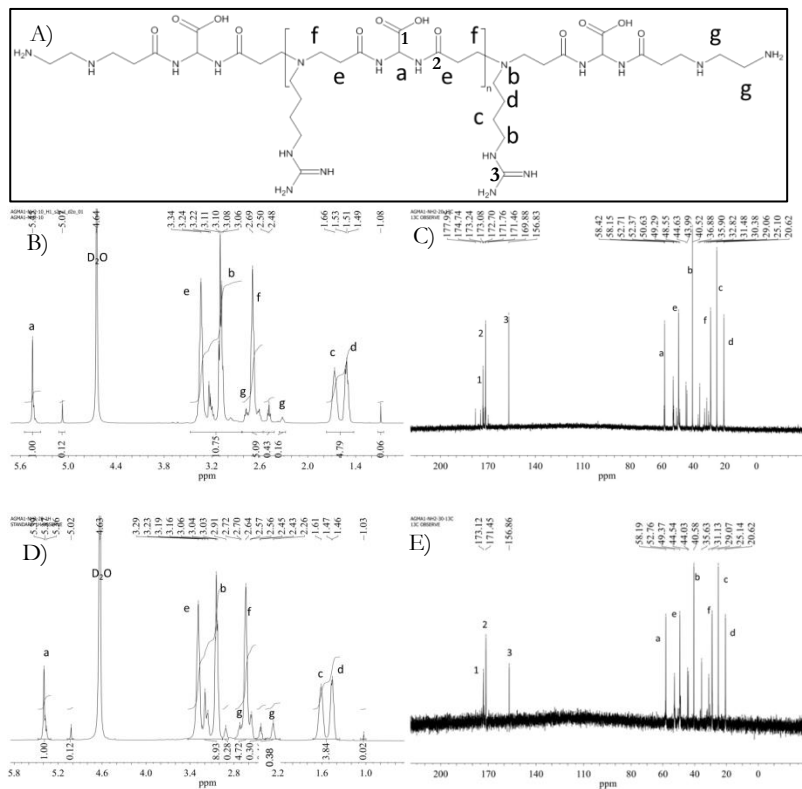
Figure 5.4. Nuclear magnetic resonance characterization of AGMA$_{10}$ and AGMA$_{20}$ with assignments: A) amine end-terminated AGMA1 structure; B)^{1}H-NMR and C) ^{13}C-NMR spectra of AGMA$_{10}$; D) ^{1}H-NMR and E) ^{13}C-NMR spectra of AGMA$_{20}$.

HYDROGELS FOR TISSUE ENGINEERING BASED ON HYALURONIC
ACID, GELATIN AND AGMA1

5.7.2 Synthesis of hydrogels and reaction parameter optimization

Hyaluronan-gelatin-AGMA1 (HA-Gel-AGMA) hydrogels were prepared by chemical cross-linking of a mixture using DMTMM as a coupling agent (Figure 5.5). For comparison purpose, also HA-AGMA and HA-Gel hydrogel were prepared. Serotonin (Ser) was added to hydrogel recipes only for biological tests, considering that its presence did not influenced chemical and physical properties of hydrogels.
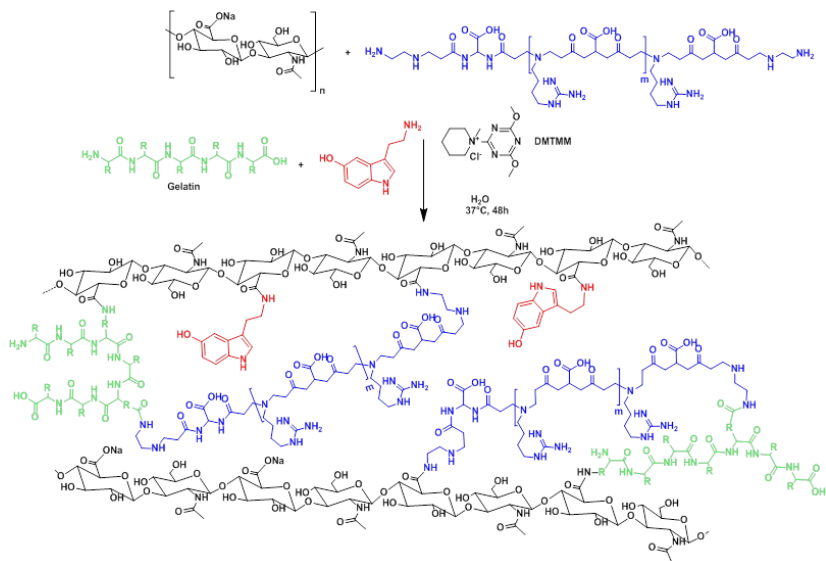
Figure 5.5. Synthesis of HA-Gel-AGMA1-Ser hydrogels.

The reaction mechanism implies the addition of a carboxylate anion to DMTMM to give an activated ester, which subsequently undergoes nucleophilic substitution by an amine group to give the corresponding amide. It should be observed that, together with chemical cross-linking, the hydrogel structure is stabilized by hydrogen bonds and Van der Waals interactions.[cvii]

In order to produce a ready-to-use hydrogels, avoiding any purification steps, DMTMM initial amount was adjusted until reaching biocompatible concentration. This choice was further dictated by the need to not use for its trace removal organic solvents (such as THF, methanol, acetonitrile), that even if present only in traces could lead to toxic effects too. Considering cell

viability test further reported in Figure 5.15A, selected DMTMM concentration was 15 mg/mL. Similarly, cell viability tests gave 10 mg/mL aqueous concentration of $AGMA_{10}$ and $AGMA_{20}$ as maximum exploitable concentrations. More detailed information on cell viability tests were further reported in paragraph 5.7.9.

As regard the best gelatin concentration to be used in hydrogel recipe, three HA-Gel hydrogels with different composition (HA:Gel 1:1, 1:2 and 1:3) were synthesised using the previously described (15mg/mL) DMTMM concentration. The reaction was allowed to proceed for 24 h and stopped lowering the temperature to -20°C and following freeze-dried. Biocompatibility and rheological properties were evaluated and described in paragraph 5.7.9 and 5.7.6. As consequence of these results, HA-Gel 1:2 was chosen as final optimal hydrogel composition.

5.7.3 FTIR characterization

FTIR hydrogels spectra were compared with those of reagent confirming the presence of all components (Figure 5.6). In particular, characteristic absorption bands of HA, gelatin and AGMA1 were following reported and found in hydrogel spectra. Hyaluronate spectrum contained five important bands: C-O stretching vibrational band (950-1200 cm^{-1}), symmetric stretching of COO^- (1400 cm^{-1}), an intense group of bands due to superposition of amides and of various carbonyl and carboxyl bands (1500-1700 cm^{-1}); symmetric and asymmetric stretching C-H band (2900 cm^{-1}) and a broad and intense band of N-H and O-H stretching bands engaged in hydrogen bonds (2500-3600 cm^{-1}). The FTIR spectrum of gelatin showed the characteristic absorption bands of a protein structure, e.g. C-O stretching band (1230 cm^{-1}), amide I vibrational band (1530-1580 cm^{-1}), asymmetric C=O stretching of carbonyl and carboxyl groups (1640-1650 cm^{-1}), H_2C-H and HC-H stretching vibration (2860 cm^{-1} and 2920 cm^{-1}, respectively) and, lastly, N-H and O-H vibrational bands (3200-3450 cm^{-1}). $AGMA_{10}$ and $AGMA_{20}$ had similar FTIR spectra, with typical bands of AGMA1 polyamidoamine: C–H and HC-H stretching bands (2960–2860 cm^{-1}), asymmetric C=O stretching (1619 cm^{-1}) and symmetric COO^- stretching (1379 cm^{-1}), as well as the amide I band (1523 cm^{-1}).

In hydrogels, a decrease of band intensities of the characteristic functional groups involved in the cross-link reaction was highlighted (v_{NH_2} at 3350 cm^{-1}, v_{CO} at 1620 cm^{-1}, v_{COO^-} at 1410 cm^{-1}). Simultaneously, a new amide band at 1680 was observed, which can be assigned to the new covalent amide bond formed between hyaluronan and gelatin or AGMA1, different to original

carbonyl band. Monitoring these signals, over 3 days of reaction, was possible to establish the end of cross-link reaction. Results indicated that after 2 days, no further modifications occurred in both FTIR spectra for the analysed hydrogels. Trend over time was reported of the only HA-AGMA$_{20}$ in Figure 5.7, highlighting the formation of a new amide band at 1680 cm^{-1} and disappearing of carboxylate one at 1410 cm^{-1}.
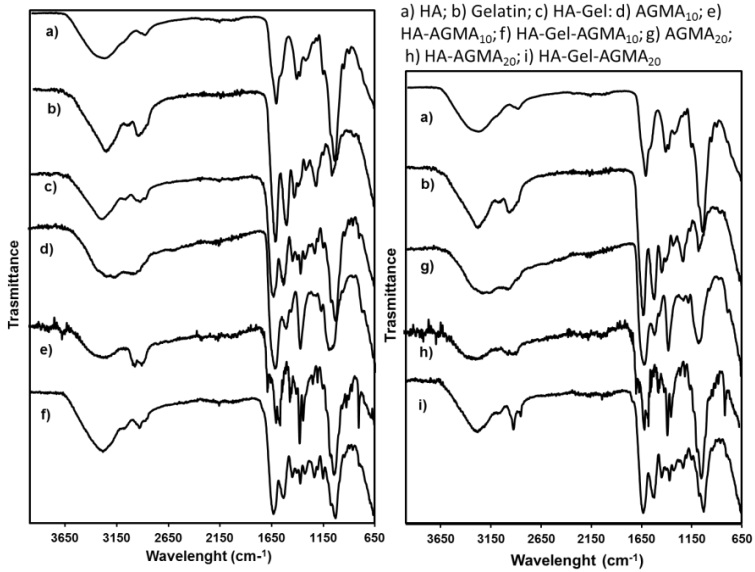
Figure 5.6. FTIR spectra of reagents and hydrogels at different compositions.

HYDROGELS FOR TISSUE ENGINEERING BASED ON HYALURONIC
ACID, GELATIN AND AGMA1
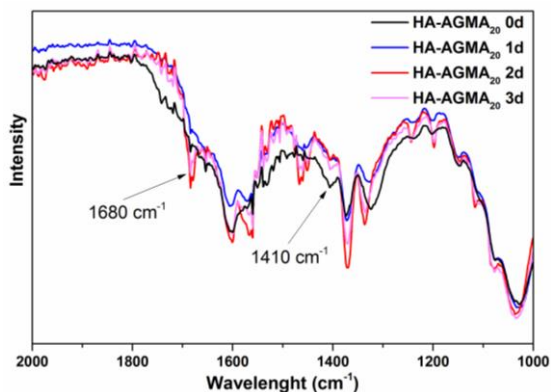
Figure 7. FTIR spectra of HA-AGMA20 hydrogels varying time reaction.

5.7.4 Water uptake measurements and Flory-Rehner calculations

Water uptake of hydrogels was measured at 37 °C after 24 h of immersion in PBS buffered solution at pH 7.4. Figure 5.8 shows the water uptake of hydrogels at different composition. Initially the system was in a solid state (xerogel), forming a rigid network. When the system started to hydrate the polymer chains swelled and became more flexible, allowing the diffusion of water molecules in the network. When the chain relaxation reached a minimum energy state, equilibrium between chain relaxation and contraction of the polymeric network was reached, getting a stable swelled state. Water uptake was affected noticeably by the composition due to a change of crosslinking density. The level of water uptake changed from 2500% for the HA-AGMA$_{10}$ hydrogel, to 1300% for HA-Gel-AGMA$_{20}$.

These data allowed determination of the crosslinking density and the average molecular weight and distance between nodes, parameters that define the three-dimensional network structure of chemical cross-linked hydrogel. These parameters determine the mechanical properties, stiffness, and elastic behaviour of the hydrogels. Flory–Rehner equation reported in the experimental section, gave these important parameters, which are reported in Table 5.4. The Flory–Rehner model was applied to hydrogels considering the only HA contribute, as in the case of monocomponent matrix, without considering gelatin and AGMA1 influences. This coarse simplification lead to approximated values of $\bar{M}_c$, ν_c, ξ. Notwithstanding, these values were useful

HYDROGELS FOR TISSUE ENGINEERING BASED ON HYALURONIC ACID, GELATIN AND AGMA1

for making order-of-magnitude comparisons of the hydrogel chemistries in biologically relevant features in this work.

In general, a low crosslinking density gives rise to a more open network, and a higher degree of hydration and higher distance between nodes. However, a high crosslinking density implies a lower degree of hydration and a less deformable hydrogel. $v_c\%$ ranged between 10^{-4} to 10^{-3}, with a maximum in the case of HA-Gel-AGMA$_{20}$. Regarding to mesh size, in all cases a nanometric pattern was calculated, in the range of 250 nm. Considering $\bar{M}_c$ and the $\bar{M}_w$ of native HA, number of cross-links per HA chain was calculated. Results indicated that at least one node per chain was present. Data confirming rheological results in which no physical interaction was detected, in the temperature ramp. Values increased passing from HA-AGMA1 to HA-Gel (1.8) and then to HA-Gel-AGMA1, with a maximum of 3.48 cross-link nodes per chain for HA-Gel-AGMA$_{20}$.
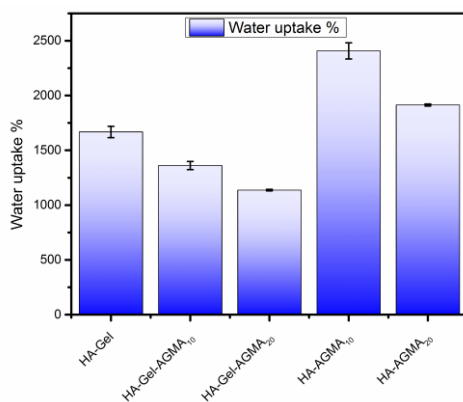
Figure 5.8. Water uptake after 24 h of immersion in PBS solution of hydrogels at different composition.

Table 5.4. Flory-Rehner calculation results, average MW between crosslinks, $\bar{M}_c$, crosslinking density %, v_c %, number of cross-links per HA chain, swollen state mesh size, ξ (nm) of all hydrogels.

Samples	Average MW between crosslinks, $\bar{M}_c$	Crosslinking density %, v_c %	Number of cross-links per HA chain	Mesh size, ξ (nm)

HYDROGELS FOR TISSUE ENGINEERING BASED ON HYALURONIC
ACID, GELATIN AND AGMA1

HA-Gel	143228	$8.58 \cdot 10^{-4}$	1.88	243
HA-Gel-AGMA$_{10}$	102021	$1.20 \cdot 10^{-3}$	2.55	227
HA-Gel-AGMA$_{20}$	74786	$1.64 \cdot 10^{-3}$	3.48	213
HA-AGMA$_{10}$	232874	$5.28 \cdot 10^{-4}$	1.12	267
HA-AGMA$_{20}$	170291	$7.22 \cdot 10^{-4}$	1.53	251

5.7.5 Thermal characterization

The thermal behaviour of hydrogels was assessed by means of thermogravimetric analysis, TGA, and differential scanning calorimetry, DSC. TGA traces (Figure 5.9 and Table 5.5) showed in all cases moisture loss at 80°C in different amounts, ranging from 5 to 15%. Table 5.5 reports the onset decomposition temperatures, obtained by the intersection of tangent lines to curves, and the relevant maximum weight loss rate temperatures, obtained by the first derivative of TGA curves. HA and gelatin degraded by a single step with maximum degradation rates, T_{max}, at 242 and 309°C, respectively. AGMA$_{10}$ and AGMA$_{20}$ showed a multi-step degradation with T_{max} at 245, 326 and 463°C.

By comparing the hydrogel degradation curves with those of each single component, it is apparent that AGMA1 and Gel had a different influence on thermal stability of HA. In particular, in the case of HA-Gel, the onset decomposition temperatures were 5°C and 23°C lower than those of native HA and Gel, respectively; similarly, the T_{max} decreased of 10°C and 8°C respectively.

Conversely, HA-AGMA$_{10}$ and HA-AGMA$_{20}$ exhibited higher thermal stability than single component. The onset degradation temperatures of HA in hydrogels was higher of 18°C and 11°C than native HA, in the cases of HA-AGMA$_{10}$ and HA-AGMA$_{20,}$ respectively. The maximum degradation rates increased of 8°C and 10°C, respectively. AGMA$_{10}$, AGMA$_{20}$ in HA-AGMA1 hydrogels and native ones started to degrade at similar temperatures, (212 and 207°C vs. 210°C, respectively), but maximum degradation rate were lower of 22 and 21°C for HA-AGMA$_{10}$ and HA-AGMA$_{20}$.

In the cases of HA-Gel-AGMA1 hydrogels, all components started to degrade early than native ones. In particular, HA presented an onset temperature lower of 15 and 22°C, in the cases of HA-Gel-AGMA$_{10}$ and HA-Gel-AGMA$_{20}$ respectively and, similarly, considering T_{max}, a decrease of 18 and 28°C. Gel showed an onset temperature variation of 32 and 39°C and T_{max} decrease of 60

HYDROGELS FOR TISSUE ENGINEERING BASED ON HYALURONIC ACID, GELATIN AND AGMA1

and 23°C for HA-Gel-AGMA$_{10}$ and HA-Gel-AGMA$_{20}$ respectively. AGMA$_{10}$ and AGMA$_{20}$ degradation steps were not detected.

Notwithstanding temperature trends, the presence of Gel and AGMA1 onto HA chains slowed down the overall degradation of hydrogels as evidenced by a less steep slope of TGA curve. Residual mass at 600°C did not significantly varied passing from native components to hydrogels.
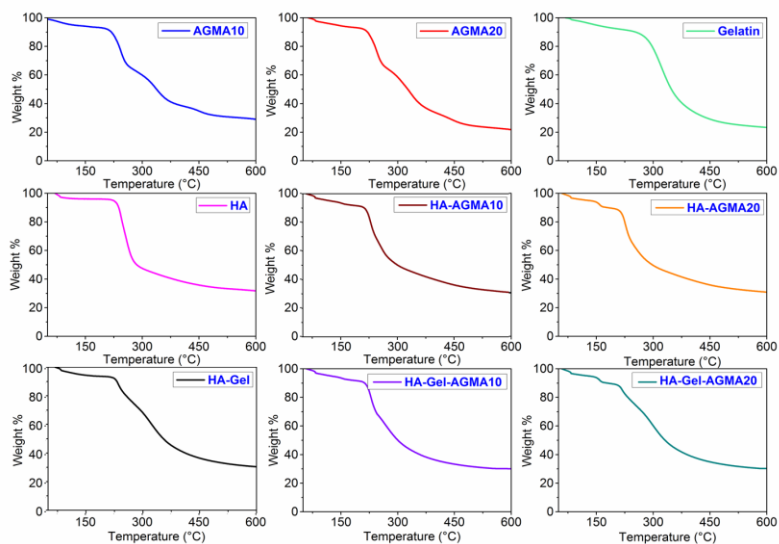

Figure 5.9. Thermogravimetric analyses of precursors and hydrogels.

Table 5.5. Hydration water loss temperature (T$_{Hydr}$) and degradation temperature (T$_{Degr}$) of reagents and hydrogels, derived by TGA. Maximum degradation rate temperatures (T$_{max}$) and onset temperatures (T$_{onset}$) are reported for each component.

Samples	T$_{Hydr}$ (°C)	T$_{Degr}$ (°C)					
		1^{rt} step		2nd step		3rd step	
		T$_{onset}$	T$_{max}$	T$_{onset}$	T$_{max}$	T$_{onset}$	T$_{max}$
HA	83	228	242				
Gelatin	82	274	316				
AGMA$_{10}$ /AGMA$_{20}$	--	210	245	304	326	432	463
HA-Gel	83	223	232	297	308		
HA-AGMA$_{10}$	82	140	142	212	224	246	250

HYDROGELS FOR TISSUE ENGINEERING BASED ON HYALURONIC
ACID, GELATIN AND AGMA1

HA-AGMA$_{20}$	82	144	150	207	223	239	252
HA-Gel-AGMA$_{10}$	82			213	224	242	256
HA-Gel-AGMA$_{20}$	83	144	150	206	214	235	293
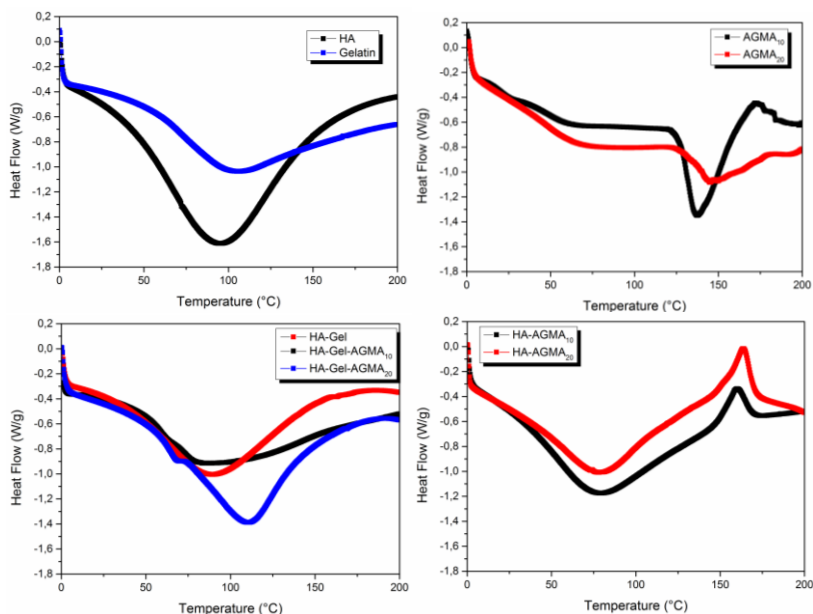
Figure 5.10. Differential scanning calorimetry thermograms of reagents and hydrogels.

The DSC traces (Figure 5.10 and Table 5.6) resulting from the first heating cycle of all polymers were characterized by broad endothermic peaks centred around 80°C associated with the loss of residual water, in agreement with TGA results. The second heating cycle lead invariably to flat curves, not reported below for seek of simplicity. HA-AGMA$_{10}$ and HA-AGMA$_{20}$ showed a degradation step centred at about 130°C, also observed in TGA curves, not present in AGMA1 and HA-Gel-AGMA1 thermograms. In the same region, the endothermic peak present in AGMA1 trace at 130 - 138°C does not correspond to any mass loss in the TGA curve.

Table 5.6. Glass transition temperature (Tg) and hydration water loss temperature (T$_{Hydr}$) and peak temperature (T$_{peak}$) of reagents and hydrogels, derived by DSC.

HYDROGELS FOR TISSUE ENGINEERING BASED ON HYALURONIC ACID, GELATIN AND AGMA1

| Samples	T_g (°C)		T_{Hydr} (°C)		T_{peak} (°C)	
	Max	Onset	Max	Onset	Max	Onset
HA	--	--	90	47	--	--
Gel	--	--	97	40	--	--
AGMA$_{10}$	50	40			130	120
AGMA$_{20}$	--	--			138	127
HA-Gel	--	--	84	32	--	--
HA-Gel-AGMA$_{10}$	50	40	79	41	--	--
HA-Gel-AGMA$_{20}$	57	38	104	38	--	--
HA-AGMA$_{10}$	--	--	74	26	152	141
HA-AGMA$_{20}$	--	--	74	24	156	143

5.7.6 Rheological experiments

The cross-linked nature (chemical or physical one) of HA-Gel hydrogels was evaluated by rotational rheometer in oscillatory mode (Figure 5.11). Three experiments were carried out, evaluating G' and G" moduli trend variation with oscillation torque, oscillation frequency and temperature, respectively.

In a first experiment, G' and G" were obtained operating at a fixed oscillation frequency, namely 1 Hz, varying oscillation torque from 0.1 to 10000 μN·m. All sample showed G" values lower than those of G', highlighting a prevailing elastic behaviour rather than a viscous one. The linear viscoelastic regions ended only for oscillation torque values higher than 2000 μN·m, indicating a high stability in a wide range of torque values. G' was not significantly sensitive to the gelatin content, and was 510, 570, 550 Pa for HA:Gel 1:1, 1:2, 1:3, respectively.
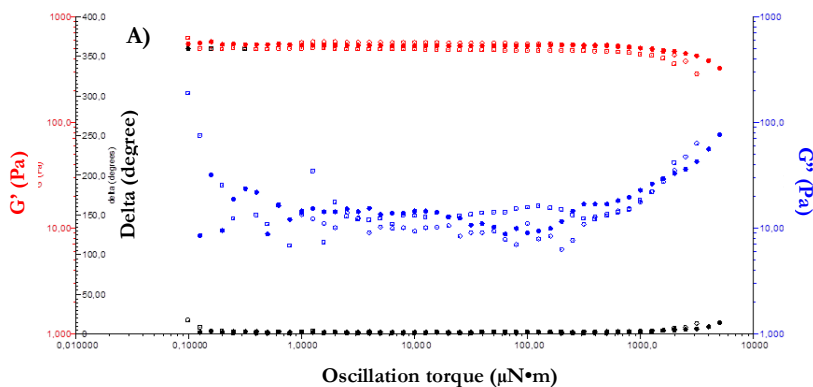
HYDROGELS FOR TISSUE ENGINEERING BASED ON HYALURONIC ACID, GELATIN AND AGMA1
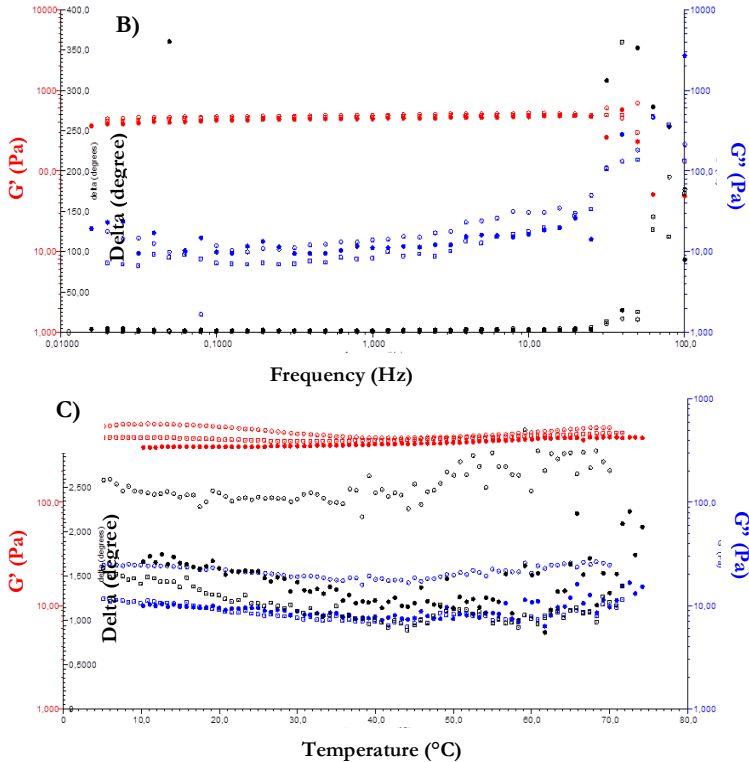
Figure 5.11. Rheological analyses of HA-Gel with different weight ratio (●1:1, □1:2, ○1:3). A) oscillation stress dependency of the modulus values G' and G", B) oscillation frequency dependency of the modulus values G' and G", C) temperature ramp.

In frequency sweep tests, G' and G" were obtained operating at a fixed oscillation torque in the linear viscoelastic region, 30 μN·m, varying oscillatory frequency from 0.01 to 100 Hz (Figure 5.11, panel B). For frequencies <30 Hz samples showed a solid response (both sinusoidal stress and deformation) and G' and the G" were constant for a wide frequency range. At frequencies >30 Hz, samples began to have liquid-like behaviour (sinusoidal stress and cosinusoidal deformation trends) in response to stress. No differences were observed among hydrogels with different gelatin content.

HYDROGELS FOR TISSUE ENGINEERING BASED ON HYALURONIC ACID, GELATIN AND AGMA1

The temperature ramp tests allowed understanding the stability of samples at high temperatures (Figure 5.11, panel C). Tests were conducted fixing oscillation torque to 30 µN·m and frequency of 1Hz. In general, for chemical cross-linked hydrogels, increasing temperature, water tends to evaporate, leading the G' increased with temperature. This trend was observed almost for all studied samples. The only exception was HA-Gel 1:3 that showed a decreasing G' with temperature, in particular in the 10 to 35ºC range, meaning that physical interactions, such as Van der Waals interactions, were present. This temperature range was typical of uncross-linked gelatin,[cviii,cix] indicating that HA:Gel 1:3 contains too high gelatin content inside. For this reason, a 1:2 weight ratio was chosen as final composition of HA-Gel hydrogels.

All hydrogels were analysed by using the same experimental conditions adopted for HA-Gel hydrogel. The viscoelastic behaviour was evaluated by determining G' and G" values varying oscillation torque, frequency of oscillation and temperature (Figure 5.12 panel A to C).

In the first experiment (Figure 5.12, panel A), G' and G" value were evaluated at fixed oscillation frequency 1 Hz varying oscillation torque from 0.01 to 10000 µN·m. Hydrogels presented an extended linear viscoelastic region ending only after 100 Pa, thus indicating a great stability also at medium – high stress. In particular, HA-AGMA$_{10}$ and HA-AGMA$_{20}$ presented the longest linear viscoelastic region, more than 1000 µN·m. The G' modulus were higher for all gelatin-based hydrogels (4, 4, 6 KPa for HA-Gel, HA-Gel-AGMA$_{10}$, HA-Gel-AGMA$_{20}$ respectively) than of HA-AGMA$_{10}$ and HA-AGMA$_{20}$ (0.7 and 2.3 KPa respectively). In panel B, a magnification of stress sweep is reported, highlighting the breakpoint of each hydrogel. HA-Gel-AGMA$_{20}$ presented the higher value, followed by HA-Gel, HA-Gel-AGMA$_{10}$, HA-AGMA$_{20}$ and HA-AGMA$_{10}$. Similar trend replicated the cross-link density one, reported before.

Oscillation frequency dependence was evaluated fixing oscillation torque of 30 µN·m (Figure 5.12, panel B). Hydrogels' behaviour did not significantly depend on frequency within a wide frequency range. For frequencies <15 Hz samples showed a solid response (both sinusoidal stress and deformation) and G' and the G" were constant for a wide frequency range. Only at really high frequency (15-100 Hz) samples involved liquid behaviour to the stress.

Temperature ramp from 25 to 100°C was performed fixing oscillation torque at 30 µN·m and frequency at 1 Hz (Figure 5.12, panel C). All hydrogels resulted stable to temperature increase. Water loss was slowed down, indeed

HYDROGELS FOR TISSUE ENGINEERING BASED ON HYALURONIC
ACID, GELATIN AND AGMA1

only slight increase of G' modulus was recorded. No physical interactions were detected. Same G' value trend of was present. Resuming all tests, the best performance was reached by HA-Gel-AGMA$_{20}$, due to its highest G' modulus and breakpoint in stress sweep, highest stability to heating in temperature ramp analysis.
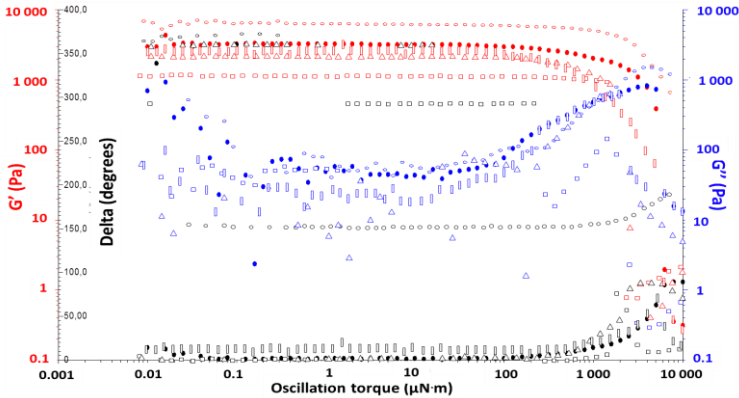
HYDROGELS FOR TISSUE ENGINEERING BASED ON HYALURONIC ACID, GELATIN AND AGMA1
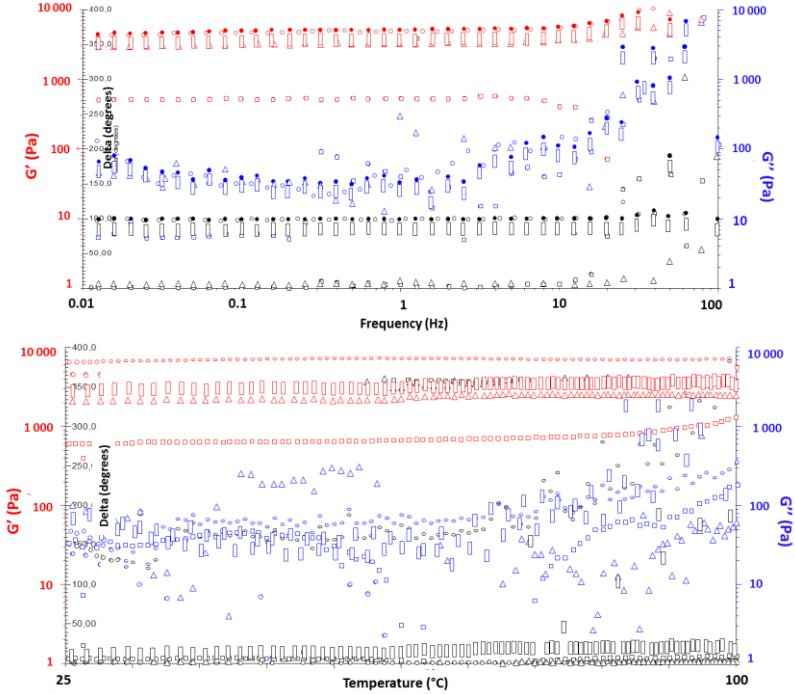
Figure 5.12. Rheological characterization of hydrogels via: (A) oscillation torque dependency of the modulus values G' (red), G" (blue) and delta (black); (B) oscillation frequency dependency of the modulus values G' (red), G" (blue) and delta (black); (C) temperature dependency of G' (red), G" (blue) and delta (black). []= HA-Gel, ●=HA-Gel-AGMA$_{10}$, ○=HA-Gel-AGMA$_{20}$, □=HA-AGMA$_{10}$, △=HA-AGMA$_{20}$.

It is important to underline that almost all synthesised hydrogels presented rheological properties comparable to those of human and bovine liver. In literature, it was reported G' and G" dependency by frequency, measured by oscillation rheology and multifrequency magnetic resonance elastography. Reported modulus values ranged between 1 and 3 KPa and between 0.4 and 1.5 KPa for respectively G' and G", varying frequency from 2 to 100 Hz.[cx] Similar values were obtained in the cases of HA-Gel-AGMA$_{20}$, HA-Gel-AGMA$_{10}$, HA-Gel and HA-AGMA$_{20}$, lower ones in the case HA-AGMA$_{10}$.

5.7.7 Degradation test

Figure 5.13 shows the residual mass of hydrogels as a function of incubation time in PBS at 37 °C. For comparison 1:2 weight ratio HA/gel blend were similarly immersed in PBS, but at 37°C they are totally soluble. After one week, HA/Gel blend started to smell bad, probably due to their decomposition, but pH solution did not change. For all hydrogels, the extent of degradation regularly and slowly increased with time. No smells or pH variation were spotted during time experiment. After 1 week, only 5-10 % of weight loss was recorded, after 4 week 25-35%. It may be noted that the highest weight loss percentage occurred for HA-Gel, the lowest for HA-Gel-$AGMA_{20}$. These results corroborated the water uptake studies and cross-linked degrees. In particular, hydrogels presented a high degradation degree were the same showing low cross-linked density. As well as, HA-Gel-$AGMA_{20}$ showed the lowest degradation degree possessed the highest cross-linked density.
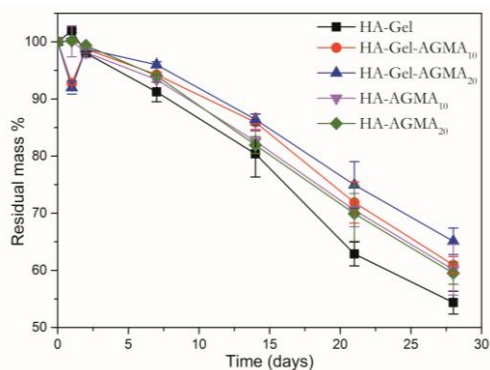
Figure 5.13. Residual mass % of hydrogels after immersion in PBS solution
for 28 days at 37°C.

5.7.8 Morphological studies by AFM

Morphology of hydrogels was examined by AFM. Images of xerogels are shown in Figure 5.14 with a size bar of 3 μm. The topographical image of HA-AGMA1 and HA-Gel-AGMA1 revealed a rough surface. However, the topographical image of HA-Gel was characterized by a smooth surface without any indication of the presence of orientated polymer chains or aggregates or organized systems domains. The surface characteristics of xerogels were composition and cross-ling degree dependent. Roughness was higher for xerogels presented lower values of cross-link degree, as showed in

HYDROGELS FOR TISSUE ENGINEERING BASED ON HYALURONIC ACID, GELATIN AND AGMA1

the case of HA-AGMA$_{20}$ and more in HA-AGMA$_{10}$. Analysis of phase images revealed an absence of phase separation in the microdomains at all compositions, what can be attributed to the total miscibility of reagents.

**Figure 5.14.** AFM images of hydrogels (3 µm bar).

5.7.9 Cell biocompatibility

One of the most popular and convenient ways to determine cell viability is the rapid colorimetric tetrazolium dye procedure commonly referred to as the MTT assay. This assay is based on the cleavage of the yellow-coloured tetrazolium salt, 3-(4,5-dimethylthiazol-2-yl)-2,5-diphenyl tetrazolium bromide, into a blue-coloured formazan by the mitochondrial enzyme succinate-dehydrogenase.[cxi] In order to disregard any cytotoxic product's influence on fibroblast proliferation, an MTT assay was carried out for reagents and final hydrogels, staying in contact with the culture medium for determined time periods. Cell viability of DMTMM, $AGMA_{10}$ and $AGMA_{20}$ PBS solutions was monitored for maximum 24h, incubating them with fibroblast cells dispersed in DMEM matrix.

Results indicated that 15 mg/mL was the maximum concentration of DMTMM after 2 h of incubation, but it resulted toxic after 18 h (Figure 5.15, panel A). Notwithstanding, this concentration was chosen in consideration that the major extent of coupler agent was consumed in the first part of reaction.

In the case of NH_2-end-capped AGMA1 products, 10 mg/mL concentration as maximum biocompatible concentration for both oligomers (Figure 5.15, panel B).
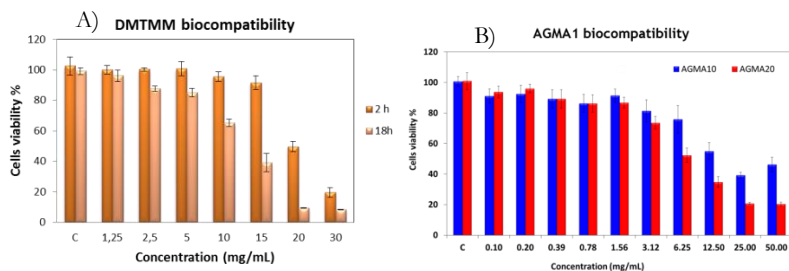
Figure 5.15. MTT tests with BALB/3T3 fibroblast cell line in presence of A) DMTMM and B) AGMA1 at different concentrations.

Biocompatibility of HA-Gel hydrogels and final hydrogels were studied (Figure 5.16 and 5.17), evaluating cell viability over 21 days on fibroblast cells and compared to PBS solution as control. The cell viability was approximately or higher than 80% in all cases. Thus, under the experimental conditions,
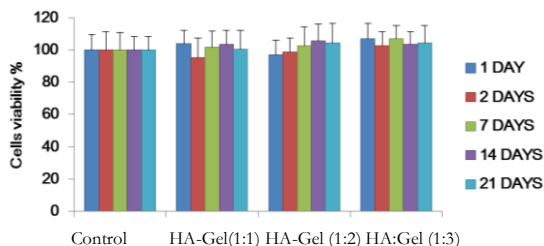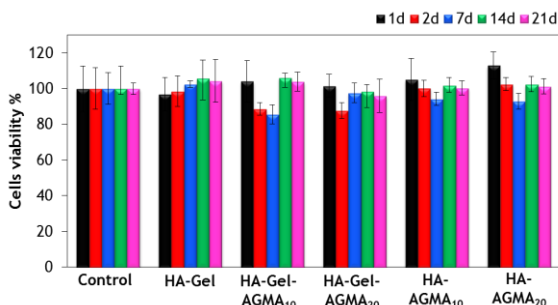
biocompatibility was not compromised and the samples did not produce cytotoxic products.

Proliferation tests on containing serotonin hydrogels are actually in progress with hepatocytes in order to evaluate the adhesion, proliferation and morphologies of cells.

Figure 5.16. Cell viability % of HA-Gel hydrogels over 21 days with BALB/3T3 fibroblast cell line.

Figure 5.17. Cell viability of hydrogels evaluated by MTT test at determined times.

5.8 CONCLUSIONS

In this work, chemical cross-linked hydrogels intended as scaffolds for tissue regeneration, in particular of liver tissue, were produced. Sodium hyaluronate and gelatin (HA-Gel) were selected as scaffolding material to mimic the crucial components of ECM, in order to enhance cell proliferation, migration, and differentiation of liver tissue. Two different NH_2-end-capped AGMA1 oligomers were opportunely synthesised and used as co-reagent in hydrogel synthesis. AGMA 1 was used to favour cell adhesion on hydrogel surface by RGD sequence enrichment in the porous hydrogel structure. Thanks to its

HYDROGELS FOR TISSUE ENGINEERING BASED ON HYALURONIC ACID, GELATIN AND AGMA1

efficacy without control pH solution, DMTMM was chosen as coupler agent in the cross-link reaction between hyaluronate, gelatin and AGMA1. Reaction parameters were finely tuned in order to increase cross-link degree at body temperature. FTIR spectra of final products confirmed the presence of all initial components and, in particular, after 48 h of reaction, the formation of new amides groups and a reduction of carboxylate groups of HA. These results confirmed the presence of chemical cross-linked hydrogels.

Thermal analysis showed lower onset temperatures and maximum rate ones of HA-Gel-AGMA1 component compared to native ones. In contrast, onset temperatures and maximum rate ones of HA-AGMA1 were higher of equal to native ones. Huge amount of moisture was retained in hydrogel structure.

Swelling analysis performed in PBS solution for 24 h allowed evaluating cross-link degrees by using of Flory-Rehner equation. Cross-link density degrees and the other mesh properties depended on composition. At least one cross-link node was present in all hydrogels, but, among others, HA-Gel-AGMA$_{20}$ hydrogel showed the highest cross-link density, number of nodes per HA chain, and the smallest distance between two cross-links nodes. Results found explanation considering the amine content in AGMA$_{20}$ higher than AGMA$_{10}$ and gelatin. Flory-Rehner results indicated that HA-Gel-AGMA$_{20}$ should be the most stable hydrogel; hypothesis confirmed by degradation tests, where, it presented the slowest degradation rate compared to the others. Notwithstanding, all hydrogel presented an high stability in water, indeed a maximum of 35 % weight loss was recorded after 28 days in PBS solution.

Rheological tests revealed that synthesised hydrogels presented good rheological properties for liver regeneration. In particular, HA-Gel-AGMA$_{20}$ gave the best performance under oscillation stress and temperature heating, presenting the highest G' modulus and highest water retention when heated.

The *in vitro* results revealed that the scaffolds did not induce cytotoxic effects and were suitable for cell growth. Biocompatibility was not compromised and the samples did not produce cytotoxic products over time. On the other hand, the cell adhesion and proliferation tests on hydrogels are actually in progress. In particular, these tests will be conducted with hydrogels contained also serotonin, a neurotransmitter also involved in DNA synthesis activation of liver cells after hepatectomy in rats and humans.

HYDROGELS FOR TISSUE ENGINEERING BASED ON HYALURONIC
ACID, GELATIN AND AGMA1

In conclusion, HA-Gel-AGMA1 hydrogels, combining the advantages of hyaluronan, gelatin and AGMA1, might be a suitable candidate for use in soft tissue engineering.

Acknowledgements

HYDROGELS FOR TISSUE ENGINEERING BASED ON HYALURONIC ACID, GELATIN AND AGMA1

Bibliography

i K. Y. Lee, D. J. Mooney, *Chemical Reviews*, **2001**, 101, 1869-1879

ii E. M. Ahmed, *Journal of Advanced Research*, **2015**, 6, 105-121

iii J.M. Guenet, *Thermoreversible gelation of polymers and biopolymers*, New York: Academic Press, **1992**

iv M.L. Markey, M.L. Bowman, M.Y. Bergamini, *Chitin and chitosan*. London: Elsevier Applied Science, **1989**

v I.M. El-Sherbiny, M. H. Yacoub, *Global Cardiology Science and Practice*, **2013**, 38, 316-342

vi O. Wichterle, D. Lim, *Nature*, **1960**, 185, 117

vii S. Woerly, *Porous Materials for Tissue Engineering*, **1997**, 250, 53-68

viii M. Borkenhagen, J.F. Clemence, H. Sigrist, P. Aebischer, *Journal of Biomedical Materials Research*, **1998**, 40, 392-400

ix V.F. Sechriest, Y.J. Miao, C. Niyibizi, A. Westerhausen-Larson, H.W. Matthew, C.H. Evans, F.H. Fu, J.K. Suh, *Journal of Biomedical Materials Research*, **1999**, 49, 534-541

x E. Caló, V. V. Khutoryanskiy, *European Polymer Journal,* **2015**, 65, 252–267

xi R. Singhal, K. Gupta, *Polymer-Plastics Technology and Engineering,* **2016**, 55, 54-70

xii J.E. Babensee, J.M. Anderson, L.V. McIntire, A.G. Mikos, *Advanced Drug Delivery Reviews,* **1998**, 33, 111

xiii B. Rihova, *Advanced Drug Delivery Reviews*, **2000**, 42, 65

xiv K.Y. Lee, D.J. Mooney, *Chemical Reviews*, **2001**, 101, 1869-1877

xv P. B. Malafaya, G.A. Silva, R. L. Reis, *Advanced Drug Delivery Reviews,* **2007**, 59, 207–233

xvi X.D. Guo, Q.X. Zheng, J.Y. Du, S.H. Yang, H. Wang, Z.W. Shao, E.J. Sun, *Journal of Wuhan University of Technology*, **2002**, 17, 30-34

xvii J. Necas, L. Bartosikova, P. Brauner, J. Kolar, *Veterinary Medicina*, **2008**, 53, 397-411

xviii M. N. Collins, C. Birkinshaw, *Carbohydrate Polymers,* **2013***,* 92, 1262– 1279

xix H. S. Yoo, E.A. Lee, J. J.Yoon, T. G.Park, *Biomaterials*, **2005**, 26, 1925–1933

xx I.Hargittai, M. Hargittai, *Structural Chemistry*, **2008**, 19, 697-717

xxi U.B.G. Laurent, R.K. Reed, *Advanced Drug Delivery Reviews*, **1991**, 7, 237-256.

xxii B.P. Toole, *Journal of Internal Medicine*, **1997**, 242, 35-40

xxiii J.Y. Lee, A.P. Spicer, *Current Opinion in Cell Biology*, **2000**, 12, 581–586

xxiv J.B. Leach, C.E. Schmidt C.E., *Encyclopedia of Biomaterials and Biomedical Engineering*: Hyaluronan, Marcel Dekker, New York, **2004**

xxv K. Mio, R. Stern, *Matrix Biology*, **2002**, 21, 31-37

xxvi T.A. Dechert, A.E. Ducale, S.I. Ward, D.R. Yager, *Wound Repair and Regeneration*, **2006**, 14, 252-258

xxvii K.R. Taylor, J.M. Trowbridge, J.A. Rudisill, C.C. Termeer, J.C. Simon, R.L. Gallo, *Journal of Biological Chemistry*, **2004**, 279, 17079-17084

HYDROGELS FOR TISSUE ENGINEERING BASED ON HYALURONIC
ACID, GELATIN AND AGMA1

xxviii E.A. Turley, P.W. Noble, L.Y. Bourguignon, *Journal of Biological Chemistry*, **2002**, 277, 4589-4592

xxix J. Leach, K.A. Bivens, C.W. Patrick, J.C. Schmidt, *Biotechnology and Bioengineering*, **2003**, 82, 578-589

xxx Y. Lei, M. Rahim, Q. Ng, T. Segura, *Journal of Controlled Release*, **2011**, 153, 255-261

xxxi Y.D. Park, N. Tirelli, J.A. Hubbell, *Biomaterials*, **2003**, 24, 893-900

xxxii T.J. Brown, U.B. Laurent, J.R. Fraser, *Experimental Physiology*, **1991**, 76, 125-134

xxxiii T.C. Laurent, J.R.E. Fraser *FASEB Journal*, **1992**, 6, 2397–2404

xxxiv C.E. Schanté, G. Zuber, C. Herlin, T. F. Vandamme, *Carbohydrate Polymers*, **2001**, 85, 469–489

xxxv M.H.M. Oudshoorn, R. Rissmann, J.A. Bouwstra, W.E. Hennink, *Polymer*, **2007**, 48, 1915–1920

xxxvi S. Ghosh, I. Kobal, D. Zanette, W.F. Reed, *Macromolecules*, **1993**, 26, 4685-4693

xxxvii A. Maleki, A.L. Kjøniksen, B. Nyström, *Macromolecular Symposia*, **2008**, 274, 131–140

xxxviii H.S. Nam, J. An, D.J. Chung, J.H. Kim, C.P. Chung, *Macromolecular Research*, **2006**, 14, 530–538

xxxix H.P. Tan, C.R. Chu, K.A. Payne, K.G. Marra, *Biomaterials*, **2009**, 30, 2499–2506

xl L.M. Zhang, C.X. Wu, J.Y. Huang, X.H. Peng, P. Chen, S.Q. Tang, *Carbohydrate Polymers*, **2012**, 88, 1445-1452

xli SK. Seidlits, C.T. Drinnan, R.R. Petersen, J.B. Shear, L.J. Suggs, C.E. Schmidt, *Acta Biomaterialia*, **2011**, 7, 2401–2409

xlii Y. Lei, M. Rahim, Q. Ng, T. Segura, *Journal of Controlled Release*, **2011**, 153, 255-261

xliii F. Zhang, C. He, L. Cao, W. Feng, H. Wang, X. Mo, *International Journal of Biological Macromolecules*, **2011**, 48, 474-481

xliv X. Wang, H. Jin, Y. Wang, F.Z. Cui, *Interface Focus*, **2012**, 2, 278-291

xlv L.J. Nesti, W.J. Li, R.M. Shanti, Y.J. Jiang, W. Jackson, B.A. Freedman, *Tissue Engineering:Part A,* **2008**, 14, 1527–1537

xlvi J.K. Park, J.H. Shim, K.S. Kang, J. Yeom, H.S. Jung, J.Y. Kim, *Advanced Functional Materials*, **2011**, 21, 2906-2912

xlvii U. Freymann, M. Endres, K. Neumann, H.J. Scholman, L. Morawietz, C. Kaps, *Acta Biomaterialia*, **2011**, 8, 677-685

xlviii C. Radhakumary, A.M. Nandkumar, P.D. Nair, *Carbohydrate Polymers*, **2011**, 85, 439-445

xlix S. Van Vlierberghe, P. Dubruel, E. Schacht, *Biomacromolecules*, **2011**, 12, 1387-1408

l J.V. Forrester, J. M. Lackie, *Journal of Cell Science*, **1980**, 50, 329-344

li F.A. Johnston-Banks, P. Harris, *Food gels: Gelatin.* Elsevier Applied Food Science Series, London, **1990**

HYDROGELS FOR TISSUE ENGINEERING BASED ON HYALURONIC ACID, GELATIN AND AGMA1

[lii] K.B. Djagny, Z. Wang, S. Xu, *Critical Reviews in Food Science and Nutrition*, **2001**, 41, 481-492

[liii] E. Hoch ,C. Schuh, T. Hirth, G.E.M. Tovar, K. Borchers, *Journal of Materials Science: Materials in Medicine,* **2012**, 23, 2607-2617

[liv] J.R. Loofbourow, B.S. Gould, I.W. Sizer, *Archives of Biochemistry and Biophysics*, **1949**, 22, 406

[lv] S.L. Bellis, *Biomaterials*, **2011**, 32, 4205-4210

[lvi] J.E. Eastoe, *Biochemical Journal*, **1955**, 61, 589-900

[lvii] R.E. Newman,. *Archives of Biochemistry and Biophysics*, **1949**, 24, 289-298

[lviii] M. De Clerq, E. Quanten, *Amino Acid Composition of Gelatins*, International Congress of Photographic Science, KÖln, Germany, **1986**

[lix] T. Kobayashi, *Foods Food Ingredients Journal*, Jpn., **1996**, 170, 82–88

[lx] A.G. Ward, A. Courts, *The Science and Technology of Gelatin*, Academic Press, New York, **1977**

[lxi] A.J. Kuijpers, G.H.M. Engbers, J. Krijgsveld, S.A.J.Zaat, J. Dankert, J. Feijen, *Journal of Biomaterials Science: Polymer Edition*, **2000**, 11, 225-243

[lxii] S. Van Vlierberghe, P. Dubruel, E. Schacht, *Biomacromolecules*, **2011**, 12, 1387-1408

[lxiii] A. Jayakrishnan, S.R. Jameela, *Biomaterials*, **1996**, 17, 471-484

[lxiv] L.H. Olde Damink, P.J. Dijkstra, M.J. Van Luyn, P.B. Van Wachem, P. Nieuwenhuis, J. Feijen, *Journal of Materials Science: Materials in Medicine*, **1995**, 6, 429-434

[lxv] S. Bozzini, P. Petrini, L. Altomare, M.C. Tanzi, *Journal of Applied Biomaterials & Biomechanics*, **2009**, 7, 194-199

[lxvi] C.M. Ofner, W.A. Bubnis, *Pharmaceutical Research*, **1996**, 13, 1821-1827

[lxvii] S.M. Lien, L.Y. Ko, T. Huang, *Acta Biomaterials*, **2009**, 5, 670-679

[lxviii] H.W. Sung, H.L. Hsu, C.C. Shih, D.S. Lin, *Biomaterials*, **1996**, 17, 1405-1410

[lxix] H. Petite, I. Rault, A. Huc, P. Mesnache, D. Herbage, *Journal of Biomedical Materials Research*, **1990**, 24, 179-188

[lxx] S. Sakai, I. Hashimoto, K. Kawakami, *Journal of Bioscience and Bioengineering*, **2007**, 103, 22-26

[lxxi] J. Franchini, E. Ranucci, P.Ferruti, M. Rossi, R. Cavalli, *Biomacromolecules*, **2006**, 7, 1215-1222

[lxxii] C. Moinarda, L. Cynobera, J.P. de Bandta, *Clinical Nutrition*, **2005**, 24, 184-197

[lxxiii] P. Ferruti, S. Manzoni, S.C.W. Richardson, R. Duncan, N.G. Pattrick, R. Mendichi, M. Casolaro, *Macromolecules,* **2000**, 33, 7793-7800

[lxxiv] U. Hersel, C. Dahmen, H. Kessler, *Biomaterials*, **2003**, 24, 4385-4415

[lxxv] E. Jacchetti, E. Emilitri, S.Rodighiero, M. Indrieri, A. Gianfelice, C. Lenardi, A. Podestà, E. Ranucci, P. Ferruti, P. Milani, *Journal of Nanobiotechnology*, **2008**, 6, 14

[lxxvi] P. Ferruti, S. Bianchi, E. Ranucci, F. Chiellini, A.M. Piras, *Biomacromolecules* **2005**, 6, 2229-2235

lxxvii V. Magnaghi, V. Conte, P. Procacci, G. Pivato, P. Cortese, E. Cavalli, G. Pajardi, E. Ranucci, F. Fenili, A. Manfredi, P. Ferruti, *Journal of Biomedical Materials Research: Part A,* **2011**, 98A, 19–30

lxxviii N. Mauro, F. Chiellini, C. Bartoli, M. Gazzarri, M. Laus, D. Antonioli, P. Griffiths, A. Manfredi, E. Ranucci, P. Ferruti, *Journal of Tissue Engineering and Regenerative Medicine*, **2016**, On line available, DOI:10.1002/term.2115

lxxix F. Zhang, C. He, L. Cao, W. Feng, H. Wang, X. Mo, J. Wang, *International Journal of Biological Macromolecules*, **2011**, 48, 474-481

lxxx S. Xu, J. Li, A. He, W. Liu, X. Jiang, J. Zheng, C.C. Han, B.S. Hsiao, B. Chu, D. Fang, *Polymer*, **2009**, 50, 3762-3769

lxxxi B. Demirdögen, A.E. Elçin, Y.M. Elçin, *Journal Growth Factors*, **2010**, 28, 426-436

lxxxii N.T.B. Linh, L. Byong-Taek, *Tissue Engineering Part A*, **2014**, 20, 1993-2004

lxxxiii X. Hu, D. Li, F. Zhou, C. Gao, *Acta Biomaterialia*, **2011**, 7, 1618–1626

lxxxiv X. Zheng Shu, Y. Liu, F. Palumbo, G. D Prestwich, *Biomaterials*, **2003**, 24, 3825-3834

lxxxv P.A. Levett, F.P.W. Melchels, K. Schrobback, D.W. Hutmacher, J. Malda, T.J. Klein, *Acta Biomaterialia*, **2014**, 10, 214-223

lxxxvi J.P.Chen, Y.L. Leu, C.L. Fang, C.H. Chen, J.Y. Fang, *Journal of pharmaceutical sciences*, **2011**, 100, 655–666

lxxxvii J. Kim, I.S. Kim, T.H. Cho, K.B. Lee, S.J. Hwang, G. Tae, I. Noh, S.H. Lee, Y. Park, K. Sun, *Biomaterials*, **2007**, 28, 1830–1837

lxxxviii J.Y. Lai, *Colloids and Surfaces B: Biointerfaces*, **2014**, 122, 277-286

lxxxix Y.C. Chen, W.Y. Su, S.H. Yang, A. Gefen, F.H. Lin, *Acta Biomaterialia,* 2013, 9, 5181–5193

xc L.F.M. Zadeh, L. Moses, S.M.G. Brant, *Journal of Veterinary Pharmacology and Therapeutics*, **2008**, 31, 187-199

xci M. Lesurtel, R. Graf, B. Aleil, D.J. Walther, Y. Tia, W. Jochum, C. Gachet, M. Bader, P.A. Clavien, *Science*, **2006**, 312, 104-107

xcii P. Starlinger, A. Assinger, S. Haegele, D. Wanek, S. Zikeli, D. Schauer, P. Birner, E. Fleischmann, B. Gruenberger, C. Brostjan, T. Gruenberger, *Hepatology*, **2014**, 60, 257-266

xciii G.K. Papadimas, K.N. Tzirogiannis, M.G. Mykoniatis, A.D. Grypioti, G.A. Manta, G.I. Panoutsopoulos, *Swiss Medical Weekly*, **2012**, 142, 13548

xciv M. Kunishima, C. Kawachi, J. Morita, K. Terao, F. Iwasaki, S. Tani, *Tetrahedron*, **1999**, 55, 13159-13170

xcv M. D'Este, D. Eglin, M. Alini, *Carbohydrate Polymers*, **2014**, 108, 239–246

xcvi A. Falchi, G. Giacomelli, A. Porcheddu, M. Taddei, *Synlett*, **2000**, 2, 275-277

xcvii P.Farkaš, S. Bystrický, *Carbohydrate Polymers*, **2007**, 68, 187-190

xcviii P. Ferruti, E. Ranucci, F. Trotta, E. Gianasi, E. G. Evagorou, Mohammed

xcix P.J. Flory, Principles of polymer chemistry, Ithaca, New York Cornell University Press, **1953**

HYDROGELS FOR TISSUE ENGINEERING BASED ON HYALURONIC ACID, GELATIN AND AGMA1

[c] A.T. Metters, K.S. Anseth, C.N. Bowman, *Biomedical sciences instrumentation Journal,* **1999**, 35, 33-38

[ci] E. Marsano, S. Gagliardi, F. Ghioni, E. Bianchi, *Polymer*, **2000**, 41, 7691-7698

[cii] M.B. Huglin, M.M. Rehab, M.B. Zakaria, *Macromolecules*, **1986**, 19, 2986-2991

[ciii] S.J. de Jong, B. van Eerdenbrugh, C.F. van Nostrum, J.J. Kettenes-van den Bosch, W.E. Hennink, *Journal of Controlled Release*, **2001**, 71, 261-275

[civ] A.M. Lowman, N.A Peppas, E. Mathiowitz, *Encyclopedia of controlled drug delivery*, New York, Wiley, **1999**

[cv] R.L. Cleland, *Biopolymers,* **1970**, 9, 811-824

[cvi] J. Baier Leach, K.A. Bivens, C.W. Patrick, C.E. Schmidt, *Biotechnology and Bioengineering*, **2003**, 82, 578-589

[cvii] M. Kunishima, C. Kawachi, J. Morita, K. Terao, F. Iwasaki, S. Tani, *Tetrahedron*, **1999**, 55, 13159-13170

[cviii] M. Djabourov, J. Leblond, P. Papon, *Journal de Physique France*, **1988**, 49, 319-332

[cix] S.M. Tosh, A.G. Marangoni *Applied Physics Letters*, **2004**, 84(21):4242 - 4244

[cx] D. Klatt, C. Friedrich, Y. Korth, R. Vogt, J. Braun, I. Sack, *Biorheology*, **2010**, 47, 133-141

[cxi] Sylvester PW. *Optimization of the tetrazolium dye (MTT) colorimetric assay for cellular growth and viability, Drug Design and Discovery. Methods and Protocols*, Los Angeles, Humana Press, 2011

List of pubblications

"One-Step Synthesis of Poly(lactic-co-glycolic acid)- g-Poly-1-Vinylpyrrolidin-2-One Copolymers", E. Ranucci, G. Capuano, A.Manfredi, P. Ferruti, *Journal of Polymer Science, Part A: Polymer Chemistry*, **2016**, 54, 1919-1928

"Preparation and characterization of poly (lactic-glycolic acid)–g-poly (1-vinylpyrrolidin-2-one) (PLGA-g-PVP) nanoparticles for controlled release of doxorubicin", In preparation

"PLGA-g-PVP -based nanocapsules for the controlled delivery of antimalarials", In preparation

"Enhanced stability and proliferation properties of hyaluronan-gelatin-AGMA1-serotonin hydrogels for liver tissue engineering", In preparation

List of attended conferences and schools

G. Capuano, P. Ferruti, A. Manfredi, E. Ranucci, L. Paltrinieri, C. Gualandi, M. L. Focarete. "The use of novel PLGA-g-PVP amphiphilic copolymers for fabrication of nanostructured materials." (Poster), Nanomedicine Congress 2014, September 17th-19th **2014**, University of Viterbo, VT, Italy.

E. Ranucci, G. Capuano, A. Manfredi, P. Ferruti. "PLGA-g-PVP amphiphilic bioactive and biocompatible copolymers for fabrication of nanostructured materials" (Oral) Biotechnology **2014**, June 24th-27th **2014**, China.

G. Capuano, P. Ferruti, A. Manfredi, E. Ranucci, L. Paltrinieri, C. Gualandi, M. L. Focarete. "The use of novel PLGA-g-PVP amphiphilic copolymers for fabrication of nanostructured materials." (Poster), XIX congresso nazionale divisione di chimica industriale della società chimica italiana" Salerno, September 14th-17th **2015**

XXXVII Convegno-Scuola AIM "Mario Farina" – Caratterizzazione di materiali polimerici: tecniche per polimeri fusi e allo stato solido, Gargnano, May 1rt-6th **2016**

G. Capuano, J. Alongi, A. Manfredi, R. Cavalli, E. Marti, X. Fernandez-Busquets, P. Ferruti, E. Ranucci. "Copolimeri ad innesto PLGA-g-PVP per la veicolazione e il rilascio controllato di farmaci antimalariali" (Poster), XXII Convegno nazionale dell'associazione italiana di scienza e tecnologia delle macromolecole-AIM, Genova, September 11th-14th **2016**

J. Alongi, G. Capuano, A. Manfredi, R. Cavalli, X. Fernandez-Busquets, E. Marti, P. Ferruti, E. Ranucci. "PLGA-g-PVP -based nanocapsules for the controlled delivery of antimalarials" (Poster), Nanomedicine, Viterbo, September 21th-23th **2016**